The Environment of Iron in Silicate Glasses

Paul A. Bingham

University of Sheffield

June 2000

A thesis submitted for the degree of Doctor of Philosophy at the University of Sheffield

Department of Engineering Materials

Sir Robert Hadfield Building

Mappin Street

Sheffield

Abstract

Iron species in glass are vital to applications such as solar control, and greater understanding of these species is required. Redox, coordination, distribution and environment of iron in alkali-alkaline earth-silica glasses containing 0-5 molar % Fe_2O_3 have been studied using a multi-technique approach.

Wet chemical analysis provided values of the $Fe^{2+}/\Sigma Fe$ redox ratio and these are in agreement with those obtained from optical and Mössbauer techniques over a wide range of glass compositions and Fe_2O_3 contents. The $Fe^{2+}/\Sigma Fe$ ratio is independent of iron content in the glasses studied, provided that melting conditions allow sufficient equilibration with the furnace atmosphere.

As iron content increases, Fe-Fe near-neighbour interactions have an increasing influence on measured properties. Mössbauer parameters indicate a wider range of site occupancies by Fe^{2+} and Fe^{3+} at low iron contents. Electron spin resonance suggests some clustering of Fe ions even at low iron concentrations. The amount of clustering is proportional to the square of the molar Fe_2O_3 content. Increasing alkali / alkaline earth ionic radius ratio promotes clustering at all Fe_2O_3 contents.

The effects of alkali and alkaline earth ions on the redox, distribution, coordination and environment of Fe ions in these glasses generally fall into two behavioural categories which have been termed "collective" and "selective".

Collective behaviour occurs when alkali and alkaline earth ions have similar effects on a property and the overall effect is cumulative. This is characterised by proportionality with theoretical optical basicity of the glass. Many parameters associated with Fe^{2+} ions fall into this category.

Selective behaviour occurs when alkali and alkaline earth ions have opposing effects on a property, suggesting competition or selectivity between ion types. This is characterised by proportionality with the alkali / alkaline earth ionic radius ratio. The redox ratio and several parameters associated with the clustering, coordination and environment of Fe^{3+} ions fall into this category.

Glasses containing MgO can exhibit behaviour dissimilar to the other alkaline earth oxides; molar volume, redox, coordination and clustering are affected. These phenomena may be due to some Mg^{2+} ions occupying tetrahedral sites.

Acknowledgements

In completing this thesis I have been fortunate to have worked with many helpful and enthusiastic people. Firstly I wish to thank my academic supervisors, Dr. John Parker and Dr. Tim Searle, for their help, guidance and encouragement throughout this PhD. Thanks also to my industrial supervisor at Pilkington Technology Centre, Ken Fyles.

Secondly I would like to thank Dr. John Williams, who was so helpful and enthusiastic with the Mössbauer studies.

My thanks also go to: Prof. Michael Cable for many useful and informative conversations ; Ian "Killer" Watts and Dean Hemlock for help with glass melting (just one more melt.....) ; Beverley Lane for optical absorption spectroscopy (well it was working ok when I left it....) ; Ashley, Stan, Glen, Helen, Clive and all at Pilkington Technology Centre ; Glass Technology Services for allowing the use of printing facilities for this thesis; and to Kyle Williams for that vital Mössbauer help.

I must also thank my friends who have been around for the past years and meant things were never dull: Raych Cubbon for putting up with me (I was going to wash up, honest!), the Eng Mats and Baggers Old Boys 6-a-side footy teams, and all my friends (you know who you are!). Thanks for all the good times.

Finally I want to thank my family for being so supportive and having faith in me – I told you I'd finish it eventually! This thesis is dedicated to you all.

The Environment of Iron in Silicate Glasses

Abstract

Acknowledgements

Contents

Chapter 1. Introduction **1**

Chapter 2. Background **6**

2.1. The Nature, Structure and Properties of Glass 6

2.2. Reduction – Oxidation (Redox) of Iron in Glass 10

2.2.1. The "Classic Model" 11

2.2.2. Temperature of Melting 12

2.2.3. Time of Melting 12

2.2.4. Furnace Atmosphere 13

2.2.5. Glass Composition 13

2.2.6. Fe_2O_3 Concentration 14

2.2.7. Glass Viscosity 15

2.2.8. Methods of Redox Measurement 16

2.3. Coordination and Environment of Iron in Glass 16

2.4. References 18

Chapter 3. Experimental **22**

3.1. Glass Making 22

3.1.1. Standard Composition 22

3.1.2. Other Compositions 23

3.1.3. Batch 23

3.1.4. Melting 23
3.2. Density Measurement 25
3.3. X-Ray Diffraction (XRD) 25
3.4. Inductively-Coupled Plasma (ICP) 25
3.5. Redox Measurements 26
3.5.1. Wet Chemical Redox Measurements 26
3.6. Optical Absorption Spectroscopy 27
3.6.1. Sample Preparation 27
3.6.2. Spectral Measurement 28
3.6.3. Normalisation of Spectra 28
3.7. Photoluminescence (PL) Spectroscopy 30
3.7.1. PL Sample Preparation 30
3.7.2. Measurement of PL Spectra 30
3.7.3. Normalisation of PL Spectra 31
3.8. Electron Spin Resonance (ESR) Spectroscopy 32
3.8.1. ESR Sample Preparation 32
3.8.2. Measurement of ESR Spectra 32
3.9. Mössbauer Spectroscopy 32
3.9.1. Mössbauer Sample Preparation 32
3.9.2. Measurement of Mössbauer Spectra 33
3.10. References 34

Chapter 4. Optical Spectroscopy 35

4.1. Background & Literature Survey 35
4.1.1. Electronic Transitions in Transition Metal (TM) Complexes 36
4.1.1.1. Spin Selection Rules 36
4.1.1.2. Laporte Selection Rule 37
4.1.1.3. Spin Multiplicity Selection Rule 37
4.1.1.4. Spin Coupling Interactions 38
4.1.1.5. Charge Transfer Transitions 38
4.1.1.6. Widths of Absorption Bands 39

4.1.1.7. The Jahn-Teller Effect 40
4.1.2. Optical Spectra 41
4.1.2.1. Ultra-Violet (UV) 41
4.1.2.2. Visible 42
4.1.2.3. Infra-Red (IR) 43
4.1.3. Application of Ligand Field Theory to Fe^{2+} and Fe^{3+} Ions in Glass 43
4.1.3.1. Electronic Spectra and *Dq* 45
4.1.3.2. Factors Affecting *Dq* 46
4.1.3.3. Spectroscopic Notation and Racah Parameters 48
4.1.3.4. Energy Level Diagrams 49
4.1.4. Optical Spectroscopy of Iron in Glass 52
4.1.4.1. Fe^{2+} d-d Absorptions 53
4.1.4.2. Fe^{3+} d-d Absorptions 54
4.1.4.3. Luminescence of Fe^{3+} Ions 57
4.1.4.4. Charge-Transfer Absorptions and the Effects of Iron Concentration 59
4.1.4.5. Coordination and Redox 60
4.1.4.6. Extinction Coefficients 60
4.1.4.7. Effects of Composition on Spectra 62
4.1.4.8. Effects of Different Glass Formers 62
4.1.4.9. Effects of Different Glass Modifiers 63
4.2. Optical Techniques – Principles of Operation 66
4.2.1. Optical Absorption Spectroscopy 66
4.2.2. Photoluminescence (PL) Spectroscopy 66
4.3. Results 67
4.3.1. Iron-Free Glass 67
4.3.2. Glasses Containing 0.2 Molar % Fe_2O_3 69
4.3.2.1. X-Ray Diffraction (XRD) 70
4.3.2.2. Density and Concentration 70
4.3.2.3. Optical Spectra 73
4.3.2.4. SiO_2 Partial Replacement 77

4.3.2.5. Silicate and Borate Glass 77
4.3.2.6. UV Edge – Effects of Composition and Redox 78
4.3.3. Glasses Containing 0.1 – 5 Molar % Fe_2O_3 79
4.3.3.1. Glasses Containing 5 Molar % Fe_2O_3 81
4.3.4. Melting Time and Temperature of Measurement 82
4.3.4.1. Melting Time 82
4.3.4.2. Measurement Temperature 84
4.3.5. Computer Fitting and Mathematical Modelling 85
4.3.5.1. Glasses Containing 0.2 Molar % Fe_2O_3 88
4.3.5.2. Glasses Containing 0.1-5 Molar % Fe_2O_3 91
4.3.5.3. Calculation of Racah Parameters 92
4.3.6. Calculation of Extinction Coefficients 94
4.3.6.1. Fe^{2+} Extinction Coefficient, $\varepsilon(Fe^{2+})$ 95
4.3.6.2. Fe^{3+} Extinction Coefficient, $\varepsilon(Fe^{3+})$ 96
4.3.7. Wet Chemical Redox Measurements 97
4.3.7.1. Glasses Containing 0.2 Molar % Fe_2O_3 97
4.3.7.2. Varying Fe_2O_3 Content 101
4.3.7.3. Glasses Containing 5 Molar % Fe_2O_3 101
4.3.8. Redox Measurements Based on Optical Absorption Spectroscopy 102
4.3.8.1. Glasses Containing 0.2 Molar % Fe_2O_3 102
4.3.8.2. Varying Fe_2O_3 Content 103
4.3.9. Photoluminescence (PL) Spectroscopy 104
4.3.9.1. Photomultiplier Detector 104
4.3.9.2. Germanium Detector 107
4.3.9.3. Computer Fitting of PL Spectra 109
4.4. Discussion 109
4.4.1. Base Glasses 109
4.4.2. Band Assignments and Computer Fitting for Iron-Containing Glasses 110
4.4.2.1. Fe^{2+} Ions 110
4.4.2.2. Fe^{3+} Ions 111

4.4.2.3. IVCT Band 112
4.4.2.4. UV Edge 113
4.4.3. Coordination and Environment 114
4.4.3.1. Fe^{2+} Ions 114
4.4.3.2. Fe^{3+} Ions 116
4.5. Chapter Summary 118
4.6. References 119

Chapter 5. Electron Spin Resonance (ESR) 124

5.1. Principles of Operation 124
5.2. Background & Literature Survey 126
5.2.1. The Effects of Iron Content 127
5.2.2. The Effects of Glass Composition 130
5.2.3. Summary and Main Points from the Literature 133
5.3. Results 134
5.3.1. Varying Glass Composition 134
5.3.2. Changing Fe_2O_3 Content 138
5.3.3. Borate Glass 140
5.4. Discussion 140
5.4.1. Distribution of Fe Ions 140
5.4.2. The Effects of Glass Composition 141
5.5. Chapter Summary 144
5.6. References 145

Chapter 6. Mössbauer Spectroscopy 148

6.1. Principles of Operation 148
6.2. Background & Literature Survey 148
6.2.1. Mössbauer Spectroscopy of Iron in Glass 149
6.2.2. Centre Shift (δ) and Quadrupole Splitting (Δ) 150
6.2.3. Paramagnetic Hyperfine Splitting (hfs) 151
6.2.4. Debye Temperature 153

6.2.5. Recoil-Free Fraction, f 155
6.2.6. Coordination of Fe^{2+} and Fe^{3+} 156
6.2.7. Linewidth, Γ 158
6.2.8. Effects of Iron Concentration 159
6.2.9. Composition – Redox – Coordination Interactions 160
6.3. Results 163
6.3.1. Varying Fe_2O_3 Content 164
6.3.2. Varying Glass Composition 169
6.4. Discussion 172
6.4.1. The Effects of Fe_2O_3 Content 172
6.4.2. The Effects of Glass Composition 177
6.5. Chapter Summary 180
6.6. References 181

Chapter 7. Discussion **185**

7.1. Iron Redox 185
7.1.1. The Effects of Fe_2O_3 Content and Melting Conditions on Redox 186
7.1.2. The Effects of Glass Composition on Redox 187
7.2. Coordination of Iron Species 189
7.2.1. The Effects of Fe_2O_3 Content on Coordination 190
7.2.2. The Effects of Glass Composition on Coordination 191
7.3. Distribution of Iron Species 192
7.3.1. The Effects of Fe_2O_3 Content on Fe Ion Distribution 192
7.3.2. The Effects of Glass Composition on Fe Ion Distribution 193
7.4. The Effects of Other Compositional Changes 194
7.5. Connections between Redox, Coordination and Distribution 196
7.6. Local Structure Surrounding Fe Species 197
7.7. Other Structural Implications 199
7.8. Suggestions for Future Work 199

7.9. References 200

Chapter 8. Summary and Conclusions **202**

8.1. The Effects of Fe_2O_3 Content 202

8.2. The Effects of Glass Composition 203

8.3. The Unique Case of MgO 204

Appendix A **206**

Appendix B **215**

Chapter 1.

Introduction

"The purpose of glass technology is to develop quantitative relations between compositions, properties, and their ionic and electronic structures and to apply them in the making and use of glasses." Clarence Babcock [1].

The importance of the colour of glass reaches back thousands of years. In various forms, glass and in particular coloured glass, was being moulded, blown, formed, pressed and sculpted as early as 2500 BC [2]. It is often surprising, given what is known today about processing, raw materials and impurities, that glasses produced long ago were often of a very high quality, with a wide variety of colours [3]. Throughout history and even to the present day, one of the major concerns about glass has been its colour.

Until relatively recently, glass colour was only related to the choice of raw materials and to a limited extent the furnace used, but there was little further understanding. In recent times, the physics and chemistry behind the processes by which light is absorbed and emitted have become better understood. The application of this knowledge to vitreous systems has given much information on many of their structural and optical characteristics.

The 20th century saw major advances in many areas of science and technology. These changes are reflected in the scope and understanding of glass. Quantum theory has allowed understanding of atomic concepts which can be applied to

both structure and colour of glasses. Electronics and instrumentation are remarkably improved and miniaturised, hence giving a greater ability to measure properties. This is a continuous process and has seen major leaps even in the last decade. The advent of mass-produced and powerful computers has revolutionised both the manufacture and analysis of materials.

In terms of actual glassmaking, there have also been significant changes. Alternative glass-forming systems such as the chalcogenides and fluorides have been introduced, bringing new and interesting properties. New processing routes such as deposition and sol-gel introduced different properties and new potential applications for glass. Improved manufacturing skills have allowed the production of large volumes of high-quality optical fibres for telecommunications applications, which have increased dramatically in the last few years.

Perhaps the most commercially important advance of the 20th century in glass manufacturing has been the introduction of the float glass process by Pilkington. This provided a cheap, controllable and continuous method of flat glass production. The basic requirement for production of a flat, fire-polished, distortion-free glass was to have some means of preventing contact between anything solid with the molten or plastic glass, whilst preventing stress of the glass. Floating the molten glass on a flat layer of molten metal under controllable conditions was the solution. Tin was found to be the most suitable metal for this purpose. The first commercial float glass appeared in 1959, following years of intensive and highly secret development. Nowadays, float glass is produced all over the world in massive volumes.

Scientific techniques with which to investigate the properties of materials have been strongly affected by the improved technology. Currently a wide range of techniques exist which can be used to investigate many aspects of glass. These include thermodynamic techniques such as differential scanning calorimetry (DSC) and differential thermal analysis (DTA), chemical techniques such as those used for compositional analysis, optical and electron microscopies, and spectroscopy.

The interaction of radiation with matter, which leads to energy dissipation in specific spectral regions, is not fully understood or characterised. The instrumentation needed to accurately observe, record and measure this interaction is often complicated. The relationship between observations and underlying structure is often influenced by many factors, which need to be fully understood before correct conclusions can be drawn from data. Spectroscopic techniques used in the study of glass cover the whole range of the electromagnetic spectrum, from Mössbauer spectroscopy at γ-ray frequencies, to electron spin resonance (ESR) and nuclear magnetic resonance (NMR), which operate in the radio frequency and microwave regions. Use of computers for the modelling of glass structure has also proven highly successful. Powerful computers have allowed complex calculations to be made on glass systems, and their structures to be modelled with reasonable accuracy.

Colouration of glass has historically been provided by transition metal ions or rare-earth ions, or metal colloids in the case of ruby glasses. Of these colorants, the most important is iron, Fe. It is predominantly introduced to the glass by the sand used in glassmaking, although most other raw materials also contain some iron. Silicate glasses, which still constitute the bulk (95%) of glass manufacturing, usually contain some level of iron. Float glass contains typically 0.1 % by weight of iron oxide, Fe_2O_3. This has the effect of giving the glass a green tinge, which can be seen easily through a cross-section of the glass. This colour is caused by the presence of both Fe^{2+} and Fe^{3+} ions in the glass, which absorb radiation at characteristic wavelengths.

Modern applications, such as in the construction and automotive industries, often require solar control. This is the deliberate attenuation of particular wavelengths of light to give certain required optical properties. For example, an automotive glass must give adequate visible light transmission, whilst cutting out harmful UV rays, and reducing heat transmission by IR radiation. It is known that UV radiation can severely damage polymeric materials which now constitute a large proportion of vehicle interiors. With the advent of the depletion of the ozone layer, the need for UV protection is made perhaps even more important.

Approximately 50% of heat transmission occurs in the IR region below 13,000 cm^{-1} (> 770 nm), with the other 50% occurring in the visible region from 26,300 - 13,000 cm^{-1} (380 - 770 nm). Attenuation of this radiation to acceptable levels is necessary, especially in hotter climates, to keep vehicle interiors cool and to reduce the load on air conditioning systems. The IR region is an obvious target for this reduction since excessive attenuation of visible radiation would be dangerous for obvious reasons. Ionic doping is by far the most common method of achieving solar control, although other methods such as reflective coatings have been used. Dopants commonly added to glasses include Fe, Se, Co, Cr, Ni, Mn, V, Cu, Ce and S (for amber glasses). Absorption spectra are more complicated for some transition metal ions than others. Investigators of optical properties of iron, for example, face problems caused by the overlap of several different absorption bands with each other and with the UV edge. This can make interpretation difficult.

It is known that when Fe is present in glasses of commercial composition, it usually occurs in both Fe^{2+} and Fe^{3+} forms. Each of these redox states produces its own unique set of optical absorption bands and so the redox state, or the ratio of Fe^{2+} / Fe^{3+} ions in a glass has a strong effect on the colour. The sites within a glass in which these ions exist can also affect colour - the coordination of a cation with respect to the surrounding O^{2-} ions is very important. There is still much debate over the coordination of Fe^{2+} and Fe^{3+} ions in silicate glasses. The effects of glass composition upon optical properties are still not fully understood either. If a glass manufacturer were to change the composition of a glass, for example to replace some calcium with magnesium, it is important to be able to predict what effects this would have on colour and structure as well as other properties such as viscosity and liquidus temperature.

Much of the scientific work on glasses containing iron has involved glasses with no commercial importance, such as binary alkali silicates. Very few surveys had, before this work, been carried out on ternary alkali-alkaline earth silicate glasses, which are realistic simplifications of commercial compositions. None of these works had used a wide range of techniques to conduct a systematic investigation

of alkali-alkaline earth silicate glasses where the emphasis has been on *type* rather than *amount* of alkali and alkaline earth ions. Nor had they conducted this survey over a very wide range of iron contents. A study of this type was necessary to "bridge the gap" between scientific investigations of iron in glasses of no use commercially and the world of commercial float glass and solar control glass-type compositions.

Further work is still required in all areas of glass science and technology. Refinement of existing systems and techniques and formation of new ones are ongoing processes. Better understanding of all properties of glass, from optical and structural to thermodynamic and mechanical, are still required. This is to allow the production of glasses with required properties more effectively, and to further the ongoing studies into glass structure/property relationships, which are still far from comprehensive.

1.1. References

[1] Babcock, C.L., Silicate Glass Technology Methods, Wiley, 1977.

[2] Maloney, F.J.T., Glasses in the Modern World, Aldus Books, 1967, p.50

[3] Maloney, F.J.T., Glasses in the Modern World, Aldus Books, 1967, p.53

Chapter 2.

Background

2.1. The Nature, Structure and Properties of Glass

The simplest glass is formed by pure silica, SiO_2. Early studies of glass structure by Zachariasen [1] and Warren [2, 3] showed that each Si^{4+} ion is screened by four O^{2-} ions, each of which is shared by two Si^{4+} ions, thus linking tetrahedra together. This 3-dimensional network with O^{2-} ions in two-fold coordination represents a very open structure, and this explains many properties of silica.

Upon addition of alkali oxides to silica glass, the extra oxygen provided to the continuous silicate network by the alkali oxide increases the O/Si ratio in the network above its value of 2 for SiO_2. This causes the appearance of oxygens bonded to only one Si^{4+} ion. These oxygens are called "non-bridging" and are charge-compensated by the monovalent alkali ions. Addition of alkali does, however, cause weakening of the Si-O bond. This analysis became known as the Zachariasen-Warren "Random Network Theory", and soon became the most popular model of glass structure. The model survives to this day, although with some modifications.

Dietzel [4] extended the theory by developing the concept of cationic field strength from his work on compound formation. The theory works by considering the size and polarizability of constituent ions in glass, and concerns the influence of the interaction of electrostatic forces between cations and anions in the glass.

The term is known as the *cation field strength* F, such that $F = z/a^2$ where z = cation charge and a = internuclear cation-anion distance. The cation field strength concept has allowed explanation of many aspects of glass formation and properties, for example correlating the number of compounds in alkali-silica and alkaline earth-silica systems with the sizes and charges of cations involved.

Studies of SiO_2-K_2O glasses did not support the concept of a random distribution of K^+ ions in a network of SiO_4 tetrahedra [5]. The differences were due to a second structure which arose when increasing amounts of K^+ were introduced [5]. X-ray studies of SiO_2-Na_2O-RO (R = Ca, Ba) glasses showed similar behaviour [6]. With increasing BaO content, Ba^{2+} ions were not randomly distributed throughout the glass but occurred as "certain groups". These works questioned the continuity and randomness predicted by the random network theory.

More recent refinements to the accepted models of glass structure have been made possible by new and improved experimental techniques and the advent of computer modelling and molecular dynamics [7, 8, 9, 10]. Work using EXAFS and neutron scattering has modified the accepted model by showing the likelihood of the existence of domains or channels enriched in cations and percolating the silicate framework [9, 10]. The presence of such domains was suggested in superionic glasses [11], and is supported by computer simulation studies [12].

Ionic radii of constituent ions provide useful information about the chemistry of a glass. When ions approach one another, forces of repulsion set in with great abruptness near certain inter-atomic separations. Ions are often treated as rigid spheres in mutual contact. Thus, interatomic spacings measured by such techniques as X-ray diffraction (XRD), are equal to the sums of the radii of the adjacent ions. Goldschmidt [13] suggested that "field strength", Z/r^2, of an ion is proportional to its polarising power, and subsequent work by Dietzel developed cation field strength, as described earlier. Dingwall & Moore [14] found that high-temperature viscosity (η) measurements provided a good empirical method for comparison of the effects of different constituent oxides. Their data was used to plot ionic radius vs. temperature at which $\eta = 10^{12}$ Poise. Data points for the

various substituting cations lay along three well defined lines, covering the ranges 0.31 - 0.6 A, 0.6 - 1.0 A, and 1.0 - 1.6 A. These groupings reflected cation coordinations. Limiting radius ratios have been determined for crystals such as alkali nitrates and divalent fluorides, and agree well with the breaks in the line. Shelby & Day [15] found that for mixed-alkali silica glasses containing equal concentrations of dissimilar alkali ions, the activation energy varied directly with the ionic radius ratio of the two alkali ion types. This highlights the usefulness of ionic radii for investigating structure / property relationships.

It has been demonstrated in silicate glasses that Mg^{2+} ions behave somewhat differently to the other alkaline earth ions, and this has been attributed to the presence of some Mg^{2+} ions in four-fold coordination [14, 16, 17, 18, 19]. The other alkaline earth cations coordinate with 6 or more oxygen anions. The unique behaviour of Mg^{2+} explains differences in molar volume [17] and glass hardness [19], and may also explain differences in redox and optical properties observed in iron-containing alkaline earth phosphate glasses by Edwards et al [20]. Gorbachev et al [18] found that significant numbers of MgO_6 groups are only stable in soda-magnesia-silica glasses when the ratio $MgO/Na_2O > 1.5$, and with large concentrations of SiO_2.

It is often necessary to use a numerical scale which represents the glass composition in some way. Such scales include cation field strength, F, and the ionic radius ratio, as previously discussed. Another property which has been used to this end is glass basicity. The optical basicity scale developed by Duffy and co-workers [21 – 23] has been widely cited, though other glass basicity scales exist [24 - 26]. Lewis acidity / basicity is a concept which applies well to inorganic glass systems. Glasses are generally based on a series of acidic oxides such as SiO_2 and basic oxides such as Na_2O and CaO. Increasing basicity of the oxide accompanies increasing negative charge on its O^{2-} ion. Thus a measurement of the electron density of the oxygen atoms provides a scale of basicity of the glass. Duffy and co-workers have used certain probe ions such as Tl^{+} and Pb^{2+}, which signal reliably the extent to which they receive negative charge from the O^{2-} ions, to produce a quantitative scale [21 –23]. The theoretical optical basicity, Λ_{th}, can

be calculated from equation 2.1.a.

$$\Lambda_{th} = X_{AOa/2}\Lambda(AO_{a/2}) + X_{BOb/2}\Lambda(BO_{b/2}) + \ldots\ldots \quad \text{(Equation 2.1.a.)}$$

where $\Lambda(AO_{a/2})$, $\Lambda(BO_{b/2})$..... are the optical basicities of the oxides $AO_{a/2}$ and $BO_{b/2}$ and $X_{AOa/2}$, $X_{BOb/2}$ are the equivalent fractions. Individual oxide basicities were provided by the work of Duffy et al [22, 23], who calculated these values from Pauling electronegativities of the cations. Optical basicity has often been used when investigating properties of transition metals and other ions in glasses [27 – 40].

As well as calculating the average optical basicity for bulk glass, the microscopic optical basicity allows one to focus on individual sites within a glass [21, 22]. For example, bridging oxygens have different microscopic basicities to non-bridging oxygens. This may be useful for quantifying site-selective phenomena as long as the exact site and its surroundings are known.

The effect of having more than one alkali and / or alkaline earth oxide in a glass is to produce local structural changes due to changes in the local bonding forces caused by exchanging different cation types [41]. In general these effects were explained by differences between the field strengths of the cations, $\Delta(z/a^2)$. The interpretation was that it is the smallest, not the largest difference in field strength which is important. Configurations of the type R^+-O(Si)-R^{2+} were said to be more energetically favourable than separate R^+-O(Si)-R^+ and R^{2+}-O(Si)-R^{2+} groups, hence the improvements in durability on addition of alkaline earth ions to alkali silicate glasses [41]. It was asserted that if the field strengths of the different cations were similar, there is a tendency for discrete separation into structural regions of different composition, i.e. cation clustering. This agrees with similar suggestions by Greaves et al [9, 42] and Brosset [6].

2.2. Reduction – Oxidation (Redox) of Iron in Glass

Redox couples are strongly affected by glass basicity. In the case of iron, its oxidised Fe^{3+} state will be favoured as the optical basicity of the glass increases. A high value of Λ_{th} means that the oxides are able to donate more negative charge, thereby stabilising the metal ion in its oxidised form. Relationships have been found linking redox with glass optical basicity for several transition metal ion couples including Fe^{2+}/Fe^{3+} [23, 27, 31, 32, 33, 35]. This relationship is linear in Li_2O-SiO_2, Na_2O-SiO_2, and K_2O-SiO_2 glasses when $\log(Fe^{2+}/Fe^{3+})$ is plotted against Λ_{th}. Thus with increasing Λ_{th}, the $Fe^{2+} \Leftrightarrow Fe^{3+}$ equilibrium moves to the right. Other redox ion pairs exhibit similar behaviour, except for Cu^{+}/Cu^{2+}. The Cu^{+}/Cu^{2+} system shows the opposite trend to the other redox pairs: increasing glass basicity favours the reduced state [32]. It has been noted that in many cases, redox equilibria do not correlate very well with the optical basicity, indicating the existence of additional mechanisms [35].

The redox states of transition metal ions play a vital role in determining the optical characteristics of glasses in which they are present. The reader is referred to an excellent paper by Schreiber [43] discussing redox processes in glass-forming systems. In glass, Fe^{2+} and Fe^{3+} ions exist in equilibrium with one another. This equilibrium is affected by the following physical factors, according to Densem & Turner [44]:

a) Melting conditions (temperature, time, furnace atmosphere)

b) Glass composition

c) Concentration of Fe_2O_3

d) Glass viscosity

2.2.1. The "Classic Model"

A general equation used to describe the effects of oxygen partial pressure on the equilibrium is as follows;

$$M^{m+} + n/4\ O_2 \Leftrightarrow M^{(m+n)+} + n/2\ O^{2-} \quad \text{(Equation 2.2.1.a.)}$$

The equilibrium constant K is given by the expression

$$K = \frac{\left[M^{(m+n)+}\right]\left[O^{2-}\right]^{n/2}}{\left[M^{m+}\right]p(O_2)^{n/4}} \qquad \text{(Equation 2.2.1.b.)}$$

so when the metal species M = Fe, the formula is written;

$$K^* = \frac{a\left(Fe^{3+}\right)a\left(O^{2-}\right)^{1/2}}{a\left(Fe^{2+}\right)p(O_2)^{1/4}} \qquad \text{(Equation 2.2.1.c.)}$$

Keeping the Fe^{2+}/Fe^{3+} ratio constant with varying composition would require K* to vary in proportion to $[O^{2-}]^{-1/2}$. If the Fe^{2+}/Fe^{3+} ratio decreases as the glass basicity increases as suggested by Duffy and co-workers [27 – 33], then K* must vary even more strongly, so it is not constant.

Attainment of redox equilibrium in systems such as Fe^{2+}/Fe^{3+} is diffusion-controlled [43, 45 – 47]. Some have looked in detail at these phenomena and have modelled kinetics to describe transport of oxygen into and out of the melt [46, 47].

2.2.2. Temperature of Melting

Redox equilibria in oxide glass melts move towards the reduced state as temperature increases [43, 45, 48 – 50]. This is predicted by the Ellingham diagram, where all the free energy lines have positive slopes [51]. Plots of log (Fe^{2+}/Fe^{3+}) vs. 1/T also show positive slopes. Differences in melt composition affect the position and slope of these lines. Glass composition affects K, the equilibrium constant. The same relationship between log (Fe^{2+}/Fe^{3+}) and 1/T has been observed in many different glass systems [20, 45, 50 - 53].

Increasing melting temperature decreases equilibration time [47]. In complex borosilicate glasses, equilibration times decreased dramatically with increasing temperature from 1050°C to 1150°C to 1250°C [47]. Equilibration was also achieved more quickly with increasing Fe content [47].

2.2.3. Time of Melting

Equilibrium is reached with the atmosphere above glass melts only after a certain amount of time. Factors affecting equilibration times include type of crucible [54, 55] and glass composition [36, 44, 46, 51, 55, 56]. Equilibration times ranged from a few hours to over 100 hours [36, 44, 46, 51, 55, 56]. The manner in which Fe is added to the batch can determine whether the equilibrium is approached from "above" or "below". The Fe^{2+} content increases up to a maximum with time if Fe is provided by Fe_2O_3 [51].

Stirring of a glass melt ensures homogeneity and greatly accelerates diffusion by convective mixing. In a stirred Cu-containing melt, equilibrium was achieved after 6-7 hours whereas in an unstirred melt it took over 48 hours to approach equilibrium [36]. Generally, equilibrium is attained more quickly if the melt is physically agitated and held at higher melting temperatures.

2.2.4. Furnace Atmosphere

The partial pressure of oxygen, $p(O_2)$, strongly affects redox. By changing the atmosphere above a melt or by adding reducing or oxidising agents to the glass batch, control over redox can be exercised. For example, the addition of carbon to a batch will form CO_2 on heating, removing oxygen from the melt, causing the melt to become reduced. Addition of nitrate species to a batch will cause the melt to be oxidised by evolving oxygen: $2\ NO_3^- \leftrightarrow 2\ NO_2^- + O_2$. For many redox species it has been shown that log $p(O_2)$ vs. log $[Fe^{2+}/Fe^{3+}]$ gives a linear relationship with slope of ¼ as predicted by equation 2.2.1.c. [43, 45, 50, 57].

2.2.5. Glass Composition

The molar alkali oxide content of binary alkali silica glass is proportional to log [oxidised/reduced] for a number of ions including Fe [23, 31, 33, 35, 53, 55, 57]. By using different alkali oxides (Li, Na, K) the value of log [oxidised/reduced] increased in the order Li < Na < K. Thus increasing optical basicity in these simple binary glasses shifted the redox equilibrium towards the oxidised state. This is a linear relationship [23, 31, 33, 35] which is independent of Fe content [55]. An equivalent relationship exists for binary alkaline earth silicates, namely that [oxidised/reduced] increased in the order Mg < Ca < Sr < Ba [58, 59]. This redox ratio was proportional to the cation field strength z/a^2 of the alkaline earth ion [58, 59]. The Fe^{2+}/Fe^{3+} ratio was linearly correlated with the degree of polymerisation of the melt [58]. Results for binary alkaline earth phosphate glasses doped with Fe were very different: the redox ratio was found to be approximately equal for CaO, SrO and BaO glasses, but MgO glasses had a higher Fe^{3+} content [20].

One may expect that redox equilibria in ternary alkali-alkaline earth silicate

systems would behave in a similar manner to these binary systems. Indeed, this has been found to be true when Na_2O and CaO replaced each other in a soda-lime-silica glass [60]. As far as could be ascertained, no systematic study of the effects of both alkali *and* alkaline earth ions on the redox of Fe in ternary silicate glass had been undertaken previous to this study.

Linear relationships were observed for Sn, Fe, As, Cr, and Ce in binary alkali silicates between the theoretical optical basicity, Λ_{th}, and Δ log O^{2-}, the empirically-calculated free oxygen ion activity [61]. This relationship did not apply to alkaline earth ions or Zn, Pb and Cd. It was concluded in the paper that the free oxygen ion activity is a better parameter than optical basicity for representing the basicity of glasses [61].

Baucke & Duffy [31 – 33] discussed how Fe^{2+}/Fe^{3+} equilibria are influenced by the basicity of a melt. Changing basicity causes changes in activity, fugacity and standard free energies of each species. The stabilisation of higher oxidation states with increasing glass basicity is explained by chemical bonding, which predicts an empirical relationship between redox ratio and average electron density of oxygen ions in the glass. This takes place in alkali silicate glasses over a wide range of basicity values. Empirical relationship's were shown relating redox ratio with optical basicity for Fe, Cr, Ce, Sn and As.

2.2.6. Fe_2O_3 Concentration

Iron is generally added to glasses as an impurity in raw materials, but for experimental glasses it has normally been added as Fe_2O_3. Other forms such as Fe_3O_4 and FeO have sometimes been used. It has long been a matter of debate whether the Fe_2O_3 content of a glass affects the redox, and why this might be if it does occur. A famous work by Densem & Turner [44] shows their results for soda-lime-silica glasses containing 0.002 to 12.5 weight % Fe_2O_3 (0.0008 to 5 molar %). This work has often been quoted as showing that iron redox varies

considerably with iron concentration below about 3 weight % (~1 molar %) Fe_2O_3. The Fe^{2+} content increased with further decreases in Fe_2O_3 content below 3 weight %. The redox ratio was constant above 3 weight % Fe_2O_3. Similar results have been discussed for iron in glass using both wet chemical analysis and Mössbauer spectroscopy [53, 62 - 66] and for other redox ions [48, 49, 55]. A key factor is that *none* of the glasses studied in these works were shown to have properly been brought to equilibrium with the atmosphere.

Goldman [50] stated that his data did not indicate a dependence of the redox equilibrium on total iron content *under equilibrium conditions*. No differences in redox ratio were found between glasses containing 0.09, 0.17 and 0.35 weight % Fe_2O_3 over a range of $p(O_2)$ values. Glasses produced under non-equilibrium conditions exhibited the same trend as discussed in the previous paragraph. This was attributed to the oxidising action of the Fe_2O_3 itself upon the melt. Ferric oxide gives up some of its oxygen during melting, and is therefore considered an oxidising agent. *Under equilibrium conditions*, the cuprous / cupric ratio is unaffected by the concentration of copper [36]. In a study of borosilicate glasses there was almost no difference in redox ratio between glasses containing 1 and 10 weight % Fe_2O_3 *at equilibrium* [47].

2.2.7. Glass Viscosity

In order to investigate viscosity / redox relationships, the composition or temperature of a glass must be changed. These are the very parameters which must stay constant in order to make the study. Viscosity is affected by factors such as the anion to cation ratio, binding forces within polyhedra, cation polarizability and cation size [67].

The effects of composition on viscosity were investigated in a series of soda-lime-silica glasses [14]. The replacement of 8 weight % of the SiO_2 by various monovalent and divalent oxides was carried out. The effects of alkali and alkaline

earth oxides on viscosity were in opposition to one another: for both types of cation, viscosity was proportional to the field strength of the cation. The relationship had a positive slope for divalent ions such as Mg, Ca, Sr, Ba, and Pb, but had a negative slope for monovalent ions such as Li, Na and K. It has been argued that viscosity has little effect on redox when compared with the effect of the chemical composition [44]. Viscosity links both composition and temperature with redox, and a change in viscosity must be brought about by a change in these parameters.

2.2.8. Methods of Redox Measurement

Various methods exist in the literature for the measurement of iron redox. The most widely used is wet chemical analysis. The method of Close et al [68] typifies these measurements. Bamford & Hudson [69] suggested a method based on the absorption spectrum of the glass. The absorption bands at 380 nm and 1000 nm, due to Fe^{3+} and Fe^{2+} ions respectively, were used. The absorbance of the bands after correction should be equal to the extinction coefficient multiplied by the concentration of Fe^{2+} or Fe^{3+} ions multiplied by the path length. This method assumed Beer's Law holds for the measured samples. Correction must be carried out to subtract the UV tail from the spectrum. The extinction coefficients must also be known to allow this method to work.

Mössbauer spectroscopy can also measure iron redox in glass. Analysis of measured spectra allows deconvolution into Fe^{2+} and Fe^{3+} components, and comparison of the relative areas can be used to give the redox ratio.

2.3. Coordination and Environment of Iron in Glass

As discussed by Nelson & White [70], "There are various conceptual frameworks

for interpreting experimental measurements that bear on the structure of glass. The traditional concept, widely used by the glass science community, is to treat glass as if it were a disordered crystal. The glass will then contain 'sites' that can be occupied by the cations. Although many site geometries and symmetries have been proposed for special cases, much of the literature focuses on tetrahedral (network forming) and octahedral (network modifying) sites....An alternative....is to discuss glass in terms of the concepts of the liquid state. Transition metals dissolved in glass re-arrange the local structure to suit their bonding requirements and form complexes of various coordination numbers."

Many works have investigated the coordination and distribution of Fe^{2+} and Fe^{3+} ions in glass, and will be reviewed in following chapters. The ionic radius of Fe^{3+}, 64 pm, is very close to the boundary between 4- and 6- coordination, which occurs at ~60 pm based on geometrical constraints [14]. This suggests that Fe^{3+} ions can occupy either 4- or 6- coordinated sites. The ionic radius of Fe^{2+} is 74 pm. This is further away from the dividing line between 4- and 6- coordination as set down by Dingwall & Moore [14], so Fe^{2+} is more likely to occur in octahedral 6-coordinated sites. Since glasses lack long-range order, these general rules are somewhat relaxed ones, and tetrahedral 4-coordinated Fe^{2+} ions have been reported in some glasses.

The possibility of 5-coordinated Fe-ions in glass has rarely been considered, although trigonal bipyramid and square pyramid are both possible CN=5 sites [71]. Five-coordinated Fe^{2+} ions are present in eudialyte, a complex silicate mineral [71]. These ions in pyramidal sites give rise to absorptions at 10,900 cm^{-1} and 4,000 cm^{-1}, close to those expected of 6- and 4-coordinated Fe^{2+} ions respectively in many silicate glasses.

2.4. References

[1] Zachariasen, W.H., J. Amer. Chem. Soc., 1932, vol. 54, p. 3841.

[2] Warren, B.E., J. Appl. Phys., 1937, vol. 8, p. 645.

[3] Warren, B.E., J. Appl. Phys., 1942, vol. 13, p. 602.

[4] Dietzel, A., Z. Elektrochem., 1942, vol. 48, p. 9.

[5] Hartleif, G., Z. Anorg. U. Allgem. Chem., 1938, vol. 238, p. 353.

[6] Brosset, C., J. Soc. Glass Tech., 1958, vol. 42, p. 125.

[7] Shackelford, J.F., J. Non-Cryst. Solids, 1982, vol. 49, p. 299.

[8] Goodman, C.H.L., J. Non-Cryst. Solids, 1985, vol. 71, p. 1.

[9] Greaves, G.N., J. Non-Cryst. Solids, 1985, vol. 71, p. 203.

[10] Gaskell, P.H., Eckersley, M.C., Barnes, A.C., Chieux, P., Nature, 1991, vol. 350, p. 675.

[11] Börjesson, L., Torell, L.M., Dahlborg, U., Howells, W.S., Phys. Rev., 1989, vol. B39, p. 3404.

[12] Abramo, M.C., Caccamo, C., Pizzimenti, G., J. Chem. Phys., 1992, vol. 96, p. 9083.

[13] Goldschmidt, V.M., Geochem. Verteil. der Elemente, VIII Schrift, Nordske Vidensk. Akad., Oslo, 1927.

[14] Dingwall, A.G.F., Moore, H., J. Soc. Glass Tech., 1953, vol. 37, p. 316.

[15] Shelby, J.E., Day, D.E., J. Amer. Ceram. Soc., 1970, vol. 53, p. 182.

[16] Weyl, W.A., Marboe, E.C., The Constitution of Glasses: A Dynamic Interpretation, vol. 2, part 1, Interscience, London, 1964.

[17] Din, A., Sheikh, M.R., Pakistan J. Sci. Ind. Res., 1974, vol. 17, p. 93.

[18] Gorbachev, V.V., Bystrikov, A.S., Vasil'ev, S.K., Bogomolova, L.V., Soviet J. Phys. Chem. Glasses, 1983, vol. 9, p. 447.

[19] Petzold, A., Wishmann, F.G., von Kamptz, H., Glastech. Ber., 1961, vol. 34, p. 56.

[20] Edwards, R.J., Paul, A., Douglas, R.W., Phys. Chem. Glasses, 1972, vol. 13, p. 137.

[21] Duffy, J.A., Ingram, M.D., J. Non-Cryst. Solids, 1976, vol. 21, p. 373.

[22] Duffy, J.A., Ingram, M.D., J. Non-Cryst. Solids, 1992, vol. 144, p. 76.

[23] Duffy, J.A., Geochim. Cosmochim. Acta, 1993, vol. 57, p. 3961.

[24] Balta, P., Spurcaciu, C., Radu, D., Dumitrescu, O., J. Non-Cryst. Solids, 1985, vol. 71, p. 69.

[25] Balta, P., Radu, D., Rev. Roumaine de Chimie, 1995, vol. 40, p. 977.

[26] Morinaga, K., Yoshida, H., Takebe, H., J. Amer. Ceram. Soc., 1994, vol. 77, p. 3113.

[27] Blair, J.A., Duffy, J.A., Phys. Chem. Glasses, 1995, vol. 36, p. 12.

[28] Duffy, J.A., Phys. Chem. Glasses, 1997, vol. 38, p. 289.

[29] Duffy, J.A., Grant, R.J., Phys. Chem. Glasses, 1975, vol. 16, p. 124.

[30] Kamitsos, E.I., Chryssikos, G.D., Patsis, A.P., Duffy, J.A., J. Non-Cryst. Solids, 1996, vol. 196, p. 249.

[31] Baucke, F.G.K., Duffy, J.A., Phys. Chem. Glasses, 1991, vol. 32, p. 211.

[32] Baucke, F.G.K., Duffy, J.A., Phys. Chem. Glasses, 1993, vol. 34, p. 158.

[33] Baucke, F.G.K., Duffy, J.A., Phys. Chem. Glasses, 1994, vol. 35, p. 17.

[34] Burkhard, D.J.M., Phys. Chem. Glasses, 1997, vol. 38, p. 317.

[35] Jeddeloh, G., Phys. Chem. Glasses, 1984, vol. 25, p. 163.

[36] Cable, M., Xiang, Z., Glastech. Ber., 1989, vol. 62, p. 382.

[37] Klonkowski, A., Phys. Chem. Glasses, 1983, vol. 24, p. 166.

[38] Klonkowski, A., J. Non-Cryst. Solids, 1987, vol. 95-96, p. 381.

[39] Klonkowski, A., Phys. Chem. Glasses, 1981, vol. 22, p. 163.

[40] Klein, R.M., Onorato, P.I.K., Phys. Chem. Glasses, 1980, vol. 21, p. 199.

[41] Dietzel, A.H., Phys. Chem. Glasses, 1983, vol. 24, p. 172.

[42] Greaves, G.N., Phil. Mag. B, 1989, vol. 60, p. 793.

[43] Schreiber, H.D., J. Non-Cryst. Solids, 1986, vol. 84, p. 129.

[44] Densem, N.E., Turner, W.E.S., J. Soc. Glass Tech., 1938, vol. 22, p. 372.

[45] Johnston, W.D., J. Amer. Ceram. Soc., 1964, vol. 47, p. 198.

[46] Goldman, D.S., Gupta, P.K., J. Amer. Ceram. Soc., 1983, vol. 66, p. 188.

[47] Schreiber, H.D., Kozak, S.J., Merkel, R.C., Balazs, G.B., Jones, P.W., J. Non-Cryst. Solids, 1986, vol. 84, p. 186.

[48] Gottardi, V., Paoletti, G., Tornati, M., Proc. VI Int. Congr. Glass, p. 412.

[49] Paul, A., Douglas, R.W., Phys. Chem. Glasses, 1965, vol. 6, p. 212.

[50] Goldman, D.S., J. Amer. Ceram. Soc., 1983, vol. 66, p. 205.

[51] Paul, A., J. Non-Cryst. Solids, 1990, vol. 123, p. 354.

[52] Kumar, A., Singh, S.P., Glastech. Ber., 1992, vol. 65, p. 69.

[53] Majumdar, R., Lahiri, D., J. Amer. Ceram. Soc., 1975, vol. 58, p. 99.

[54] Baak, T., Hornyak, E.J., J. Amer. Ceram. Soc., 1961, vol. 44, p. 541.

[55] Paul, A., Douglas, R.W., Phys. Chem. Glasses, 1965, vol. 6, p. 207.

[56] Hahn, B., Buhler, P., Weissmann, R., Fundamentals Glass Sci. Tech., Venice, 1993, p. 205.

[57] Douglas, R.W., Nath, P., Paul, A., Phys. Chem. Glasses, 1965, vol. 6, p. 216.

[58] Mysen, B.O., Virgo, D., Seifert, F.A., Amer. Mineral., 1984, vol. 69, p. 834.

[59] Mysen, B.O., Amer. Mineral., J. Non-Cryst. Solids, 1987, vol. 95-96, p. 247.

[60] Levy, R.A., Lupis, C.H.P., Flinn, P.A., Phys. Chem. Glasses, 1976, vol. 17, p. 94.

[61] Pyare, R., Nath, P., J. Non-Cryst. Solids, 1991, vol. 128, p. 154.

[62] Taragin, M.F., Eisenstein, J.C., J. Non-Cryst. Solids, 1970, vol. 3, p. 311.

[63] Labar, C., Gielen, P., J. Non-Cryst. Solids, 1973/74, vol. 13, p. 107.

[64] Williams, K.F.E., Johnson, C.E., Thomas, M.F., J. Non-Cryst. Solids, 1998, vol. 226, p. 19.

[65] Dunn, A.G., Beales, K.J., Newns, G.R., Wilson, J.L., Phys. Chem. Glasses, 1978, vol. 19, p. 1.

[66] Dyar, M.D., Amer. Mineral., 1985, vol. 70, p. 304.

[67] Weyl, W.A., Marboe, E.C., The Constitution of Glasses: A Dynamic Interpretation, Interscience Publishers, 1962, vol. 2, p. 669.

[68] Close, P., Shepherd, H.M., Drummond, C.H., J. Amer. Ceram. Soc., 1958, vol. 41, p. 455.

[69] Bamford, C.R., Hudson, E.J., Proc. 7th Int. Congr. Glass, Brussels, 1965, vol. 1, p. 1.

[70] Nelson, C., White, W.B., Phys. Chem. Glasses, 1993, vol. 34, p. 219.

[71] Burns, R.G., Mineralogical Applications of Crystal Field Theory, 2nd Ed., Cambridge Univ. Press, 1993.

Chapter 3.

Experimental

3.1 Glass Making

A full listing of the glasses investigated in this study can be found in appendix A, table A1.

3.1.1 Standard Composition

The ternary system SiO_2 - R_2O - R'O was used in this study. Iron was introduced as Fe_2O_3, with proportionate molar reductions of the other constituents to compensate. Glass compositions were calculated in molar percent, enabling atom for atom replacement of one component with another. The standard compositions melted were, in molar percent:

70	SiO_2
15	R_2O (R = Li_2O, Na_2O, K_2O, Rb_2O, Cs_2O)
15	R'O (R' = MgO, CaO, SrO, BaO)
0 - 5	Fe_2O_3

It was necessary to melt some glasses where the 15 % R_2O consisted of 7.5 % each of two alkali oxides. Most of the glasses containing 15 % Li_2O exhibited phase separation, rendering optical spectroscopy impossible. It was therefore necessary to make mixed-alkali samples containing 7.5 % each of Li_2O and Na_2O. Some samples containing a similar mixture of Na_2O and K_2O were also melted.

3.1.2. Other Compositions

Some melts had carbon added to the batch as a reducing agent. As a subset of the standard glasses, a few were made with a standard 0.2% Fe_2O_3 - CaO - Na_2O composition, but with 5 % of the SiO_2 being replaced with B_2O_3, GeO_2 or Al_2O_3. Another "non-standard" glass was melted in the B_2O_3 - SiO_2 - Na_2O - Fe_2O_3 system to allow comparison between borate and silicate glasses.

3.1.3 Batch

Only high purity raw materials were used in glassmaking, to avoid contamination by unwanted oxides and other contaminants such as sulphur. Appendix A, table A2 gives raw material assays where available. SiO_2 was provided by ultra-high purity Japanese quartz, and all R_2O and R'O was provided by high purity carbonates. Iron oxide was introduced as Fe_2O_3.

3.1.4 Melting

Glasses were melted in air in Pt-2%Rh crucibles at 1450°C in electric furnaces. This kept contamination of the glass by undesirable transition metals from the

crucible to a minimum, whilst providing the same melting temperature and atmosphere for every glass. Temperature and atmosphere have been shown to strongly affect redox of iron in glass (see chapter 2.2.), so these usually had to be kept constant. A few glasses were melted with different melting time, temperature or redox conditions to investigate their effects.

Batches were made to produce either 100 g or 300 g of glass. Expensive raw materials such as Rb_2CO_3 and Cs_2CO_3 necessitated smaller 100 g melts.

Batch was added stepwise to the crucible which was placed in the furnace, then 1 hour batch-free time was allowed. A motorised Pt-Rh stirrer was then lowered into the melt and switched on. The melt was stirred for 5 hours before the stirrer was switched off and removed. The glass was poured into preheated moulds. As the glass cooled it was removed from the moulds and placed in an annealing furnace at 550°C. The furnace was programmed to hold at this temperature for 1 hour then to cool by 1°C per minute to room temperature.

Investigation of the effects of melting time on homogeneity and redox necessitated changing the melting schedule. Where this was done, the melting schedule was essentially the same, with only time in furnace or stirring time being altered. Table 3.1.4.a categorizes the different melting schedules used.

Table 3.1.4.a. Melting Schedules Used

Melting Conditions	**Furnace Type**	**Temperature / °C**	**Melting Time/ hours**	**Stirred?**
"Standard"	Electric	1450	5	Yes
"Gas 1"	Gas	1450	5	No
"Gas 2"	Gas	1380	2	No

3.2. Density Measurement

The Archimedes method was used to calculate the densities of some samples. This involved weighing the sample in air and in distilled water of a known temperature, then performing the calculation shown in equation 3.2.

$$\delta_{TRUE} = \frac{W_A}{W_A - W_W} * \delta_W \qquad \text{(Equation 3.2.)}$$

where δ_{TRUE} = true density, W_A= weight in air, W_W = weight in water, δ_W = density of water at measured temperature.

3.3. X-Ray Diffraction (XRD)

XRD was carried out on powdered samples using CuKα radiation on a Philips goniometer. Scan rate was 2°2θ / minute. Step size was 0.2°. Samples were measured between 10° and 80°, 2θ.

3.4. Inductively-Coupled Plasma (ICP)

Measurement of chemical composition of samples was done using the Inductively Coupled Plasma (ICP) technique. An Applied Research Laboratories 3410 ICP was used. Samples in the form of aqueous solutions were introduced as aerosols into the flame of a high temperature (10,000 K) Ar plasma flame. The technique is suitable to ppm levels.

3.5. Redox Measurements

Redox was measured by three different techniques: wet chemical, Mössbauer spectroscopy and optical absorption spectroscopy. The wet chemical method is detailed in chapter 3.5.1. The methods of measuring redox by Mössbauer spectroscopy and by optical absorption spectroscopy are discussed in chapters 6 and 4.3.8., respectively.

3.5.1. Wet Chemical Redox Measurements

These measurements were made using two methods, one for glasses with < 2 molar % Fe_2O_3 and one for glasses with ≥ 2 molar % Fe_2O_3. Errors associated with the technique for low iron contents were very low, ± 1 % of ΣFe. For high iron contents, errors were ± 2 % of ΣFe. Special thanks go to the staff at Pilkington who carried out these procedures.

For < 2 molar % Fe_2O_3, the method used was similar to that of Close et al [1]. The glass was decomposed using HF in a Pt beaker under an oxygen-free atmosphere of CO_2 and the Fe^{2+} was determined colorimetrically using o-phenanthroline.

Glasses with > 2 molar % Fe_2O_3 were analysed titrimetrically. Again the glass was decomposed in HF in a CO_2 atmosphere. The solution was extracted into a polythene beaker and neutralised with boric acid. It was then titrated with potassium dichromate with ferroin as an indicator.

The procedure used was as follows:

i) 20ml of distilled H_2O, 2.5ml of o-phenanthroline solution (1% w/v), 8.0ml of HF (40% w/w), and 2.0ml of H_2SO_4 (1:2 v/v) were added to a Pt crucible.

ii) A lid was placed over the crucible and CO_2 bubbled through the solution at a steady rate.

iii) The crucible was heated slowly on a sand bath until the solution was just boiling; then cooled by standing the crucible in cold water.

iv) Approx. 0.5g of finely ground sample was weighed onto a watch glass and transferred to the Pt crucible

v) The lid was replaced and the crucible heated on the sand bath to boiling over a period of 20 mins. The solution was swirled occasionally.

vi) The crucible was cooled in cold water. The contents were transferred to a polythene beaker with the aid of a fine jet of distilled water, and 8g of boric acid (1g per ml of HF used) was added. This was stirred and allowed to stand for 5 mins.

vii) Ammonia solution was added until the pH = 3.2, then the solution was transferred to a 100ml flask, made up to volume and mixed thoroughly.

viii) The solution was filtered through a dry medium filter paper into a cell, and the absorbance vs. a distilled water blank was measured at 510nm.

The nominal total Fe content was known from batch calculations, and ICP analysis showed losses during melting were minimal. Thus Fe^{2+}/Fe^{3+} and $Fe^{2+}/\Sigma Fe$ could be calculated using nominal ΣFe values. Errors associated with this technique are thought to be very low. These have been estimated at ± 1 % for $Fe^{2+}/\Sigma Fe$.

3.6. Optical Absorption Spectroscopy

3.6.1. Sample Preparation

The cast glass was cut to size using a diamond cutting wheel, then ground to the required dimensions on a grinding wheel. A cerium rouge impregnated wheel was

used to chemically polish the sample. Samples were typically 2 cm * 2cm, with thickness varying between 0.2 and 4 mm depending on iron content.

3.6.2. Measurement of Optical Absorption Spectra

Optical spectra were measured and recorded using a Hitachi U-3501 Spectrometer connected to a PC. The spectrometer was a dual-beam instrument which was used to take measurements between 4,545 - 33,900 cm^{-1} (2,200 - 295 nm). An integrating sphere was placed in the spectrometer during the measurement of spectra. This greatly reduced the effects of "wedging" of the sample, i.e. deviation from constant thickness, and imperfections with polishing quality. Data points were taken every 1 nm between 295 and 2,200 nm. Some spectra were also recorded using other spectrometers. A Unicam UV/Vis spectrometer and a Perkin-Elmer Spectrum 2000 FT-IR spectrometer were used to record low-temperature spectra described in chapter 4.3.4.2.

3.6.3. Normalisation of Optical Absorption Spectra

In order to compare spectra from different samples, normalization was carried out. To quote Bamford [2], "The measurement of spectral transmission is normally made on an homogenous glass sample of defined thickness, having plane, polished and parallel surfaces, with the spectral radiation incident to the glass surface.....factors producing attenuation are: the reflection at the glass-air interface; the optical absorption of the body of the glass". All spectra were first corrected for reflection losses. The reflection coefficient (R) is related to the refractive index (N) of the glass as shown in equation 3.6.3.a.

$$R = \left[\frac{N-1}{N+1}\right]^2 \qquad \text{(Equation 3.6.3.a.)}$$

The refractive index of glass is an important spectral property; R at each surface measures thus:

for N = 1.5, R = 0.040 or 4.0 %

for N = 1.7, R = 0.067 or 6.7 %

for N = 1.9, R = 0.096 or 9.6 %

Thus the reflection losses must be subtracted first from any spectral transmission data. Spectral absorption is the difference between the energy incident on the glass and that transmitted or reflected. Correcting for reflection gives the Lambert-Beer Law shown in equation 3.6.3.b.

$$I = I_0 \exp(-\alpha c l) \qquad \text{(Equation 3.6.3.b.)}$$

where I = transmitted intensity, I_0 = incident intensity, α = absorption coefficient, c = concentration of absorbing species (units often g mole / litre), and l = path length. Rearranging equation 3.6.3.b., we have equation 3.6.3.c.

$$A = \log(I/I_0) = -\alpha c l \qquad \text{(Equation 3.6.3.c.)}$$

To convert transmission spectra into absorption spectra, the $\log_{10}$ of the corrected transmission data gives A.

3.7. Photoluminescence (PL) Spectroscopy

3.7.1. PL Sample Preparation

This technique does not require that samples have a particular geometry, so it was usually sufficient to use any piece of glass of approximately the same dimensions as the optical samples.

3.7.2. Measurement of PL Spectra

Spectra were measured from 20,000 – 12,500 cm^{-1} with a Thorn EMI extended-S20 photomultiplier tube and from 16,600 – 8,300 cm^{-1} with a liquid N_2-cooled North Coast EO-817-L germanium detector. Spectra were recorded at 293 K. The measurement parameters such as laser power, time constants, settle time and data averaging time were set to give optimal noise reduction whilst recording spectra in an acceptable time period.

A ¼-m Jarrell-Ash monochromator blazed at 25,000 cm^{-1} was used with the Extended-S20 photomultiplier. For the EO-817-L Ge detector both the Jarrell-Ash and a Bentham M300 monochromator blazed at 10,000 cm^{-1} were used.

A Brookdeal precision lock-in amplifier and an Acorn Archimedes microcomputer were used for data capture. Excitation was provided by the 20,986 cm^{-1} (476.5 nm) line of a Lexel model 95(4) Ar-ion laser. A Gould type 3405 oscilloscope was used to monitor signal strength and phase. Entrance and exit slits on the monochromators were set at 2000 μm. Data points were measured every 2 nm or 5 nm.

3.7.3. Normalization of PL Spectra

The response of the system, i.e. filter, monochromator and detector, changed with wavelength. Correction was carried out by measuring the luminescence of a light source with known spectral characteristics. A tungsten filament bulb at known temperature has a luminescence spectrum close to that of an ideal black body. An accurate luminescence spectrum of a tungsten bulb can therefore be generated by applying an emissivity correction, E(λ), to the radiancy of a black body, B(λ). This is generated using Planck's radiation law shown in equation 3.7.3.a.

$$B(\lambda)d\lambda = \frac{2\pi hc^2}{\lambda^5(e^{hc/\lambda kT} - 1)}d\lambda \quad \text{(Equation 3.7.3.a.)}$$

where c is the velocity of light, h is Planck's constant, λ is the wavelength of light, k is Boltzmann's constant and T is the temperature of the black body. Thus the spectral radiance of a tungsten bulb, W(λ) can be calculated using equation 3.7.3.b.

$$W(\lambda) = E(\lambda).B(\lambda) \qquad \text{(Equation 3.7.3.b)}$$

The measured spectrum of the tungsten bulb at a known temperature, MW(λ), is equal to the actual spectrum of the bulb multiplied by the spectral response, R(λ), of the system. We can therefore write equation 3.7.3.c.

$$MW(\lambda) = R(\lambda).E(\lambda).B(\lambda) \qquad \text{(Equation 3.7.3.c)}$$

Bulb temperature was measured using an optical pyrometer. Error was estimated at ± 40 K. Emissivity data for tungsten was given in 200 K intervals rendering this error small, since emissivity varied little over 200 K intervals.

3.8. Electron Spin Resonance (ESR) Spectroscopy

3.8.1. ESR Sample Preparation

A few grams of powdered sample were required by this technique. Samples were prepared in the same manner as for Mössbauer spectroscopy, but without the need for grinding to a fine powder with pestle and mortar. The main priority was that samples fit the sample tube, diameter ~3 mm. The crushing equipment was cleaned after crushing each sample to avoid cross-contamination.

3.8.2. Measurement of ESR Spectra

Spectra were measured using two different Varian spectrometers. One was connected to a BBC "B" Microcomputer for data capture. The second spectrometer allowed data capture onto a chart recorder. Spectral normalisation was unnecessary because for the samples measured in this study, all comparisons were in terms of parameters which were unaffected by sample size, i.e. intensity ratios and linewidths.

3.9. Mössbauer Spectroscopy

3.9.1. Mössbauer Sample Preparation

This technique required only small amounts (100 mg) of sample in powdered form. The average particle size was not critical as long as the larger particles were removed. A small lump of sample was cut from the annealed blocks, put in a percussion mortar and crushed into powder. The powder was then finely ground with a pestle and mortar and sieved to 100 mesh. The percussion mortar and

mortar and pestle were cleaned thoroughly after each sample to avoid contamination. The sample holder was comprised of two plastic discs, known to be iron-free, between which a small amount of sample, approximately 100mg, was sandwiched. The discs were then fastened together and placed in the spectrometer for measurement. It was not necessary to weigh out exactly equal amounts of different samples: this would have no useful purpose because volume and concentration correction was not carried out.

3.9.2. Measurement of Mössbauer Spectra

A schematic of the spectrometer used is shown in figure 3.9.2.a. Due to financial and time restrictions, it was only possible to measure two samples at 7 K, so only samples which were expected to show the greatest effects were measured. Most spectra were measured at ambient temperature, 293 K. Spectra for the 3 % Fe_2O_3 sample were measured at a range of temperatures between 293 K and 7 K to allow calculation of the Debye temperature. A 25 mCi ^{57}Co source embedded in Rh or Pd was used. A correction of 0.053 mm/s had to be added to δ measured using the Pd matrix source, to allow direct comparison with those measured with the Rh matrix source. Spectra were recorded on a 512-channel recorder, and quoted centre shift values are relative to α-Fe. Velocity ranges of $\pm$ 4, $\pm$ 5 or $\pm$ 12 mm/s were used. The wider velocity ranges were used for the lower iron contents, and the necessity of this are explained in chapter 6.2.3. Depending on the Fe_2O_3 content, spectra usually took between 2 days and 2 weeks to collect. Once an acceptable spectrum had been recorded, it was fitted using a computer program developed in-house named MOSS. This program fitted Lorentzian lines to the spectra.

Figure 3.9.2.a. Mössbauer Spectrometer Schematic

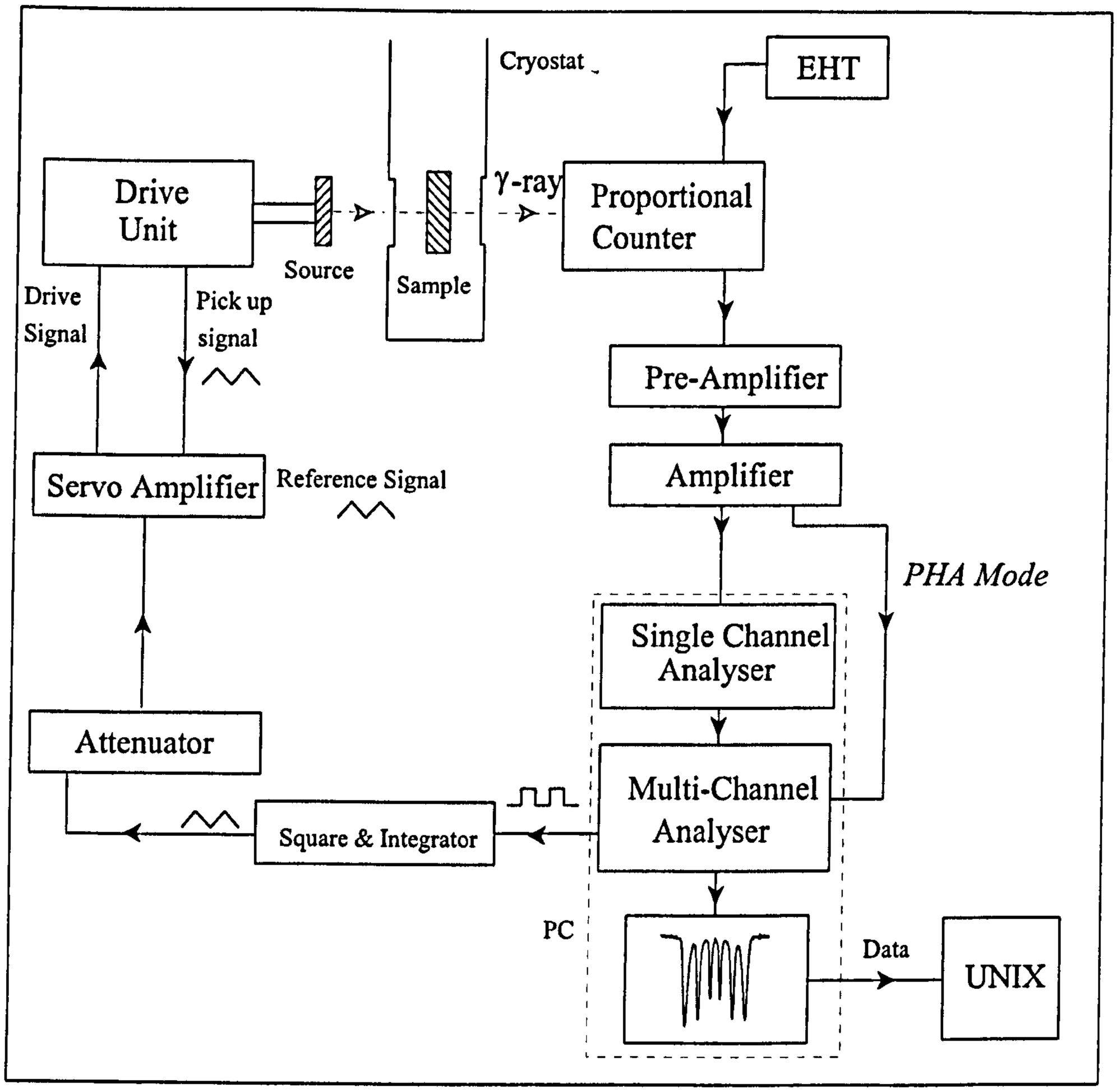

3.10. References

[1] Close, P., Shepherd, H.M., J. Amer. Ceram. Soc., 1958, vol. 41, p. 455.

[2] Bamford, C.R., Colour Generation and Control in Glass, Elsevier, New York, 1977.

Chapter 4

Optical Spectroscopy

4.1. Background & Literature Survey

Coloured glass has been widely studied for many years. Weyl's book "Coloured Glasses" [1] is a comprehensive investigation and discussion of the nature of colouring in glasses which covers the state of the art through the 1950's. The book discusses the structure of glass and its effects on colour as they were then understood. For example, absorptions due to Fe^{2+} and Fe^{3+} ions were known to occur in the red visible and near-IR for Fe^{2+} and the UV and blue visible for Fe^{3+}. They have the effect of colouring glass green or blue, depending upon the redox equilibrium. It was recognised that Fe^{3+} exists in both 4- and 6- coordinated sites. The iron concentration itself was known to affect colour and redox, whilst the composition of a glass affects most optical properties.

This early work brought together many areas of glass research and formed what has become possibly the most widely known and comprehensive work on the colour of glasses. Some ideas it discusses have since been modified or replaced. The majority, however, are as useful to the glass technologist now as when the book was written, and the reader is referred to it regarding many aspects of this thesis.

The advent of ligand field theory [2 – 4] in the late 1950's and early 1960's allowed better understanding and interpretation of the optical spectra of ionic

colourants. The absorption of transition metals in glass is nowadays generally studied on the basis of ligand field theory.

4.1.1. Electronic Transitions in Transition Metal (TM) Complexes

The intensities of electronic transitions of transition metal (TM) ions in the solid state are influenced by several factors. Physical conditions such as temperature and pressure can have strong effects, but these parameters are approximately constant for most applications. The main factors concerned with iron in glass are discussed in this chapter.

4.1.1.1. Spin Selection Rules

Electronic transitions can generally be separated into two main groups:

1. Transitions occurring within one ion.
2. Transitions involving more than one ion.

Within each of these groups exist the following two subsets:

a) Intrashell transitions. These include *d-d* type transitions.

b) Intershell transitions, involving electron transfer between orbital types, e.g. *s-p* type transitions.

Optical absorption by TM ions is usually due to intrashell transitions within one ion (i.e. categories 1-a above), although intershell transitions do also occur. The

intensities of the intrashell transitions are governed by the probabilities of transitions between split 3*d* orbital energy levels. A series of selection rules in turn govern the probabilities of the transitions.

4.1.1.2. Laporte Selection Rule

All electronic *d-d* transitions are forbidden by the Laporte rule, since ground and excited states have the same number of *d*-electrons, but some transitions are forbidden more strongly than others. The rule is relaxed somewhat if there is no centre of symmetry to the TM ion coordination polyhedron. If an Fe ion is octahedrally coordinated with the surrounding oxygen anions then there is a centre of symmetry and the Laporte rule applies strongly, weakening the absorption. If, however, the Fe ion is tetrahedrally coordinated then the lack of a centre of symmetry relaxes the Laporte rule and the absorption is stronger. The Laporte rule is relaxed further for a tetrahedral site, where some mixing of *d* and *p* orbitals can occur. The result of this is that absorptions from tetrahedral sites are 10-100 times more intense than from octahedral sites. For basaltic glasses containing iron, the absorption due to tetrahedral Fe^{2+} ions and occurring at ~5,000 cm^{-1}, is comparable in strength with the absorption at ~10,000 cm^{-1} due to octahedral Fe^{2+} ions, with only 1 % of the Fe^{2+} ions in tetrahedral sites and the other 99 % in octahedral sites [5].

4.1.1.3. Spin Multiplicity Selection Rule

This rule states that the total number of unpaired electrons on an ion must remain unchanged during an electronic transition. Spin-allowed transitions are, similarly to Laporte-allowed transitions, approximately 10 - 100 times stronger than spin-forbidden transitions. An example of a spin-allowed transition is the $^5T_2(D) \rightarrow$

$^5E(D)$ transition for Fe^{2+} ions in octahedral sites, which occurs at ~10,000 cm^{-1} in many crystalline and amorphous solids (notation is discussed in chapter 4.1.3.3.). Fe^{2+} is a $3d^6$ ion and always has four unpaired electrons in the $3d$ shell when the transition $^5T_2(D) \rightarrow {}^5E(D)$ occurs. All transitions involving Fe^{3+}, a $3d^5$ ion, are spin-forbidden. Each of the five orbitals is occupied by one electron, so any transition must change the number of unpaired electrons. Spin-forbidden transitions of Fe^{2+} are possible, and involve different orbital energy levels.

4.1.1.4. Spin Coupling Interactions

If Fe ions occupy next-nearest neighbour sites to one another, intensities of spin-forbidden transitions may be enhanced. This is caused by magnetic coupling of electron spins, and has been observed in Fe^{3+}- bearing structures [5]. Selection rules for Fe^{3+}-Fe^{3+} coupled ions are different than for isolated ions. It is also possible to have additional transitions from simultaneous excitations within both the interacting Fe^{3+} ions. For example an absorption occurs in yellow sapphire at 18,690 cm^{-1} which is due to the simultaneous excitation $^6A_1(S) + {}^6A_1(S) \rightarrow {}^4T_1(G) + {}^4T_1(G)$ involving two Fe^{3+} in adjacent octahedra [5]. Spectral enhancement can also be caused by mixed valence Fe^{2+}-Fe^{3+} transitions, and these are discussed in chapter 4.1.1.5.

4.1.1.5. Charge-Transfer Transitions

There are two charge-transfer mechanisms, each producing different effects:

a) Oxygen - Metal Charge Transfer (OMCT)

Absorption of photons of light may result from the transfer of an electron from oxygen ligands to a $3d$ orbital of the TM ion, or vice versa. The distances

involved in this transfer are relatively large, so the dipole moment is large. The transition itself is also Laporte-allowed. The spectra arising from OMCT transitions are generally 100 - 1000 times stronger than *d-d* transitions. These transitions usually occur in the UV region. For some species such as Fe^{3+} the tails of these OMCT bands reach into the visible and can obscure some of the absorptions associated with *d-d* transitions.

b) Inter-Valence Charge Transfer (IVCT)

Electron exchange can occur between ions of the same element with differing redox states, e.g. Fe^{2+} and Fe^{3+}. If the coordination polyhedra are edge-sharing, IVCT takes place. Strong coupling between Fe^{2+} and Fe^{3+} ions removes the symmetry of 3*d* orbitals at the Fe^{2+} site, making Fe^{2+} *d-d* transitions Laporte-allowed and enhancing the intensity of absorption [5]. The absorptive effects of Fe^{2+}-Fe^{3+} IVCT bands have been documented for minerals, for which they can occur in the visible region. IVCT bands have been found at 11,000 - 18,000 cm^{-1} in silicate minerals [4], and near 14,500 cm^{-1} in lead silicate glasses [6].

4.1.1.6. Widths of Absorption Bands.

Surrounding anions strongly affect *d-d* transitions of TM ions. Changes affecting the anions affect the energy separations in the TM ion, and hence widths of absorption bands. Energy level diagrams of the type used by Tanabe & Sugano [2, 3], help to explain peak widths. The more strongly a transition is affected by ligand field, the broader the absorption band. Metal – ligand distances vary about a mean position due to vibrational modes caused by thermal energy, thus the parameter *Dq* (see chapter 4.1.3.1.) also varies about a mean energy corresponding to the mean separation. These vibrational modes can be reduced by decreasing the temperature. Lattice disorder and Stokes shift (see chapter 4.1.4.3.) effects also cause broadening of absorption bands in glasses.

4.1.1.7. The Jahn-Teller Effect

The Jahn-Teller effect causes broadening and asymmetry of absorption bands, due to distortions of coordination polyhedra from regular symmetry. Jahn and Teller [7] proved that if the orbitals in the ground state of a molecule are degenerate (i.e. have the same energy), the molecule distorts spontaneously to a lower symmetry to remove the degeneracy and make one energy level more stable. Degenerate electron distributions exist in high-spin $3d^6$ complexes (Fe^{2+}), suggesting that Jahn-Teller distortions may occur. Van Vleck [8] showed, however, that these Jahn-Teller distortions are small when there is degeneracy in the t_{2g} ground state orbital group, as in the case of Fe^{2+}. In regular octahedral environments provided by MgO or aqueous solutions, cations such as Ti^{3+} ($3d^1$), V^{3+} ($3d^2$), and Fe^{2+} ($3d^6$) experience ground state splittings of the order of 10 - 100 cm^{-1}.

The Jahn-Teller theorem also predicts the splitting of energy levels whilst cations are in their excited states following absorption of a photon. During the short lifetime of the transition the upper energy levels are split. This phenomenon is known as the *dynamic* Jahn-Teller effect. A dual transition to the resolved energy levels of the E_g excited state can lead to asymmetry and broadening of spectra, especially for ions such as Fe^{2+} and Ti^{3+}. An example of the *dynamic* Jahn-Teller effect occurs in the spectrum of $[Fe(H_2O)]^{2+}$ ions in crystal or solution, where the main spin-allowed band due to the $^5T_2(D) \rightarrow {}^5E(D)$ transition occurs at ~10,400 cm^{-1}. The peak is broad and exhibits two maxima with a separation of ~2,000 cm^{-1} [9]. The ground state splitting is less than 1,000 cm^{-1}, indicating that the asymmetry observed in iron-containing minerals and glasses is probably due to the *dynamic* Jahn-Teller effect and not the static Jahn-Teller effect [9]. Ookawa et al [6] attributed a peak at approximately 7,500 cm^{-1} in lead silicate glasses to dynamic Jahn-Teller splitting of the main octahedral Fe^{2+} peak near 10,000 cm^{-1}.

4.1.2. Optical Spectra

Optical spectra are comprised of the ultra-violet (UV), visible (Vis) and infra-red (IR) regions of the electromagnetic spectrum. Many glasses show a transmission "window" starting in the UV and reaching through the visible into the IR. The extent of the transmission range is determined by the glass composition, and to a lesser extent by the glass production route.

4.1.2.1. Ultra-Violet (UV)

For solar control applications, the UV transmission must be decreased to acceptable limits to protect eyes and polymeric upholstery. Ultraviolet absorption in silicate glasses arises from three principal sources:

1) Intrinsic electronic excitations of the Si-O network.
2) The introduction of network modifying and / or network forming cations.
3) The presence of impurities, particularly TM ions.

As the cation field strength of the glass-forming oxide increases, the UV edge moves to greater wavenumbers such that $P_2O_5 > SiO_2 > B_2O_3 > HPO_3^- > GeO_2$ [10]. The UV transmission of SiO_2 and B_2O_3 glass is diminished by the addition of metal oxides [11]. The rapid onset of absorption in the UV is caused by the transition of an electron from a bound state with an oxygen ion to an excited state [12]. The absorption edge is less sharp than it might be, due to the nature and structure of glasses. In pure SiO_2 and B_2O_3 glasses the UV absorption is caused by bridging oxygens, i.e. O^{2-} anions which connect Si^{4+} cations. The addition of other oxides moves the absorption to lower wavenumbers [13]. The UV edge in $2SiO_2.Na_2O$ glass occurs at ~33,300 cm^{-1}, whereas in fused SiO_2 it occurs at

~58,800 cm^{-1}. The absorption becomes a function of non-bridging oxygen ions. These are O^{2-} ions which coordinate the modifier cations, breaking up the continuous network. Increasing the size of alkali or alkaline earth modifier ions shifts the UV edge of silicate glasses to lower wavenumbers [14].

The presence of iron, even at parts-per-million (ppm) levels, has a dramatic effect upon the UV absorption edge of glass, which shifts to lower wavenumbers with increasing iron content [6, 15 - 19]. In silicate glasses, the UV edge obeys Urbach's rule [20] over the range 27,000 – 32,000 cm^{-1} [21]. Urbach's rule can be expressed in such a way as shown in equation 4.1.2.1.a.

$$A = e^{(a + b/\lambda)} \qquad \text{(Equation 4.1.2.1.a.)}$$

Where A = absorbance, a and b are constants, and λ = wavelength. Both Fe^{2+} and Fe^{3+} ions contribute to the UV absorption [15, 21]. In oxidised silicate glasses, Fe^{3+} gives the largest contribution due to a strong band centred at 43,500 cm^{-1}. The Fe^{2+} contribution is somewhat weaker and its maximum lies at greater wavenumbers than Fe^{3+}, ~50,000 cm^{-1} [15, 21]. UV charge-transfer absorptions due to Fe in glass are typically 10-100 times stronger than the absorptions caused by *d-d* transitions. They are of the type OMCT (Oxygen-Metal Charge-Transfer) discussed in chapter 4.1.1.5.

4.1.2.2. Visible

In glasses containing iron, visible absorptions tend to be caused by *d-d* transitions, however these transitions can also occur in the UV and near-IR regions. The exact characteristics of Fe ion absorptions are affected by glass composition and melting conditions, and these are discussed in more detail in chapter 4.1.4.

Other factors such as the crucible type can also affect the colour of glass: ionic

platinum and rhodium give rise to optical absorptions, which can cause the glass to appear faintly yellow in colour [13, 22 - 24]. The absorptions are generally weak, although high lead or barium contents may enhance their strength [22]. For Pt^{4+} ions in glass, absorptions were found at ~22,000 cm^{-1} (very weak spin-forbidden) and ~27,500 cm^{-1} (stronger spin-allowed) [23]. Rh^{3+} ions caused absorptions at ~22,500 cm^{-1} and ~28,000 cm^{-1} [24].

4.1.2.3. Near Infra-Red (NIR)

The near-IR or NIR region encompasses the range of wavenumbers from ~13,000 to ~4,000 cm^{-1}. The two main absorptions attributed to Fe^{2+} ions in glass occur in the NIR region [6, 19, 21, 25 - 32]. Vibrational absorptions generally occur below 4,000 cm^{-1} in silicate glasses. Groups of –OH molecules produce very strong absorptions in this region, and transmission generally falls to zero between 3,000 cm^{-1} and 2,000 cm^{-1}. Many borate glasses show an affinity for atmospheric water, and react readily with it. Hence -OH absorptions in the NIR are stronger in borate glasses than silicate glasses [33]. This may also be partially due to generally lower melting temperatures for borate glasses.

4.1.3. Application of Ligand Field Theory to Fe^{2+} and Fe^{3+} Ions in Glass

The chemical properties of the transition metals are more complex than those of other elements in the periodic table due to electrons being located in incompletely-filled 3*d* orbitals having different energy levels. Interactions with radiation in or near the visible region of the electromagnetic spectrum causes electrons to be excited between split 3*d* orbital energy levels, hence absorption bands. The origin of the splitting of these 3*d* orbital energy levels can be described by three models: molecular orbital theory, crystal field theory and

ligand field theory.

Molecular orbital theory concentrates on exchange interactions and orbital overlap between the central ion and the surrounding ligands. Crystal field theory treats the interactions between the central ion and its ligands as purely electrostatic in nature with the ligands as point negative charges. Ligand field theory closely resembles crystal field theory, but introduces the empirical Racah B and C parameters to account for covalent bonding interactions.

Mineralogically it is generally considered that silicates are ionic in nature, and thus crystal field theory has often been used to describe transition metals in silicate minerals. Ligand field theory has been more commonly used when discussing transition metals in glasses since the composition, distortion and relative randomness of the structure introduce some covalent character to bonding of TM ions therein.

In the early use of valence bond theory in the form developed by Pauling [34], complexes in which the electronic configuration of the TM ion was the same as in the free gaseous ion were labelled *ionic complexes*. Compounds in which the electrons were paired as far as possible were termed *covalent complexes.* These terminologies are equivalent to spin states in ligand field theory:

High spin ≡ Ionic ≡ Weak Field

Low Spin ≡ Covalent ≡ Strong Field

Ligand field theory has been used extensively over the years to explain and predict optical absorption properties of TM – containing compounds [2 – 5]. It should be stressed that ligand field theory is an approximation and cannot predict and explain every aspect of TM complex chemistry with complete accuracy.

A brief mention should be made of molecular orbital (MO) theory, which can be used as an alternative method of spectral interpretation. The theory rests on the basic assumption that if two nuclei are at equilibrium distance and electrons are

added, they will go into molecular orbitals, which are in many ways analogous to atomic orbitals. This approach is somewhat more complicated than ligand field theory.

4.1.3.1. Electronic Spectra and *Dq*

When the five-fold degeneracy of a 3*d* orbital is removed by the presence of a ligand field, the energy gap between the lower and upper split levels (the t_{2g} and e_g orbitals) is called 10*Dq* or Δ, as shown schematically in figure 4.1.3.1.a. The parameter 10*Dq* or Δ is known as the *ligand field strength*. The value of *Dq* is affected by coordination, and it occurs that *Dq* for a tetrahedral site ≈ 4/9 *Dq* for an octahedral site.

An octahedral field splits the 3*d* orbitals of TM ions in such a way as to produce the lower-level group of three t_{2g} orbitals and a higher-level group of two e_g orbitals, as in figure 4.1.3.1.a. The separation between the two electronic states, t_{2g} and e_g, increases with increasing ligand field strength. A tetrahedral site experiences the reverse situation. The lobes of the e_g orbitals now lie between the ligands; those of the t_{2g} ligands, whilst not pointing directly towards the ligands, lie closer to them. Hence the t_{2g} orbitals are destabilised with respect to the e_g orbitals.

The magnitude of *Dq* can often be measured by analysing the wavenumbers of *d-d* absorption bands. The energy used to excite a 3*d* electron from one orbital to another orbital with higher energy often corresponds to wavenumbers in the visible and NIR. This is a very important parameter and can give information on the environment and bonding of TM ions.

Figure 4.1.3.1.a. Energy Levels of the d-orbitals in Octahedral and Tetrahedral Fields

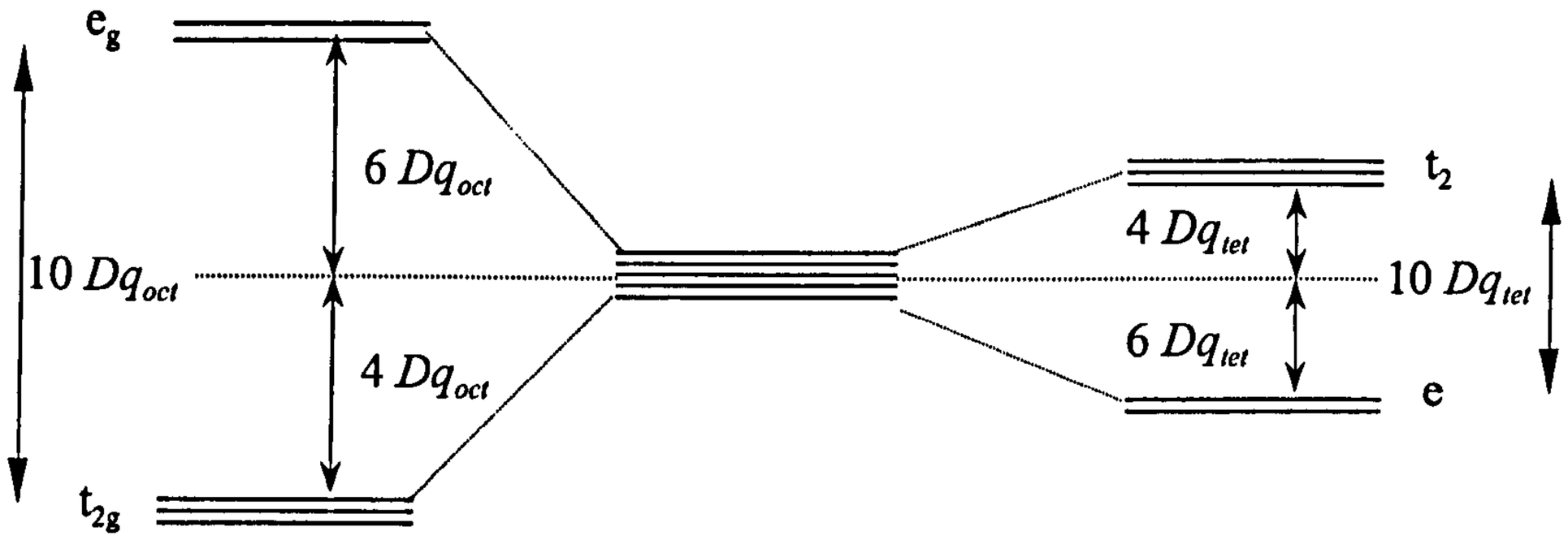

4.1.3.2. Factors Affecting *Dq*

The parameter *Dq* is affected by several factors: type of cation, type of ligand, interatomic distance, pressure, temperature, and symmetry of the ligand environment.

1) Cation and Anion Effects

The greater the charge on the metal ion, the greater is *Dq*. Increasing charge should cause the ligands to be attracted more strongly to the metal ion, thus interacting more strongly with its *d*-orbitals. Generally *Dq* is higher for trivalent ions than divalent ions: *Dq* for Fe^{2+} and Fe^{3+} ions in aqueous solutions are 1,040 cm^{-1} and 1,370 cm^{-1} respectively [5]. The *spectrochemical series* highlights the effects of ligands on *Dq*:

$$I^- < Br^- < Cl^- < OH^- < CO_3^{2-} < O^{2-} < H_2O < NH_3 < SO_3^{2-} < NO_2^- < S^{2-} < CN^-$$

Transition metal ions with $3d^4$ - $3d^7$ configurations, which include Fe^{2+} and Fe^{3+} ions, coordinated with ligands at the left of this series usually have high-spin configurations. Low-spin configurations tend to exist with anions on the right of the series. Iron is usually present in its high-spin form in oxide minerals and glasses. The effects of changing anion on iron absorption in glass is highlighted by the differences between spectra of Fe^{2+} in fluoride glasses [35] and oxide glasses [19].

2) Metal-Oxygen (M-O) Interatomic Distance

An inverse fifth-power relationship exists between *Dq* and the M-O distance, so *Dq* is greatly affected by relatively small variations in the M-O distance. The M-O distance is strongly dependent upon both the coordination of the cation and the glass matrix. Modern techniques such as X-ray absorption spectroscopy, EXAFS and neutron diffraction have been used to estimate the Fe-O distance in various silicate glasses [32, 36 - 42). As expected from packing restrictions, the Fe-O distance is greater with Fe in octahedral sites than in tetrahedral sites. Measured Fe^{3+}-O distances [37, 42] show that in silicate glasses, Fe^{3+} ions exist mainly in tetrahedral sites and the Fe^{3+}-O distance is approximately 1.89 Å. The octahedral Fe^{3+}-O distance is approximately 2.18 Å. Values falling between these two distances can be explained by the presence of some octahedrally coordinated Fe^{2+} ions, and / or by the presence of both tetrahedral and octahedral Fe^{3+} ions.

3) Temperature

The temperature variation of *Dq* can be expressed as:

$$\frac{10Dq_T}{10Dq_{T_0}} = \left(\frac{V_0}{V_T}\right)^{5/3} \qquad \text{(Equation 4.1.3.2.a.)}$$

where Dq_0, Dq_T, V_0 and V_T are ligand field splittings and molar volumes at room temperature (0) and elevated temperatures (T). Generally $V_T > V_0$ so that increasing

the temperature causes a decrease in *Dq*.

4) Symmetry of the Ligand Environment

The symmetry of the ligands surrounding a transition metal ion strongly affects *Dq*. For example, according to the simple electrostatic model, the ideal value of *Dq* for a tetrahedral site = 4/9 *Dq* for an octahedral site. These splittings can be further modified by distortion of the coordination site.

4.1.3.3. Spectroscopic Notation and the Racah Parameters

A brief discussion of spectroscopic notation is necessary to explain the meanings of the nomenclature. Transition metal ions with between two and eight 3*d* electrons have their energies characterised by quantised values of L and S, the total orbital angular momentum and total spin momentum, respectively. This type of coupling is known as L-S or Russell-Saunders, and only breaks down when spin-orbit coupling becomes large.

Each state is identified by the spectroscopic term: $^{2S+1}L_J$, where 2S+1 is the spin multiplicity (number of unpaired electrons in the configuration, plus one), L is the orbital angular momentum such that:

S	P	D	F	G	H	I .....
L =	0	1	2	3	4	5	6 .....

and the subscript J denotes total angular momentum. A $3d^1$ ion such as Ti^{3+} has one such term, ^2D, but $3d^5$ and $3d^6$ ions such as Fe^{3+} and Fe^{2+} have 16 terms each, so the full energy level diagrams for Fe^{2+} and Fe^{3+} are complicated. The ground states for the ligated ions in high-spin octahedral symmetries are denoted by

$^5T_2(D)$ and $^6A_1(S)$ for Fe^{2+} and Fe^{3+} ions respectively. The bracketed letter is the spectroscopic term.

Energy separations between spectroscopic terms can be expressed by the Racah B and C parameters. These are semi-empirical parameters reflecting the covalency of bonding. It is common for C/B ≈ 4, but by no means the rule. The value of B increases with both oxidation state and number of 3*d* electrons. High valences and large numbers of electrons influence cation sizes such that ionic radii decrease with increasing oxidation state and fuller 3*d* orbitals. The Racah B and C parameters are often known for free ions, but B always has a lower value in inorganic solids than the free-ion state. This implies that when a transition metal ion is bonded to ligands in a coordination site, the mean radial displacement of 3*d* electrons increases and the effective charge experienced by the electrons decreases. Deviations in B and C from free ion values can therefore indicate the covalency of bonding.

Evaluation of Racah B and C is particularly easy for $3d^5$ ions (Fe^{3+}), irrespective of coordination. There are two energy levels which are virtually unaffected by ligand field, so the energy separations from the ground state are approximately constant:

$$^6A_1(S) \rightarrow {}^4A_1,{}^4E(G) = 10B + 5C$$

$$^6A_1(S) \rightarrow {}^4E(D) = 17B + 5C$$

4.1.3.4. Energy Level Diagrams

The relative energies of the ligand field states can be illustrated on an energy level diagram, sometimes called a Tanabe-Sugano diagram. This plots the energy levels based on the Racah B and C parameters alone against the strength of the ligand field. The parameter *Dq* for Fe^{2+} ions in octahedral sites, $Dq(Fe^{2+}_{oct})$, can be easily

evaluated by measuring the position of the only spin-allowed transition, $^5T_2(D) \rightarrow {}^5E(D)$. This usually occurs near 10,000 cm^{-1} in silicates. Hence Dq for Fe^{2+} in tetrahedral sites, $Dq(Fe^{2+}_{tet})$, can be estimated by applying the rule $Dq_{tetrahedral} = 4/9 * Dq_{octahedral}$, giving an expected wavenumber of ~ 4,500 cm^{-1}.

For Fe^{3+}, the configuration is $3d^5$ and the same Tanabe-Sugano diagram applies irrespective of coordination since the energy levels are the same for both octahedral and tetrahedral coordinations.

Tanabe-Sugano diagrams best highlight the relationship between Dq and the wavenumbers at which transitions occur. As discussed in chapter 4.1.3.1., the ligand field strength $10Dq = \Delta$, hence Dq is one-tenth of the ligand field strength. Figure 4.1.3.4.a. shows a Tanabe-Sugano diagram for Fe^{2+} ($3d^6$). A change in spin-state for an atom in its ground state occurs at the critical ligand field value of $Dq/B = 2$. Below this value, Fe^{2+} ions exist in the high-spin state. For silicate glasses only the high-spin case is relevant. The exact predicted transition wavenumbers depend on Dq/B.

For Fe^{3+} ions some transitions are independent of ligand field, and appear as horizontal lines on the diagram. Other transitions are strongly affected by ligand field. Figure 4.1.3.4.b. illustrates the manifestation of particular transitions in optical spectra of Fe^{3+} ions in yellow sapphire, from [5].

Figure 4.1.3.4.a. Tanabe-Sugano Diagram for Fe^{2+} in Octahedral Coordination, from Burns [5]

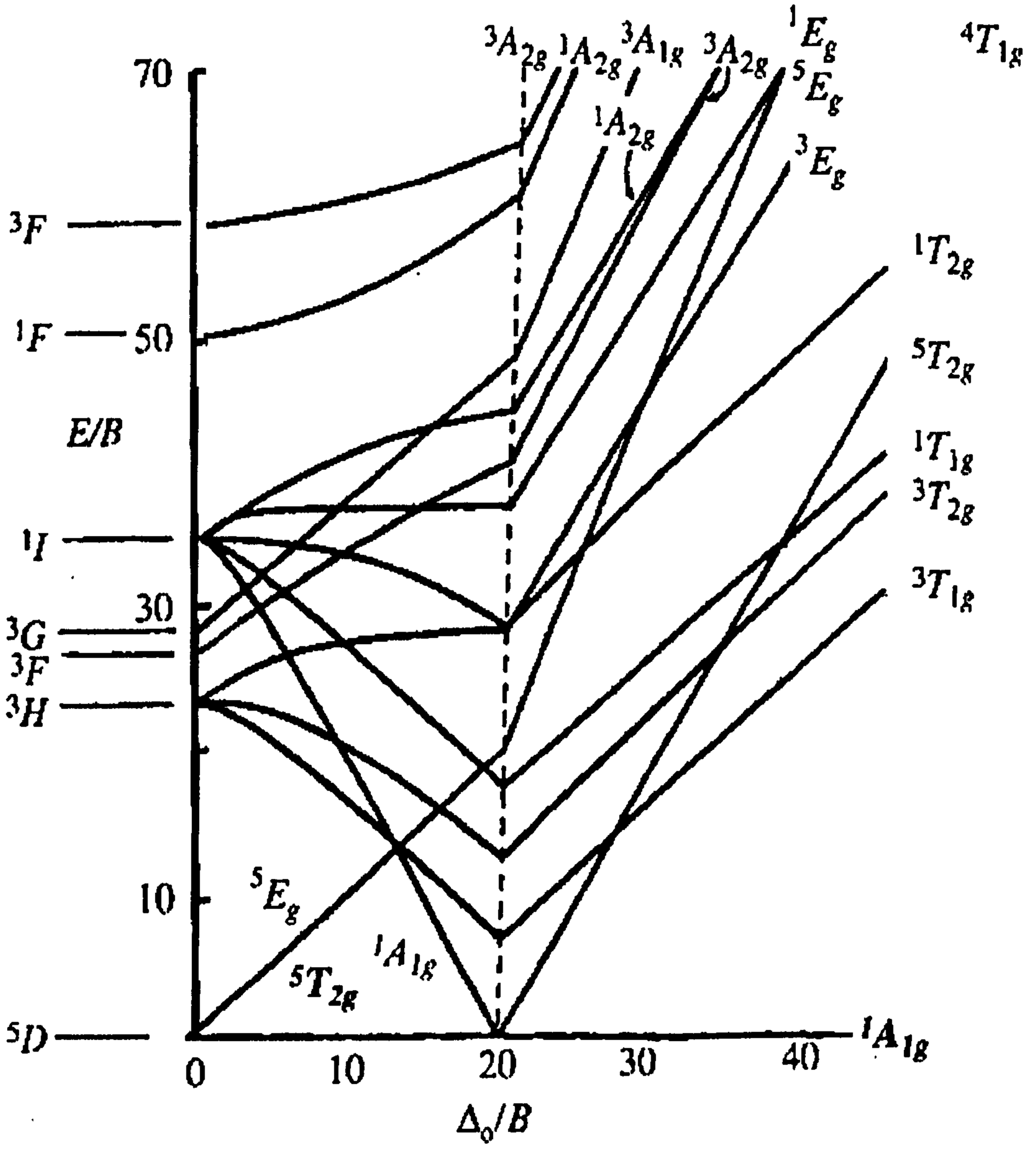

Figure 4.1.3.4.b. Tanabe-Sugano Diagram for Fe^{3+} and Corresponding Absorptions in Yellow Sapphire, from Burns [5].

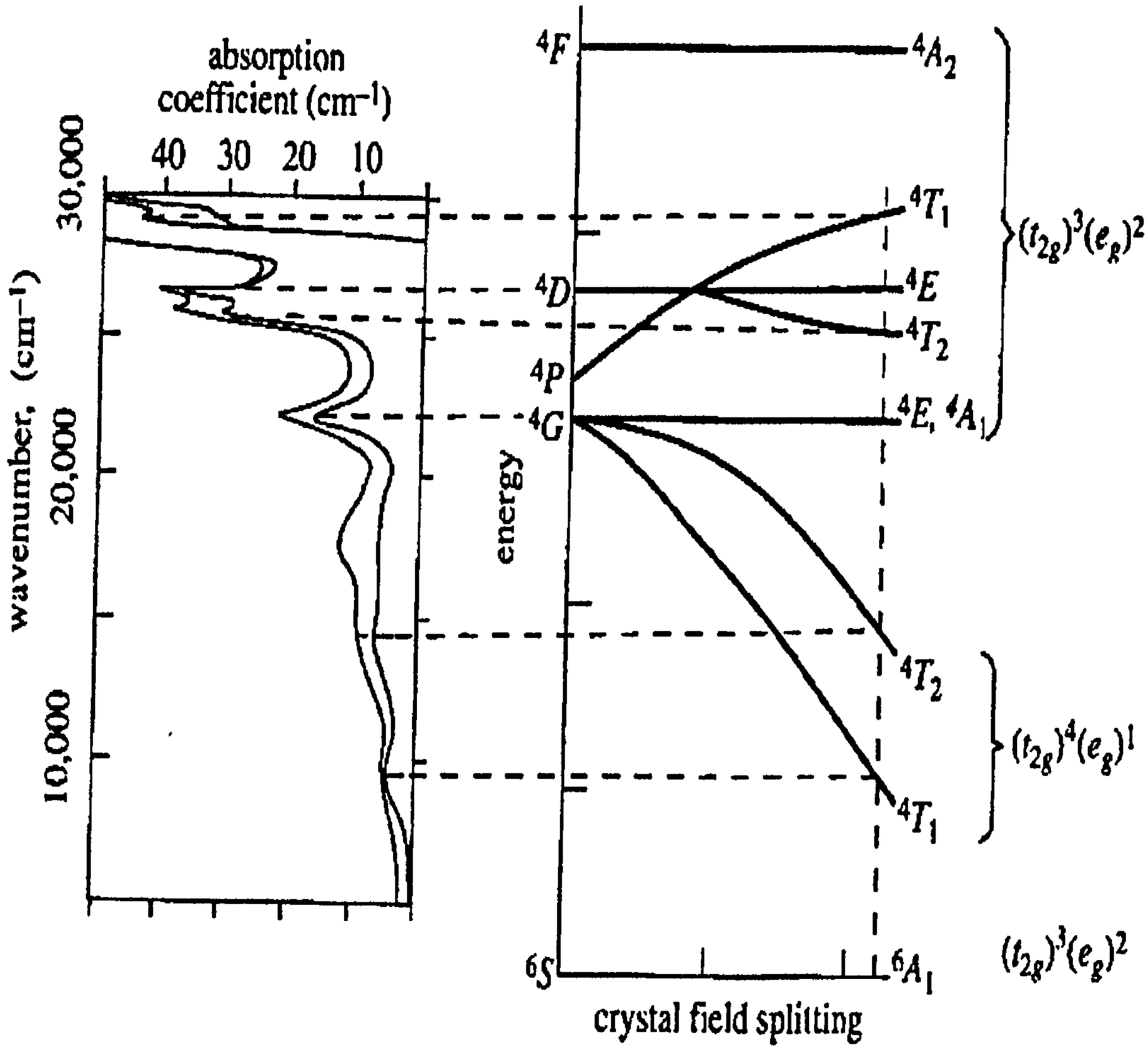

4.1.4. Optical Spectroscopy of Iron in Glass

Optical absorption spectroscopy has been extensively used for the investigation of Fe in glasses and minerals. In this way a large amount of data on *Dq*, Racah parameters, coordination and environment has been acquired. Using Tanabe-Sugano matrices it is possible to predict the wavenumbers at which absorption bands occur. It is also possible to obtain estimates of the values of *Dq* and the Racah B and C parameters in different glasses by observing the absorption bands.

4.1.4.1. Fe^{2+} *d-d* Absorptions

Only one spin-allowed transition is expected for Fe^{2+}, corresponding to the $^5T_2(D) \rightarrow {}^5E(D)$ transition for octahedral sites and $^5E(D) \rightarrow {}^5T_2(D)$ for tetrahedral sites. These are expected to occur at ~10,000 cm^{-1} and ~4,500 cm^{-1}, respectively [19, 25, 28]. The octahedral band at ~10,000 cm^{-1} is particularly wide and asymmetric. This is mainly due to the range of distortions of the octahedral Fe^{2+} sites. The asymmetry may be caused by the dynamic Jahn-Teller effect (see chapter 4.1.1.7.). Mathematical fitting and observation of spectra has revealed the presence of just such a band [6, 19, 27, 29]. Other transitions predicted for Fe^{2+} should occur in the blue visible and near-UV. Transitions include $^5T_2(D) \rightarrow {}^3T_1(H)$ and $^5T_{2g} \rightarrow {}^3T_2(H)$, which occur at ~20,000 cm^{-1} and ~22,200 cm^{-1} in $Fe^{2+}(H_2O)_6$ [5]. These and other spin-forbidden Fe^{2+} transitions have generally been ignored in glass research since they are expected to be very weak. The predominance of Fe^{3+} ions in oxidised glasses also means that the stronger Fe^{3+} absorptions in this region obscure the spin-forbidden Fe^{2+} bands. Two absorptions due to Fe^{2+} were found in a silicate glass at 23,250 cm^{-1} and 25,000 cm^{-1} [43].

Racah parameters for Fe^{2+} ions in glasses have not been widely discussed or investigated. The free-ion values B = 917 cm^{-1} and C = 4040 cm^{-1} have been used by some workers, but in complexes B and C are decreased from their free-ion values due to partially covalent bonding [4, 5]. It is likely that $B < 900$ in silicate glasses.

The Fe^{2+} ion has an ionic radius of 74 pm. Geometrical constraints suggest it will occur in octahedral sites in glasses [44]. There is strong evidence from a number of different techniques, however, that tetrahedral Fe^{2+} ions do exist in many systems [6, 17, 19, 29 – 32, 36, 41, 45 - 49]. The ratio of tetrahedral Fe^{2+} to octahedral Fe^{2+} in silicate glasses is generally small. X-ray absorption work on silicate glasses showed about 15 % of the Fe^{2+} ions to be in tetrahedral sites with the remainder in octahedral sites [36]. Optical spectroscopy of various silicate glasses indicated that less than 5 % of Fe^{2+} ions were tetrahedrally coordinated

[29, 30, 45]. Tetrahedrally coordinated ions absorb 10 - 100 times more strongly than octahedrally coordinated ions, hence the number of Fe^{2+} ions causing the absorption at ~4,500 cm^{-1} is likely to be small. There has been much debate over the origin of this band. Many workers [6, 17, 19, 31, 45, 29, 30, 32] have attributed it to the $^5E(D) \rightarrow {}^5T_2(D)$ transition of Fe^{2+} ions in distorted tetrahedral sites. Irradiation with x-rays led to a similar conclusion [47]. The possibility of this band being caused by a site distortion of octahedral sites has also been discussed [25, 27, 28, 50].

4.1.4.2. Fe^{3+} *d-d* Absorptions

Fe^{3+} is a $3d^5$ ion, and direct evaluation of *Dq* from the absorption spectrum is not easy because all transitions are spin-forbidden (see chapter 4.1.1.3.). There is, however, much information on Fe^{3+} parameters in the literature, some of which are reproduced in table 4.1.4.2.a. Free-ion values are B = 1015 cm^{-1}, C = 4800 cm^{-1}.

There has been much debate regarding the coordination of Fe^{3+} ions in glass. Most of those who have studied this with optical techniques agree that both octahedral and tetrahedral Fe^{3+} ions can occur in silicate glasses, with the majority being tetrahedral [18, 19, 21, 25, 26, 31, 51 - 56] although some EXAFS work has suggested that Fe^{3+} ions are largely octahedrally coordinated in sodium silicate glasses [38, 39].

Data in table 4.1.4.2.a. represents a wide range of Fe^{3+} environments. Data for glasses which are close in composition to those studied in this work [4, 19, 51, 56, 58, 61] suggest the approximate values shown after table 4.1.4.2.a.

Table 4.1.4.2.a. Fe^{3+} Parameters from Literature

Reference	Coordination	*Dq* / cm^{-1}	Racah B / cm^{-1}	Racah C / cm^{-1}
[57]	-	1600	-	-
[9]	OCT	1400	-	-
	TET	620	-	-
[58]	-	1230	720	-
[59]	-	1400	540	3410
	-	1532	590	3490
	-	1541	560	3510
	-	1595	610	3470
[60]	-	1151	788	2907
[56]	OCT	1278	730	-
	TET	568	730	-
[51]	OCT	1400	600	3300
	TET	900	520	3570
[19]	OCT	1370	-	-
	TET	672	-	-
[5]	Various	1000-1500	500-700	-
[61]	OCT	1050	715	2262
	TET	660	867	2023
[4]	OCT	1230	720	-
	TET	550	720	-

Literature on specifically silicate glasses suggests the following range of values:

$$Dq_{\text{octahedral}} \approx 1{,}200 - 1{,}400\ \text{cm}^{-1}$$

$$Dq_{\text{tetrahedral}} \approx 500 - 900\ \text{cm}^{-1}$$

$$\text{Racah B} \approx 500 - 700\ \text{cm}^{-1}$$

$$\text{Racah C} \approx 3500\ \text{cm}^{-1}$$

Interpretation of the $3d^5$ (Fe^{3+}) energy level diagram is strongly dependent upon the values of Dq and B. Hannoyer et al [51], in a detailed study of Fe^{3+} ions in soda-lime-silica glass, gave the interpretation shown in table 4.1.4.2.b.

Table 4.1.4.2.b. Fe^{3+} Transitions in Soda-Lime-Silica Glass from [51]

Transitions	**Tetrahedral / cm^{-1}**	**Octahedral / cm^{-1}**
$^6A_1(S) \rightarrow {}^4T_1(G)$	16,800	11,200
$^6A_1(S) \rightarrow {}^4T_2(G)$	20,500	15,600
$^6A_1(S) \rightarrow {}^4E_1, {}^4A_1(G)$	23,000	22,500
$^6A_1(S) \rightarrow {}^4T_2(D)$	24,200	24,300
$^6A_1(S) \rightarrow {}^4E(D)$	26,600	26,600
Optical Parameters		
Dq / cm^{-1}	900	1,400
B / cm^{-1}	520	600
C / cm^{-1}	3,570	3,300

Bands such as those for the lowest energy Fe^{3+} transition, $^6A_1(S) \rightarrow {}^4T_1(G)$ are usually not directly observed by absorption spectroscopy because they are obscured by stronger Fe^{2+} bands. So how do we know a) that they exist, and b) in which part of the spectrum they occur? The answer is in two parts. Firstly, the bands have been observed in many materials, for example in several polymorphs of Fe_2O_3 and FeOOH [59], and these band positions fit very well with those in table 4.1.4.2.b. Secondly, some bands can be observed with luminescence spectroscopy, and this is discussed further in chapter 4.1.4.3.

4.1.4.3. Luminescence of Fe^{3+} Ions

The energy of an electronically excited state may be dissipated in a number of ways. Non-radiative decay is a common loss mechanism, where the excess energy is transferred into thermal energy (phonons) affecting the vibration, rotation and translation of surrounding atoms or ions. Radiative decay (luminescence or fluorescence) occurs when the energy loss is achieved by emission of a photon of light, which happens when the energy difference between the excited and ground states is too great to achieve relaxation by phonons alone. Luminescence occurs at lower wavenumbers than absorption because the radiation is emitted after some vibrational energy has been lost to the surrounding molecules. This effect is called the *Stokes shift*. Luminescence spectroscopy is particularly useful for studying absorptions which cannot easily be measured with absorption spectroscopy.

The main expected luminescence from Fe^{3+} ions is due to the transition from the first excited state to the ground state, $^4T_1(G) \rightarrow {}^6A_1(S)$. Luminescence of Fe^{3+} has been investigated in various crystalline inorganic hosts: $LiAl_5O_8$ [62, 63], $LiGa_5O_8$ [63], α-Ga_2O_3 [62], $NaAlO_2$ [62], γ-Al_2O_3 [62], γ-AlF_3 [64] and zeolites [62]. In these crystalline hosts, the $^4T_1(G) \rightarrow {}^6A_1(S)$ transition of tetrahedral Fe^{3+} ions produces luminescence in the red part of the visible spectrum (13,000 – 15,500 cm^{-1}). The $^4T_1(G) \rightarrow {}^6A_1(S)$ transition of octahedral Fe^{3+} ions is expected to produce

luminescence at lower wavenumbers (11,000 – 12,000 cm^{-1}).

Luminescence of Fe^{3+} ions in various oxide glasses has been investigated by researchers at Pennsylvania State University: sodium and calcium phosphates [65], sodium silicates [25], lithium silicates [66] and sodium and potassium aluminosilicates [55]. Another research group has investigated borosilicates [67]. The lowest excited states of Fe^{3+} in oxide glasses were found to occur at 14,000 - 16,000 cm^{-1} for tetrahedral Fe^{3+}[25, 54, 55, 65 - 67] and at ~11,500 cm^{-1} for octahedral Fe^{3+} [25, 65].

The effects of glass composition on the environment of Fe^{3+} ions can be analysed by changes in luminescence band wavenumbers. Comparison of band positions from the literature suggested that for tetrahedral Fe^{3+} ions, $Dq_{tet} \approx 800$ cm^{-1}, and for octahedral Fe^{3+} ions, $Dq_{oct} \approx 1250$ cm^{-1}. The luminescence band was shifted to greater wavenumbers by increasing the size of the alkali ion, from 14,000 cm^{-1} in lithium silicates [66] to 14,600 cm^{-1} in sodium silicates [25], and from 14,500 cm^{-1} in sodium aluminosilicates [55] to 14,900 cm^{-1} in potassium aluminosilicates [55]. Stokes shifts of 1400 - 1700 cm^{-1} were attributed to these luminescences [25, 55, 65]. Since the $^4T_1(G)$ level has a strong negative slope on the $3d^5$ Tanabe-Sugano diagram, the wavenumbers of absorption and emission decreased with increasing ligand field strength, Dq. It can therefore be inferred that increasing the size of the alkali ion lowers the ligand field strength of the Fe^{3+} coordination complex.

Platinum in lead silicate glasses exhibits luminescence [68]. At ambient temperatures the luminescence spectrum was approximately flat from 16,700 – 13,300 cm^{-1}. This fact coupled with the weakness of the luminescence suggests that the presence of Pt complexes in iron-containing glass would not appreciably affect the Fe^{3+} luminescence spectra.

It is assumed that all the luminescence data in the literature was corrected for the response of the systems used to measure the spectra.

4.1.4.4. Charge-Transfer Absorptions and the Effects of Iron Concentration

The UV absorption edge is influenced by both glass composition and iron content. OMCT bands discussed in chapter 4.1.1.5. occur at approximately 43,500 cm^{-1} and 50,000 cm^{-1} for Fe^{3+} and Fe^{2+} ions, respectively [19, 21, 52]. The extinction coefficient is greater for the Fe^{3+}-O interaction than Fe^{2+}-O interaction [21], therefore a shift in redox toward the reduced state decreases UV absorption and shifts the UV edge to higher wavenumbers. The UV edge exhibits an exponential relationship [6, 19, 21, 52], and the strength of OMCT bands increase more rapidly than d-d transitions as the iron content increases. For this reason the UV edge occurs at lower wavenumbers with increasing iron content [6, 16 - 19]. Figures 4.3.3.a. and 4.3.3.b. show typical spectra of glasses containing increasing amounts of Fe, illustrating the characteristics discussed above.

Increasing the iron content of glass also leads to intervalence charge-transfer bands (see chapter 4.1.1.5.) and possibly spin-coupling bands (see chapter 4.1.1.4.). The presence of IVCT bands has been suggested in iron-containing glasses [31], and has been observed by computer fitting of spectra of iron lead silicate glasses [6]. Spin-coupling bands have been demonstrated in minerals (see chapter 4.1.1.4.). Both IVCT bands and spin-coupling bands have been found at visible wavenumbers [5, 6].

Increasing iron content naturally leads to stronger absorption. When Beers' Law applies, the absorbance of *d-d* bands increases linearly with increasing iron content. The exponential relationship which explains the behaviour of the UV edge means that as iron content increases, the UV edge moves to lower wavenumbers, obscuring some weaker *d-d* transitions. This effect may be compounded by the appearance of bands due to IVCT and / or spin coupling in the visible.

4.1.4.5. Coordination and Redox

Intensive work on iron in glasses comprising a wide range of compositions, redox ratios and iron contents, has shown that in general a mixture of Fe^{2+} and Fe^{3+} ions are present in 4-coordinated tetrahedral network-forming (nwf) sites and 6-coordinated octahedral network-modifying (nwm) sites [10, 18, 19, 25, 26, 28, 32, 36 - 39, 41, 45, 51, 52, 56]. For silicate glasses, the vast majority of Fe^{2+} ions occupy octahedral sites, whilst there is a mixture of both tetrahedral and octahedral Fe^{3+} ions.

The possibility of 5-coordinated Fe ions in glass was briefly discussed in chapter 2.3.

The effects of redox have been discussed in detail in chapter 2.2. Optical spectra can be strongly affected by redox, since Fe^{2+} and Fe^{3+} exhibit different absorption characteristics (see chapters 4.1.3. and 4.1.4.). To the human eye, an oxidised iron-containing glass appears green, whereas a more reduced sample appears more blue. This is because the reduced sample absorbs more red light than the oxidised sample due to the stronger Fe^{2+} band in the near-IR.

4.1.4.6. Extinction Coefficients

The extinction coefficient, ε, also known as the absorption coefficient α, remains constant for a given system in the concentration range in which Beer's law applies. Extinction coefficients of Fe^{2+} and Fe^{3+} in glass are affected by changes in coordination: a change in the proportion of tetrahedral and octahedral site occupancies causes a change in extinction coefficient. Values of $\varepsilon(Fe^{3+}) = 4.1$ l mol^{-1} cm^{-1} at 26,300 cm^{-1} and $\varepsilon(Fe^{2+}) = 31.7$ l mol^{-1} cm^{-1} at 9090 cm^{-1} were found in SiO_2-Na_2O-CaO glasses [69]. In calcium aluminoborosilicate glasses, $\varepsilon(Fe^{2+}) = 17.7$ l mol^{-1} cm^{-1} at 9435 cm^{-1} [70]. The differences are attributable to differences between glass matrices. Extinction coefficients shown in table 4.1.4.6.a. were

calculated for eight gaussian bands fitted to the spectrum of a SiO_2 – Na_2O – CaO glass containing < 0.8 weight % Fe_2O_3 [71].

Table 4.1.4.6.a. Extinction Coefficients of Computer Fitted Absorptions from [71]

Wavenumber / cm^{-1}	Extinction Coefficient / $lmol^{-1}cm^{-1}$
26,315	4.86
24,390	2.56
22,420	0.98
20,000	1.39
17,545	0.75
13,605	4.93
9,435	53.85
5,000	12.90

It has been suggested that the breakdown of the selection rule which gives rise to the high values of $\varepsilon(Fe^{2+})$ relative to crystalline compounds [4], may arise for structural reasons which cause static distortion of the octahedral environment [72].

Duran et al [73] found a linear decrease in $\varepsilon(Cu^{2+})$ with increasing ionic radius of alkali ion in 30 R_2O-70 SiO_2 glasses. Although the alkali ions incorporated in the glass break up Si-O-Si bonds, the distortion produced in the network depends upon the size and polarising power of the cation, say the authors. The smaller the alkali ion, the more easily it is accommodated in the network and the smaller the distortion of the network. On the other hand, a cation with a high field strength will exert an ordering effect over neighbouring oxygens and it is therefore possible to predict that, for a constant alkali content the distortion increases with increasing field strength and decreasing polarisability of the alkali cation. In terms

of $\varepsilon(Cu^{2+})$, an increase in its value implies a greater order and stability of the network [73].

4.1.4.7. Effects of Composition

The interconnection of properties of iron in glass is highly intricate and thus cannot be explored fully by the scope of this work. For example, coordination and redox of Fe have been shown to be affected by one another in several silicate glasses [74, 75]. Similarly, Fe-O distances are interwoven with coordination, glass composition and redox. These phenomena, amongst several others, present difficulties with data interpretation. So many variables exist that when a single variable is studied, it may emerge that several other variables come into play. For example, replacement of MgO by CaO in a simple glass may seem like a small change; however this will affect redox, coordination, environment, extinction coefficients, etc. Each of these variables may in turn affect others, and so on.

4.1.4.8. Effects of Different Glass Formers

Many of the effects due to different network-forming ions on optical spectra of transition metals in glass have been covered by Fanderlik [10], and the reader is referred to that work for further details. Within oxide systems, Fe has been widely studied in silicate, borate and phosphate glasses. Several differences exist between these systems. For example Fe^{2+} ions absorb much more strongly in silicate glasses than in borate glasses and the Fe^{2+} absorption found near 10,000 cm^{-1} in silicate glass occurred at higher wavenumbers in a borate glass [21]. The UV edge was much stronger in the borate glass, and obscured the Fe^{3+} *d-d* transitions found in silicate glasses at >20,000 cm^{-1}. It was suggested that colloidal dispersions may be partly responsible for this. Differences in optical parameters of particularly Fe^{3+}

ions in different glass systems are evident from the literature [60, 18, 45, 26, 27, 21, 19, 57]. Comparison of band fitting work in silicate [19] and phosphate [60] systems shows many differences. The UV edge occurs at higher wavenumbers in the phosphate systems, and absorption bands due to Fe^{3+} occur at higher wavenumbers. For example, the $^6A_{1g} \rightarrow {}^4E_g$ transition, which is unaffected by ligand field, occurs at 28,500 cm^{-1} in phosphate glasses [60], but at 26,300 cm^{-1} in silicate glasses [19]. Other transitions of Fe^{3+} are similarly affected. Similar differences in band positions were found for Cu^{2+} ions in silicate, borate and germanate glasses [76].

It is well documented that Fe^{2+} and Fe^{3+} occur in octahedral sites in phosphate glasses [18, 27, 60, 77], so spectral differences from silicates can be expected. Redox changes brought about by differences in composition also affect optical spectra. Iron in silicate glasses occurs in both redox states, with a typical Fe^{2+} content being 20% of the total Fe in float glass.

4.1.4.9. Effects of Different Glass Modifiers on Spectra

The position of the absorption band near 10,000 cm^{-1} due to octahedral Fe^{2+} ions in silicate glasses is strongly affected by composition [25 - 27, 78, 79]. Other transition metal ions show similar behaviour [10, 76, 80, 81]. These changes in band position indicate changes in the values of *Dq*, B and C.

The position of the main Fe^{2+} absorption in alkaline earth phosphate glasses occurred at ~9,000 cm^{-1} [27, 79]. The peak position moved to smaller wavenumbers in the series Mg < Ca < Ba [27, 79]. A linear relationship was established between cation field strength of the alkaline earth ion and Fe^{2+} band position in these glasses [27]. It was asserted that the modifier cation was expected to reduce the ligand field strength of the oxygen ligands and that this effect would be greatest for the cation with the greatest polarizing power, namely Mg^{2+}. Hence the band would move to lower wavenumbers as the cation field

strength of the alkaline earth decreased. In ternary alkali-alkaline earth silicate glasses, the opposite occurs: with increasing field strength of alkali and / or alkaline earth ion, the peak position of the peak near 10,000 cm^{-1} moved to higher wavenumbers [78]. Possible explanations explored by these workers for the movement of the band were changes in the number of non-bridging oxygens and medium-range order effects due to modifier cations. Non-bridging oxygens (nbo's) are bonded to one network-former and one network-modifier, hence they do not form bridges between glass-forming ions such as Si^{4+}.

The value of *Dq* increases linearly with the number of non-bridging oxygens (nbo's) in silicate glasses [54, 78]. In alkaline earth phosphate glasses, *Dq* increased linearly with alkaline earth ionic radius [54]. In both cases the largest values of *Dq* were found in glasses with the largest interstitial sites and the most open structure, as would be supplied by larger network-modifying ions or more nbo's. This agrees with work on phosphate glasses [27], but does not apply to silicate glasses [78], where increasing cation field strength of the modifier moves *Dq*(Fe^{2+}) to higher values. Similar findings have been reported for Cu^{2+} in silicate and germanate glasses [76].

In sodium silicate glasses, the peak wavenumber of the Fe^{2+} bands at ~4,500 cm^{-1} and ~10,000 cm^{-1} changed with increasing Na_2O content such that the former peak moved to lower wavenumbers whilst the latter increased in peak wavenumber [25]. Greater Si-O bond lengths occurred with increased Na_2O content. It was postulated that this caused the effective negative charge on oxygen ions to increase, hence the stronger ligand field experienced by Fe^{2+} ions. At low Na_2O contents, Fe^{2+} ions were said to occupy somewhat larger sites dictated by the size requirements of the Na^+ ion. As the glass becomes more depolymerised, increased flexibility of the non-bridging bonds permits Fe^{2+} to assume an octahedral coordination polyhedron appropriate to its ionic size. Thus *Dq* for Fe^{2+} in high-Na_2O glasses is very close to its value in crystalline Fe^{2+} compounds.

Shifts of absorption peaks were found for Cu^{2+} in alkali silicate glasses [73, 76]. An approximately linear relation was found between the ionic radius of the alkali cation and the peak frequency of the main Cu^{2+} absorption near 13,000 cm^{-1}, such

that increasing ionic size resulted in lower peak frequencies [76]. Similar results were found by Klonkowski [80] for Cu^{2+} in alkali aluminosilicate glasses. Mixed-alkali glasses showed deviations from linearity in terms of peak frequency. This was attributed to the alkali-oxygen bond being more ionic than expected. Alkali germanate glasses behaved similarly to alkali silicates [76], but different alkali ions in alkali borate glasses had no effect on Cu^{2+} peak position [73, 76]. It was suggested the discrepancy is caused by the fact that the addition of alkali ions to silicate and germanate glasses introduces non-bridging oxygens. These are subjected to the influence of alkali ions. There is a good chance that the Cu^{2+} ions are coordinated by such non-bridging oxygens, and the effects of a particular type of alkali will be evident. On the other hand, the addition of alkali ions to borate glasses causes changes in boron coordination from 3 to 4, and therefore does not necessarily introduce non-bridging oxygens. The bridging oxygens do not directly reflect the type of alkali ion, so the coordination of Cu^{2+} ions by these oxygens does not greatly affect spectral positions [76].

Combes et al [78] found that the peak frequency of the main Fe^{2+} absorption band near 10,000 cm^{-1} changed dramatically with composition in a number of silicate glasses. Decreasing SiO_2 content resulted in a large increase in peak frequency. A plot using cation field strength, Z/a^2, of the various cations showed an approximately linear relation between peak wavenumber and FS (alkali + alkaline earth) / FS (Si + Al). To quote their work, "More polymerised glasses, which contain more SiO_2, have a higher number of bridging oxygens. The oxygens as first neighbours to Fe^{2+} are mainly bridging oxygens. They carry a smaller effective charge, hence the ligand field experienced by Fe^{2+} is smaller and absorption moves to lower energies."

Variation of *Dq* and B with different glass compositions for various transition metal ions was discussed by Nelson and White [82]. It was found that in each case *Dq* and B were remarkably constant across the compositional range of sodium silicate glasses. This is somewhat at odds with the results of White & Knight [54]. The ligand field parameters illustrate two types of behaviour, say Nelson and White [82]. In the first case, the value of *Dq* is in the same range as in oxides and

hexaquo complexes. Since *Dq* varies with $(R_{M-O})^{-5}$, the small shifts observed indicate that the transition metal-oxygen distances are not very different from those expected from the ionic radii. On the other hand, Racah B is much smaller than the free ion value, indicating substantial covalent bonding. The second type of behaviour is exhibited by transition metal ions for which the *Dq* values are depressed from that of a hexaquo complex, but the Racah B value is closer to the free ion value. The interpretation of this pattern is that the transition metal ions are in an environment where the metal-oxygen distances are larger than those in the reference compounds, and there is little covalent interaction between the transition metal ion and the oxygen ligands.

4.2. Optical Techniques - Principles of Operation

4.2.1. Optical Absorption Spectroscopy

Optical absorption spectroscopy involves passing a beam of light through a flat, polished sample of glass. By comparing the transmitted light with the incident light (with use of a reference beam) over a specified wavelength range, the absorption characteristics of the glass can be measured. The strengths, positions and widths of these absorption bands can give important information on the environment, coordination and redox of the Fe ions in the glass.

4.2.2. Photoluminescence (PL) Spectroscopy

Photoluminescence spectroscopy measures emission of light (in this case Fe^{3+} ions in glass samples) following excitation by high-energy light of a very narrow energy range, provided by a laser. Relaxation of Fe^{3+} ions from an excited state to the ground state takes place by emission of phonons (heat) or photons. Phonons are emitted as relaxation occurs in the upper excited states, but the energy gap between the lowest excited state of Fe^{3+} and the ground state is too great to permit relaxation by phonon emission. Instead, photons of light are emitted. In this study

the transition being stimulated occurs in the visible region, and thus the glass glows faintly red when excited. By measuring the amount of light emitted by the sample over a range of energies, information could be gained which optical absorption spectroscopy could not provide. The transition being excited was a weak spin-forbidden transition due to Fe^{3+}. It occurs in absorption in a region where it is totally obscured by the tail of the much stronger Fe^{2+} absorption in the near-IR region. Luminescence spectroscopy has thus provided information on the bonding and environment of the Fe^{3+} ions associated with this emission.

4.3. Results

4.3.1. Iron-Free Glass

Figure 4.3.1.a. shows the optical spectra of the nominally iron-free glasses melted in Pt-2% crucibles. The absorption band centred at ~27,800 cm^{-1} was present in all four of these glasses (samples 1 – 4). This band was most intense in sample 4, which contains BaO as the alkaline earth oxide. This glass was tinged a straw yellow colour.

Three glasses of the type SiO_2-BaO-R_2O (samples 5-7) were melted in mullite crucibles. Figure 4.3.1.b. shows their optical spectra. These melts were not stirred, and the resulting glasses contained a little inhomogeneity.

The slight change in measured absorption at ~12,000 cm^{-1} was due to a lamp or grating change in the spectrometer, but the change in measured absorption was negligible.

Figure 4.3.1.a. Optical Spectra of SiO_2-Na_2O-RO Base Glasses (Samples 1 - 4)

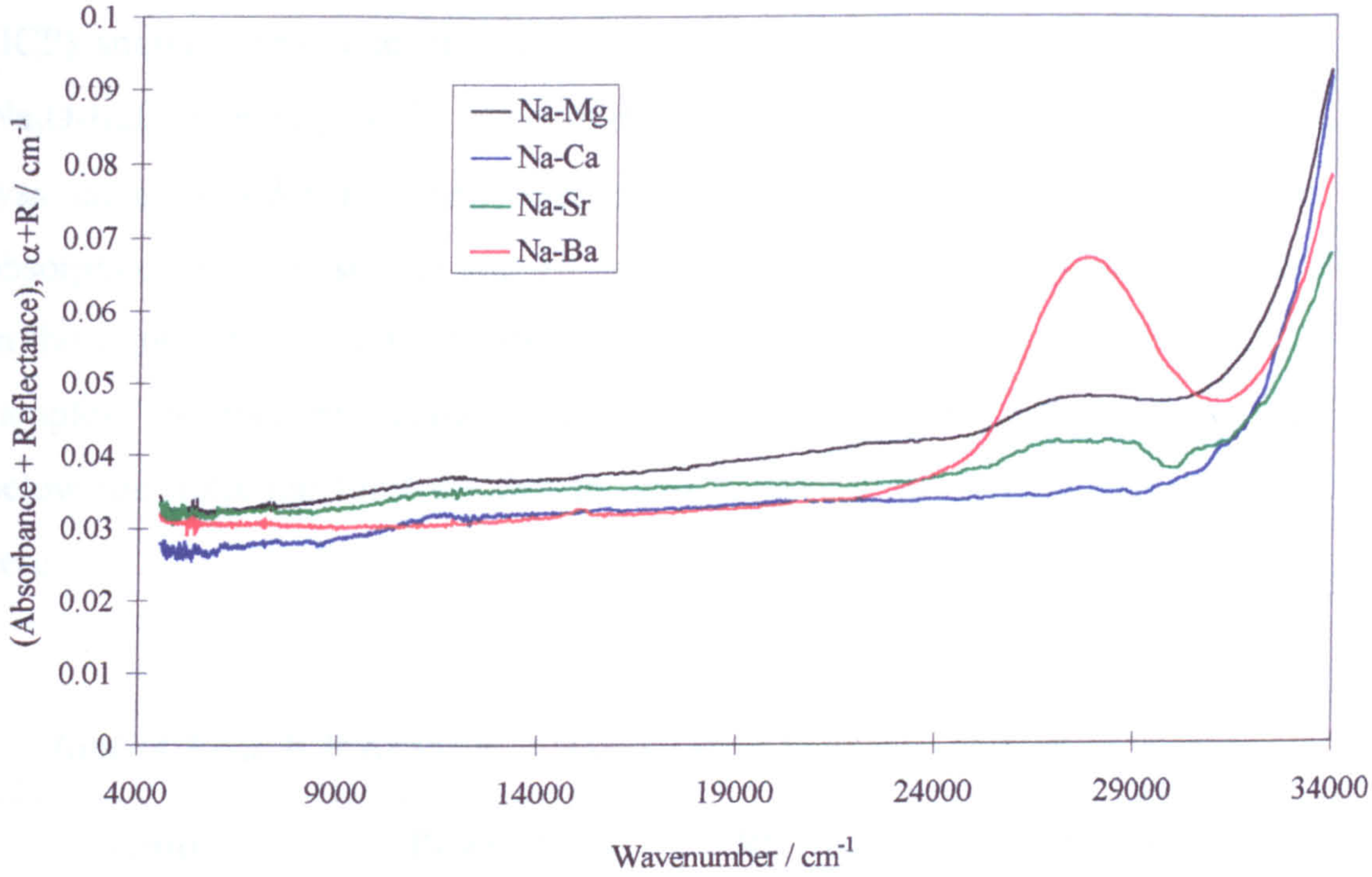

Figure 4.3.1.b. Optical Spectra of SiO_2-R_2O-BaO Base Glasses (Samples 5 - 7)

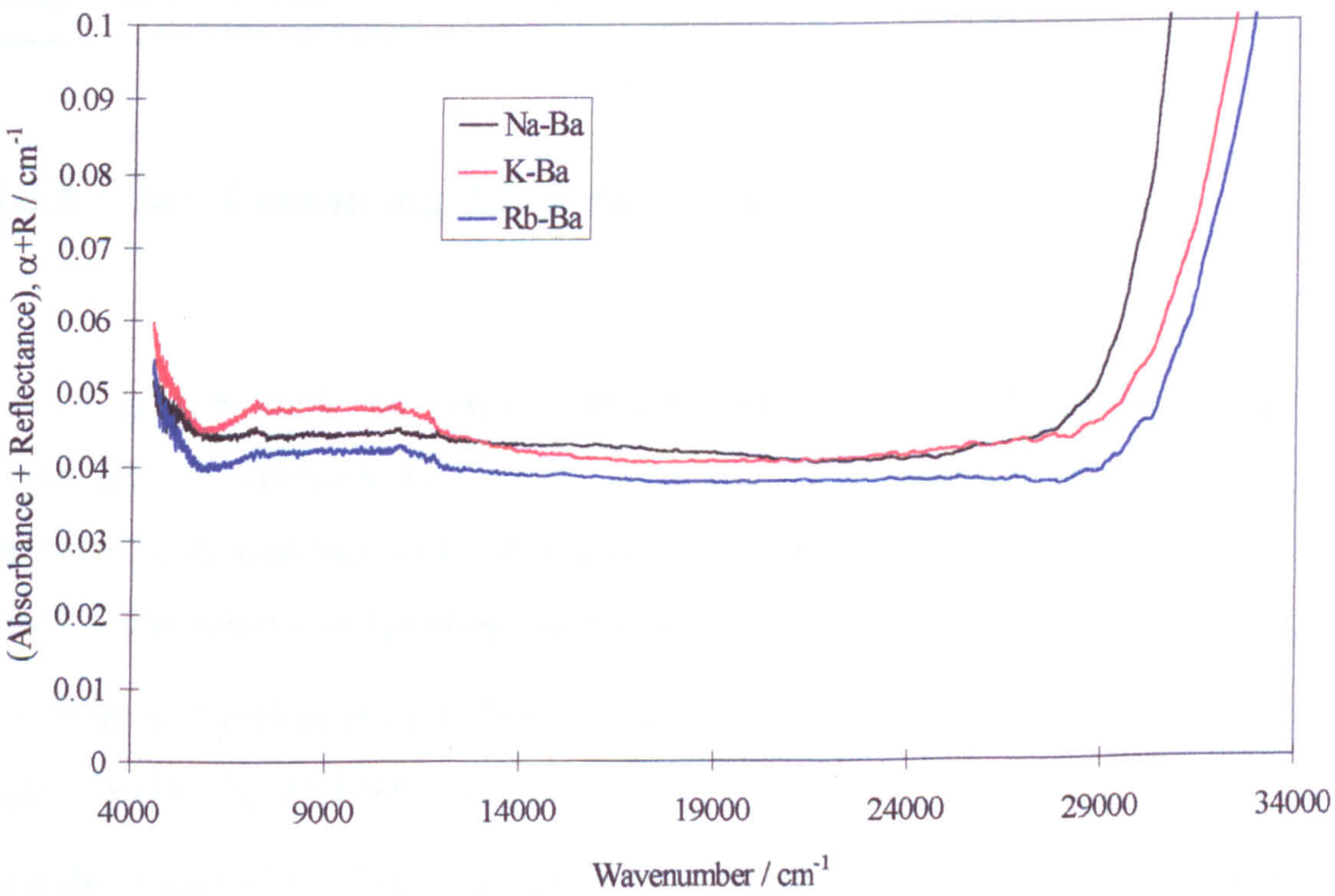

The absorption band at ~27,800 cm^{-1} in the glasses from Pt-2%Rh crucibles was absent from the glasses melted in mullite crucibles. Inductively-charged plasma (ICP) analysis was conducted on two base glasses; SiO_2-Na_2O-MgO and SiO_2-Na_2O-BaO (samples 1 and 4 respectively). Results are shown in table 4.3.1.a. This was done in order to detect any impurities which may have explained the absorption bands present in glasses melted in Pt-2%Rh crucibles but not present in those melted in mullite crucibles. Very low levels of Pt were detected in both samples, however the yellow sample gave readings of Rh and Fe which were below the detection limit for this technique, effectively making these readings zero.

Table 4.3.1.a. ICP Analysis of Base Glasses Melted in Pt-2%Rh Crucibles

Sample	**Pt weight %** ± **0.0005**	**Rh weight %** ± **0.0005**	**Fe weight %** ± **0.02**
Na_2O-MgO (clear)	0.00274	0.0017	0.04
Na_2O-BaO (yellow)	0.00186	< 0.0005	< 0.02

4.3.2. Glass Containing 0.2 Molar % Fe_2O_3

All the glasses could be poured when molten at 1450°C. There were large differences in viscosity (η) between samples of different composition. No quantitative measurements of η were made, but the following general points were noted whilst melting and pouring the glasses:

i) η increased with relative molecular mass of substituting alkali oxide such that $Li_2O < Na_2O < K_2O < Rb_2O < Cs_2O$.

ii) η decreased with relative molecular mass of substituting alkaline earth oxide such that $MgO > CaO > SrO > BaO$.

iii) η decreased as the Fe_2O_3 content of the glass increased.

4.3.2.1. X-Ray Diffraction (XRD)

Glasses of the system SiO_2-Li_2O-RO where R = Mg, Ca and Sr were opaque, so X-Ray Diffraction (XRD) was used to determine whether this was due to crystallisation. Some samples containing 5 molar % Fe_2O_3 were also analysed to determine if any crystalline phases occurred at high Fe_2O_3 contents.

All samples gave spectra equivalent to figure 4.3.2.1.a., which shows sample 10, SiO_2-Li_2O-MgO, the most severely opaque glass.

Figure 4.3.2.1.a. XRD Spectrum of Sample 10.

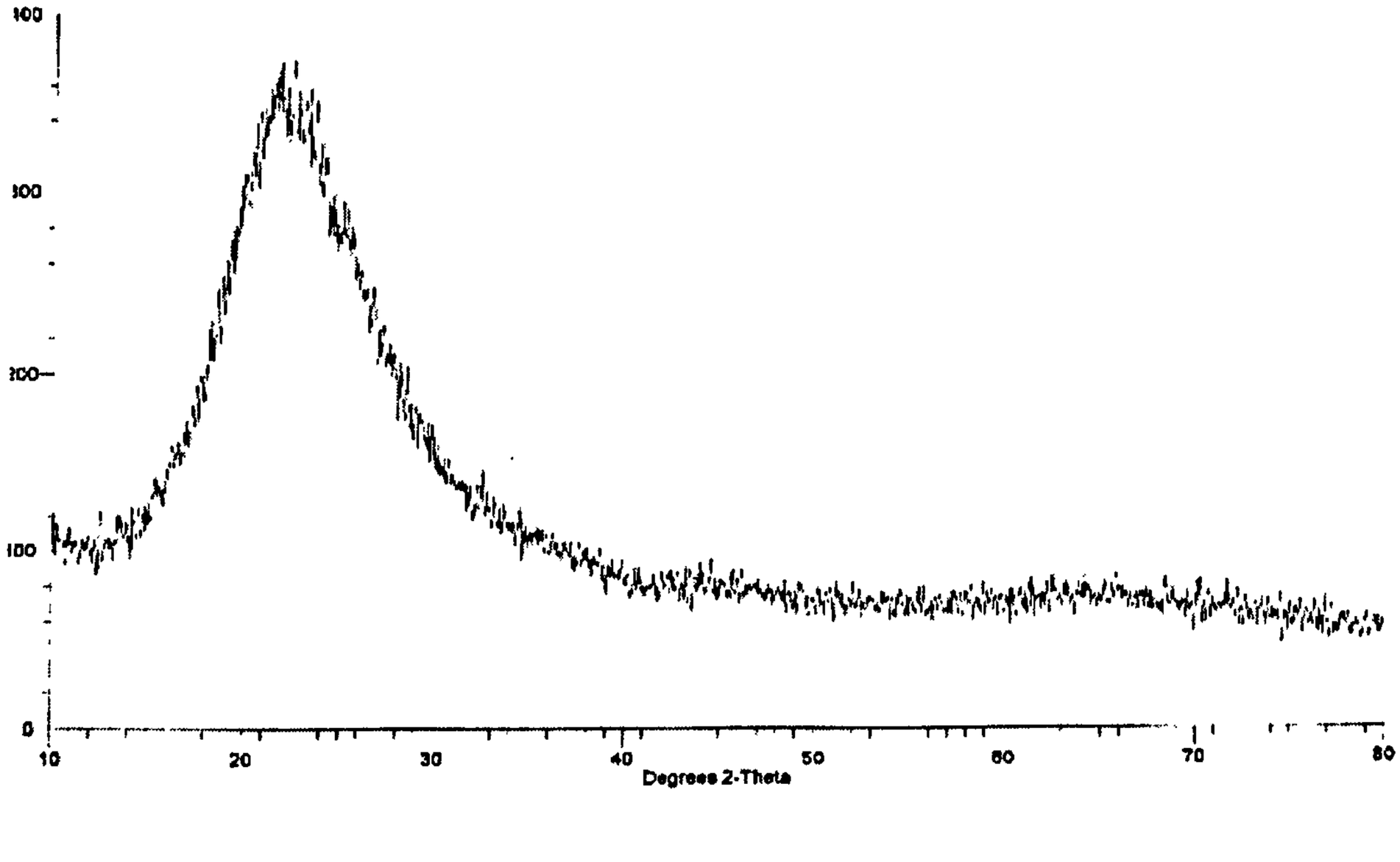

4.3.2.2. Density and Concentration

Measured densities are given in appendix B, table B1. These measurements were

made to facilitate calculation of extinction coefficients and to estimate the $Fe^{2+}/\Sigma Fe$ ratio from optical spectra. Figures 4.3.2.2.a. and 4.3.2.2.b. both highlight the effects of glass composition on density. Density remains largely unchanged for alkali ions smaller than Rb. Indeed, density actually decreases very slightly between Li and K, before rising sharply through Rb and Cs. This trend occurred for all types of alkaline earth ion.

The unique behaviour of MgO is illustrated well in figure 4.3.2.2.b., and shows that regardless of alkali type, the molar volumes of Mg glasses are higher than corresponding Ca glasses. Despite this, density increases linearly in the order Ca < Sr < Ba.

Figure 4.3.2.2.a. Densities of 0.2 % Fe_2O_3 Glasses Plotted vs. Alkali Ionic Radius

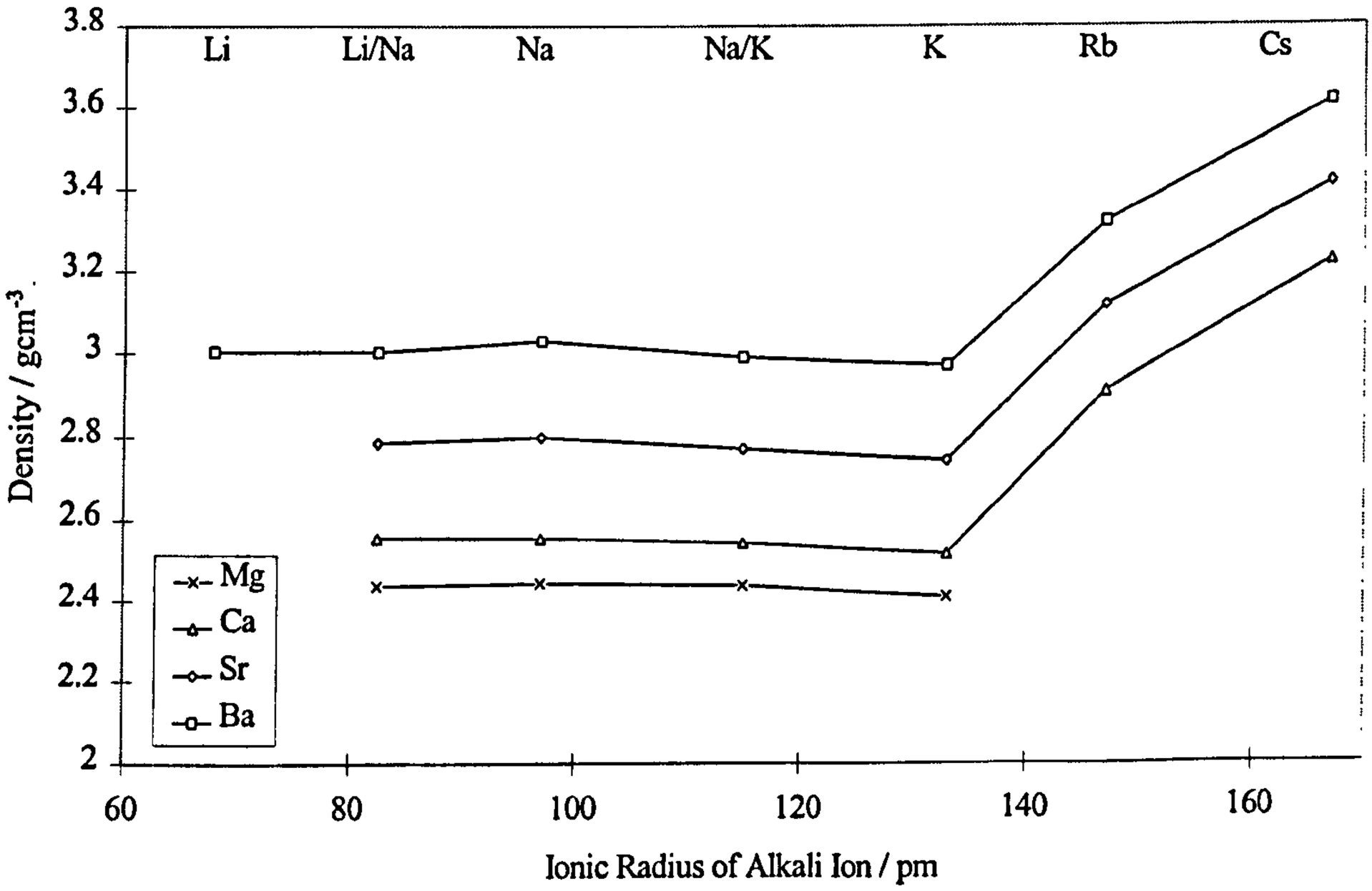

Figure 4.3.2.2.b. Density vs. Molar Volume of 0.2 % Fe_2O_3 Glasses

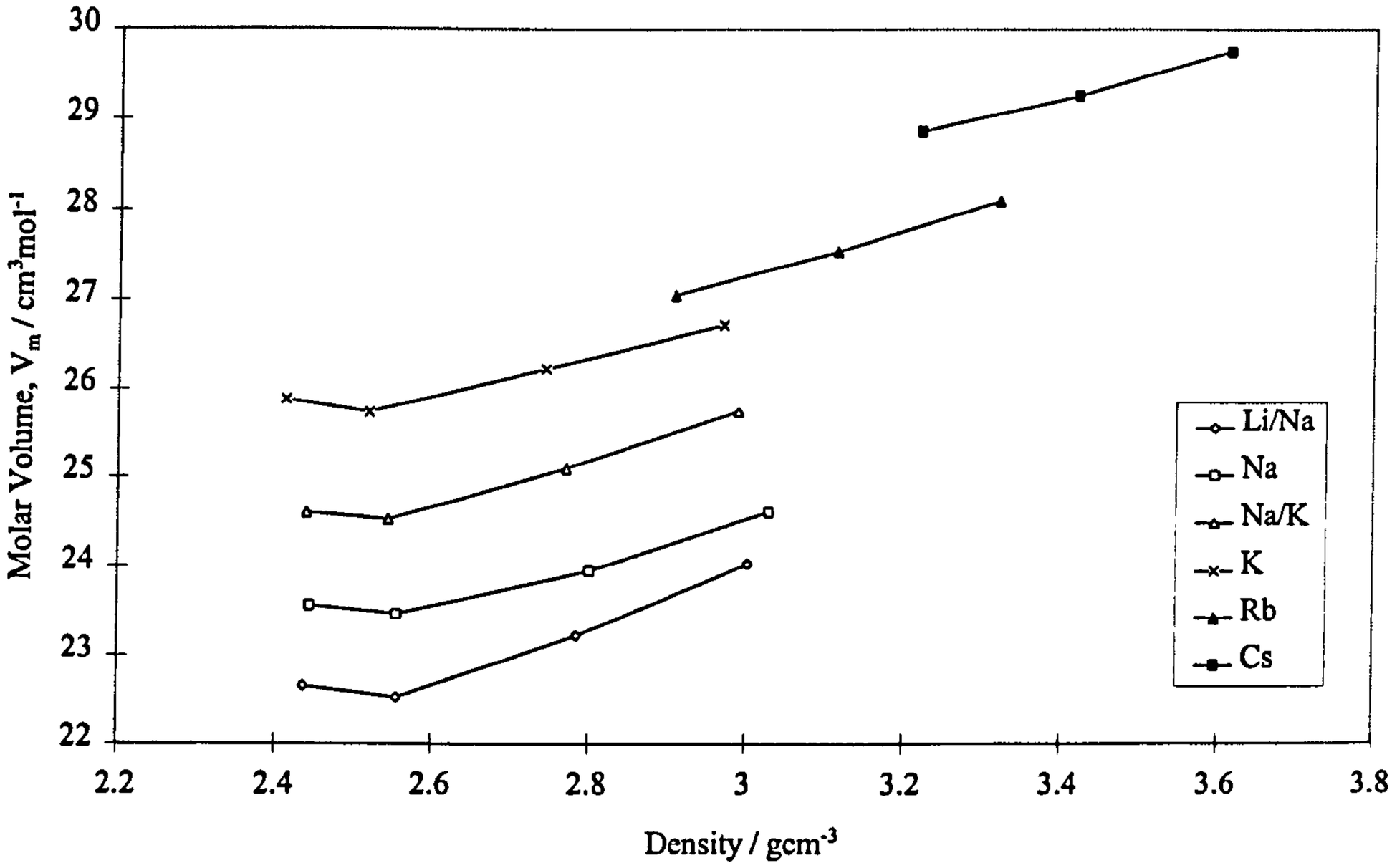

Volume concentrations of total Fe calculated as Fe_2O_3 were calculated from density measurements and batch calculations. It was assumed that nominal composition = actual composition, i.e. that there were no losses due to volatilisation during melting. Figure 4.3.2.2.c. shows calculated volume concentrations for each sample. Over the compositional range studied, concentration of Fe_2O_3 varies between ~ 0.09 mol/l and ~ 0.065 mol/l, a change of over 25 %. This means that for glasses containing equimolar concentrations of Fe_2O_3, large differences in actual iron concentration per unit volume can occur which depend on the base glass composition.

The volume concentration of Fe_2O_3 decreases with increasing alkali size. The linear relationship shown in figure 4.3.2.2.b. linking Ca, Sr and Ba regardless of alkali type also occurs when considering concentration of Fe_2O_3. Once again, MgO glasses do not obey this trend but actually contain a *lower* concentration of Fe_2O_3 than comparable CaO glasses due to their voluminous structure.

Figure 4.3.2.2.c. Concentration of Fe_2O_3 for 0.2 % Fe_2O_3 Glasses

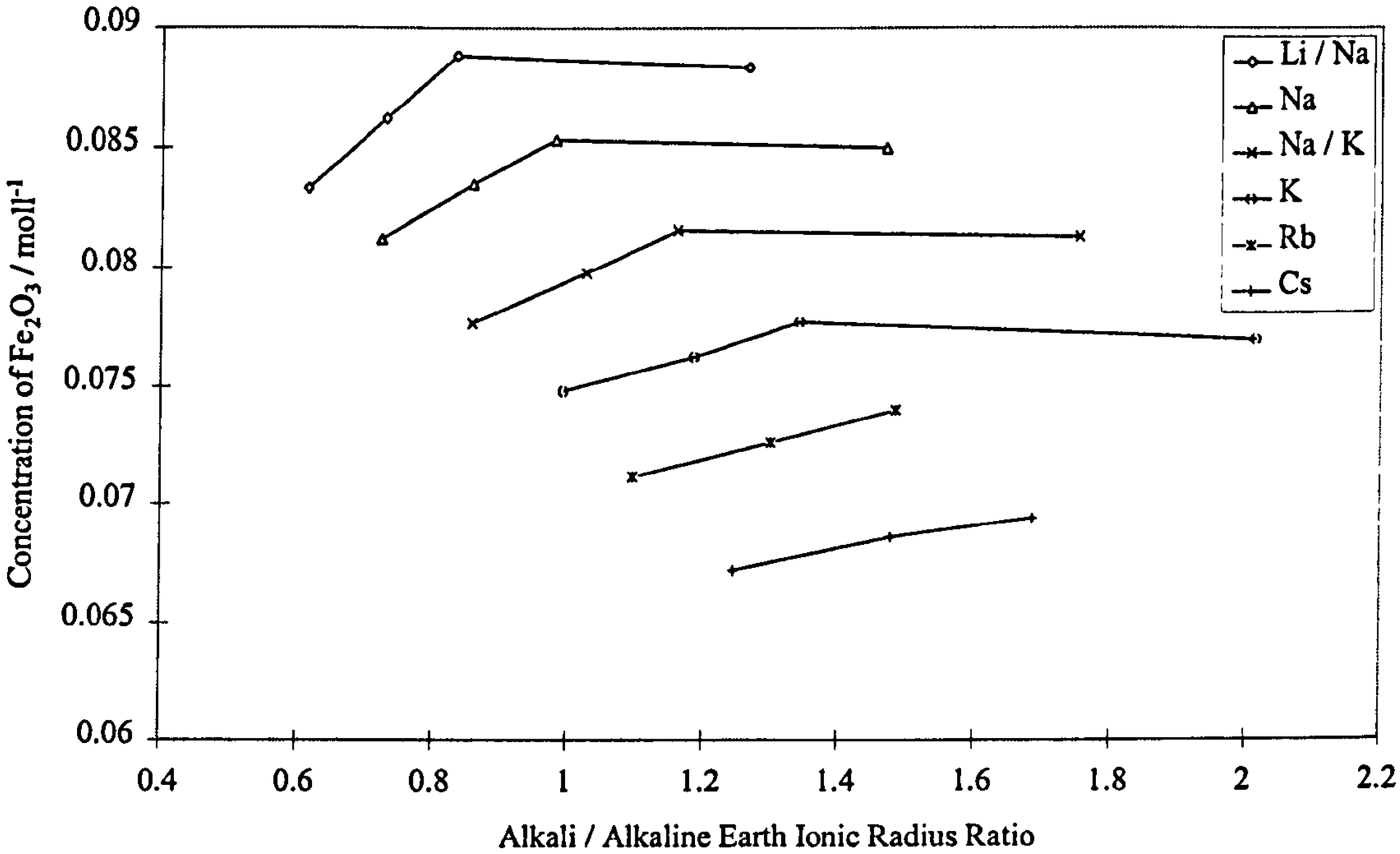

4.3.2.3. Optical Spectra

Systematic reproduction of optical absorption spectra of all the glasses in this series is in order of increasing average alkali size. Spectra are shown in figures 4.3.2.3.a.to 4.3.2.3.f.

Figure 4.3.2.3.a. SiO_2-Li_2O-BaO-0.2 % Fe_2O_3 Glass (Sample 15)

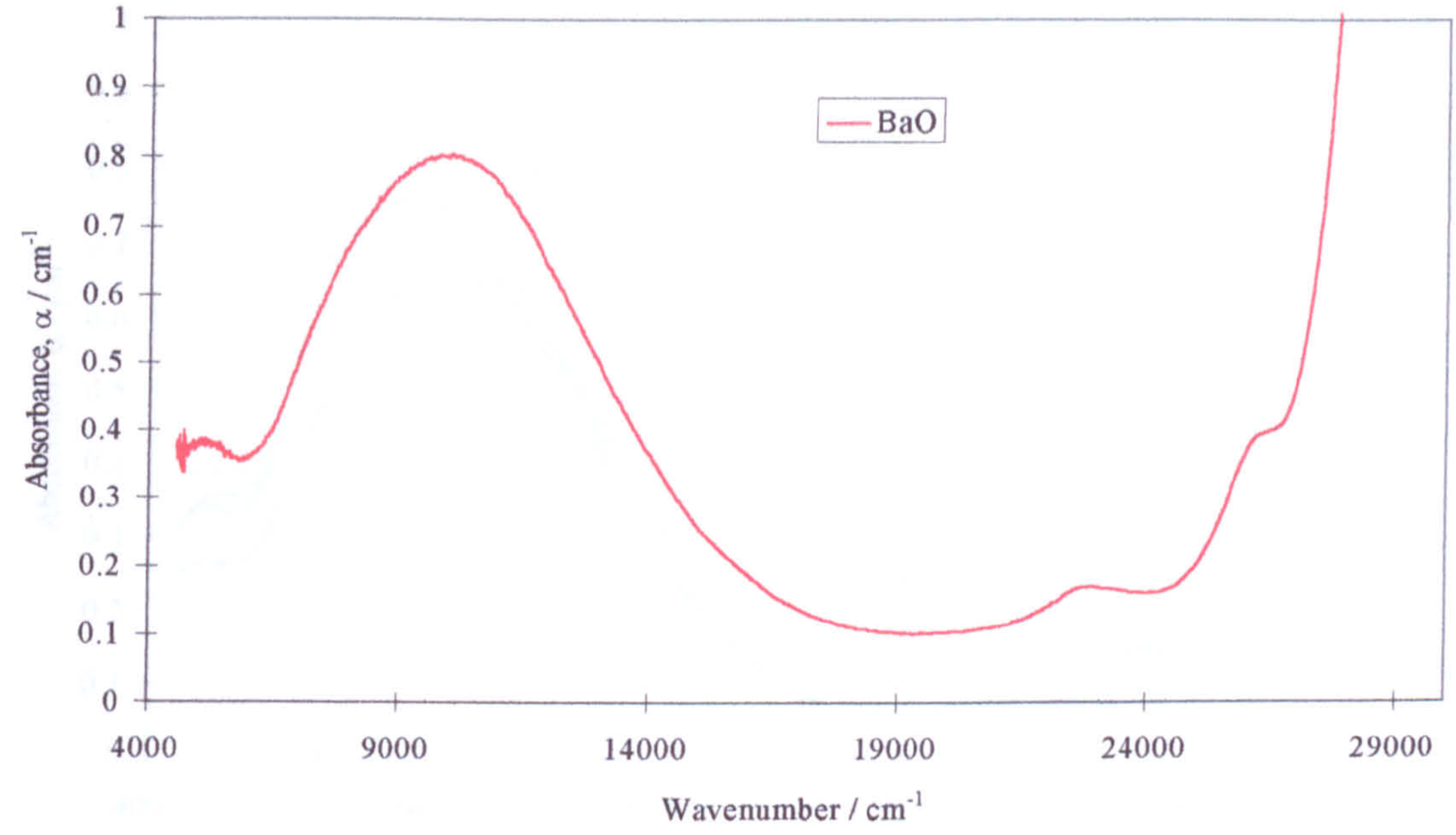

Figure 4.3.2.3.b. SiO_2-Li_2O-Na_2O-RO-0.2 % Fe_2O_3 Glasses (Samples 17 - 20)

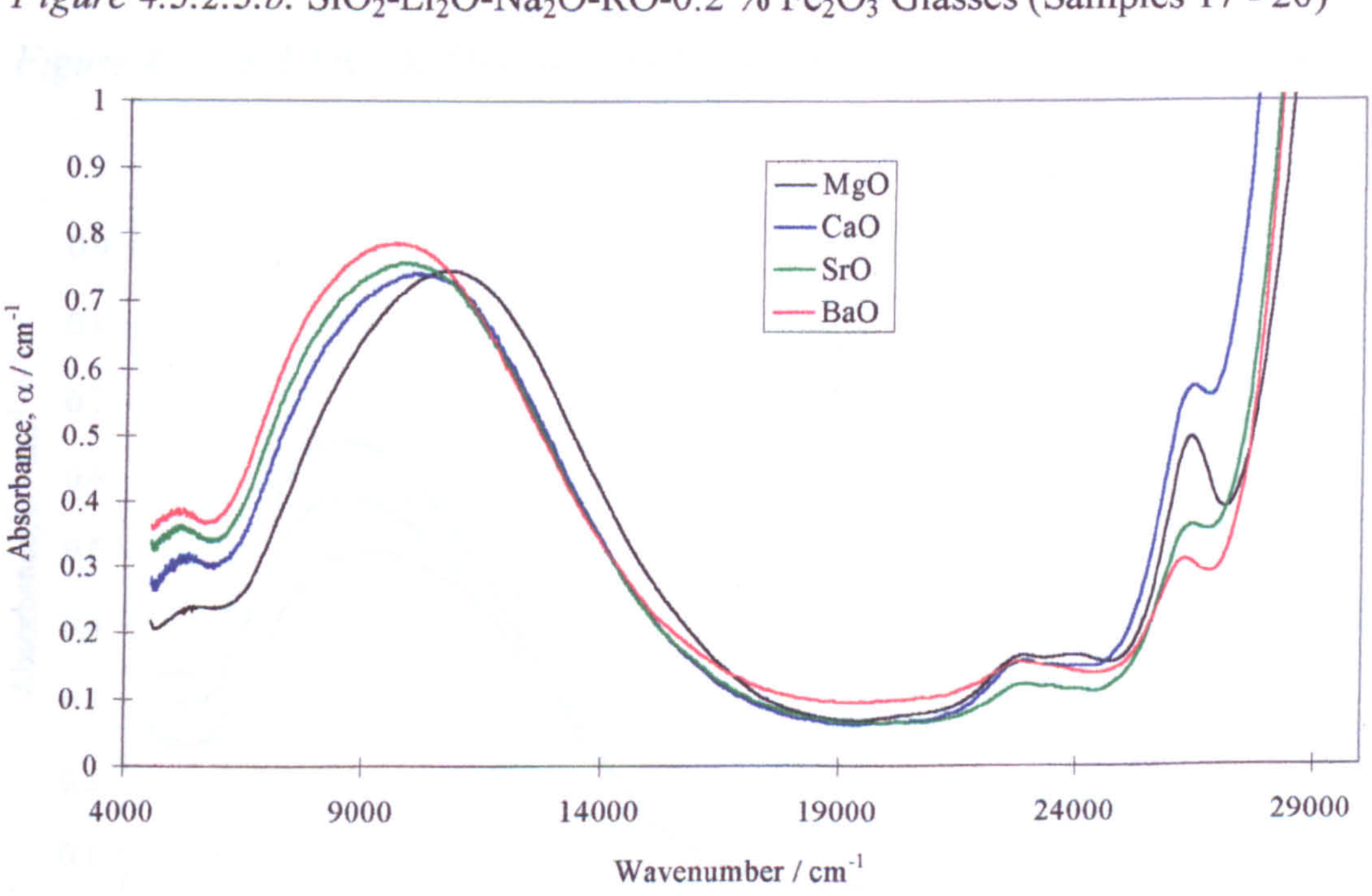

Figure 4.3.2.3.c. SiO_2-Na_2O-RO-0.2 % Fe_2O_3 Glasses (Samples 21, 24, 29, 32)

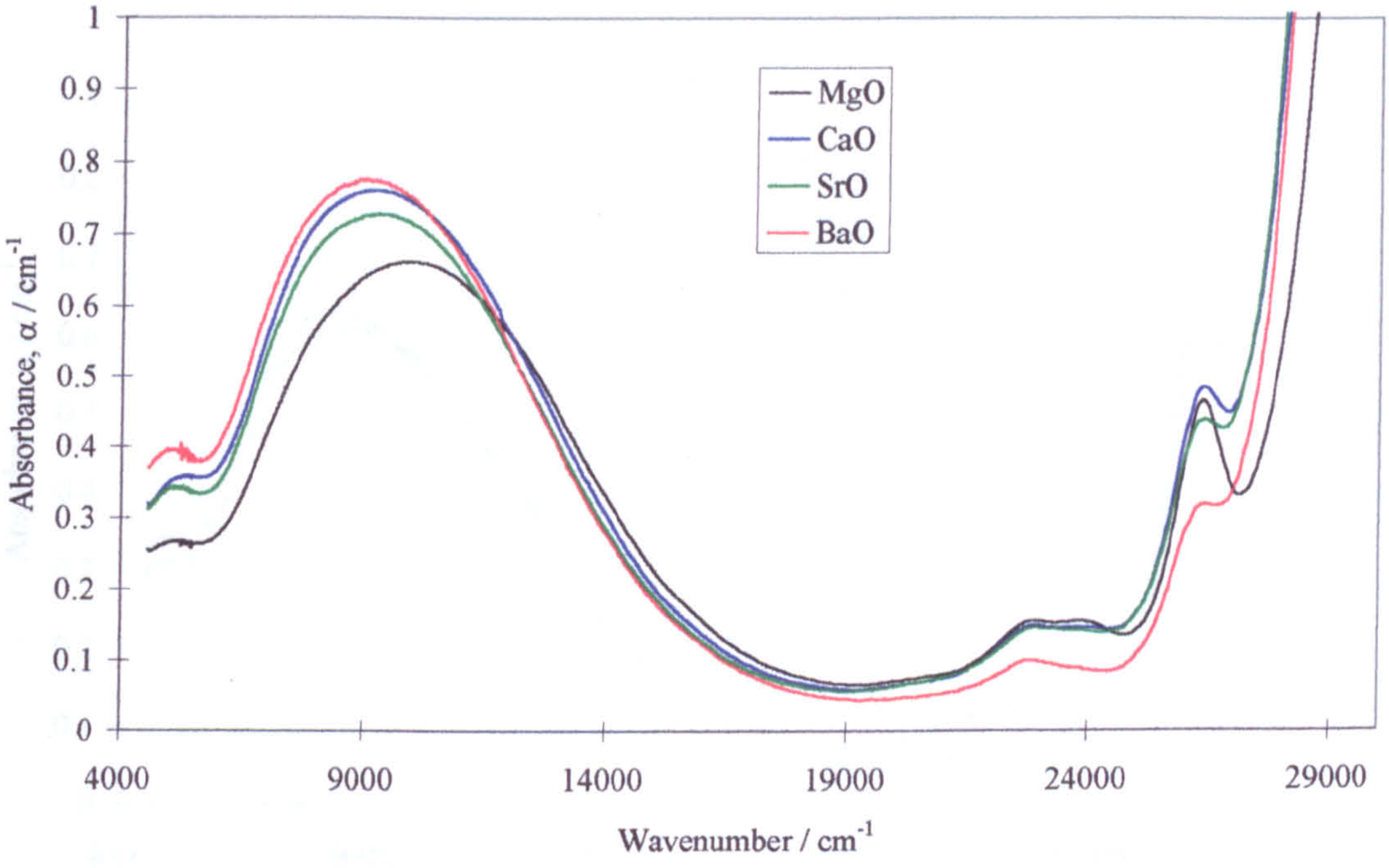

Figure 4.3.2.3.d. SiO_2-K_2O-RO-0.2 % Fe_2O_3 Glasses (Samples 40, 42, 45, 48)

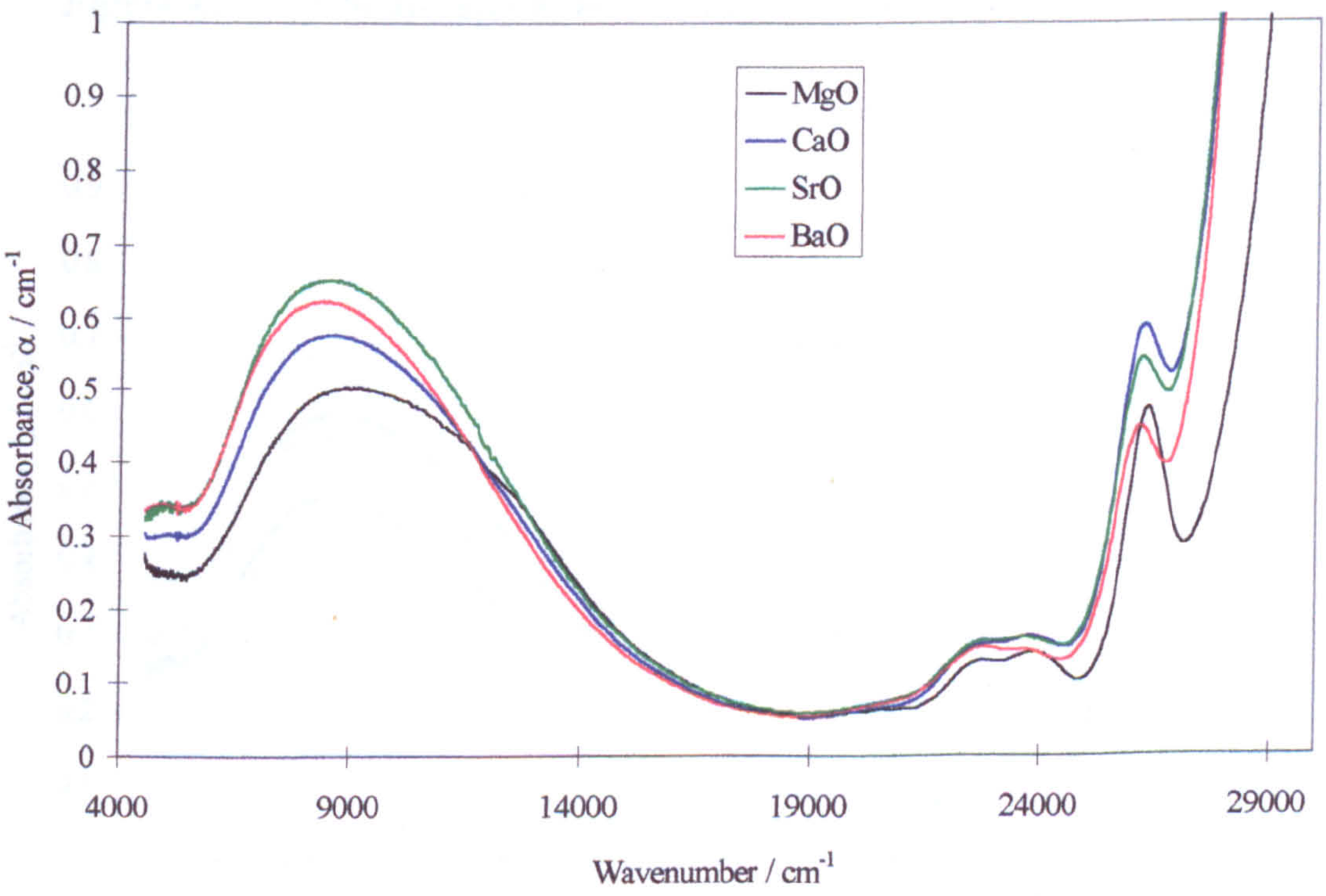

Figure 4.3.2.3.e. SiO_2-Rb_2O-RO-0.2 % Fe_2O_3 Glasses (Samples 51 - 53)

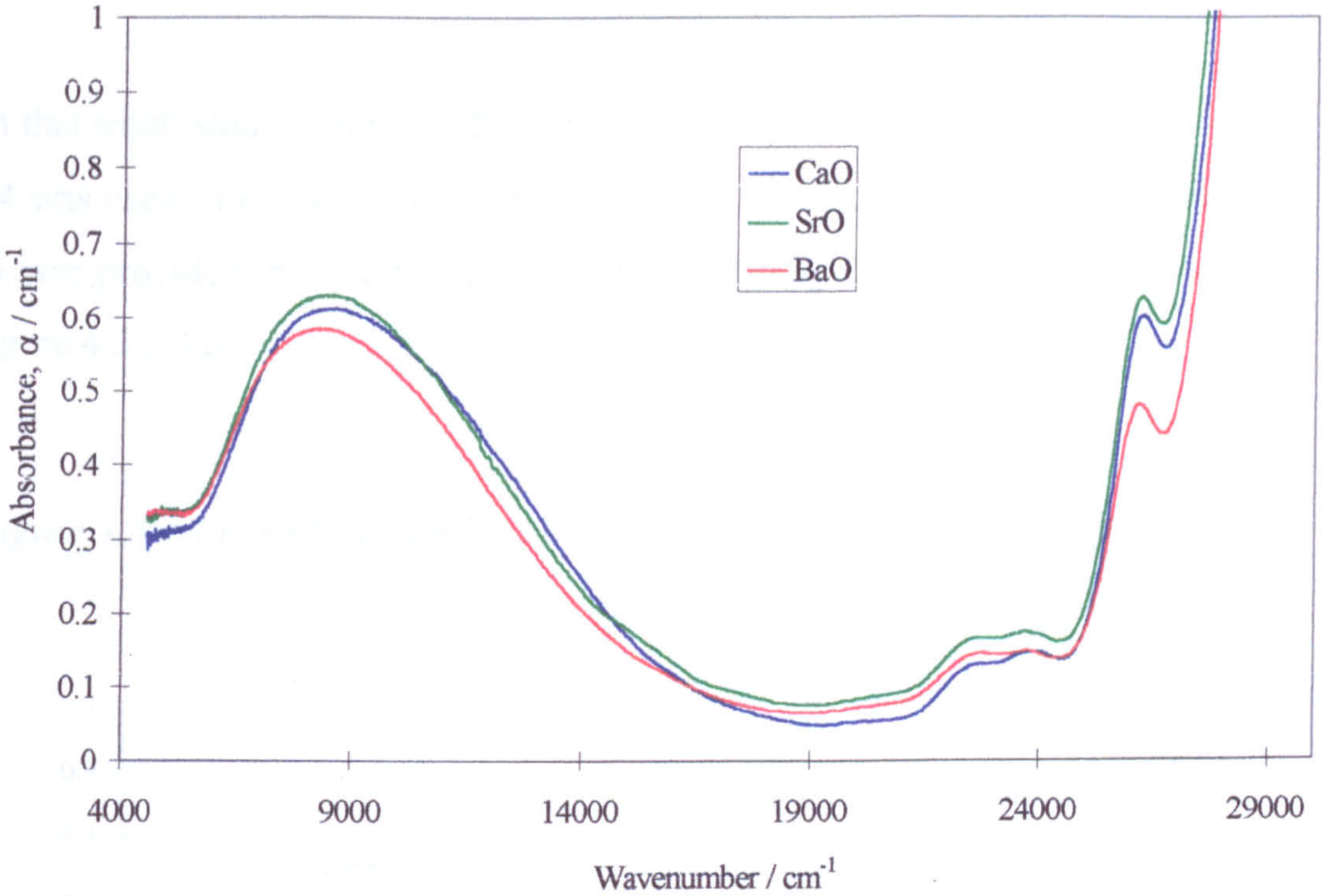

Figure 4.3.2.3.f. SiO_2-Cs_2O-RO-0.2 % Fe_2O_3 Glasses (Samples 54 - 56)

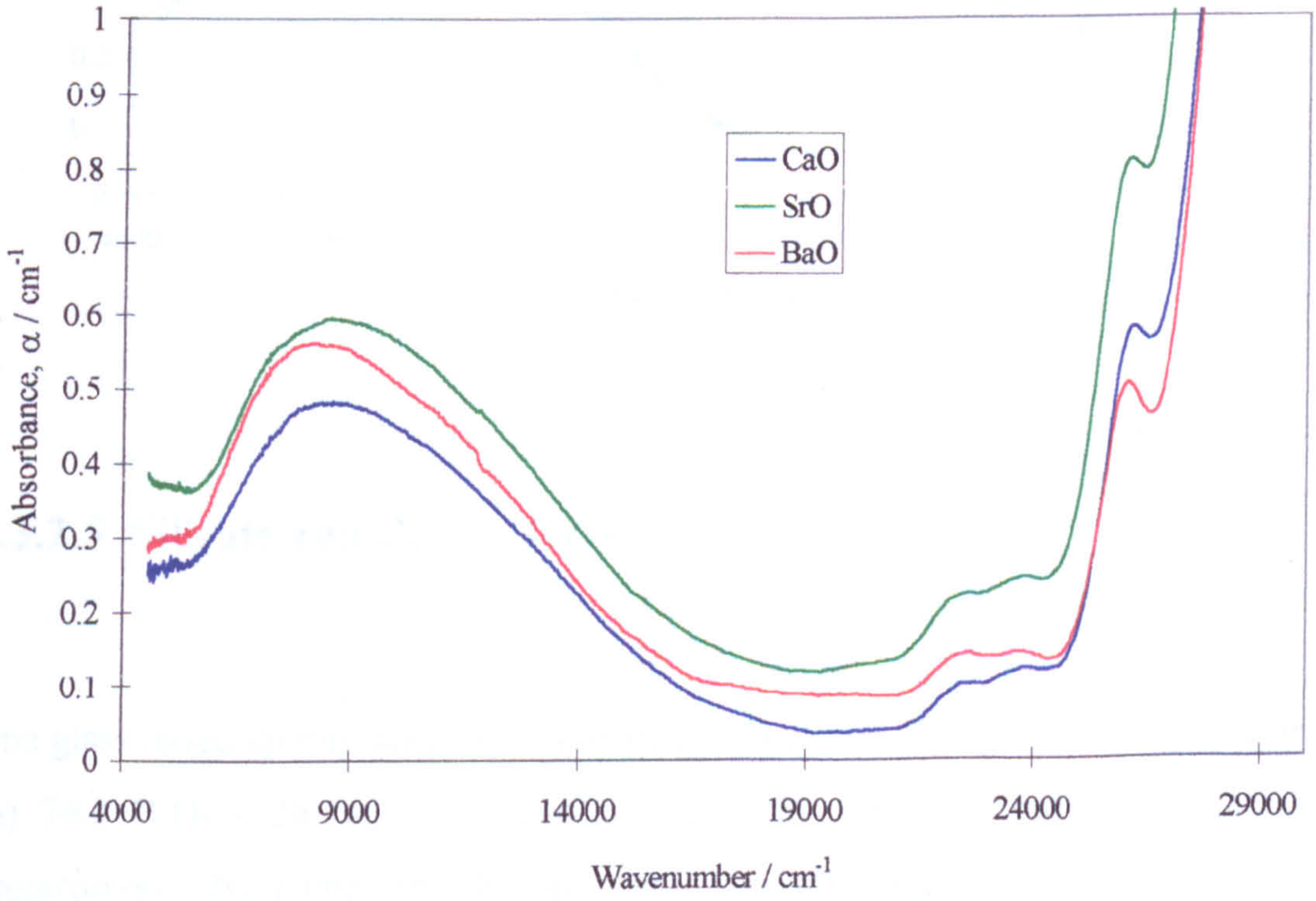

4.3.2.4. SiO_2 Partial Replacement

In this small study a standard SiO_2-Na_2O-CaO-0.2% Fe_2O_3 glass based on sample 24 was used. It contained 64.8 molar % SiO_2 instead of 69.8%. The remaining 5 % was provided instead by Al_2O_3, B_2O_3, and GeO_2. Optical spectra are shown in figure 4.3.2.4.a.

Figure 4.3.2.4.a. Partial Replacement of SiO_2 by Al_2O_3, B_2O_3 and GeO_2 (Samples 24, 57, 58, 60)

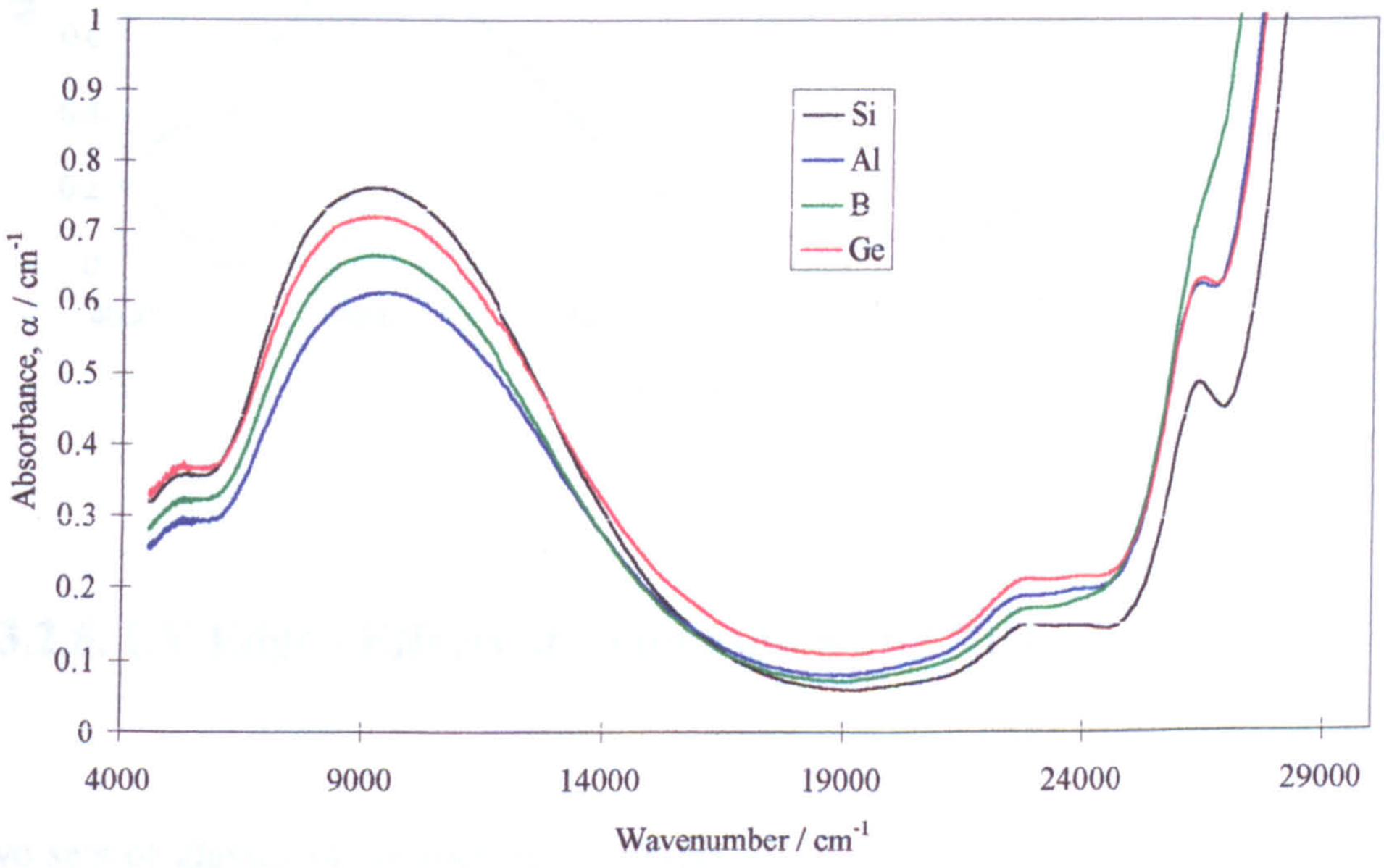

4.3.2.5. Silicate and Borate Glass

One glass based largely upon B_2O_3 was made (sample 62), of composition (molar %) 74.8 B_2O_3 - 20 SiO_2 - 5 Na_2O - 0.2 Fe_2O_3, and analysed using optical spectroscopy. By comparing the spectrum with that of a typical silicate glass (sample 24), of composition (molar %) 69.8 SiO_2 - 15 Na_2O - 15 CaO - 0.2 Fe_2O_3,

it can be seen from figure 4.3.2.5.a. that the spectra are very different.

Figure 4.3.2.5.a. Silicate and Borate Glasses Containing 0.2 Molar % Fe_2O_3

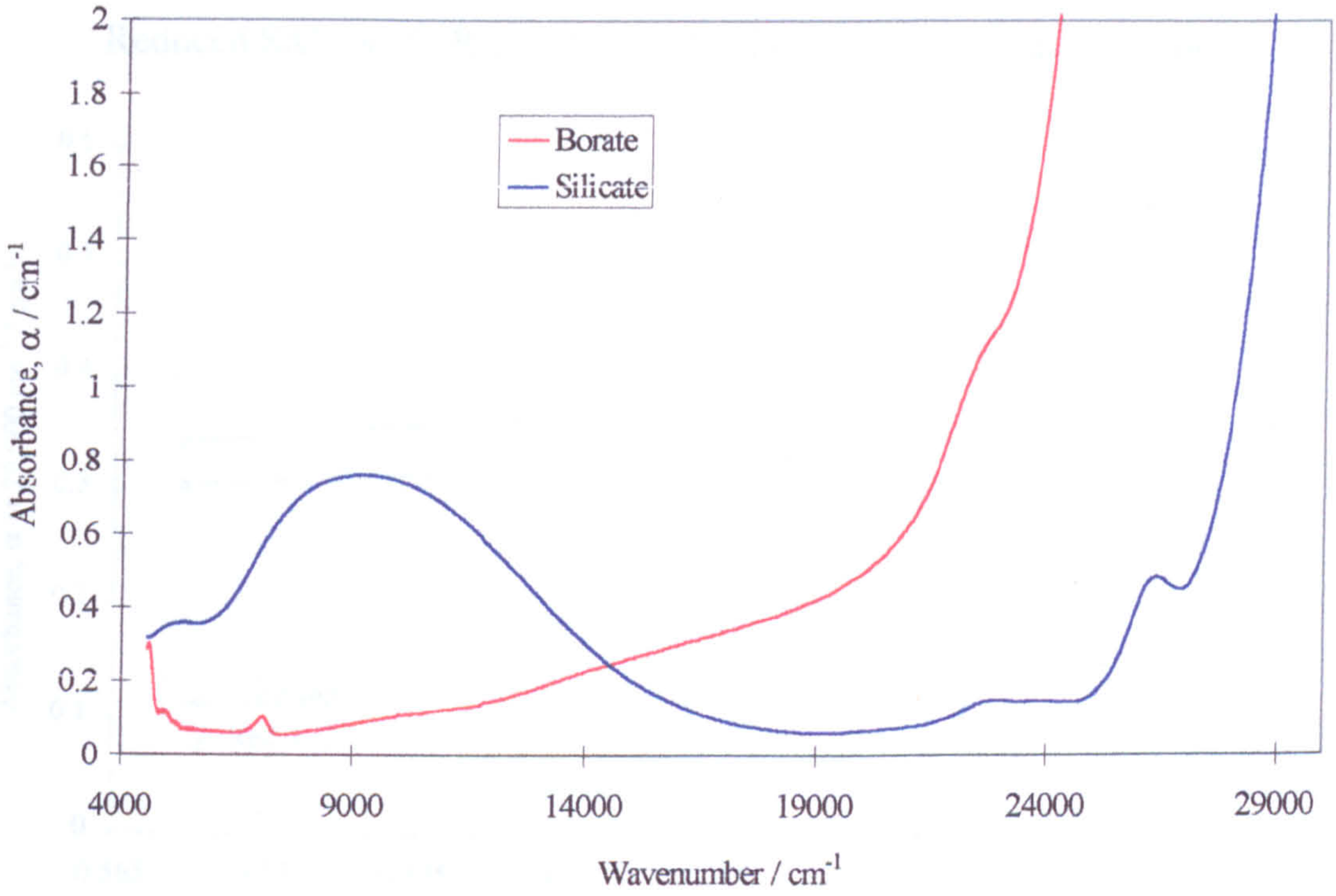

4.3.2.6. UV Edge - Effects of Composition and Redox

Two sets of glasses of composition SiO_2-Na_2O-RO-0.2 molar % Fe_2O_3 (R = Mg, Ca, Sr, Ba) were melted in a gas furnace (Gas 2 in melting conditions, see chapter 3.1.4.), with the aim of producing two glasses of each composition, but with different redox states. This was done by adding 0.1g of carbon powder to the batch for one glass of each composition. Samples for optical spectroscopy were prepared by the workshop at Pilkington, where the glasses were also melted. Samples 22, 23, 27, 28, 30, 31, 34 and 35 were prepared in this way. It was possible to produce optical samples of exactly equal path length, so accurate investigation of the effects of redox on the UV edge was possible. This was done by plotting the absorbance of the UV edge at a given wavenumber, in this case

29,000 cm^{-1}, as shown in figure 4.3.2.6.a. Points are plotted against optical basicity, i.e. Mg, Ca, Sr, Ba from left to right.

Figure 4.3.2.6.a. Absorbance of UV Edge at 29,000 cm^{-1} in Oxidised and Reduced SiO_2-Na_2O-RO-0.2% Fe_2O_3 Glasses of Equal Path Length

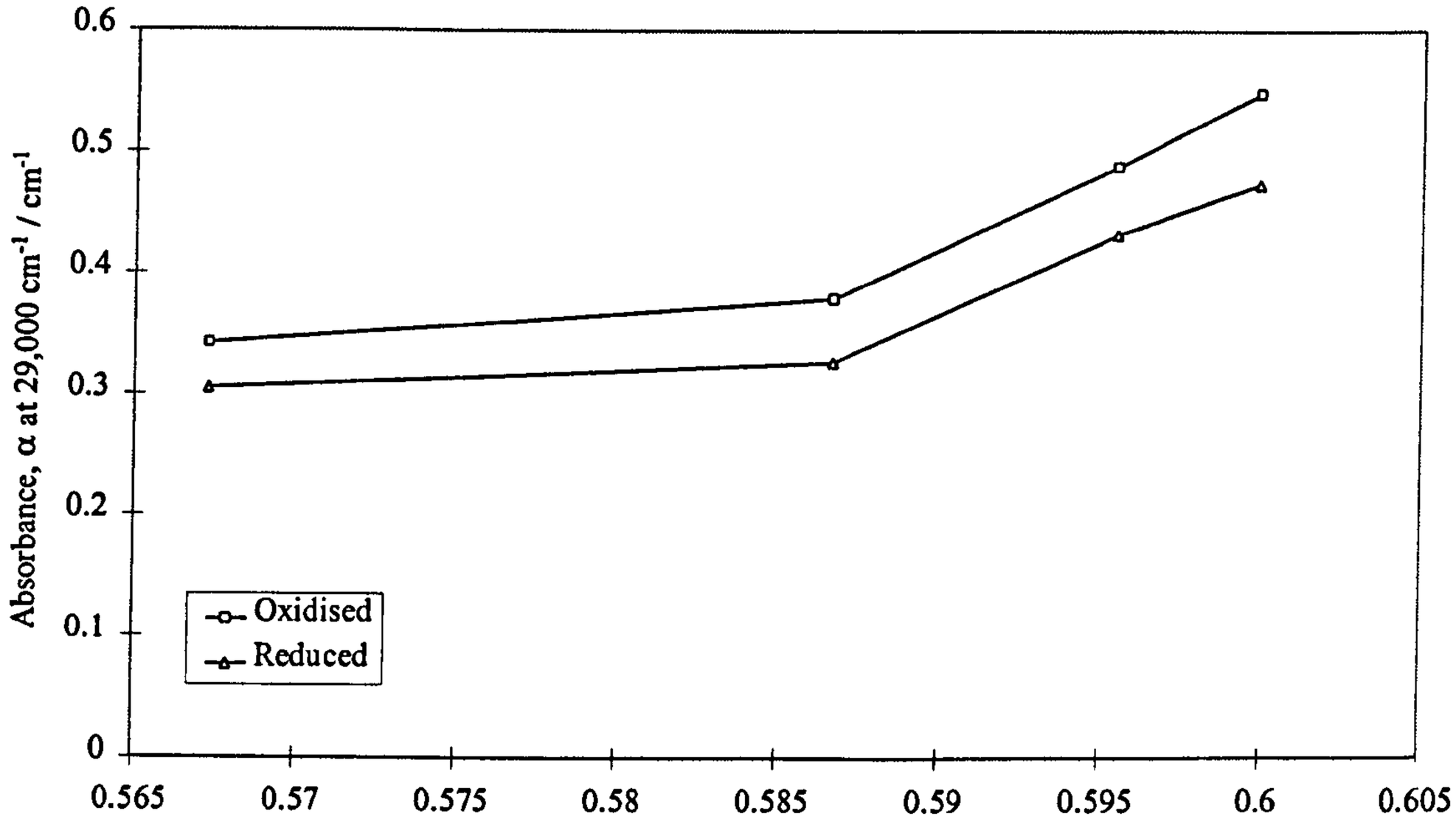

4.3.3. Glass Containing 0.1 – 5 Molar % Fe_2O_3

Studies were made on the effects of different iron contents on a range of glass compositions:

- SiO_2 - Na_2O - CaO (0.1, 0.2, 0.5, 1, 2, 3, 4, 5) % Fe_2O_3
- SiO_2 - K_2O - CaO (0.2, 1, 2, 3, 4, 5) % Fe_2O_3

Figures 4.3.3.a. and 4.3.3.b. show spectra for the series with Na_2O as alkali. These figures show that the shape of the spectrum, as well as the strength of absorption, changes with increasing Fe_2O_3 content. Absorption in the visible and near-UV regions becomes stronger relative to the broad peak near 10,000 cm^{-1}. The glass

absorbed more strongly with increasing iron content, and it was necessary to take thinner sections for optical spectroscopy. The colour of these sections changed from green at lower iron levels, to a more amber colour with higher iron levels.

Figure 4.3.3.a. SiO_2-Na_2O-CaO Glasses containing 0.1 - 1 Molar % Fe_2O_3

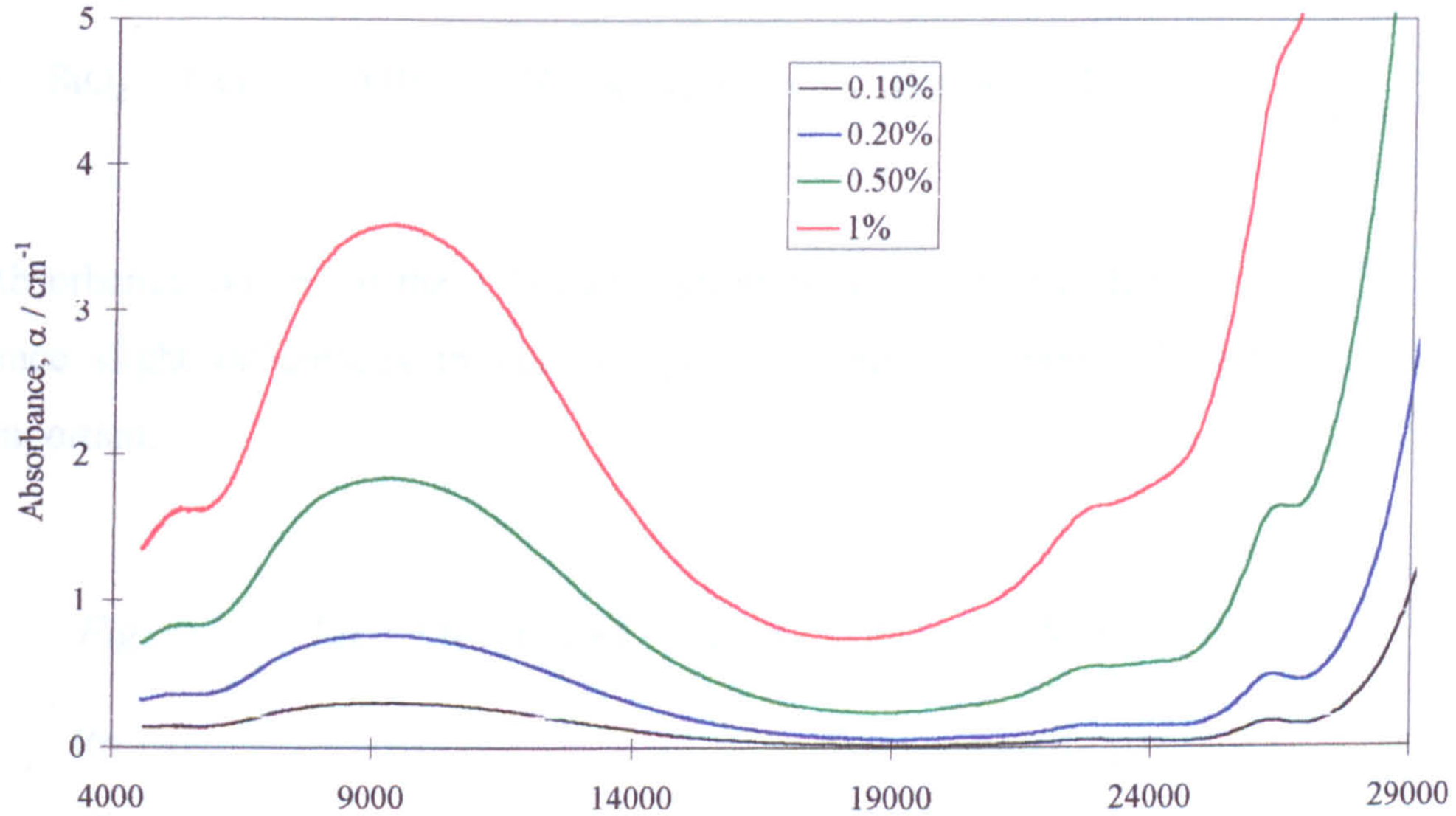

Figure 4.3.3.b. SiO_2-Na_2O-CaO Glasses Containing 1 - 5 Molar % Fe_2O_3

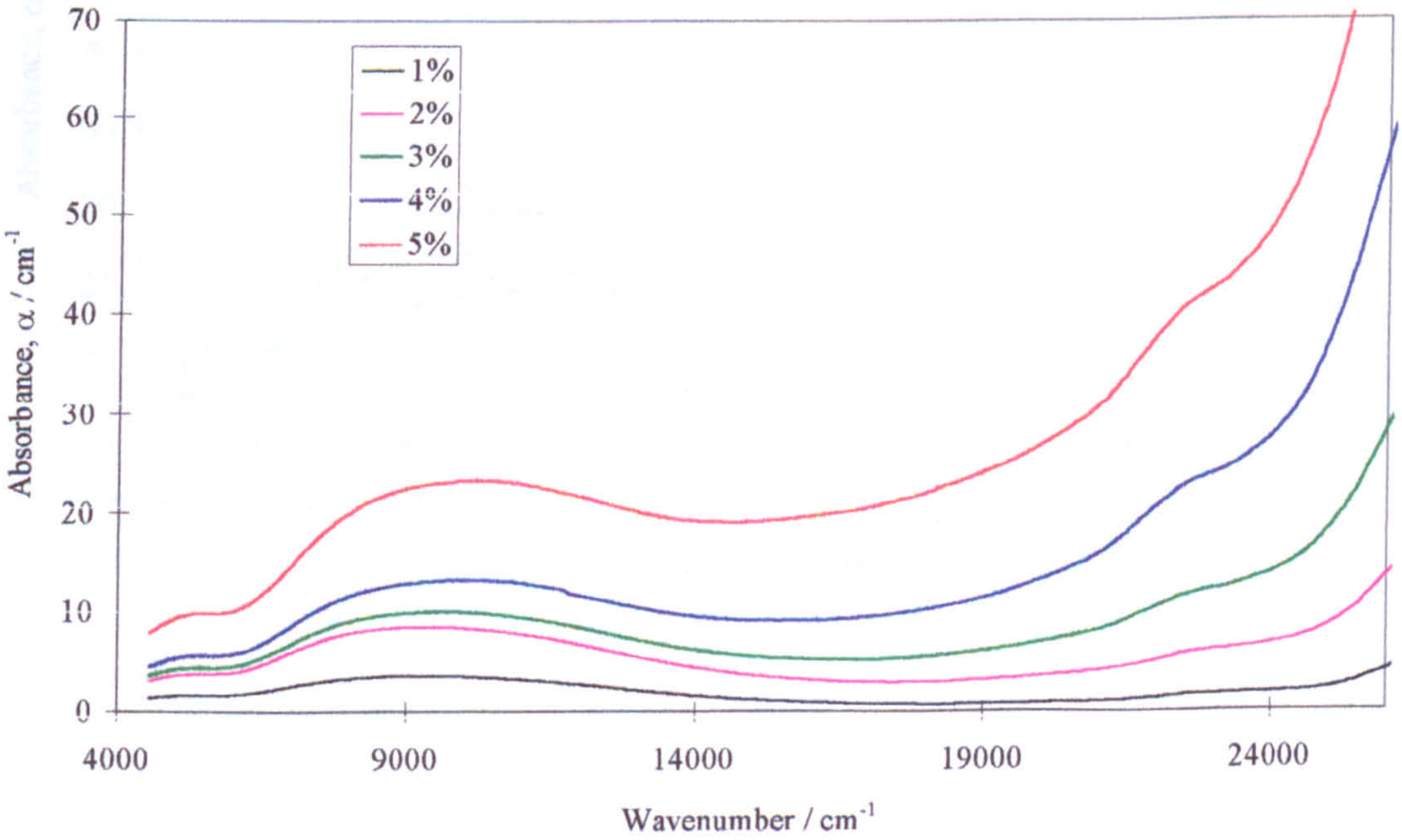

4.3.3.1. Glass Containing 5 molar % Fe_2O_3

Studies were made on a range of glass compositions containing 5 molar % Fe_2O_3:

- SiO_2 - Na_2O – RO (R = Mg, Ca, Sr, Ba) – see figure 4.3.3.1.a.
- SiO_2 – R_2O – BaO (R = Li/Na, Na, K, Rb, Cs) – see figure 4.3.3.1.b.

Absorbance values for the 5 % Fe_2O_3 samples are lower than for 0.2 % Fe_2O_3, since slight differences in path length and sample geometry become more important.

Figure 4.3.3.1.a. SiO_2-Na_2O-RO Glasses Containing 5 Molar % Fe_2O_3

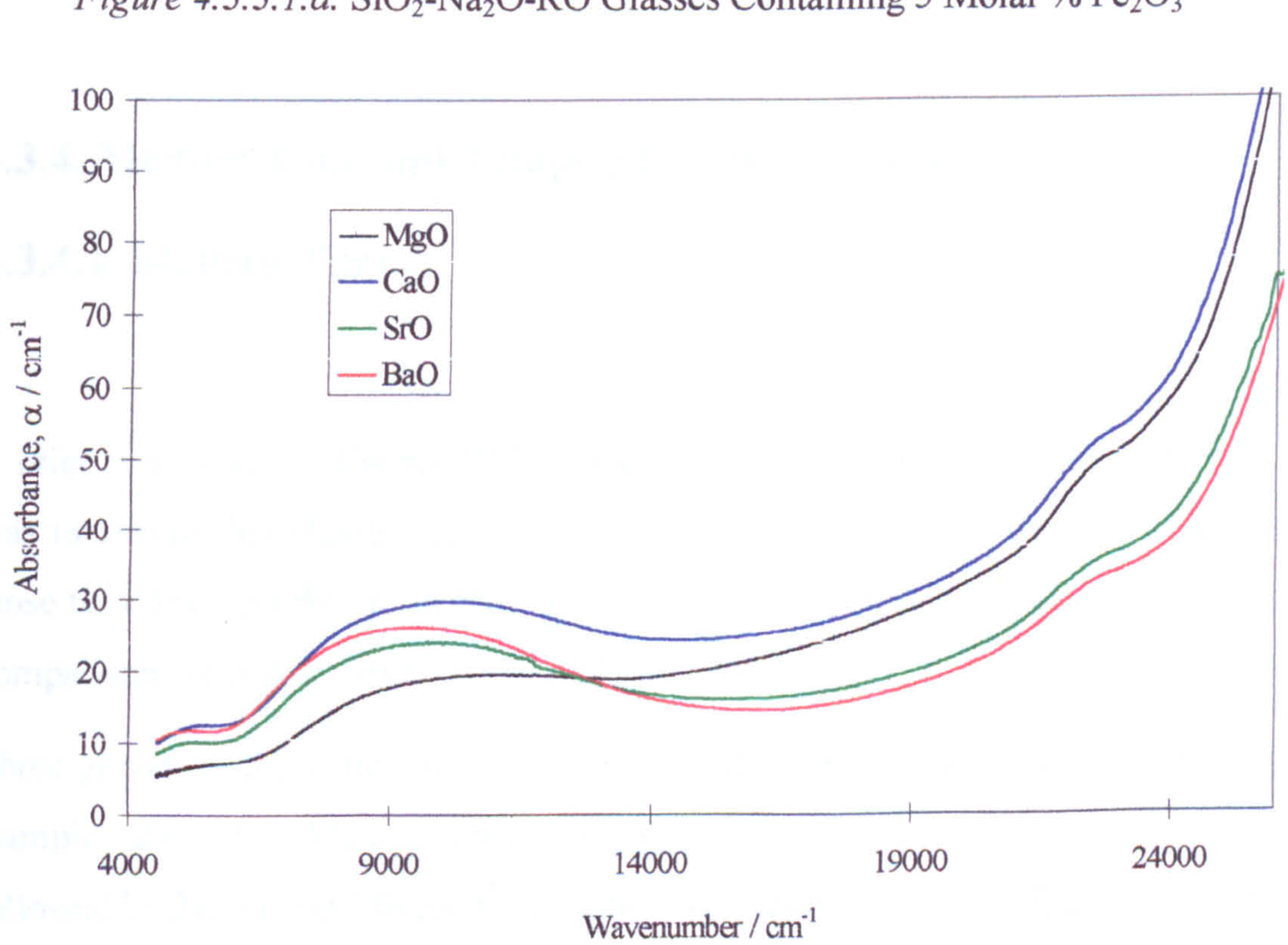

Figure 4.3.3.1.b. SiO_2-R_2O-BaO Glasses Containing 5 Molar % Fe_2O_3.

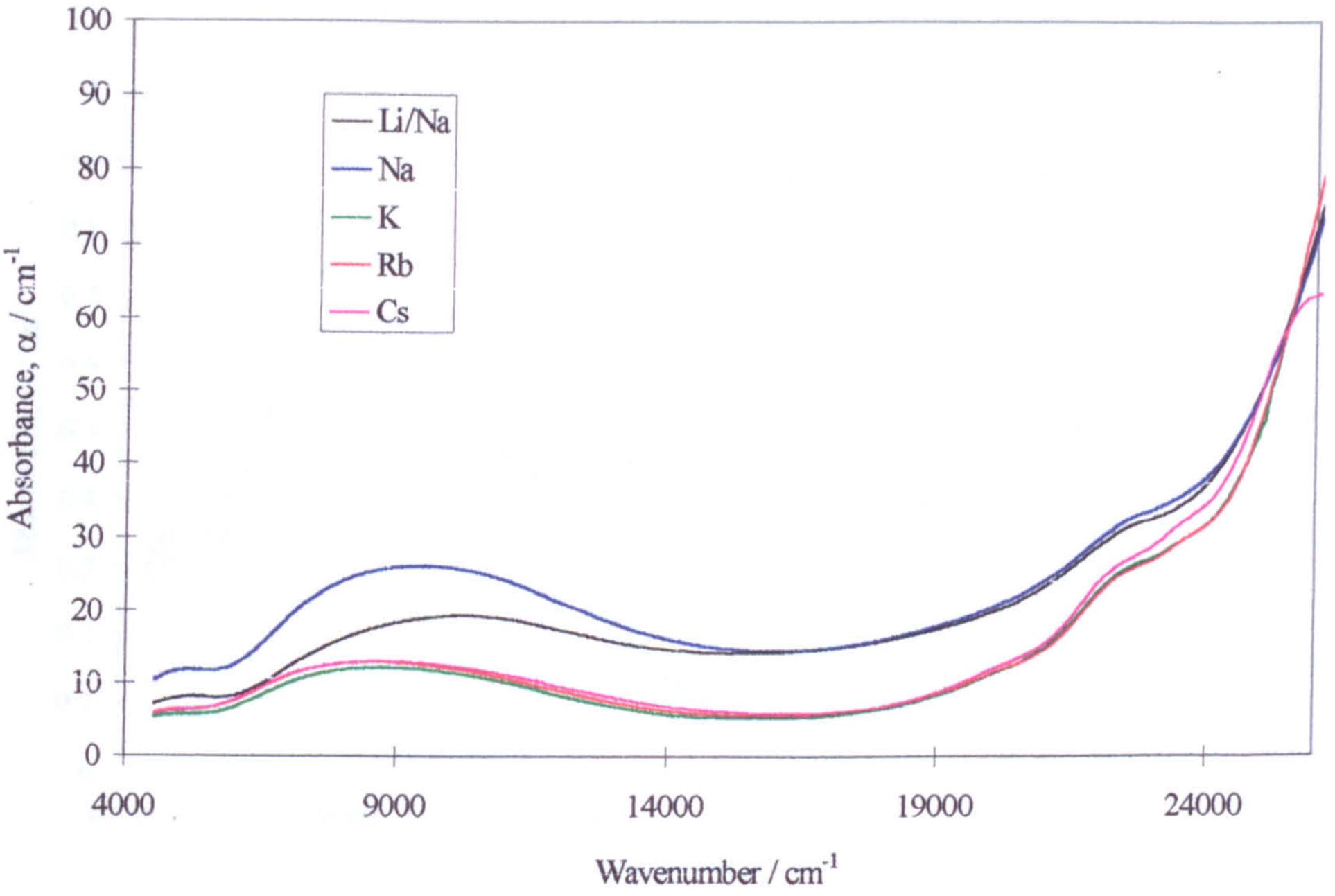

4.3.4. Melting Time and Temperature of Measurement

4.3.4.1. Melting Time

A brief investigation of some of the effects of melting time was undertaken. This was to ensure that glasses melted under the standard schedule were sufficiently close to redox equilibrium. If they were not, it would introduce inaccuracies into comparisons of redox data between different samples.

Three glasses of the same composition were melted: SiO_2-Na_2O-CaO-0.2% Fe_2O_3 (samples 24 - 26). Melting times for all glasses included 1h batch-free time followed by 2h, 5h and 21h melting. Optical spectra are shown in figure 4.3.4.1.a. It was only possible to perform wet chemical redox measurements on one of the samples. The redox state in all of the glasses was determined by comparing the optical absorption spectra, and in particular the intensity of the absorption due to Fe^{2+} ions at ~10,000 cm^{-1}.

Figure 4.3.4.1.a. SiO_2-Na_2O-CaO-0.2% Fe_2O_3 Glass with Different Melting Times

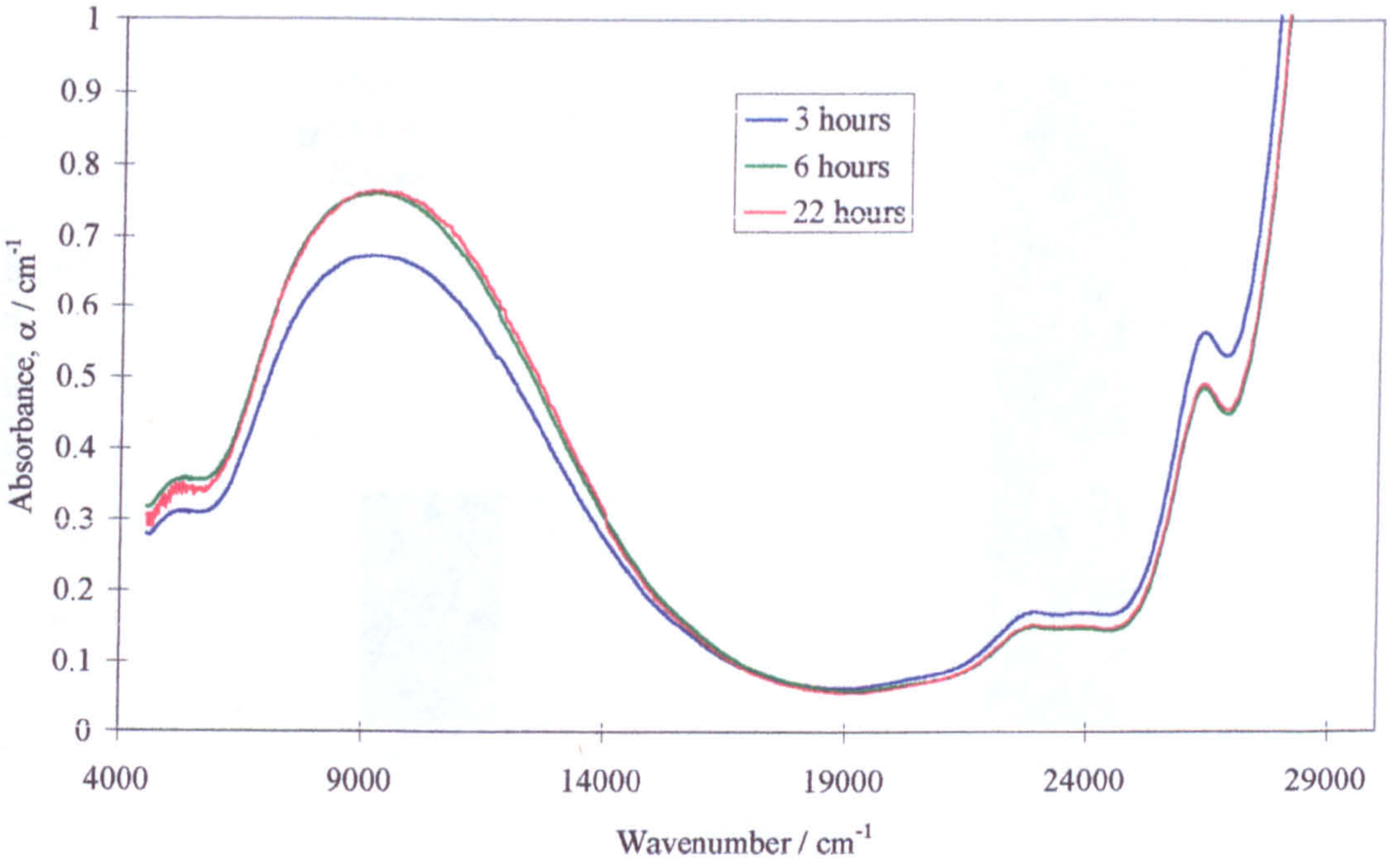

The bands at 26,300 cm^{-1} and 10,000 cm^{-1} have been attributed to Fe^{3+} and Fe^{2+} ions, respectively (see chapter 4.1.4.). The absorbance of the peak at ~10,000 cm^{-1} is virtually the same for the 6h and 22h samples, whereas it is noticeably lower in the 3h sample. Likewise, the peak near 26,300 cm^{-1} is stronger in the 3h sample than the other two. Computer modelling was carried out on these spectra, the data for which is in appendix B, table B4. Figure 4.3.4.1.b. shows the fitted absorption peak intensities which confirmed that $Fe^{2+}/\Sigma Fe$ was lower in the 3h sample, and that it was approximately equal in the 6h and 22h samples.

Figure 4.3.4.1.b. Intensities of Computer Modelled Absorption Bands of SiO_2-Na_2O-CaO-0.2% Fe_2O_3 Glass with Different Times of Melting

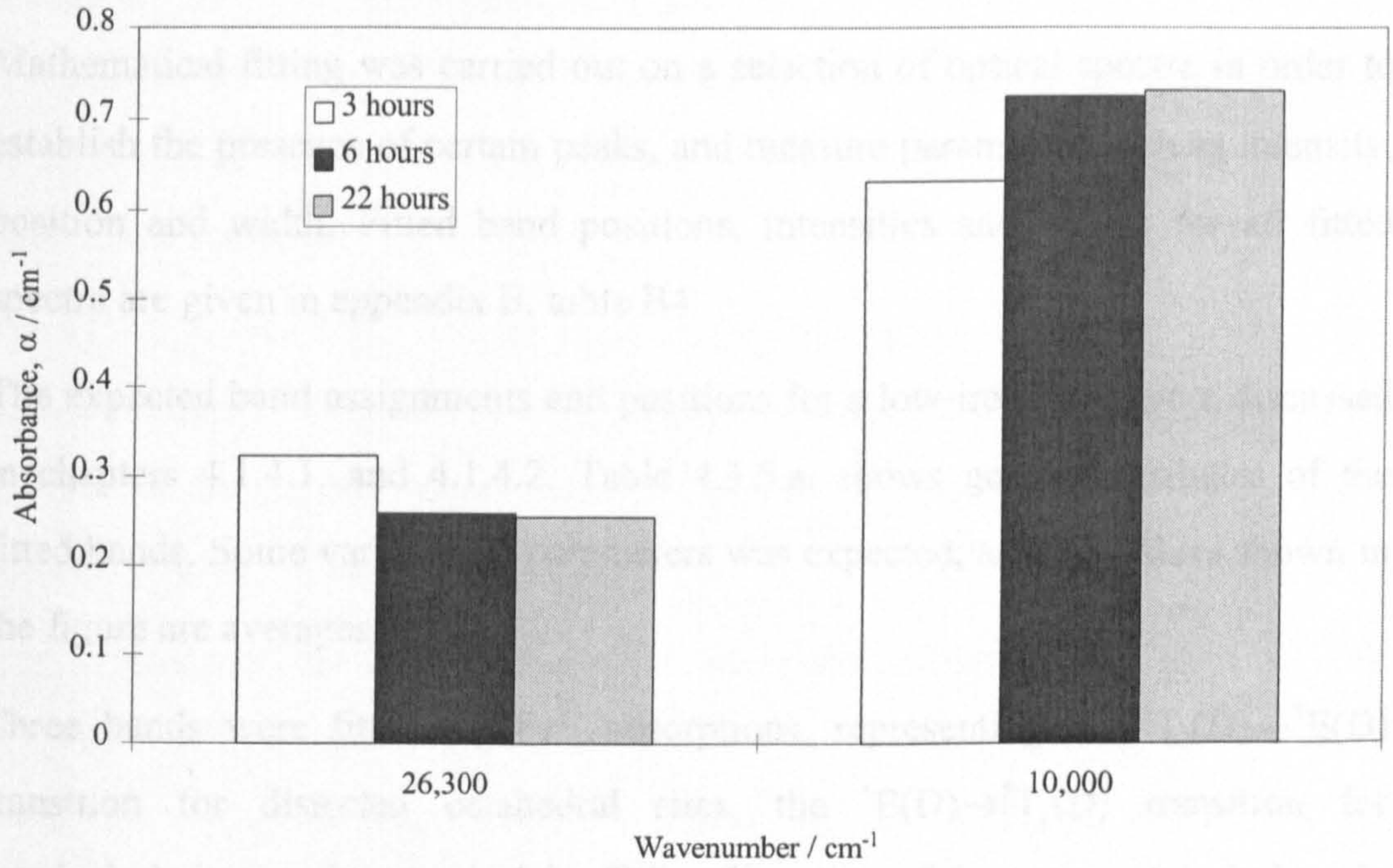

4.3.4.2. Measurement Temperature

Several spectra were recorded at ~77 K in an attempt to improve the resolution. By removing vibrational modes, it was hoped that broadening, especially of the absorption near 10,000 cm^{-1}, could be reduced. A cryostat containing the sample was placed in the beam path of the spectrometer. The cavity of the cryostat was pumped to a high vacuum by rotary and diffusion pumps. Liquid N_2 was then poured into the cavity, which cooled the sample by conduction to ~77 K. Spectra were then measured.

Spectra were virtually unaffected by temperature, so have not been reproduced here. These results showed that the vibronic coupling interactions have little broadening effect on the Fe absorption spectra in these glasses, even at relatively low wavenumbers in the near-IR.

4.3.5. Computer Fitting and Mathematical Modelling

Mathematical fitting was carried out on a selection of optical spectra in order to establish the presence of certain peaks, and measure parameters such as intensity, position and width. Fitted band positions, intensities and widths for all fitted spectra are given in appendix B, table B4.

The expected band assignments and positions for a low-iron glass were discussed in chapters 4.1.4.1. and 4.1.4.2. Table 4.3.5.a. shows general attributes of the fitted bands. Some variation in parameters was expected, and the values shown in the figure are averages.

Three bands were fitted for Fe^{2+} absorptions, representing the $^5T_2(D) \rightarrow {}^5E(D)$ transition for distorted octahedral sites, the $^5E(D) \rightarrow {}^5T_2(D)$ transition for tetrahedral sites, and dynamic Jahn-Teller distortion of the main octahedral peak. No bands were fitted for the expected spin-forbidden Fe^{2+} bands in the near-UV. They would have been obscured by the stronger Fe^{3+} bands which also occur in this region.

A total of ten Fe^{3+} absorption bands were identified in chapter 4.1.4.2. In this work, five Gaussian bands were fitted to represent them for glasses containing 0.2 molar % Fe_2O_3. This is because many of these bands overlap. Details of the actual fitted bands and the transitions they represent are shown in table 4.3.5.a. Several bands were fitted for the same transition in both octahedral and tetrahedral coordinations, because they occur at the same wavenumbers and it is impossible to separate them. The band fitted at ~16,000 cm^{-1} incorporates components from the $^6A_1(S) \rightarrow {}^4T_1(G)$ transition for tetrahedral Fe^{3+}, the $^6A_1(S) \rightarrow {}^4T_2(G)$ transition for octahedral Fe^{3+}, and any Fe^{2+}-O-Fe^{3+} coupling which produces an IVCT band in this region. Again the reason for this is that in reality the bands overlap. Some inaccuracy occurred as a result of this, but it is estimated that the fitted band maximum position is within 1000 cm^{-1} of the band maxima for all three bands. No band was fitted to represent the $^6A_1(S) \rightarrow {}^4T_1(G)$ transition for octahedral Fe^{3+} ions, predicted to occur at ~11,200 cm^{-1}. The band also represents octahedral Fe^{3+}

ions, which give much weaker absorption than tetrahedral ions. The fitted tetrahedral bands are themselves weak, and an octahedral band in this region would be 10-100 times weaker still (see chapter 4.1.1.2.). The band was also obscured by the strong, broad Fe^{2+} absorption centred ~10,000 cm^{-1}. Any attempts to fit this band proved fruitless, and fitting a band here would serve no purpose beyond the statistical.

The UV edge was fitted with an exponential function, as in previous work [6, 19, 21]. Modelling of 5 molar % Fe_2O_3 samples required fewer fitted bands due to the strength of the UV edge obscuring some of those at higher wavenumbers. This is discussed further in chapter 4.3.5.2.

Curve fitting of the spectra was done using the statistical package SPSS for Windows. This process required that optical spectra were broken up into sections, otherwise fitting became impossible. Especially at low Fe_2O_3 contents, if the whole spectrum were modelled at once, this produced inaccurate fitting. The spectra were therefore generally fitted in the following sections and order:

i) Exponential function fitted to the UV edge between about 27,000 and 30,000 cm^{-1}, of the form:

$$A = b_0 \times EXP(b_1 \times E) \qquad \text{(Equation 4.3.5.a.)}$$

where A = absorbance / cm^{-1}, b_0 = constant, b_1 = constant, E = wavenumber / cm^{-1}

ii) Gaussian absorption bands. All Gaussian distributions were fitted according to the formula:

$$y = I \times EXP\left(\frac{-(a-E)\times(a-E)}{(w\times w)}\right) \qquad \text{(Equation 4.3.5.b.)}$$

where I = intensity of absorption, E = wavenumber, w = half width at half height, a = wavenumber of measurement, y = intensity of measured absorbance at

a given wavenumber. Spectra were split into three parts for fitting: the near-UV (20,000 - 30,000 cm^{-1}), the visible (13,000 - 20,000 cm^{-1}), and the near-IR (4,500 - 13,000 cm^{-1}). The near-UV and near-IR parts were fitted separately, then these were used to fit the whole spectrum. This then allowed accurate fitting of the visible region.

Table 4.3.5.a. Bands Fitted to Optical Spectra at 0.2 molar % Fe_2O_3

Band	**Valence State**	**Transition / Coord^n.**	**Position / cm^{-1}**	**½ Width @ ½ Height / cm^{-1}**	**Absorbance α / cm^{-1}**
A	2+	$^5E(D) \rightarrow {}^5T_2(D)$ Tetrahedral	~ 4,800	~1,000	0.14 - 0.22
B	2+	Jahn-Teller	~ 7,500	~ 2,000	0.05 - 0.21
C	2+	$^5T_2(D) \rightarrow {}^5E(D)$ Octahedral	~ 10,000	~ 4,000	0.38 – 0.75
D	3+	$^6A_1 \rightarrow {}^4T_1(G)$Tet $+{}^6A_1 \rightarrow {}^4T_2(G)$ Oct + IVCT	~ 16,000	~ 2,500	0.04 – 0.20
E	3+	$^6A_1 \rightarrow {}^4T_2(G)$ Tetrahedral	~ 20,000	~ 2,000	0.02 – 0.09
F	3+	$^6A_1 \rightarrow {}^4E, {}^4A_1(G)$ Oct + Tet	~ 23,000	~ 1,500	0.02 – 0.18
G	3+	$^6A_1 \rightarrow {}^4T_2(D)$ Oct + Tet	~ 24,200	~ 1,000	0.03 – 0.15
H	3+	$^6A_1 \rightarrow {}^4E(D)$ Oct + Tet	~ 26,300	~ 650	0.15 – 0.40

4.3.5.1. Glass Containing 0.2% Molar Fe_2O_3

Figures 4.3.5.1.a. and 4.3.5.1.b. show typical modelled spectra. Problems were encountered when fitting the region 20,000 - 30,000 cm^{-1} for most samples. Figure 4.3.5.1.a. shows a case where the fitting program fitted this region poorly, and figure 4.3.5.1.b. shows a case where the fitted spectrum more closely resembled that expected from literature [19, 51]. The UV edge was fitted for all samples with an exponential function, but the program had particular difficulty fitting the two peaks near 23,000 and 24,000 cm^{-1}. It often fitted one large, broad peak instead of two smaller ones, accompanied by a small peak near 25,000 cm^{-1}, for which no justification can be found. It was necessary to fit the peak near 26,300 cm^{-1} separately.

Figure 4.3.5.1.a. Computer Model of the Optical Absorption Spectrum of Sample 24, SiO_2-Na_2O-CaO-0.2 % Fe_2O_3 Glass

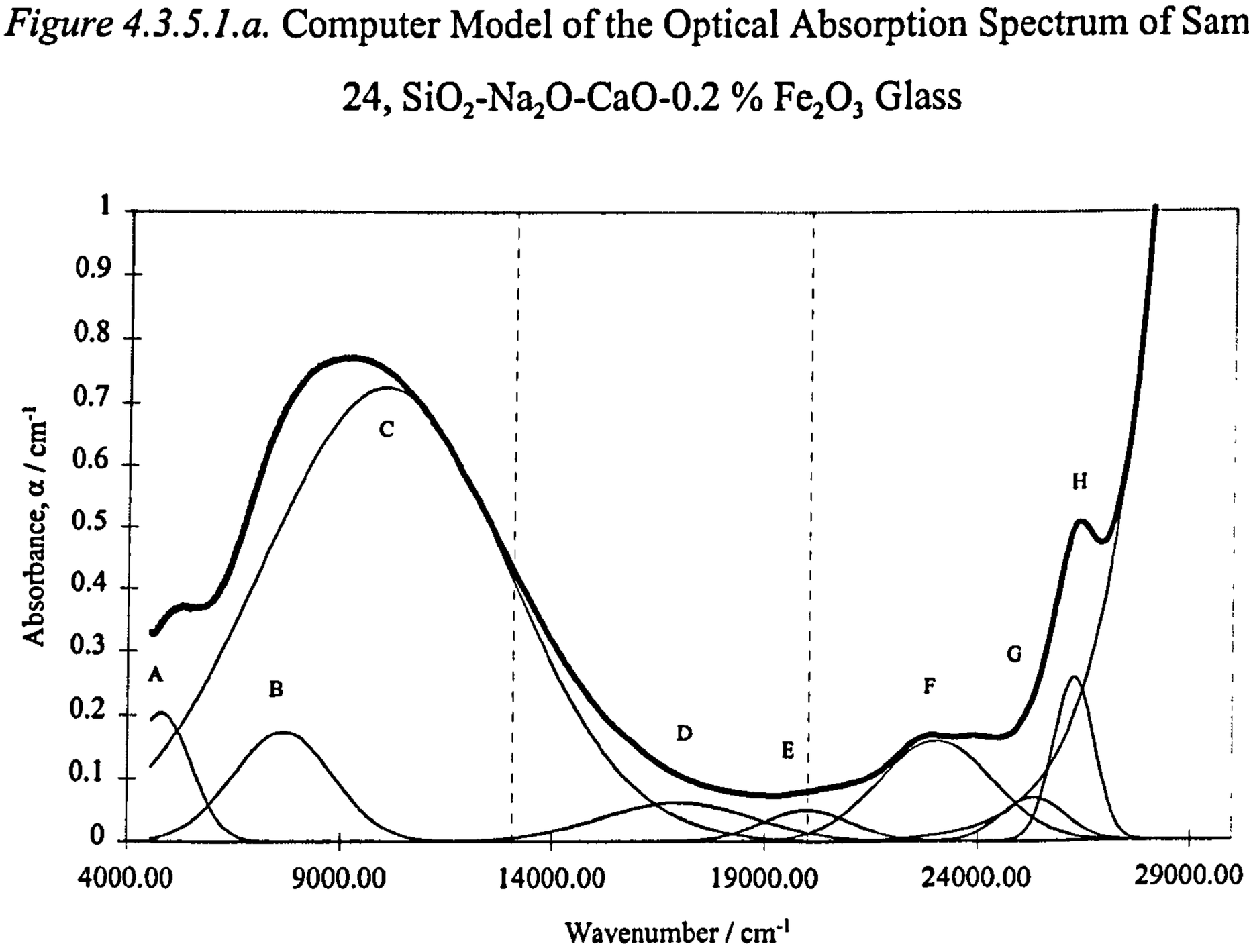

Figure 4.3.5.1.b. Computer Model of the Optical Absorption Spectrum of Sample 54, SiO_2-Cs_2O-CaO-0.2 % Fe_2O_3 Glass

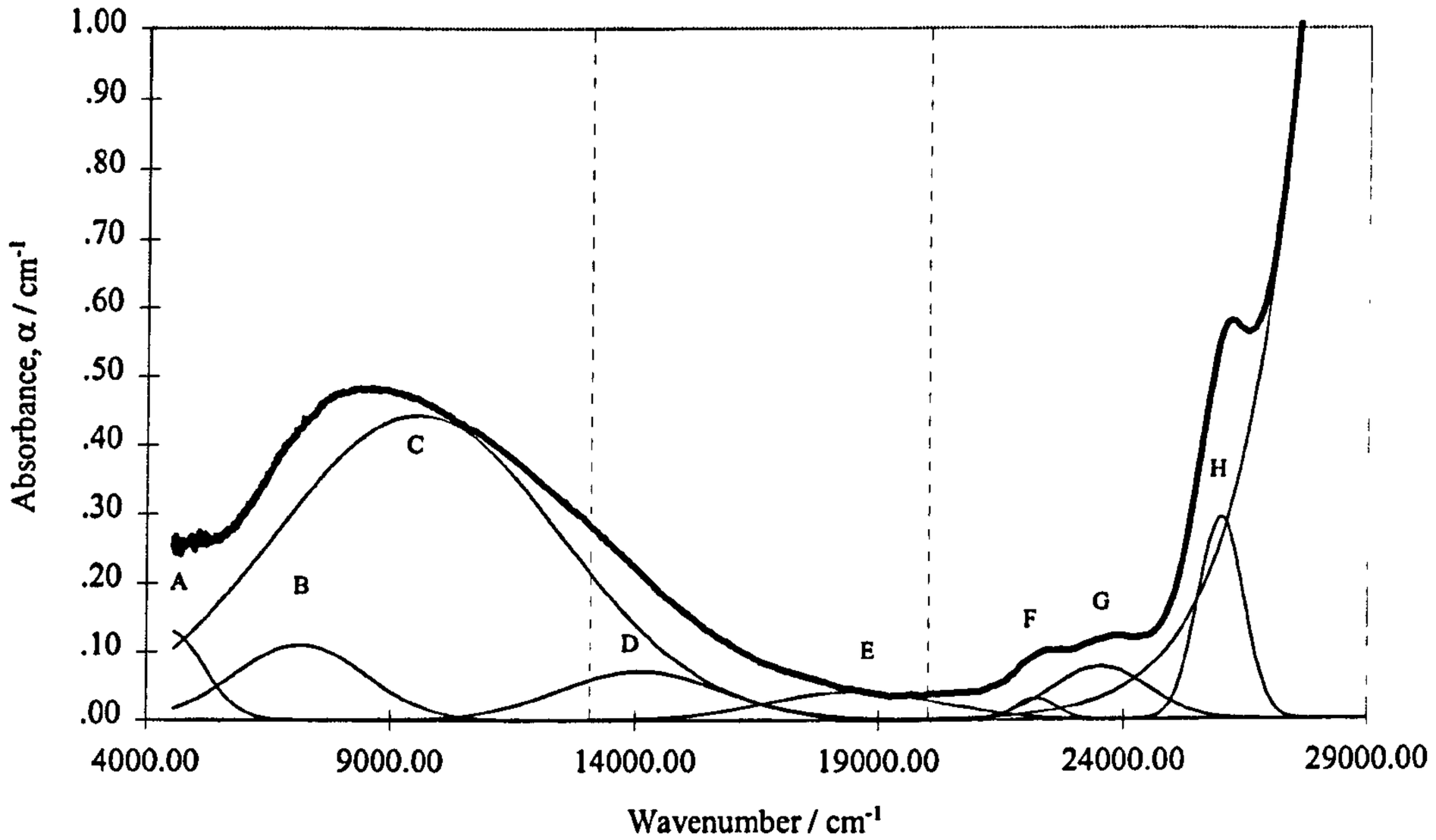

Peak wavenumbers of the three fitted bands associated with Fe^{2+} ions showed systematic changes with changing glass composition, as described by Λ, the optical basicity of the glass, shown in figure 4.3.5.1.c. These changes were such that increasing optical basicity of the glass moved the fitted bands to lower wavenumbers. There was no relationship with alkali / alkaline earth ionic radius ratio. The lines shown in figure 4.3.5.1.c. constitute linear best fits to each data set.

Figure 4.3.5.1.c. Fitted Peak Wavenumber vs. Optical Basicity for Fe^{2+} Bands

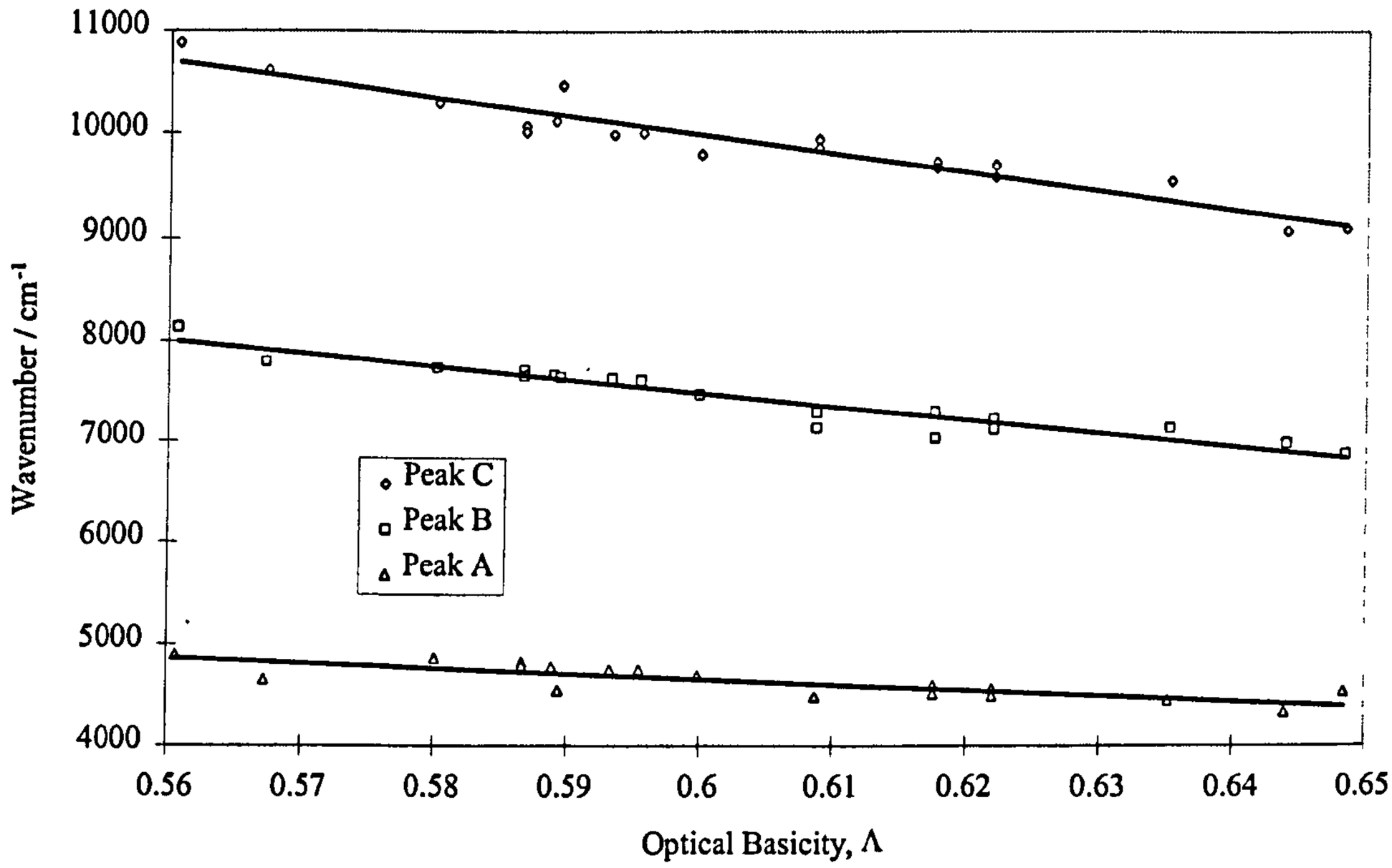

The most characteristic Fe^{3+} absorption, caused by the $^6A_1(S) \rightarrow {}^4E(D)$ transition, occurs at ~26,300 cm^{-1} (380 nm), where it is predicted to occur by Tanabe-Sugano matrices for tetrahedral and octahedral coordination. This band is barely affected by ligand field (i.e. by *Dq*). Despite this fact, the position of the fitted band moved linearly with optical basicity Λ, as shown in figure 4.3.5.1.d. It should be noted that these changes in peak wavenumber represent a change of less than 7 nm between extreme cases. Data points were only measured every 1 nm, so errors are relatively high. A change of less than 7 nm is an extremely small change when compared with the effects composition has on the Fe^{2+} absorption bands.

Figure 4.3.5.1.d. Fitted Absorption Maxima of Fe^{3+} $^6A_1(S) \rightarrow {}^4E(D)$ Transition with varying Optical Basicity

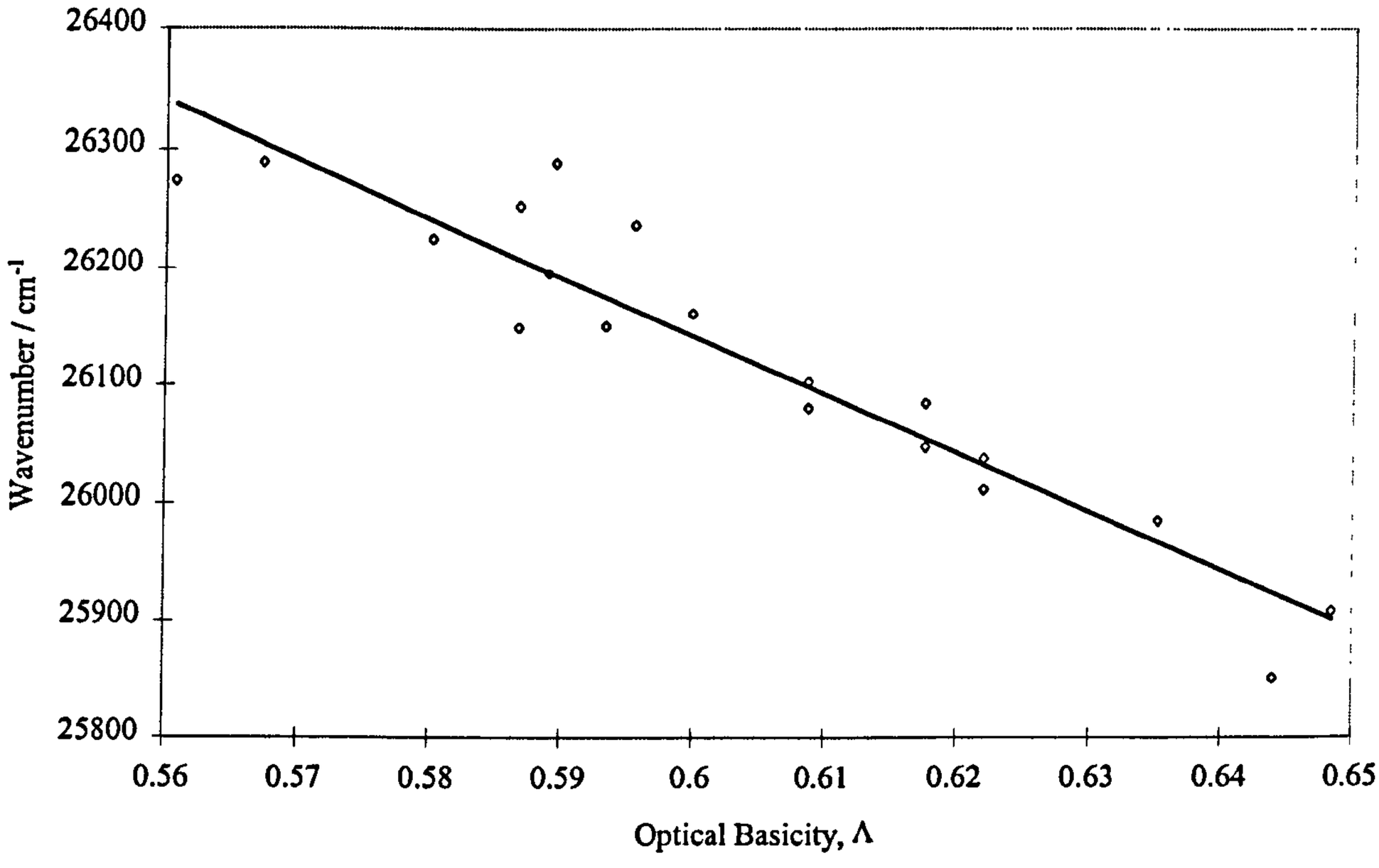

4.3.5.2. Glass Containing 0.1 – 5 Molar % Fe_2O_3

Spectra for the series SiO_2-Na_2O-CaO-(0.1, 0.2, 0.5, 1, 2, 3, 4, 5% Fe_2O_3) were computer fitted. With increasing Fe_2O_3 content the UV edge moved to lower and lower wavenumbers. Absorption coefficients rose dramatically, and certain absorption bands became more prominent. For example the area contained by the band fitted ~16,000 cm^{-1} showed a large increase with increasing iron content.

To the eye, some bands, such as that at ~10,000 cm^{-1}, appeared to change both in width and position with changing iron content, but fitted peak wavenumbers and widths were largely unaffected by Fe_2O_3 content. Peak intensities and thus peak areas, on the other hand, were strongly affected by Fe_2O_3 content, as shown in figure 4.3.5.2.a. In particular the intensities of the peak fitted near 10,000 cm^{-1} and the peak fitted near 16,000 cm^{-1} increased strongly with Fe_2O_3 content. From examination of the spectra in chapter 4.3.3., with increasing Fe_2O_3 content, the

position of the absorption peak near 10,000 cm^{-1} moves to higher wavenumbers. The computer modelling shows that this comes about through the increased absorption in the visible region by the band near 16,000 cm^{-1} rather than from the 10,000 cm^{-1} band actually changing position.

Figure 4.3.5.2.a. Areas of Modelled Absorptions with Varying Fe_2O_3 Content

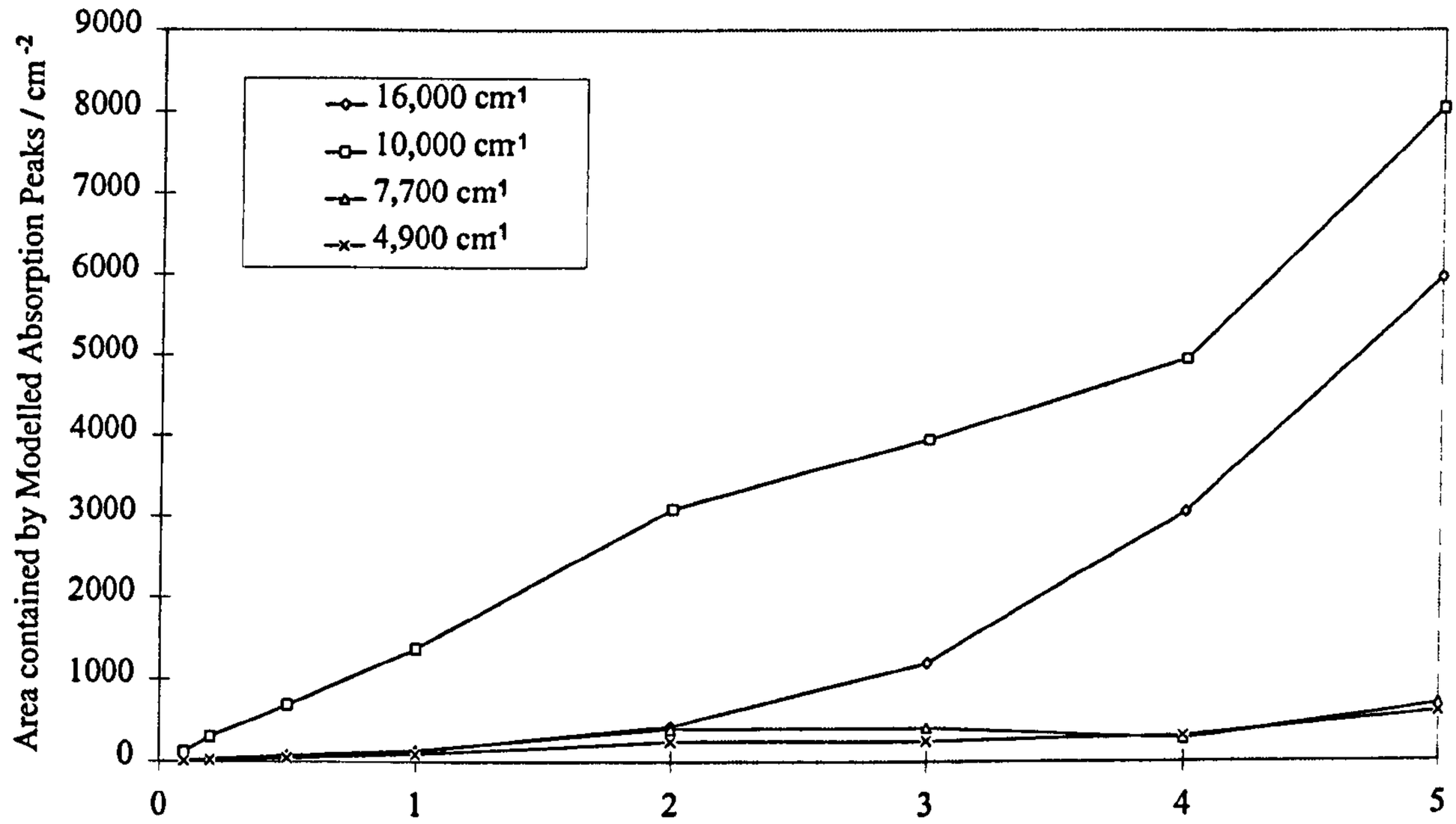

The area contained by the peak near 16,000 cm^{-1} with increasing iron content was very similar to a trend found in ESR spectra (see chapter 5), which links the amount of clustering of Fe^{3+} ions with Fe_2O_3 content. The band intensity I is approximately proportional to the square of the Fe_2O_3 content, such that:

$$I \propto (Fe_2O_3\ \%)^2 \quad \text{(Equation 4.3.5.2.a.)}$$

4.3.5.3. Calculation of Racah Parameters

As shown in chapter 4.1.3.3., it is possible to calculate the Racah B and C

parameters for Fe^{3+} ions directly from their optical spectrum. The actual wavenumbers of the two absorption bands move slightly with composition, but some error is introduced by the complicated nature of the absorption in this part of the spectrum. Computer modelling failed to give accurate data on the positions of these bands, so peak positions were found by subtracting the fitted exponential UV edge component from the corrected spectrum, then visually checking the data. Figures 4.3.5.3.a. and 4.3.5.3.b. show the calculated Racah B and C parameters, which observe approximate proportionality with the alkali / alkaline earth ionic radius ratio and cation field strength ratio. Ionic radius ratio is used in the figures. Errors were calculated as approximately 2 % for Racah B and 1 % for Racah C.

Figure 4.3.5.3.a. Fe^{3+} Racah B Parameter with Changing Composition

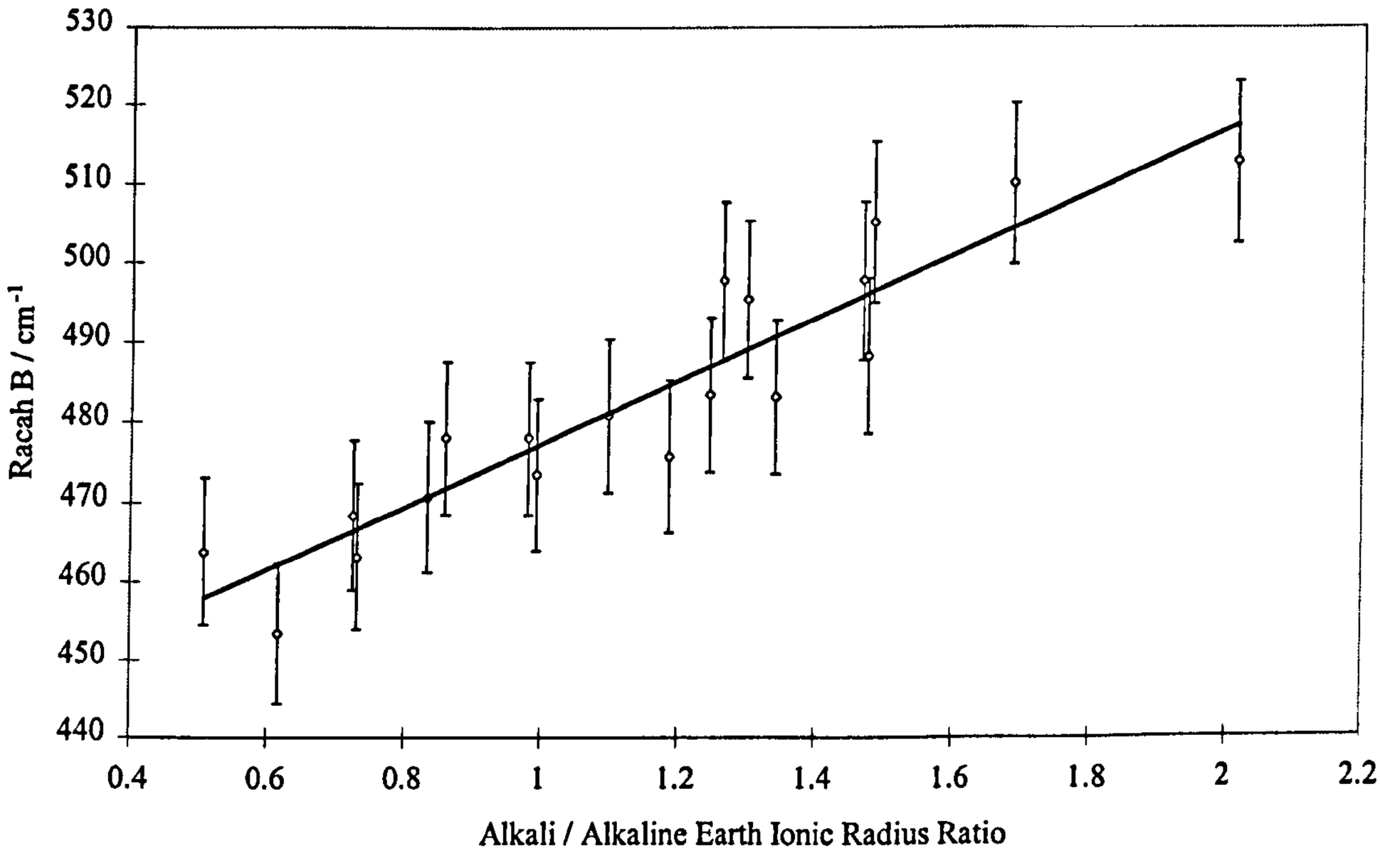

Figure 4.3.5.3.b. Fe^{3+} Racah C Parameter with Changing Composition

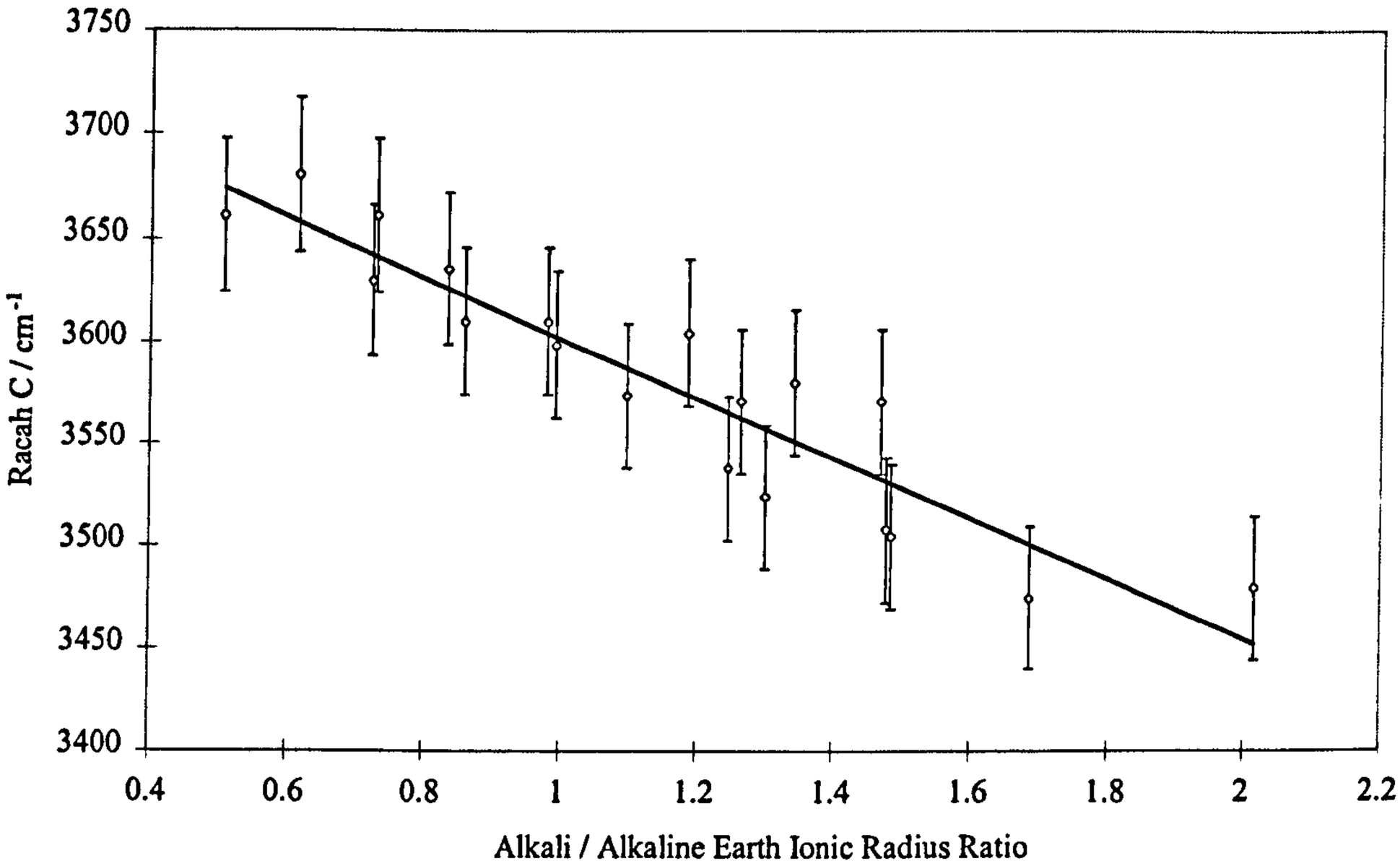

4.3.6. Calculation of Extinction Coefficients

Calculations of the extinction coefficients for Fe^{2+} and Fe^{3+} were carried out. This allowed calculation of redox ratios from optical spectroscopy. Quantitative analysis of the extinction coefficient can also provide structural and environmental information about the Fe ions in glass.

The density of the glass had to be measured in order to obtain the concentration of total iron present, as this varied with glass composition. The total volume of glass was found from the mass and density, then the mass of Fe_2O_3 obtained from batch calculations, hence the number of moles of Fe_2O_3 calculated. Concentration was found from the number of moles of Fe_2O_3 / volume of glass.

In order to obtain extinction coefficients for Fe^{2+} and Fe^{3+} ions, several quantities must be known:

- Absorbance. For Fe^{2+} this was provided by measured absorbances from the peak near 10,000 cm^{-1}. For Fe^{3+}, the curve-fitted absorbance values for the peak near 26,300 cm^{-1} was used.
- Fe_2O_3 concentration. This was calculated from density values provided by the Archimedes method.
- Redox $Fe^{2+}/\Sigma Fe$ measurements. This allowed calculation of the concentration of Fe^{2+} and Fe^{3+} ions per unit volume. Redox values were either taken from wet chemical measurements or regressions therefrom.

The Beer-Lambert Law states that:

$$A = -\varepsilon cl$$

where A = absorbance (arbitrary units), ε = extinction coefficient (litres mol^{-1} cm^{-1}), c = concentration of absorbing species - Fe^{2+} or Fe^{3+} (mol l^{-1}), l = path length (cm). Manipulation of the formula and using the values of A, c and l which are known, gives the extinction coefficient.

Wet chemical redox measurements were used where available. Where they were not, predicted values were used (see chapter 4.3.7.1.).

4.3.6.1. Fe^{2+} Extinction Coefficient, $\varepsilon(Fe^{2+})$

Figure 4.3.6.1.a. shows $\varepsilon(Fe^{2+})$ for all the 0.2 molar % Fe_2O_3 glasses melted under standard conditions. For all compositions studied, alkali / alkaline earth ionic radius ratio is proportional to $\varepsilon(Fe^{2+})$. An identical relationship links glasses containing CaO, SrO and BaO. Glasses containing MgO give lower values of $\varepsilon(Fe^{2+})$, but obey the proportionality with an identical gradient.

Figure 4.3.6.1.a. Fe^{2+} Extinction Coefficient (ε) with Varying Alkali / Alkaline Earth Ionic Radius Ratio

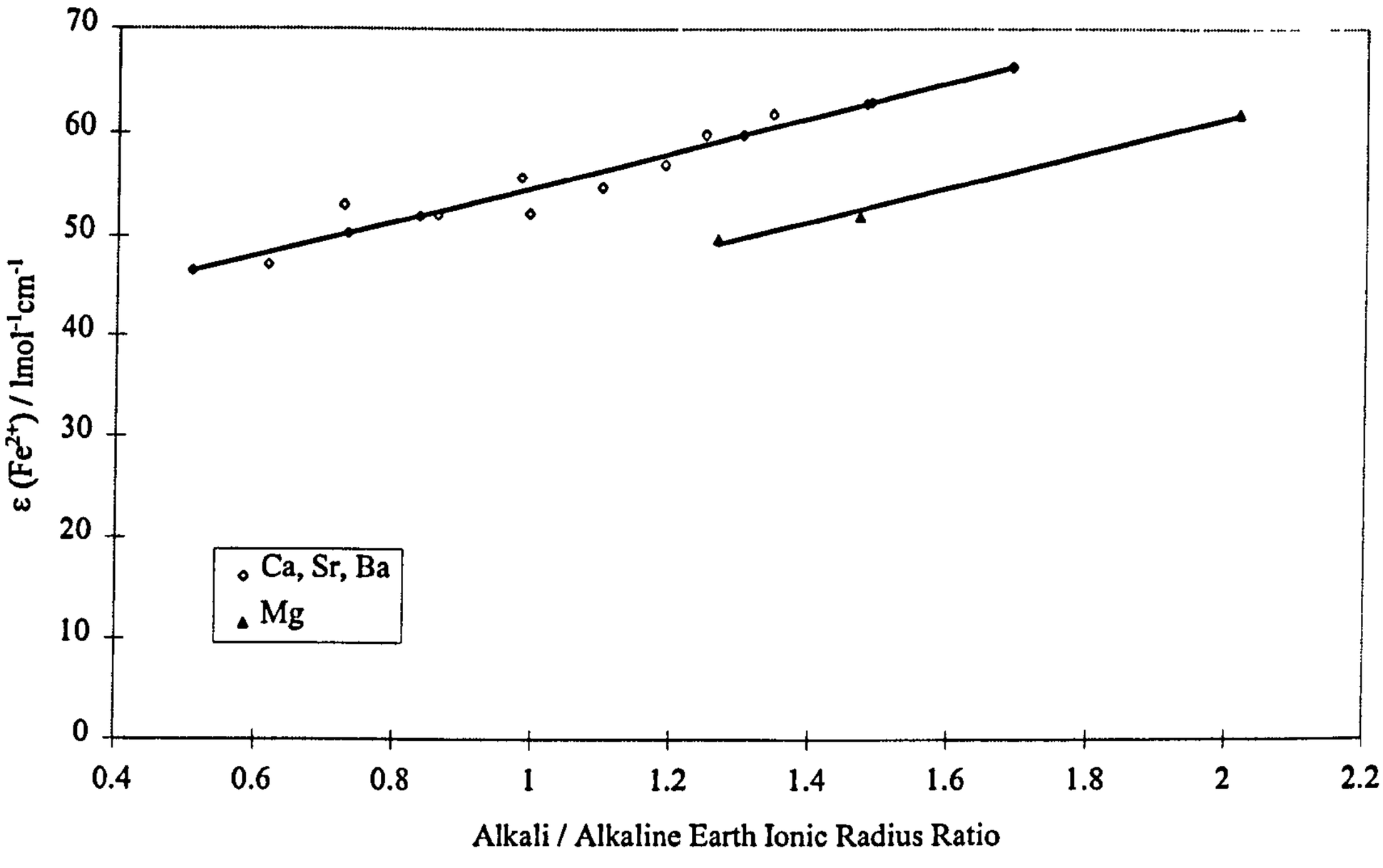

4.3.6.2. Fe^{3+} Extinction Coefficient, ε(Fe^{3+})

The calculation of ε(Fe^{3+}) was based upon the absorbance of the peak at ~26,300 cm^{-1}, widely attributed to Fe^{3+} in both tetrahedral and octahedral sites (see chapter 4.1.4.2.). Computer fitting was carried out to separate this peak from the UV edge and other nearby bands. From this, ε(Fe^{3+}) was calculated in the same way as ε(Fe^{2+}). Figure 4.3.6.2.a. shows ε(Fe^{3+}) for many of the 0.2 molar % Fe_2O_3 glasses studied. Again it can be seen that the MgO glasses, which are highlighted as black triangles, behave somewhat differently to the other alkaline earths.

Figure 4.3.6.2.a. ε(Fe^{3+}) from Optical Measurements, with Varying Alkali / Alkaline Earth Ionic Radius Ratio

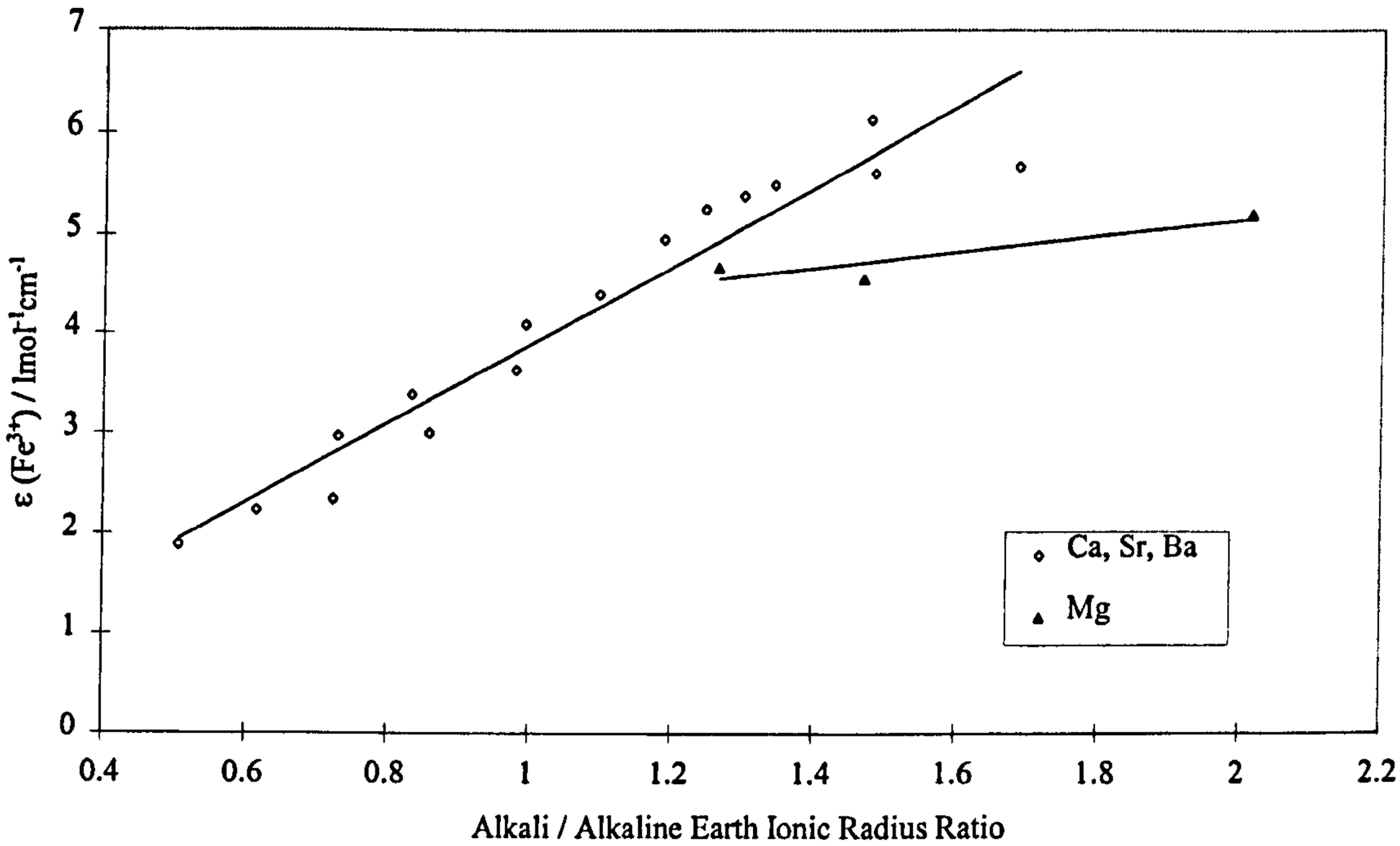

4.3.7. Wet Chemical Redox Measurements

Wet chemical redox analyses were both costly and time consuming to Pilkington, so only a selection of analyses could be made. The compositions to be analysed were chosen carefully as a result. Results for all the samples measured by this technique are given in appendix B, table B3.

4.3.7.1. Glasses Containing 0.2 Molar % Fe_2O_3

The relationship between redox and composition in these glasses is complex. The optical basicity scale can be used to show trends in redox with composition, but only with variation in one oxide type at a time. For a given alkaline earth oxide, increasing optical basicity brought about by variation in type of alkali oxide (i.e.

$Li_2O \rightarrow Cs_2O$), resulted in a *decrease* in the $Fe^{2+}/\Sigma Fe$ ratio (see figure 4.3.7.1.a.). On the other hand, for any given alkali oxide, increasing optical basicity brought about by variation in alkaline earth oxide (i.e. MgO → BaO) results in an *increase* in the $Fe^{2+}/\Sigma Fe$ ratio (see figure 4.3.7.1.b.). Hence the influences of alkali oxide and of alkaline earth oxide upon iron redox in these glasses are in opposition to one another. Redox values in these plots were taken from wet chemical measurements where possible, and from optical redox measurements where no wet chemical data was available.

Figure 4.3.7.1.a. Effect of Optical Basicity on Redox (1)

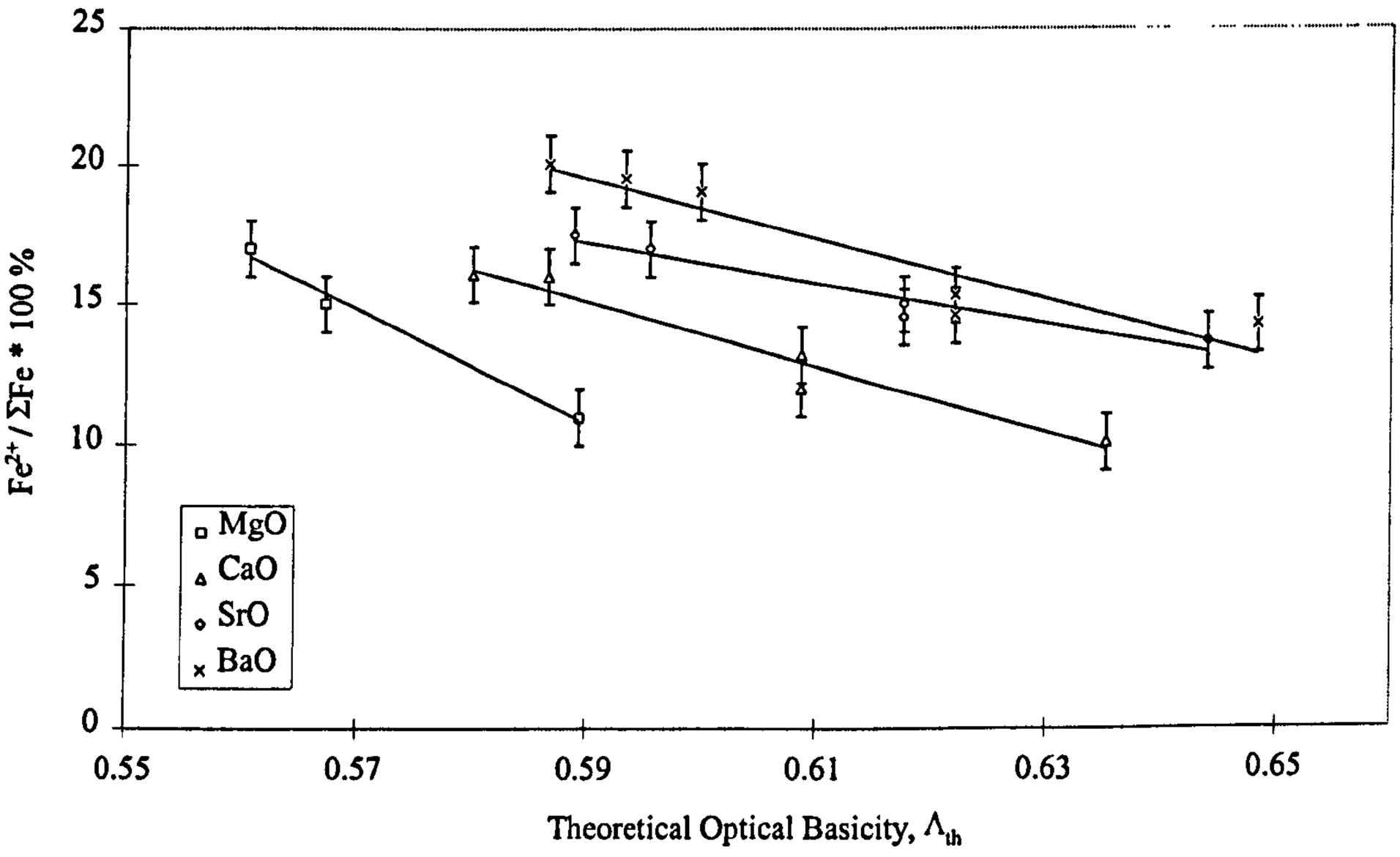

Figure 4.3.7.1.b. Effect of Optical Basicity on Redox (2)

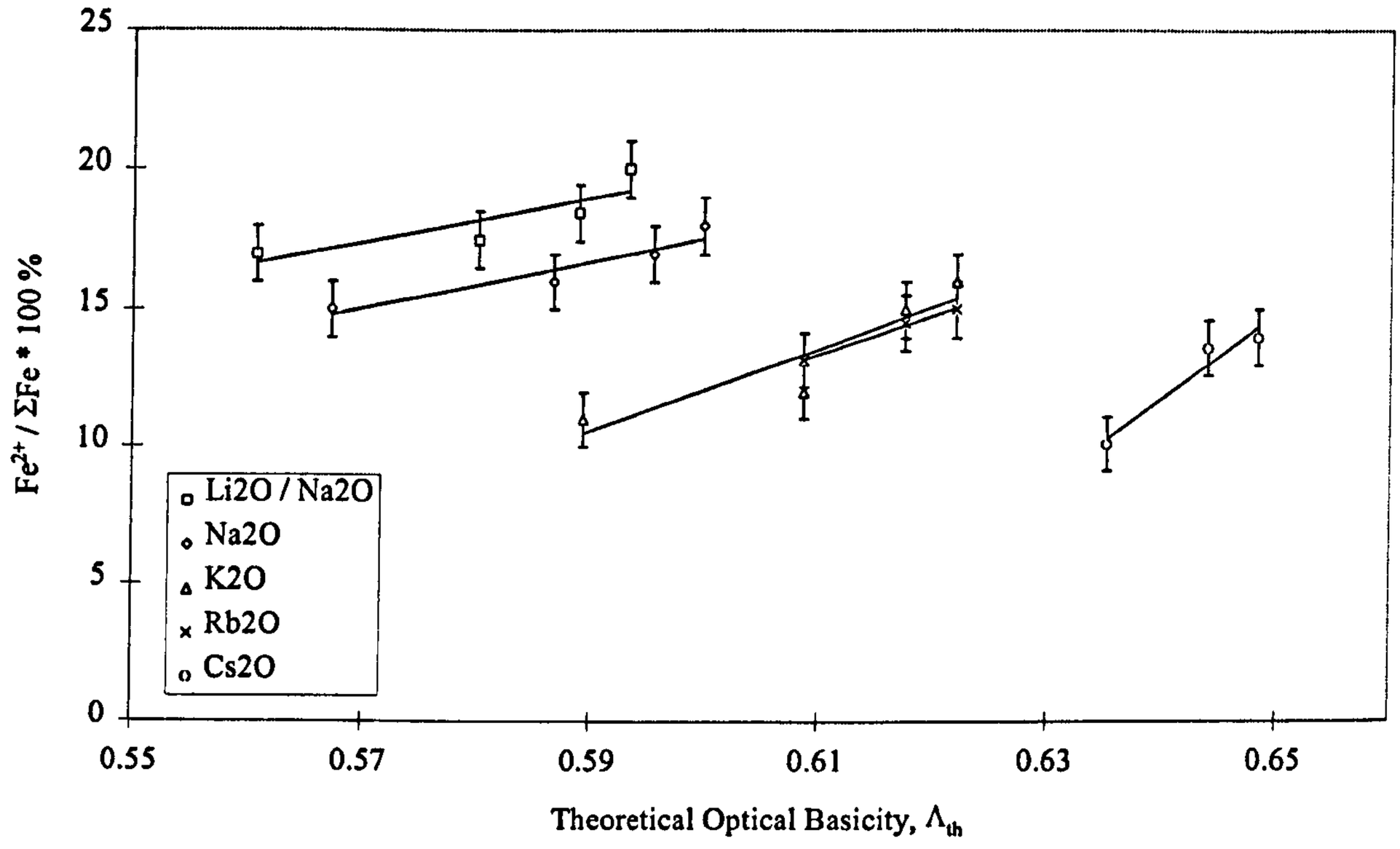

Plotting the redox ratio, $Fe^{2+}/\Sigma Fe$, against the alkali / alkaline earth ratio of either the Pauling ionic radii, the cation field strength, Z/a^2, or the optical basicities of the individual oxides, yielded linear relationships. Figure 4.3.7.1.c. shows only $Fe^{2+}/\Sigma Fe$ ratios measured by wet chemical analysis. Figure 4.3.7.1.d. extends the data series to include points for those glasses for which no wet chemical data was available. This was done using linear regressions of the wet chemical data: one for CaO, SrO and BaO glasses and another for MgO glasses, which are shown to behave differently. The Fe^{2+} content of samples containing MgO is somewhat higher than indicated by the linear relationship linking the other results, and these points are highlighted in the figures as black triangles. MgO glasses follow a similar linear relationship, but removed somewhat from that linking glasses containing CaO, SrO and BaO.

Using linear regressions to predict redox ratios in glasses for which no wet chemical data was available was reasonable since there was very little deviation over the wide range of samples which *were* measured. There may be slightly larger error bars associated with these predicted points, however the data is considered relevant. If the predicted redox values were inaccurate, these deviations would be revealed through extinction coefficients. They did not do so

(see figure 4.3.6.1.a.).

Figure 4.3.7.1.c. $Fe^{2+}/\Sigma Fe$ Ratio versus Ionic Radius Ratio from Wet Chemical Measurements

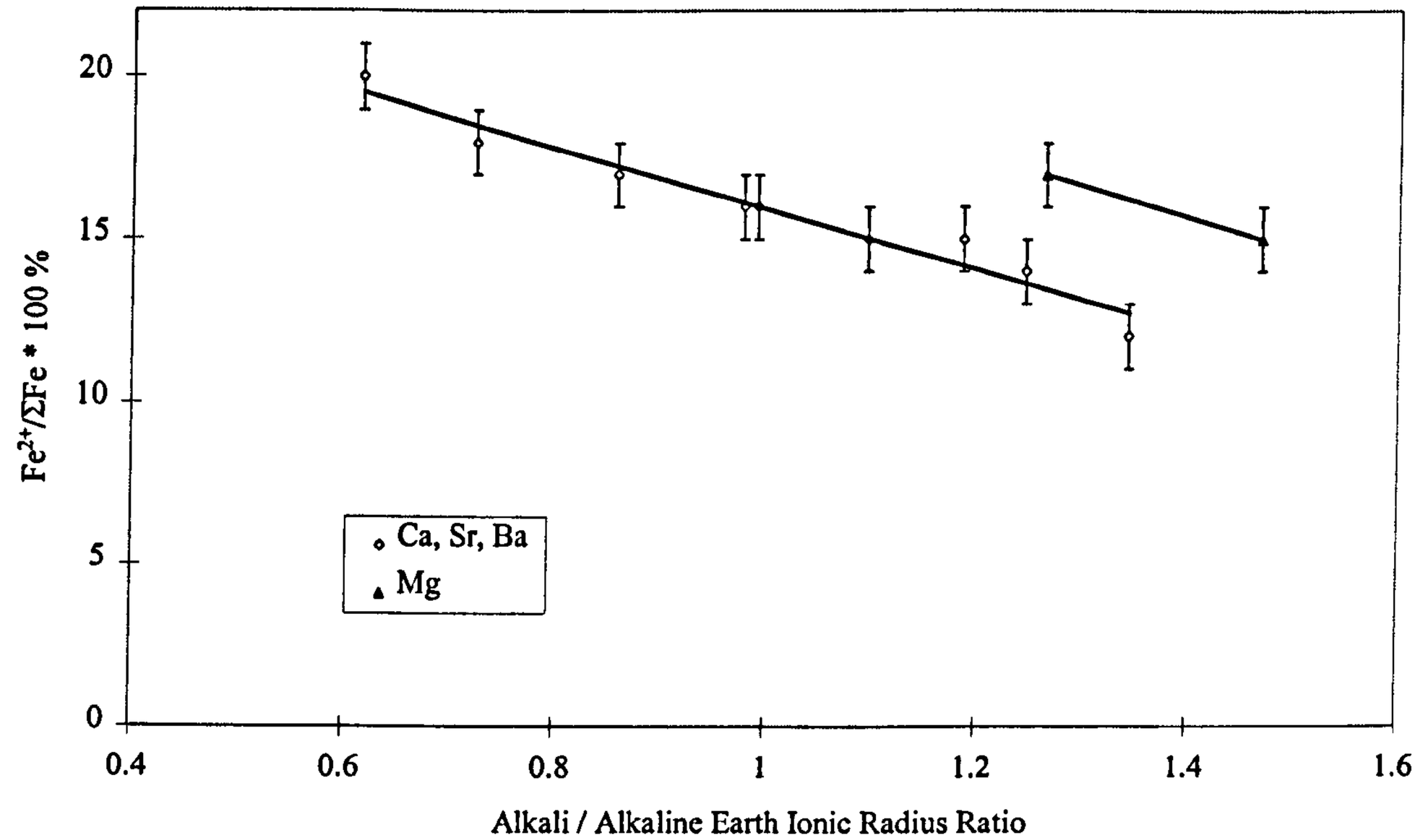

Figure 4.3.7.1.d. $Fe^{2+}/\Sigma Fe$ Ratio versus Ionic Radius Ratio including Estimated Values

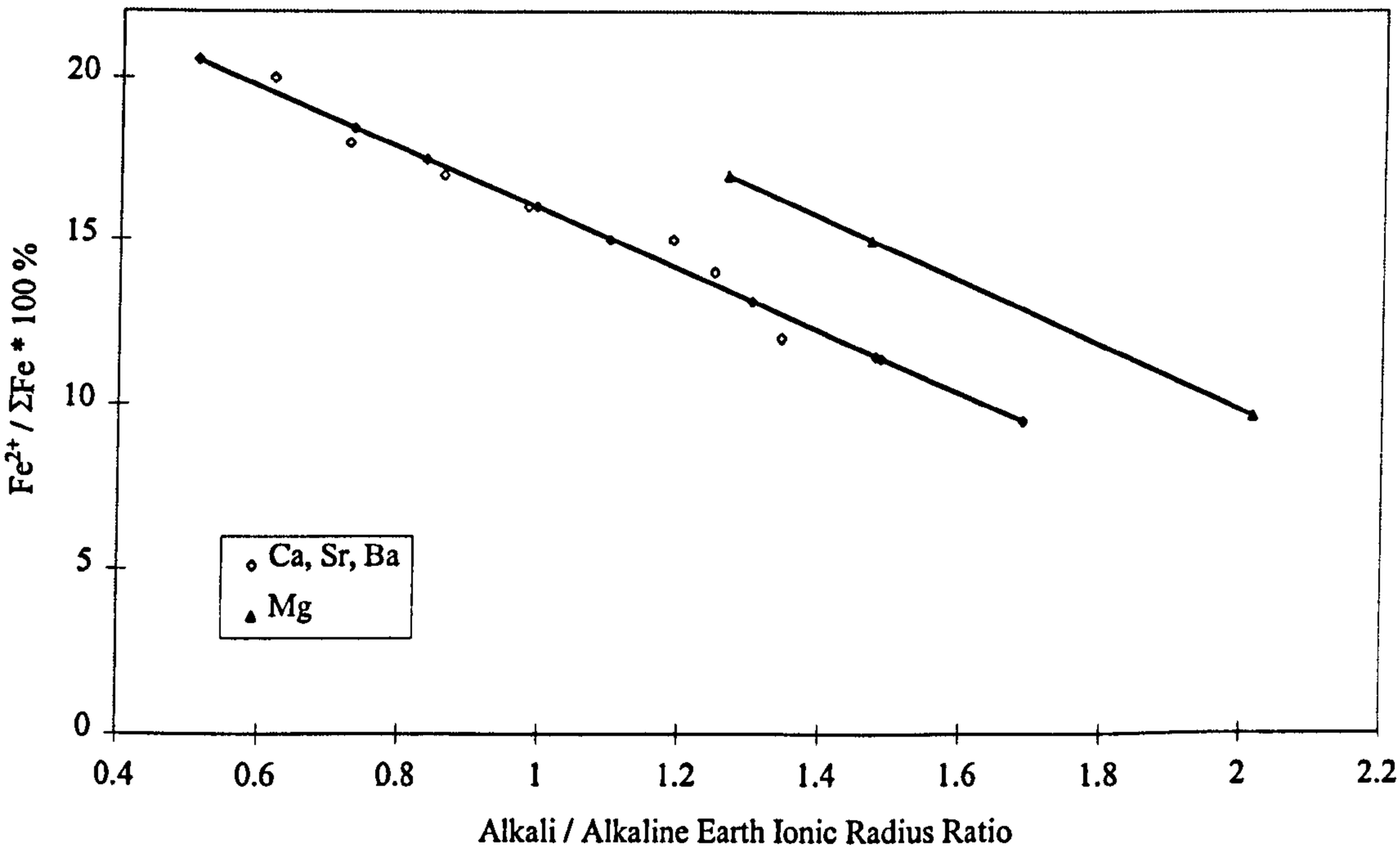

4.3.7.2. Varying Fe_2O_3 Content

Wet-chemical redox measurements in figure 4.3.7.2.a. indicate that samples in the system SiO_2-Na_2O-CaO-(0.1 to 5 % Fe_2O_3) show little change in redox with Fe_2O_3 content. A linear regression of the data gives the best fit at ~ 16.5 %. The sample containing 2 % Fe_2O_3 appeared to have somewhat higher Fe^{2+} levels than suggested by the other samples. This could have been caused by a slight contamination of batch, crucible or stirrer.

Figure 4.3.7.2.a. Wet Chemical Redox Results for SiO_2 - Na_2O - CaO Glasses with Varying Fe_2O_3 Content

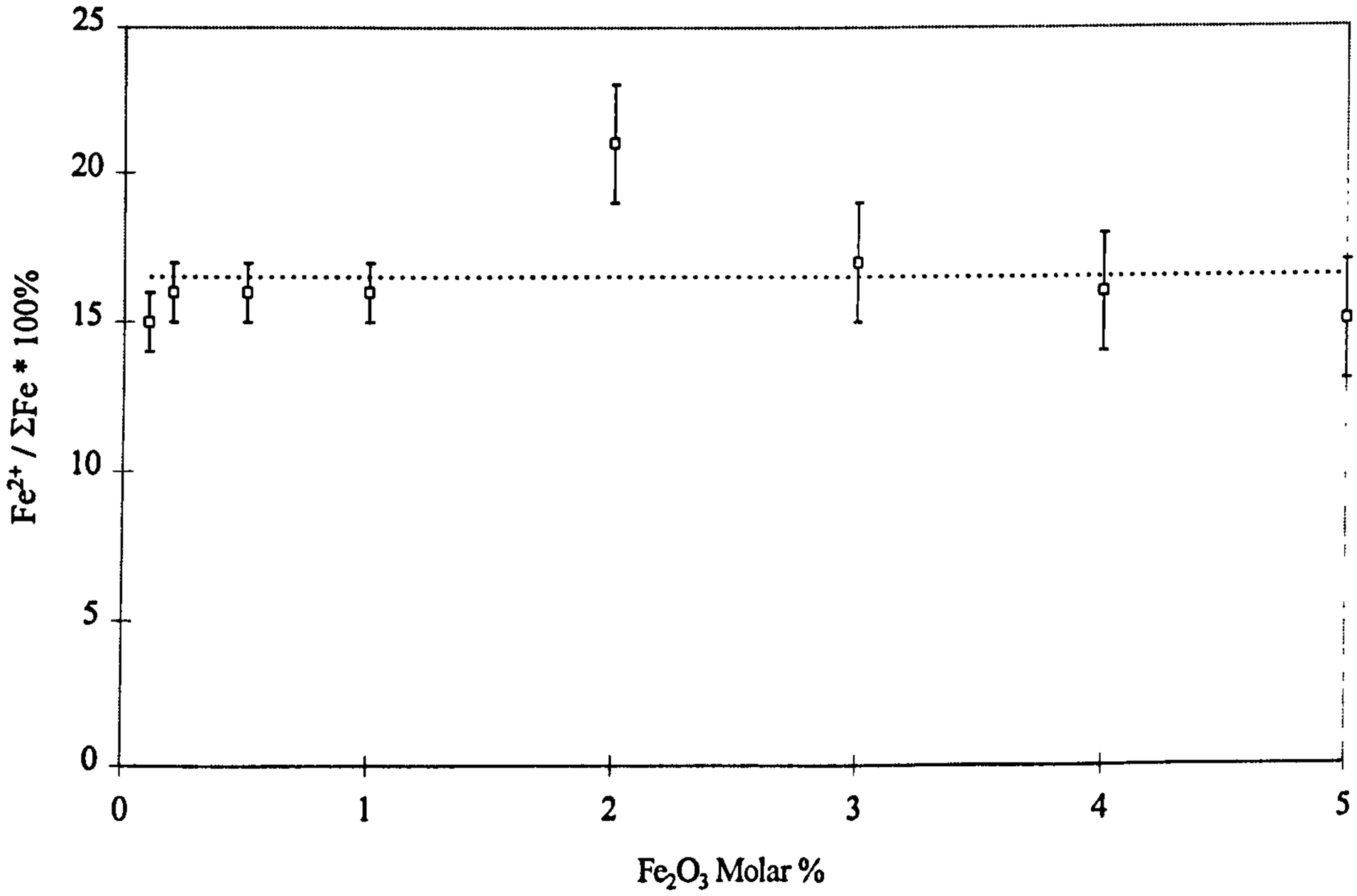

4.3.7.3. Glasses Containing 5 Molar % Fe_2O_3

Results for various glasses containing 1 or 5 molar % Fe_2O_3 showed no change in

redox within stated errors from the same base glasses containing 0.2 molar % Fe_2O_3, as shown in table 4.3.7.3.a., and in appendix B, table B3.

Table 4.3.7.3.a. Wet Chemical Redox Measurements of Other Glasses

Sample Numbers	Composition in Brief	$Fe^{2+}/\Sigma Fe$ at 0.2 % Fe_2O_3	$Fe^{2+}/\Sigma Fe$ at 1 % Fe_2O_3	$Fe^{2+}/\Sigma Fe$ at 5 % Fe_2O_3
20, 81	Li/Na-Ba	(20 ± 1) %	-	(18 ± 2) %
53, 83	Rb-Ba	(15 ± 1) %	-	(14 ± 2) %
56, 84	Cs-Ba	(14 ± 1) %	-	(15 ± 2) %
21, 65	Na-Mg	(15 ± 1) %	(14 ± 1) %	-

4.3.8. Redox Measurements Based on Optical Spectroscopy

4.3.8.1. Glasses Containing 0.2 % Fe_2O_3

Results for all the samples measured by this technique are given in appendix B, table B3.

Following calculation of extinction coefficients as detailed in chapter 4.3.6., prediction of the redox ratio $Fe^{2+}/\Sigma Fe$ could be carried out for all samples, again using the formula $A = -\varepsilon cl$, since the values of A, ε and l were known as well as the total Fe content.

Correlation of the $Fe^{2+}/\Sigma Fe$ ratio measured from both wet chemistry and this "optical Fe^{2+}" method agreed exceptionally well, within 1% for most samples. This method of calculating redox does require that the Fe^{2+} extinction coefficient be known. It is not necessarily a "quick and easy" method of redox determination.

Measurement of the $Fe^{2+}/\Sigma Fe$ ratio by optical methods has generally been

restricted to glasses of constant base composition with only the iron content and redox varying [71, 83]. This avoids the problems associated with changes in extinction coefficients brought about by changing the glass composition. The method used in this study accurately predicts the redox from optical spectra over a range of base compositions, although some initial measurements of a selection of the glasses must be carried out using a different technique such as wet chemistry in order to establish extinction coefficients, and the concentration of iron ions would have to be known. It is unnecessary to reproduce the results of this method for these glasses since they mirror so closely the wet chemical results discussed in chapter 4.3.7.1.

4.3.8.2. Varying Fe_2O_3 Content Glasses

The optical Fe^{2+} method used for estimating $Fe^{2+}/\Sigma Fe$ in glasses of composition SiO_2-Na_2O-CaO containing 0.1 - 5% Fe_2O_3 was an empirical method based on the combination of wet chemical and optical measurements. It was assumed that the extinction coefficient $\varepsilon(Fe^{2+})$ remained constant with all Fe_2O_3 contents investigated.

A single wet chemical measurement was used for predicting the redox in this series of glasses. The result chosen was that for the 0.2 % Fe_2O_3 sample, at $Fe^{2+}/\Sigma Fe$ = 16 %. The absorbance of the main Fe^{2+} peak near 10,000 cm^{-1} for each sample was compared with that of the 0.2 % Fe_2O_3 sample, and weighted according to actual Fe_2O_3 content. This gave a factor by which the original chemical measurement was multiplied to give the predicted $Fe^{2+}/\Sigma Fe$ value, as shown in figure 4.3.8.2.a. where they are compared with wet chemical and Mössbauer measurements of redox for the same glasses. Errors introduced by deviations in sample thickness and flatness have increasing effects on the optical Fe^{2+} value as Fe_2O_3 content increases.

The chart looks slightly confusing, and there is no easy way to plot all the data

and error bars. It can be seen, however, that though there is some spread in results a straight, flat line could be drawn across the chart at a $Fe^{2+}/\Sigma Fe$ of about 16 -17 %.

Figure 4.3.8.2.a. Comparison of Redox Measurements using Mössbauer, Wet Chemical and Optical Techniques

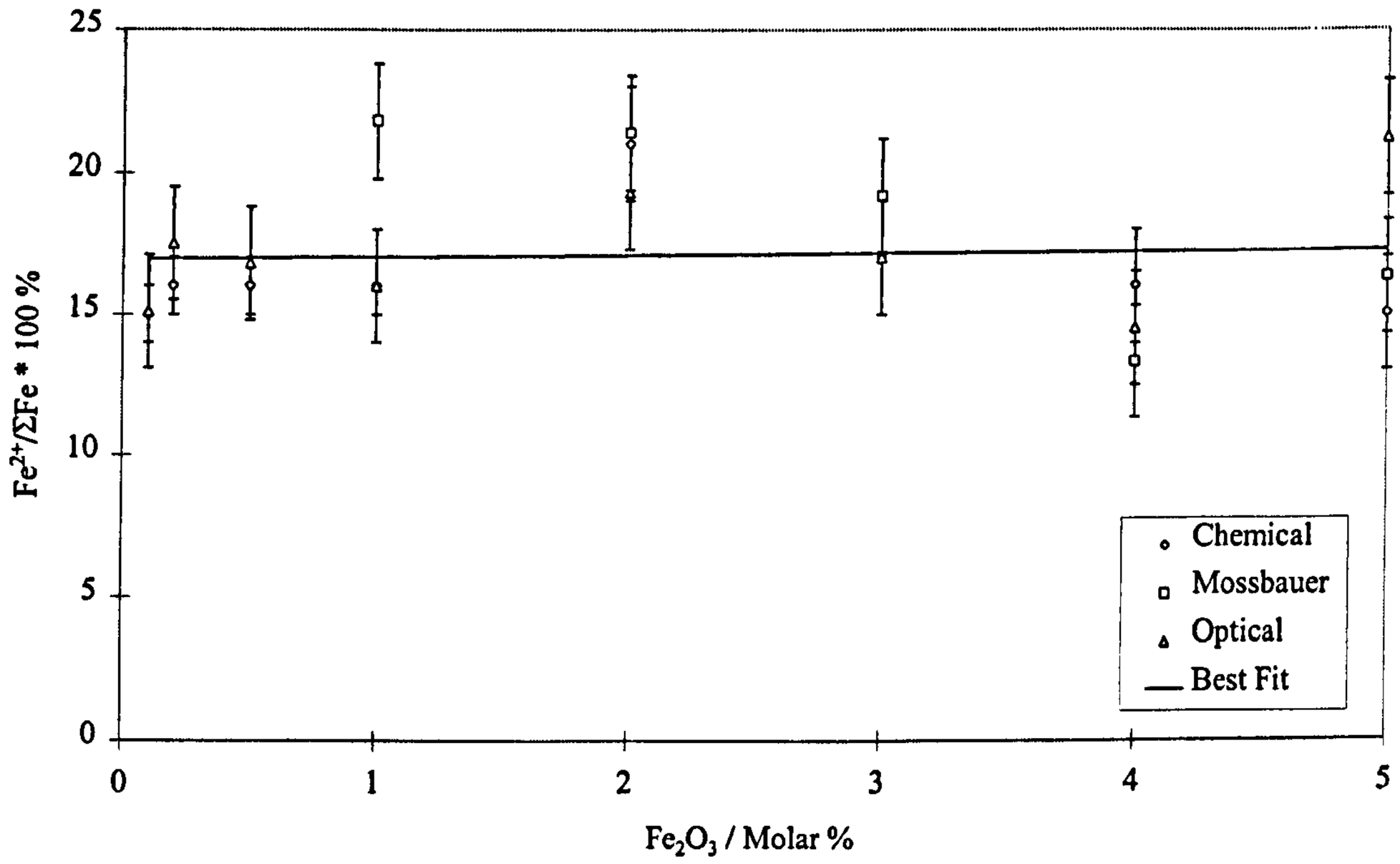

4.3.9. Photoluminescence (PL) Spectroscopy

Photoluminescence studies were carried out on all glasses containing 0.2 molar % Fe_2O_3 and one each of 0.5 and 1 % Fe_2O_3. At higher than 1 % Fe_2O_3, luminescence quenching meant that no luminescence was observed.

4.3.9.1. Photomultiplier Detector

The photomultiplier has a good response at visible wavenumbers, but which tailed

off rapidly below 12,500 cm^{-1} (above 800 nm). A 20,200 cm^{-1} (495 nm) high-pass filter was used. Entrance and exit slits on the monochromator were set at 2000 μm, which gave adequate light throughput. Spectra were measured from 20,000 to 12,500 cm^{-1} (500 to 800 nm). Measured spectra showed one low-intensity, broad luminescence peak centred in the red-visible, the exact wavelength of which varied with glass composition. Correction of this data for system response showed the band generally occurred at 13,000 - 15,000 cm^{-1} (667 – 770 nm). This peak appeared to have a gaussian profile and was so broad that measurement of the exact peak energy was difficult. Errors in peak position were therefore estimated at ± 200 cm^{-1} (10 nm).

Figure 4.3.9.1.a. shows a typical corrected PL spectrum, in this case sample 17, SiO_2-Li_2O-Na_2O-MgO-0.2 % Fe_2O_3. The peak position is shown to be 14,285 ± 200 cm^{-1} (700 ± 10 nm).

Figure 4.3.9.1.a. Corrected PL Spectrum of Sample 17

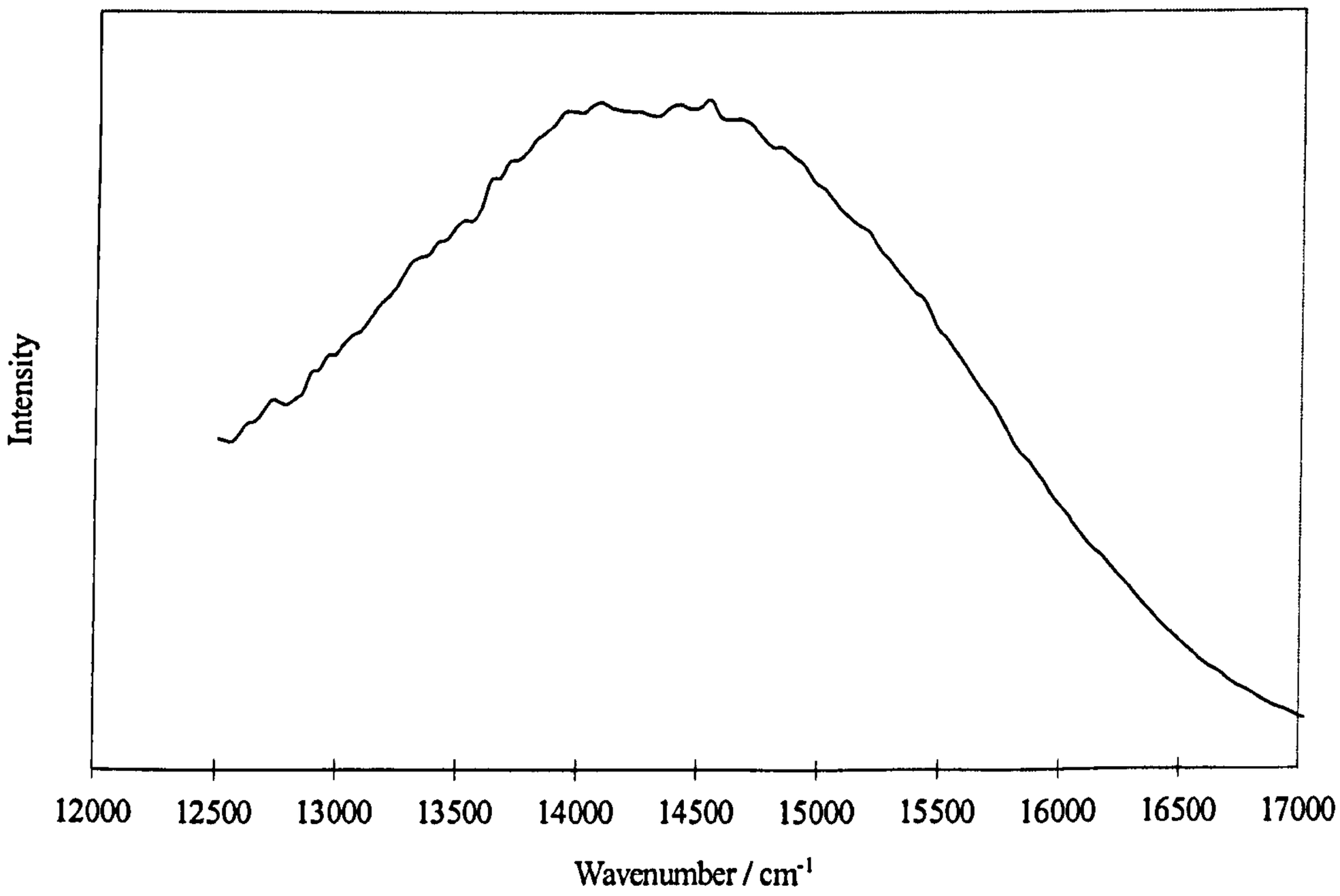

PL measurements were taken for all glasses containing 0.2 % Fe_2O_3, and also

certain glasses containing 0.1 – 1 % Fe_2O_3. Above 1 % Fe_2O_3, luminescence quenching rendered impossible the measurement of spectra.

Peak wavenumbers from some corrected spectra are shown in table 4.3.9.1.a. and show that varying the Fe_2O_3 content had no effect on luminescence wavenumbers.

Table 4.3.9.1.a. Corrected PL Peak Positions with Varying Fe_2O_3 Content

Fe_2O_3 / Molar %	**Peak Wavelength / nm**	**Peak Wavenumber / cm^{-1}**
0.1	705 ± 10	14,185 ± 200
0.2	710 ± 10	14,085 ± 200
0.5	705 ± 10	14,185 ± 200
1	700 ± 10	14,285 ± 200

The corrected parameters for all glasses of composition SiO_2-R_2O-RO-0.2 % Fe_2O_3 plus several other glasses containing 0.2 % Fe_2O_3, appear in appendix B, table B1. Of all samples containing Li_2O as the sole alkali oxide, only the sample also containing BaO was sufficiently free of phase separation to give an adequate PL spectrum.

Plots of the peak wavenumber against the ionic radius ratio of the alkali / alkaline earth cations yielded a linear relationship with some spread, as shown in figure 4.3.9.1.c.

Figure 4.3.9.1.c. PL Peak Position vs. Alkali / Alkaline Earth Ionic Radius Ratio

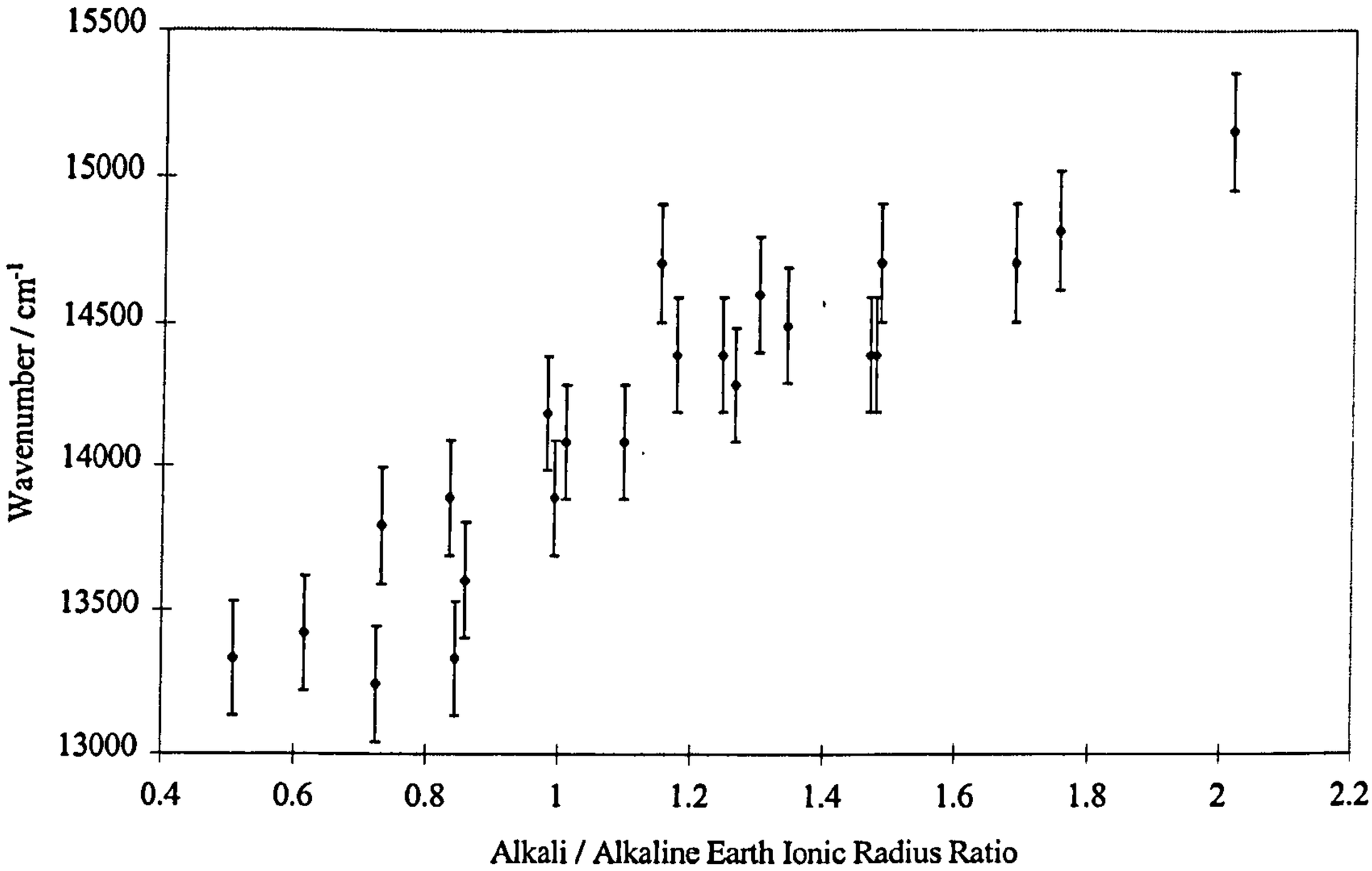

4.3.9.2. Germanium Detector

Luminescence spectra were measured in the red visible and near - IR using a North Coast EO-817-L germanium detector, which has a range of 5,555 - 16,667 cm^{-1} (1800 - 600 nm). Two different monochromators were used; a Jarrell-Ash monochromator blazed at 25,000cm^{-1} (400 nm), and a Bentham M-300 monochromator blazed near 10,000 cm^{-1} (1 μm).

Spectra were measured from 8,333 - 16,667 cm^{-1} (1200 - 600 nm). The measurement of the main luminescence band occurring in the range 13,000 - 15,000 cm^{-1} may have been affected by the response of the EO-817-L detector as the response dropped sharply as wavenumber approached 16,000 cm^{-1}. Tests showed that the photomultiplier gave better results in this region than the germanium detector.

Spectra recorded using the Jarrell-Ash monochromator all showed similar characteristics: a broad luminescence in the region of 14,000 cm^{-1} and a weaker,

narrower peak at approximately 11,400 cm^{-1}. This second peak was viewed with some caution: it may have been an artifact: a second-order laser line at double the laser wavelength; filter fluorescence; re-entrant spectra due to reflections in the monochromator; or some form of scattering effect were all possibilities. Spectra were re-measured using a series of different high-pass filters, all of which had no apparent effect on the peak measured at 11,000 – 12,000 cm^{-1}. The monochromator was checked internally to ensure no reflected or re-entrant light got through to the detector, although checking for this by eye was not infallible.

Spectra measured using the Bentham monochromator were similar to those measured using the Jarrell-Ash monochromator. Figure 4.3.9.2.a. shows a comparison of spectra from the two monochromators. The second peak near 11,000 cm^{-1} was at slightly lower wavenumbers to that measured using the Jarrell-Ash monochromator. The difference can be explained by the fact that the monochromators were blazed at very different wavelengths, and the Bentham is considered more accurate at these wavenumbers.

Figure 4.3.9.2.a. Corrected PL Spectra using Different Monochromators

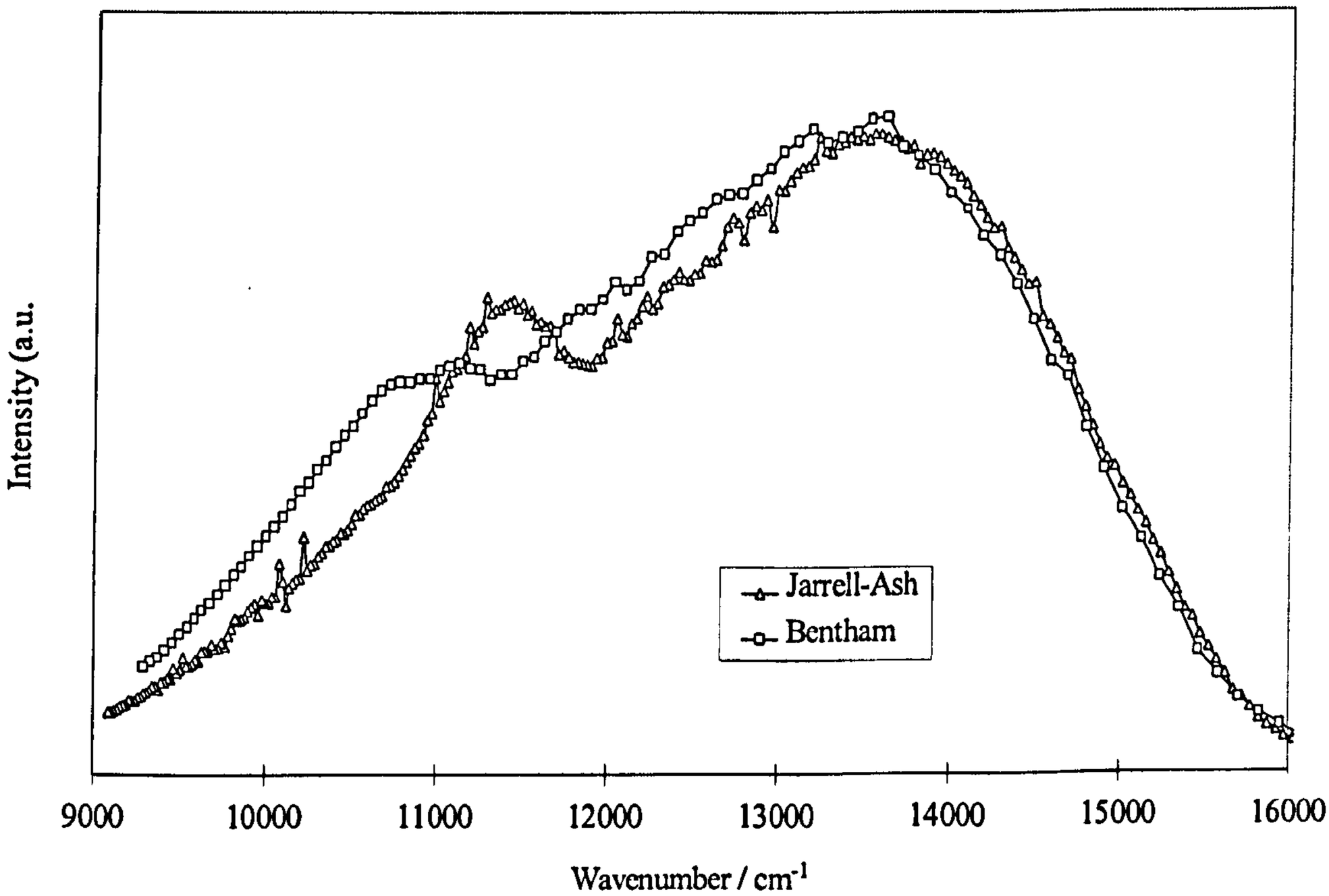

4.3.9.3. Computer Fitting of PL Spectra

The statistical package SPSS was used to fit one Gaussian peak to the corrected photomultiplier PL spectra. The fitting procedure was the same as was used for optical spectra (see chapter 4.3.5.) Intensity values are inconsequential since intensity data was qualitative only, however values of half-width at half-height and peak position could be modelled. A small selection of samples were fitted, giving the results shown in table 4.3.9.3.a. The results show that peak wavenumber changed significantly with glass composition, and peak width was of the order of 2000 - 2500 cm^{-1}.

Table 4.3.9.3.a. Parameters of Gaussian Band Fitted to PL Spectra

Sample Code	Composition	Peak / cm^{-1}	Peak Width / cm^{-1}
20	Si-Li-Na-Ba-0.2Fe	13,605	2615
42	Si-K-Ca-0.2Fe	14,530	1925
56	Si-Cs-Ba-0.2Fe	14,142	2560
63	Si-Na-Ca-0.5Fe	14,230	1880

4.4. Discussion

4.4.1. Base Glasses

Figures 4.3.1.a. and 4.3.1.b. show spectra of base glasses melted in Pt-2%Rh and mullite crucibles, respectively. The visible absorption bands in figure 4.3.1.a. indicate the presence in the glass of Pt^{4+} and / or Rh^{3+} ions [23, 24]. ICP chemical analysis (see chapter 4.3.1.) does not support this conclusion, because ICP measurements indicated that levels of Pt and Rh were lower in the discoloured

glass (SiO_2-Na_2O-BaO, sample 4) than in the colourless glass (SiO_2-Na_2O-MgO, sample 1). The ICP results were close to the limit of measurement of the technique, and must therefore be viewed with caution.

The UV edge occurred at lower wavenumbers in the glasses melted in mullite crucibles than in similar glasses melted in Pt-2%Rh crucibles. These differences were probably caused by dissolution of iron from the mullite crucible walls into the glass melt. Strong oxygen-metal charge-transfer (OMCT) bands shift the UV edge to lower wavenumbers (see chapter 4.1.2.1.).

4.4.2. Band Assignments and Computer Fitting for Iron-Containing Glasses

Computer fitting of spectra of iron-containing glasses, and subsequent band assignments (see chapter 4.3.5.) generally agreed with similar work on both low-iron [19] and high-iron [6] silicate glasses. This agreement was in terms of band intensities and assignments.

The number of bands fitted generally decreased with increasing Fe_2O_3 content. Increasing strength of the OMCT bands shifted the UV edge to lower wavenumbers, such that above certain Fe_2O_3 contents it obscured some of the Fe^{3+} *d-d* bands. In addition the increasing intensity of the Fe^{2+}-O-Fe^{3+} IVCT band fitted at ~16,000 cm^{-1} gave added complication. At 0.2 molar % Fe_2O_3, eight absorption bands plus the UV edge were fitted, but at 3, 4, and 5 molar % Fe_2O_3, six bands plus the UV edge were fitted.

4.4.2.1. Fe^{2+} Ions

Computer fitting of optical spectra (see chapter 4.3.5.) showed the presence of three absorption bands which can be attributed to Fe^{2+} ions. These three bands are

consistent with bands discussed in chapter 4.1.4.1. They represent distorted octahedral sites (~10,000 cm^{-1}), distortion splitting of the main octahedral peak, probably the dynamic Jahn-Teller effect (~7,500 cm^{-1}), and tetrahedral sites (~4,800 cm^{-1}). Changes in the ratio of peak intensities of the bands at ~10,000 cm^{-1} and ~4,800 cm^{-1} should indicate changes in the relative numbers of Fe^{2+} ions in tetrahedral and octahedral sites. Computer fitting gave no conclusive evidence on this point, although a small increase in the proportion of tetrahedral Fe^{2+} sites appears to occur with increasing alkali / alkaline earth ionic radius ratio. These changes were only small, so it can be inferred that the ratio of tetrahedral Fe^{2+} : octahedral Fe^{2+} ions is largely unaffected by glass composition. These findings are in agreement with other investigations [31, 46, 50]. As noted by Boon & Fyfe [45], the number of tetrahedral Fe^{2+} ions causing the band at ~4,800 cm^{-1} is small because the Laporte selection rule dictates that absorptions from tetrahedral sites are generally 10-100 times stronger than from octahedral sites. This lack of change with composition also indicates that both these sites are relatively stable and therefore it is difficult to cause large changes in the Fe^{2+} site occupancies in these glasses. Composition did, however, have a systematic effect on the extinction coefficient of the main Fe^{2+} band, and this is discussed in chapter 4.4.3.

Computer fitting has been particularly successful in showing the presence of an absorption band near 7,500 cm^{-1} which causes the apparent asymmetry of the absorption peak due to the $^5T_2 \rightarrow {}^5E$ transition of Fe^{2+} ions in distorted octahedral sites. This new band occurs in all samples at all measured iron contents. Comparison of the fitted band with data from the literature (see chapters 4.1.1.7. and 4.1.4.1.) indicates that it is caused by distortion splitting, probably the dynamic Jahn-Teller effect.

4.4.2.2. Fe^{3+} Ions

The fitted bands attributed to Fe^{3+} ions are shown in table 4.3.5.a. Previous work

[19] fitted an Fe^{3+} band at 13,600 cm^{-1} which was by far the strongest Fe^{3+} *d-d* band in terms of both peak height and area. There is a basis for fitting a band in this part of the spectrum: luminescence work in chapter 4.3.9. has shown the presence of the $^4T_1 \rightarrow {}^6A_1$ luminescence transition for tetrahedral Fe^{3+} ions. However there was no reason to fit a strong band such as that fitted by Ades et al [19]. Attempts at fitting another band in this region in addition to the bands near 16,000 cm^{-1} and 10,000 cm^{-1} were problematic and judged to be of little use beyond the statistical.

4.4.2.3. IVCT Band

The band fitted at ~16,000 cm^{-1} with a width of ~4,000 cm^{-1} is attributed to inter-valence charge transfer (IVCT). It has already been that this band becomes more prominent at visible wavenumbers with increasing Fe_2O_3 content in silicate glasses [5, 6]. Differences in the exact position and linewidth between the spectra in this work and that of Ookawa et al [6] are probably due to compositional differences between the two sets of glasses.

This band is direct evidence of Fe^{2+} and Fe^{3+} ions in next-nearest neighbour sites, i.e. clustered as groups of >1 ion. The area contained by this IVCT band increased approximately linearly with the square of the Fe_2O_3 content, as shown in chapter 4.3.5.2. This relationship is identical to that established by ESR as applying to Fe^{3+}-O-Fe^{3+} clusters (see chapter 5).

Computer modelling has indicated that an absorption band is present in this part of the spectrum at all Fe_2O_3 contents. For low iron concentrations the absorption had previously been attributed solely to *d-d* transitions of Fe^{3+} ions [18, 19, 51, 53, 60, 77]. It is probable that the absorption near 16,000 cm^{-1} has a contribution from IVCT interactions even at lower iron contents.

4.4.2.4. UV Edge

The UV edge in these glasses is primarily governed by their iron content: the higher the concentration of Fe ions, the lower the wavenumber at which the UV edge occurs [15, 16, 18, 21]. This phenomenon is caused by oxygen-metal charge transfer (OMCT) bands. As discussed in chapter 4.1.1.5., the strength of the OMCT bands depends not only upon the iron concentration, but on glass redox and composition. Figures 4.3.1.a, 4.3.1.b., 4.3.2.3.a. – 4.3.2.3.f., 4.3.2.4.a., 4.3.2.5.a. and 4.3.2.6.a. all show changes in UV edge position brought about by these three phenomena.

The UV edge moves to lower wavenumbers with increasing oxidation of the glass, as shown in figure 4.3.2.6.a. The OMCT band due to Fe^{3+}-O interaction has a greater extinction coefficient and is centred at a lower wavenumber than the Fe^{2+}-O OMCT band [21]. Hence a change in redox towards the oxidised state moves the UV edge to lower wavenumbers.

Both the concentration of Fe ions per unit volume (figure 4.3.2.2.c.) and redox ratio (figures 4.3.7.1.a. – d.) are strongly affected by glass composition. It was found that whilst changes in redox do affect the UV edge (see figure 4.3.2.6.a.), they are not solely responsible for differences in UV edge position. Large changes in redox between reduced and oxidised samples of equal base composition only gave rise to relatively small changes in UV edge position. Much greater changes were seen with different base compositions, for example with the replacement of MgO by BaO. Glass composition itself plays a major role in determining UV edge position of iron-containing glasses.

Increasing the ionic radii of the modifying cations, both alkali and alkaline earth, shifted the UV edge to lower wavenumbers. Shifts in UV edge also occurred when SiO_2 was partially replaced by a variety of oxides (see chapter 4.3.2.4.) or when the base glass was changed from silicate to borate (see chapter 4.3.2.5.). The major influencing factor in all these cases is the composition of the glass itself. In nominally iron-free glasses it is already known [14] that the addition of larger

alkali and / or alkaline earth ions in equimolar quantities moves the UV edge to lower wavenumbers. This study shows that this rule still applies for glasses containing iron: the influence of composition on the UV edge is far stronger than the influence of redox, or small differences in iron concentration.

The partial replacement of SiO_2 with other oxides (see chapter 4.3.2.4.) also affected the UV edge. The addition of B_2O_3, Al_2O_3 or GeO_2 moves the UV edge to lower wavenumbers. The change was greatest for added B_2O_3. This has interesting possibilities for applications which require enhancement of UV absorbance.

4.4.3. Coordination and Environment

Of the factors discussed in chapter 4.1.3.2. which affect *Dq*, only interatomic distance and symmetry of the ligand environment were likely to be affected by glass composition. The parameter *Dq* is very sensitive to changes in the metal-ligand distance, R, since it is proportional to $1/R^5$.

4.4.3.1. Fe^{2+} Ions

Work presented in chapter 4.3.5.1. showed that $Dq(Fe^{2+})$ is proportional to $1/\Lambda_{th}$, and hence Λ_{th} is proportional to R^5, where Λ_{th} is the theoretical optical basicity, and R is the metal-oxygen distance. This proportionality occurred for all three fitted Fe^{2+} bands, associated with distorted octahedral sites, dynamic Jahn-Teller splitting of those sites, and tetrahedral sites. Smaller modifier cations such as Mg^{2+} and Li^+ give smaller values of Λ_{th}, hence they give smaller values of R and greater values of $Dq(Fe^{2+})$. These cations are both small and highly polarising, thus they give rise to the greatest ligand field strengths. The fact that there is a linear relationship between *Dq* and Λ_{th} shows that non-bridging oxygen ions associated with both alkali and alkaline earth ions coordinate with Fe^{2+} ions, and

there is no obvious selectivity about the coordinating cation type.

It was not possible to measure the effects of composition on Fe^{2+} Racah parameters. Characteristic changes occurred in the Fe^{3+} Racah parameters, so it is likely that similar changes occurred for Fe^{2+} ions.

Calculated extinction coefficient, $\varepsilon(Fe^{2+})$, agreed with the literature (see chapters 4.1.4.6. and 4.3.6.1.) and in particular with similar work by Traverse et al [71]. The ionic radius ratio of alkali / alkaline earth ions was proportional to $\varepsilon(Fe^{2+})$, although notable differences occurred for glasses containing MgO, such that these glasses had greater extinction coefficients than predicted.

As discussed in chapter 4.4.2.1., there was little change in the octahedral / tetrahedral Fe^{2+} ratio, based on optical measurements. Unlike Fe^{3+} ions, where a definite shift in coordination explains the changing extinction coefficient, the changes in $\varepsilon(Fe^{2+})$ must indicate other changes. It has been suggested that increasing the size of modifier ion, whether alkali or alkaline earth, increases the distortion of the silicate network [73]. On the other hand a small, highly polarising ion such as Li^{+} or Mg^{2+}, can also cause distortion of the matrix by exerting a strong attraction on nearby oxygens, thus influencing other cations to which they are bonded. The greatest distortions arise when cations are either large or highly polarising. However alkaline earth ions carry double the charge of alkali ions, therefore they have greater polarising ability. It is possible that it is these site distortions of Fe^{2+} ions are mirrored by the proportionality of the extinction coefficient with alkali / alkaline earth ionic radius ratio.

It was indicated in chapter 4.1.4.9. that changes in the number of non-bridging oxygen ions or Si-O bond lengths could affect *Dq*. Whilst these remain possibilities, the fact that replacement of modifier ions by others was conducted on a molar basis minimised this possibility.

4.4.3.2. Fe^{3+} Ions

Values of $Dq(Fe^{3+})$ in the literature have varied somewhat (see table 4.1.4.2.a.), demonstrating both the difficulty of measuring this parameter accurately and its variation with glass composition. Computer fitting showed that the peak wavenumber of the most characteristic Fe^{3+} band, $^6A_1 \rightarrow {}^4E(D)$, normally occurring at ~26,000 cm^{-1}, decreased with increasing optical basicity (see figure 4.3.5.1.d.), despite the fact that this band is supposedly unaffected by ligand field (see chapters 4.1.3.4., 4.1.4.2., and 4.1.4.8.). Similar behaviour occurred in sodium silicate glasses with changing composition, and was attributed to changes in the Racah B and C parameters [25]. The effects of changing composition on Racah B and C for Fe^{3+}, evidenced by the alkali / alkaline earth ionic radius ratio in this study, were shown in figures 4.3.5.3.a. and 4.3.5.3.b., respectively. The values and behaviour of these parameters agreed with similar studies.

Luminescence spectroscopy in this study found that the wavenumber of the luminescence band due to the $^4T_1(G) \rightarrow {}^6A_1$ transition was unaffected by Fe_2O_3 content, but was proportional to the alkali / alkaline earth ionic radius ratio. It varied between approximately 13,300 cm^{-1} and 15,300 cm^{-1}, a range of ~2,000 cm^{-1} (see figure 4.3.9.1.c.). The literature survey indicated that the differences in B and C were not large enough to explain similar changes in luminescence band wavenumbers [25]. The changes in luminescence band position therefore indicated a change in *Dq* as well as in B and C. Addition of a Stokes shift of 1,600 cm^{-1} (see chapter 4.1.4.3.) corresponds with values for $Dq(Fe^{3+}_{tet})$ of 900 – 1,000 cm^{-1}, and an average of $Dq(Fe^{3+}_{tet}) \approx 950\ cm^{-1}$. Luminescence spectroscopy also indicated the presence of a band at 11,000 – 11,500 cm^{-1}. This correlates with the $^4T_1(G) \rightarrow {}^6A_1$ transition of octahedral Fe^{3+} ions (see chapter 4.1.4.3.). Addition of the Stokes Shift of 1,600 cm^{-1} corresponds with a value of $Dq(Fe^{3+}_{oct}) \approx 1{,}300\ cm^{-1}$, which agrees with values in the literature (see table 4.1.4.2.a).

The position of the Fe^{3+} absorption band at 26,300 cm^{-1} due to the $^6A_1 \rightarrow {}^4E(D)$ transition of tetrahedral and octahedral ions was proportional to the optical

basicity, yet the position of the Fe^{3+} luminescence band near 14,000 cm^{-1} due to the $^4T_1(G) \rightarrow {}^6A_1$ transition of tetrahedral ions was proportional to the alkali / alkaline earth ionic radius ratio. The former band was supposedly field-independent, so the only parameters affecting the band position were Racah B and C. The latter band was strongly field-dependent, and indicated that $Dq(Fe^{3+}_{tet})$ is inversely proportional to the alkali / alkaline earth ionic radius ratio.

Calculated $\varepsilon(Fe^{3+})$ agreed with the literature (see chapters 4.1.4.6. and 4.3.6.2.) and in particular with similar work by Traverse et al [71]. The trend in Fe^{3+} extinction coefficient indicated that increasing alkali / alkaline earth ionic radius ratio lead to an increase in the number of Fe^{3+} tetrahedral / octahedral ratio. Over the compositional range, the extinction coefficient $\varepsilon(Fe^{3+})$ increased from ~2 l mol^{-1} cm^{-1} to ~6 l mol^{-1} cm^{-1}. The tetrahedral / octahedral ratio therefore changed in favour of tetrahedral sites. It was not possible to quantify this change using the available data, however due to the 300 % increase in $\varepsilon(Fe^{3+})$, it can be assumed that this change was considerable. The Laporte selection rule means that the tetrahedral band should be much stronger than the octahedral band, hence the shift in coordination had such a noticeable effect.

The effects of replacing 5 molar % SiO_2 with GeO_2, B_2O_3 and Al_2O_3 were shown in figure 4.3.2.4.a. The effect on $Dq(Fe^{2+})$ was minimal, although the addition of Al_2O_3 did appear to give a slight increase. No redox measurements were made on these glasses, so it was not possible to determine whether the changes in peak intensity were caused by differences in redox or extinction coefficients. Considerable increases in the strength of the UV edge were achieved by these replacements, such that Al_2O_3 and GeO_2 gave moderate effects, but the addition of B_2O_3 gave by far the greatest change. This result comes as little surprise, since results have shown how far the UV edge is shifted by changing to a glass based predominantly on B_2O_3 (see figure 4.3.2.5.a.). Correlation of these results with ESR results (see chapter 5.3.3.) indicates that there may be a link between Fe ion distributions and the strength of the UV edge.

4.5. Chapter Summary

Increasing Fe_2O_3 content causes changes in the characteristics of optical spectra, notably due to changes in oxygen-metal charge transfer (OMCT) bands in the UV and an inter-valence charge transfer (IVCT) band in the visible.

The $Fe^{2+}/\Sigma Fe$ redox ratio was unaffected by Fe_2O_3 content, but was inversely proportional to the ratio of alkali / alkaline earth ionic radii.

Computer modelling identified three Fe^{2+} absorption bands, and these were attributed to the $^5T_2(D)\rightarrow{}^5E(D)$ transition for distorted octahedral sites, to dynamic Jahn-Teller splitting of the octahedral sites, and to the $^5E(D)\rightarrow{}^5T_2(D)$ transition for tetrahedral sites. Most Fe^{2+} ions occur in octahedral sites and distortions thereof. The ratio of octahedral / tetrahedral Fe^{2+} sites was largely unaffected by composition. The parameter $Dq(Fe^{2+})$ for both octahedral and tetrahedral coordination was inversely proportional to the glass theoretical optical basicity, indicating that non-bridging oxygens associated with both alkali and alkaline earth ions coordinate with Fe^{2+} ions.

Five absorption bands were fitted for Fe^{3+} ions in both tetrahedral and octahedral coordination. The extinction coefficient of the $^6A_1\rightarrow{}^4E(D)$ absorption band increased proportionally with alkali / alkaline earth ionic radius ratio, indicating that the Fe^{3+} tetrahedral / octahedral ratio was similarly proportional. Racah B and C parameters and $Dq(Fe^{3+}_{tetrahedral})$ all exhibited proportionality with the alkali/ alkaline earth ionic radius ratio.

Replacement of SiO_2 by various other oxides indicated the B_2O_3 in silicate glass can decrease UV edge wavenumber, and the characteristics of iron in borate glasses are different from silicate glasses.

4.6. References

[1] Weyl, W.A., Coloured Glasses, Soc. Glass Technol., Sheffield, 1961.

[2] Tanabe, Y., Sugano, S., J. Phys. Soc. Japan, 1954, vol. 9, p. 753.

[3] Tanabe, Y., Sugano, S., J. Phys. Soc. Japan, 1954, vol. 9, p. 766.

[4] Bates, T., in Modern Aspects of the Vitreous State, vol. 2, Ed. Mackenzie, J.D., Butterworths, London, 1962, p.195.

[5] Burns, R.G., Mineralogical Applications of Crystal Field Theory, 2nd Ed., Cambridge Univ. Press, 1993.

[6] Ookawa, M., Sakurai, T., Mogi, S., Yokokawa, T., Mater. Transact. JIM, 1997, vol. 38, p.220.

[7] Jahn, H.A., Teller, E., Proc. Royal Soc., 1957, vol. A161, p.220.

[8] Van Vleck, J.H., J. Chem. Phys., 1939, vol. 7, p. 79.

[9] McClure, D.S., J. Chem. Phys. Solids, 1957, vol. 3, p.311.

[10] Fanderlik, I., Optical Properties of Glass, Elsevier, 1983.

[11] Zschimmer, E., Z. Instrumkde, 1903, vol. 23, p. 360.

[12] Stevels, J.M., Proc. 11th Congr. Pure and Appl. Chem., 1947, vol. 5, p. 519.

[13] Smith, H.L., Cohen, A.J., Phys. Chem. Glasses, 1963, vol. 4, p. 173.

[14] Hensler, J.R., Lell, E., Proc. Ann. Meeting Int. Comm. Glass, Toronto, 1969, p. 51.

[15] Sigel, G.H., Ginther, R.J., Glass Technol., 1968, vol. 9, p. 66.

[16] De Jong, J., J. Soc. Glass Technol., 1954, vol. 38, p. 57.

[17] Bishay, A.M., Makar, L., J. Amer. Ceram. Soc., 1969, vol. 52, p. 605.

[18] Kurkjian, C.R., Sigety, E.A., Phys. Chem. Glasses, 1968, vol. 9, p. 73.

[19] Ades, C., Toganidis, T., Traverse, J.P., J. Non-Cryst. Solids, 1990, vol. 125, p. 272.

[20] Urbach, F., Phys. Rev., 1953, vol. 92, p. 1324.

[21] Steele, F.N., Douglas, R.W., Phys. Chem. Glasses, 1965, vol. 6, p. 246.

[22] Volf, M.B., Chemical Approach to Glass, Elsevier, Amsterdam / Prague, 1980.

[23] Paul, A., Tiwari, A.N., Phys. Chem. Glasses, 1973, vol. 14, p. 69.

[24] Paul, A., Parker, J.M., Phys. Chem. Glasses, 1975, vol. 16, p. 103.

[25] Fox, K.E., Furukawa, T., White, W.B., Phys. Chem. Glasses, 1982, vol. 23, p. 169.

[26] Edwards, R.J., Paul, A., Douglas, R.W., Phys. Chem. Glasses, 1972, vol. 13, p. 131.

[27] Edwards, R.J., Paul, A., Douglas, R.W., Phys. Chem. Glasses, 1972, vol. 13, p. 137.

[28] Keppler, H., Amer. Mineral., 1992, vol. 77, p. 62.

[29] Nolet, D.A., Burns, R.G., Flamm, S.L., Besancon, J.R., Proc. 10th Lunar Planet. Sci. Conf., 1979, p. 1775.

[30] Nolet, D.A., J. Non-Cryst. Solids, 1980, v.37, p. 99.

[31] Montenero, A., Friggeri, M., Giori, D.C., Belkhiria, N., Pye, L.D., J. Non-Cryst. Solids, 1986, vol. 84, p. 45.

[32] Calas, G., Petiau, J., in The Structure of Non-Crystalline Materials, Ed., Gaskell, P.H., parker, J.M., Davis, E.A., Taylor-Francis, 1983, p.18.

[33] Adams, R.V., Phys. Chem. Glasses, 1961, vol. 2, p. 39.

[34] Pauling, L., Nature of the Chemical Bond, 3rd Ed., Cornell Univ. Press, 1960.

[35] McKinlay, K., PhD Thesis, Univ. Of Sheffield, 1999.

[36] Calas, G., Petiau, J., Solid State Comms.,1983, vol. 48, p. 625.

[37] Wang, C.M., Chen, H., Phys. Chem. Glasses, 1987, vol. 28, p. 39.

[38] Park, J.W., Chen, H., Phys. Chem. Glasses, 1982, vol. 23, p. 107.

[39] Iwamoto, N., Umesaki, N., Atsumi, T., J. Mat. Sci. Lett., 1987, vol. 6, p. 271.

[40] Magini, M., Sedda, A.F., Licheri, G., Paschina, G., Piccaluga, G., Pinna, G., Cocco, G., J. Non-Cryst. Solids, 1984, vol. 65, p. 145.

[41] Calas, G., Levitz, P., Petiau, J., Bondot, P., Loupias, G., Rev. Phys. Appl., 1980, vol. 15, p. 1161.

[42] Johnson, J.A., Johnson, C.E., Holland, D., Mekki, A., Appleyard, P., Thomas, M.F., J. Non-Cryst. Solids, 1999, vol. 246, p. 104.

[43] Glebov, L.B., Boulos, E.N., Glebova, L.N., Smirnova, T.V., Proc. 18th Int. Congr. Glass, San Francisco, 1998.

[44] Dingwall, A.G.F., Moore, H., J. Soc. Glass Technol., 1953, v. 37, p. 316.

[45] Boon, J.A., Fyfe, W.S., Chem. Geol., 1972, vol. 10, p. 287.

[46] Levy, R.A., Lupis, C.H.P., Flinn, P.A., Phys. Chem. Glasses, 1976, vol. 17, p. 94.

[47] Kordas, G., Oel, H.J., Phys. Chem. Glasses, 1984, vol. 25, p. 76.

[48] Zhou, Z., Yuan, Y., Hu, Z., Liu, R., Xia, Y., Wanf, S., J. Non-Cryst. Solids, 1986, vol. 84, p. 34.

[49] Dyar, M.D., Amer. Mineral., 1985, vol. 70, p. 304.

[50] Goldman, D.S., Berg, J.I., J. Non-Cryst. Solids, 1980, vol. 38 & 39, p. 183.

[51] Hannoyer, B., Lenglet, M., Durr, J., Cortes, R., J. Non-Cryst. Solids, 1992, vol. 151, p. 209.

[52] Fenstermacher, J.E., J. Non-Cryst. Solids, 1980, vol. 38 & 39, p. 239.

[53] Lenglet, M., Arsene, J., Riv. Staz. Sper. Vetro, 1990, vol. 5, p. 39.

[54] White, W.B., Knight, D.S., in Defects in Glass Res. Colloq., 1986, ch. 40, p. 283.

[55] Knight, D.S., White, W.B., J. Amer. Ceram. Soc., 1988, vol. 71, p. C-342.

[56] Baiocchi, E., Bettinelli, M., Montenero, A., J. Amer. Ceram. Soc., 1982, vol. 65, p. C-39.

[57] Berretz, M., Holt, S.L., J. Amer. Ceram. Soc., 1978, vol. 61, p. 136.

[58] Fuxi, G., Optical and Spectroscopic Properties of Glass, Springer-Verlag, Shanghai, 1990.

[59] Sherman, D., Waite, D.T., Amer. Mineral., 1985, vol. 70, p. 1262.

[60] Kinawi, A.A., Transition Met. Chem., 1982, vol. 7, p. 335.

[61] Malashkevitch, G.E., Korzhik, M.V., Livshits, M.G., Paulenko, V.B., Blinov, A.L., Borik, M.A., Soviet J. Glass Phys. Chem., 1990, vol. 16, p. 397.

[62] Pott, G.T., McNichol, B.D., J. Lumin., 1973, vol. 6, p. 225.

[63] Melamed, N.T., Neto, J.M., Abritta, T., Barros, F., J. Lumin., 1981, vol. 24 / 25, p. 249.

[64] Telfer, D.J., Walker, G., J. Lumin., 1976, vol. 11, p. 315.

[65] Fox, K.E., Furukawa, T., White, W.B., J. Amer. Ceram. Soc., 1981, vol. 64, p. C-42.

[66] Brawer, S.A., White, W.B., J. Mater. Sci., 1978, vol. 13, p. 1907.

[67] Bilan, O.N., Gorbachev, S.M., Cherenda, N.G., Voropai, Y.S., Yudin, D.M., Radiation Effects and Defects in Solids, 1991, vol. 115, p. 285.

[68] Gebala, S., Sarzynski, J., Optica Appl., 1982, vol. 12, p. 49.

[69] Bamford, C.R., Hudson, E.J., Proc. 7th Int. Congr. Glass, Brussels, 1965, vol. 1, p. 1.

[70] Goldman, D.S., Berg, J.I., J. Non-Cryst. Solids, 1980, vol. 38 & 39, p. 183.

[71] Traverse, J.P., Toganidis, T., Ades, C., Glastech. Ber., 1992, vol. 65, p. 201.

[72] Dunn, A.G., Beales, K.J., Newns, G.R., Wilson, J.L., Phys. Chem. Glasses, 1978, vol. 19, p. 1.

[73] Duran, A., Fernandez-Navarro, J.M., Phys. Chem. Glasses, 1985, vol. 26, p. 126.

[74] Mysen, B.O., Seifert, F., Virgo, D., Amer. Mineral., 1980, vol. 65, p. 867.

[75] Mysen, B.O., Virgo, D., Neumann, E.R., Seifert, F.A., Amer. Mineral., 1985, vol. 70, p. 317.

[76] Sakka, S., Kamiya, K., Yoshikawa, H., J. Non-Cryst. Solids, 1978, vol. 27, p. 289.

[77] Kinawi, A.A., J. Inorg. Nucl. Chem., 1981, vol. 43, p. 1989.

[78] Combes, J.M., Calas, G., Creux, S., Proc. 17th Int. Congr. Glass, 1995, p. 90.

[79] Hirayama, C., Castle, J.G., Kuriyama, M., Phys. Chem. Glasses, 1968, vol. 9, p. 109.

[80] Klonkowski, A., Frischat, G.H., Richter, T., Phys. Chem. Glasses, 1983, vol. 24, p. 47.

[81] Klein, R.M., Onorato, P.I.K., Phys. Chem. Glasses, 1980, vol. 21, p. 199.

[82] Nelson, C., White, W.B., Phys. Chem. Glasses, 1993, vol. 34, p. 219.

[83] Cable, M., Hulme, R., Glass Technol., 1985, vol. 26, p. 170.

Chapter 5.

Electron Spin Resonance (ESR)

5.1. Principles of Operation

Electron Spin Resonance, ESR (or Electron Paramagnetic Resonance, EPR) spectroscopy has been used in this study to measure the resonant absorption of fixed-frequency microwaves (X-band, 9.45 GHz) by the unpaired electrons of Fe^{3+} ions in glass, tuned by varying the strength of an externally applied magnetic field from 0 - 500 mT. ESR spectroscopy measures the absorptions caused by transitions between energy (Zeeman) levels of the orbital ground state. Generally, these transitions depend upon the particular ion being studied, the strength and symmetry of the ligand field, spin-orbit coupling and other effects such as hyperfine interactions between electrons and nucleus. Absorptions occur at specific g-values, which can be calculated from the magnetic field and frequency of radiation, as in equation 5.1.a.

$$g = h\nu / \beta B\mu_B \qquad \text{(Equation 5.1.a.)}$$

where h = Planck's constant; ν = frequency of the radiation; β = Bohr Magneton; B = magnetic induction; μ_B = permeability of medium. For given coordinations, symmetries and environments, effective g-values can be obtained from quantum mechanical calculations. The technique is particularly useful for investigating

Fe^{3+} ions in glass since no known resonance is produced by Fe^{2+} ions at room temperature. A typical ESR spectrum of Fe^{3+} ions in silicate glass is shown in figure 5.1.a. Resonance in these glasses occurs at magnetic fields of approximately 0.075 T, 0.15 T and 0.35 T, corresponding to g-values of ~ 6, ~ 4.3 and ~ 2 respectively.

Extraction of parameters such as relative peak-to-peak derivative intensity ($I_{p\text{-}p}$) and peak-to-peak linewidth ($\Delta H_{p\text{-}p}$) is possible, illustrated in figure 5.1.a. These parameters can give useful information on the environment of the Fe^{3+} ions. Due to the sharpness of the resonance, errors associated with measuring $I_{p\text{-}p}(g = 4.3)$ and $\Delta H_{p\text{-}p}(g = 4.3)$ are relatively small. Slight problems may occur when attempting to fit a baseline to the spectrum so as to measure $I_{p\text{-}p}(g = 2)$, and also when defining the limits of $\Delta H_{p\text{-}p}(g = 2)$. For these reasons the errors associated with measurement of these parameters are larger for g = 2 than for g = 4.3. Similar difficulties apply for measurement of the g = 6 resonance.

Figure 5.1.a. Typical ESR Spectrum of Fe^{3+} Ions in a Silicate Glass

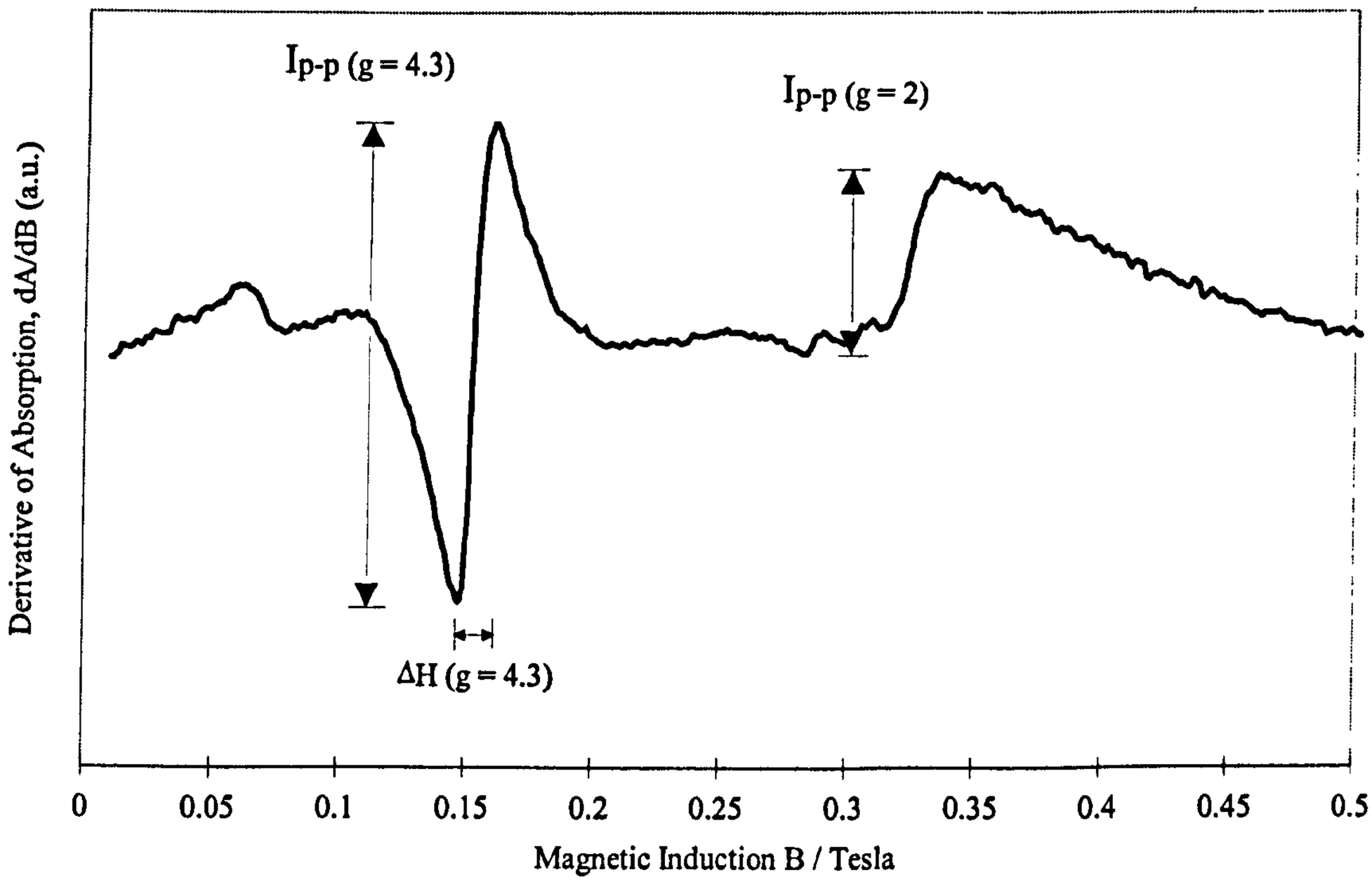

5.2. Background and Literature Survey

An excellent review article by Griscom [1] gives broad coverage of most aspects of ESR in glasses, and the reader is referred to this.

All paramagnetic centres can be described by one or more of the terms in the spin Hamiltonian $H = \beta gSB/\mu_B + IAS + SDS$, where β is the Bohr Magneton, B is the induction, μ_B = permeability of medium, S and I are the electronic and nuclear spin vectors respectively, and g, A and D are matrices expressing the energetics of the coupling between the magnetic fields associated with the vector quantities. Excluded from the equation are the nuclear Zeeman, quadrupole and higher order crystal field terms, because of the general inability to measure their effects in glasses. This Hamiltonian can be tailored to the specific needs of the user.

In ordinary paramagnetic salts, no Fe^{2+} resonance is seen at room temperature [2]. The ligand field may split the spin states by too large an amount to be observed, or spin-lattice relaxation times may be so short as to greatly broaden and weaken the resonance [2].

It is expected that Fe^{3+} will produce a resonance at or very near to the free-electron value of g = 2.0023 [2, 3]. Early work on ESR of iron in glass showed the presence of a resonance as predicted, near g = 2 [2, 4, 5]. Resonances were also found at g-values of ~ 4.3 and ~ 6. All of these resonances were assigned to Fe^{3+} ions [2].

The origins of the two main resonances at g ~ 4.3 and g ~ 2 have been intensively debated. Some have attributed them to Fe^{3+} ions occupying tetrahedral and octahedral coordination sites, respectively [4, 6 – 10].

A larger and generally more recent body of work maintains that the g = 4.3 resonance can be produced by isolated Fe^{3+} ions occupying either tetrahedral or octahedral sites with low-symmetry rhombic distortions [11 – 21]. It has been suggested that these sites have a particular symmetry, C_{2V} [12, 20, 21]. Those structural configurations having C_{2V} symmetry were discussed by Loveridge & Parke [12]. The concentration dependence of the g = 2 resonance has also been

noted and ascribed to exchange interactions between Fe^{3+} ions in close proximity, i.e. clustered [11, 13 - 15, 17, 18, 20 - 24]. The resonance at g = 6 has been assigned to either axial distortions which may result from Fe^{3+} in tetrahedral coordination but with an extra positive charge in the immediate neighbourhood [11, 19], or to Fe^{3+} with S^{2-} ions in their coordination polyhedra [12].

At low iron contents, the origin of the g = 2 resonance is less clear. It has been suggested that both tetrahedral Fe^{3+} ions with T_d symmetry and octahedral Fe^{3+} ions with O_h or C_{3v} symmetry can produce this resonance [20, 21]. Statistically, exchange interactions can occur at all iron concentrations, and indeed clustering has been found at low iron concentrations using both ESR [15, 23] and Mössbauer spectroscopy (see chapter 6.2.3).

5.2.1. The Effects of Iron Content

The peak-to-peak linewidth, $\Delta H_{p\text{-}p}$, and the peak-to-peak intensity, $I_{p\text{-}p}$, of both the g = 4.3 and g = 2 resonances exhibit characteristic changes with increasing iron content. These are shown in figure 5.2.1.a., which contains spectra of typical silicate glasses with differing iron contents. The deduced values of $I_{p\text{-}p}(g = 2) / I_{p\text{-}p}$ (g = 4.3) and $\Delta H(g = 4.3)$ are shown in appendix B, table B2.

Peak-to-peak linewidth of the g = 4.3 resonance, $\Delta H_{p\text{-}p}$ (g = 4.3), exhibited similar behaviour with increasing iron content in many different glass systems [10, 13, 16, 25]. At low iron concentrations $\Delta H_{p\text{-}p}$ (g = 4.3) increases proportionally with iron content, as shown in figure 5.2.1.b. This linear behaviour is indicative of dipolar interactions between isolated Fe^{3+} ions, and that the majority of Fe^{3+} ions occupy isolated sites [15, 16].

Figure 5.2.1.a. ESR Spectra of Glasses with Varying Fe_2O_3 Contents

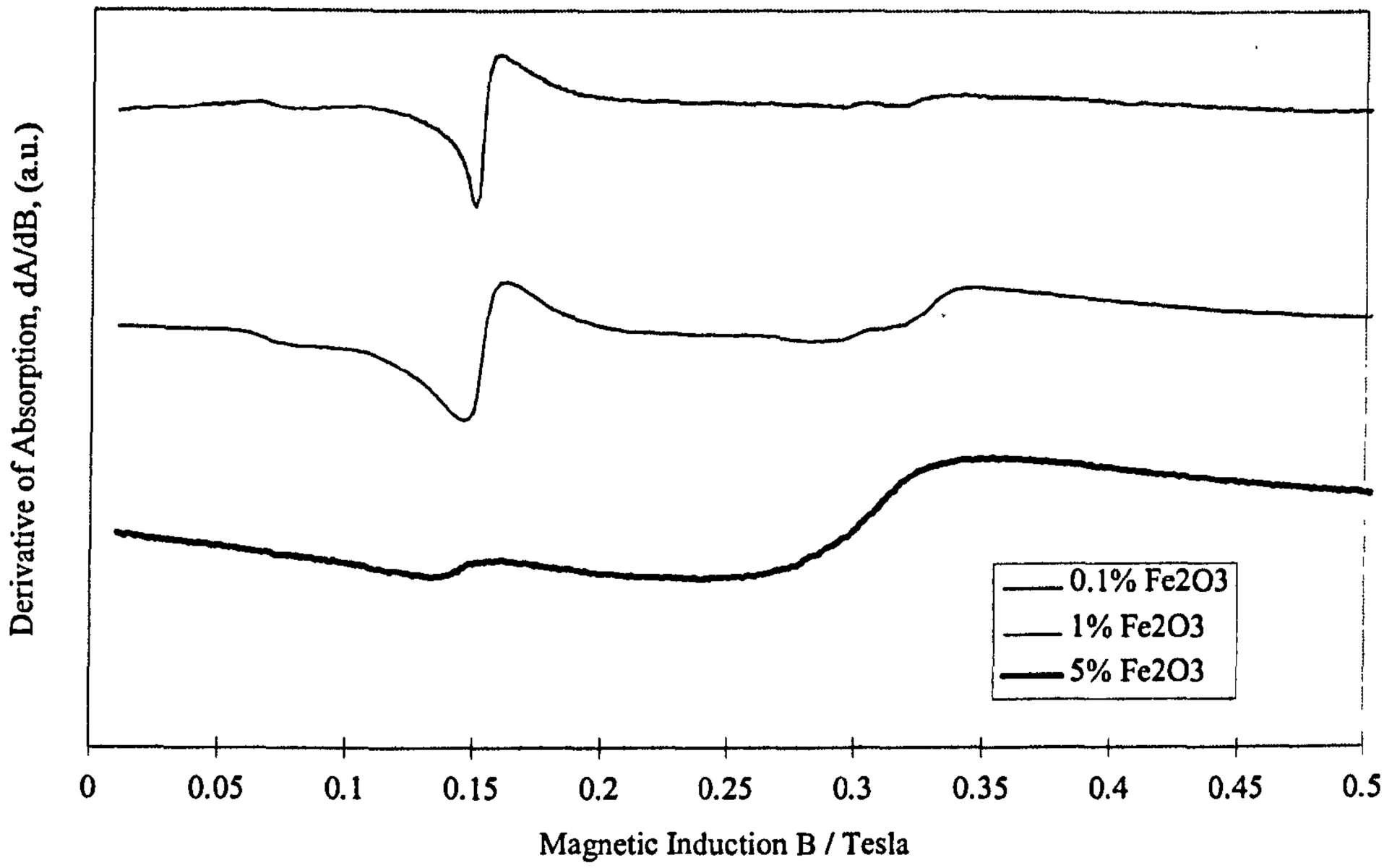

Figure 5.2.1.b. Effects of Iron Content on $\Delta H_{p\text{-}p}(g = 4.3)$ for Lead Borate Glass (adapted from Mendiratta & De Sousa [16])

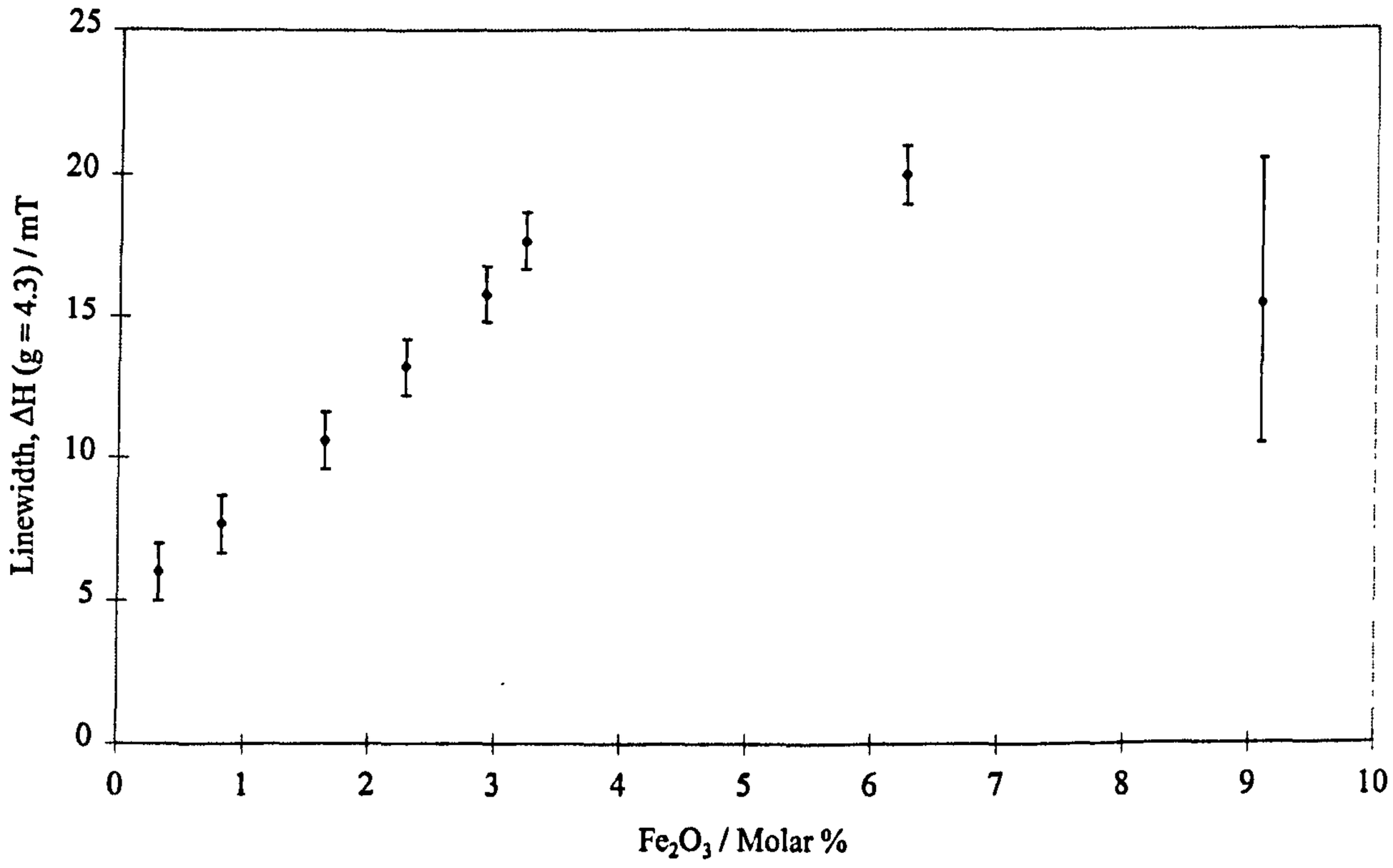

When Fe-Fe distances are large, exchange interaction is not significant and

linewidths can only be broadened by dipolar interaction, hence $\Delta H_{p\text{-}p}$ ($g = 4.3$) $\propto$ Fe_2O_3 % for low iron levels [10, 15, 16]. With further increases in iron content, the relationship deviates from linearity and $\Delta H_{p\text{-}p}$ ($g = 4.3$) tends toward saturation [13, 15, 25]. This effect is caused by the presence of increasing amounts of strong exchange interaction between Fe^{3+} ions as they are brought closer together and the orbitals of the unpaired electrons overlap. These ions are members of "clusters" of more than one Fe^{3+} ion. The point at which the relationship between $\Delta H_{p\text{-}p}$ ($g = 4.3$) and iron content deviates from linearity indicates the onset of significant amounts of clustering [16]. The range of iron contents over which the linearity exists is strongly affected by glass composition [12, 13, 15, 16, 19, 25], but generally lies in the range 1 to 3 molar % Fe_2O_3 depending upon composition. Hence the iron content above which clustering dominates is partially governed by glass composition.

The effects of iron concentration on $\Delta H_{p\text{-}p}$ ($g = 2$) has been less widely investigated [19, 22, 25]. At low iron concentrations where $\Delta H_{p\text{-}p}$ ($g = 4.3$) $\propto$ Fe_2O_3 %, the value of $\Delta H_{p\text{-}p}$ ($g = 2$) remains approximately constant [19, 25]. In these cases this was up to approximately 2 molar % Fe_2O_3. When $\Delta H_{p\text{-}p}$ ($g = 4.3$) began to saturate at about 2 molar % Fe_2O_3, there was a large jump in the value of $\Delta H_{p\text{-}p}$ ($g = 2$). At yet higher iron contents, $\Delta H_{p\text{-}p}$ ($g = 2$) increased but less rapidly.

The intensity of an ESR resonance is approximated by equation 5.2.1.a. [12, 13, 17 – 19, 22, 26].

$$\text{Intensity } I = I_{p\text{-}p} * (\Delta H_{p\text{-}p})^2 \qquad \text{(Equation 5.2.1.a.)}$$

Several characteristic trends in I or approximations of I have been identified with varying iron content [7 - 10, 12, 14, 19, 20 - 22, 26]. With increasing iron content, I ($g = 4.3$) behaves similarly to ΔH ($g = 4.3$) [10, 12, 22]; I ($g = 4.3$) increases linearly with low iron contents, followed by saturation towards a maximum value of I which occurs at approximately 3 molar % Fe_2O_3, followed by a decrease with further increases in iron content.

The resonance intensity I (g = 2) increased slowly at low Fe_2O_3 contents up to 1 molar % in silicate glasses [14] and up to 2 molar % in borate glasses [19]. Further increases in iron content resulted in swift increases in I (g = 2) which continued throughout the ranges of iron contents studied.

The ratio of the two intensities has also been studied [7, 10, 20, 21]. The ratio I (g = 2) / I (g = 4.3) was proportional to (Fe_2O_3 molar %)^2 [20, 21], i.e. I (g = 2) / I (g = 4.3) $\propto$ (Fe_2O_3 %)^2. It was also found that ΔH_{p-p} (g = 2) $\propto$ ΔH_{p-p} (g = 4.3) [20, 21]. Comparison of the ratio of peak-to-peak intensities (i.e. only the I_{p-p} component in equation 5.2.1.a.) I_{p-p} (g = 2) / I_{p-p} (g = 4.3) was therefore an accurate approximation of I since any changes in the ratio I (g = 2) / I (g = 4.3) could only be brought about by changes in the I_{p-p} components and not ΔH. This "technique" has been used previously [20, 21, 27].

5.2.2. The Effects of Glass Composition

The effects of glass composition on the ESR spectra of iron-containing silicate glasses have also been studied [6, 8 – 10, 20, 21, 28 – 30]. Some of these have concentrated on alkali calcium silicate glasses with changing alkali ion type and Fe_2O_3 content up to ~3 molar % Fe_2O_3 [8 – 10, 20, 21]. For any given Fe_2O_3 content, the ratio I_{p-p} (g = 2) / I_{p-p} (g = 4.3) increased as the alkali ion increased in size from Li $\rightarrow$ Cs [8 – 10, 20, 21]. This effect also applied in mixed-alkali calcium silicate glasses containing both Na^+ and K^+ alkali ions [21]. Changing the calcium content had a smaller effect on I_{p-p} (g = 2) / I_{p-p} (g = 4.3) [21]. This was interpreted as showing that calcium does contribute to stabilisation of the C_{2v} structure. Some workers [8 – 10] attributed specific coordinations to the two main resonances, as discussed earlier. They therefore argued that the ratio of octahedral / tetrahedral Fe^{3+} ions increased with alkali ionic radius (Li $\rightarrow$ Cs). No consideration was given to the work discussed in chapter 5.2., which argues that octahedral and tetrahedral Fe^{3+} coordinations should not be directly inferred from the g = 2 and g = 4.3 resonances.

As discussed in chapter 5.2.1., it has been found that $I_{p\text{-}p}$ (g = 2) / $I_{p\text{-}p}$ (g = 4.3) $\propto$ $(Fe_2O_3\ \%)^2$ [20, 21]. The slope A of the line increased with increasing size of the alkali ion. It was noted that the intensity ratio $I_{p\text{-}p}$ (g = 2) / $I_{p\text{-}p}$ (g = 4.3) was an effect of the *type* and not the *quantity* of alkali ion within the range studied. Thus, the author asserted, optical basicity (the average electron donor power of constituent anions) was not the determining influence and a priori does not influence the ESR spectra. Stabilisation of the structure giving rise to the g = 4.3 resonance was best achieved by small alkali cations. To achieve charge neutrality, alkali and theoretically alkaline earth ions are required by the Fe^{3+} ion [31]. If these ions are small, the stabilisation of the structure is stronger due to higher electrostatic forces and to bond angles closer to 90° which is required for octahedral coordination of the alkali cation [20, 21]. With more than one type of alkali ion present, the situation was more complicated. The probability of forming the C_{2V} symmetry changed with type alkali ion, and is probably also affected by Ca. Russel's [20, 21] interpretation of this was that when K_2O is added to a SiO_2-Na_2O-CaO glass, it destabilises the C_{2V} symmetry and promotes the formation of clusters. He stated that ln A $\propto$ 1/a where A is the slope of the relationship $I_{p\text{-}p}$ (g = 2) / $I_{p\text{-}p}$ (g = 4.3) $\propto$ $(Fe_2O_3\ \%)^2$, and a = alkali-oxygen distance. Therefore ln A $\propto$ 1/(ionic radius of alkali cation). Subsequent work used square-wave voltammetry [32], a technique which is used to directly measure the molten glass and allows determination of standard potentials, equilibrium constants and other thermodynamic data, to investigate identical glasses. It was asserted that MgO leads to more stable iron-containing clusters than CaO, and that alkaline earth ions *do* contribute to the stabilisation of tetrahedrally coordinated Fe^{3+} ions. Combining all these results indicates that increasing the size of the alkali ion and/or decreasing the size of the alkaline earth ion destabilises those symmetries giving rise to the g = 4.3 resonance and promotes formation of Fe^{3+} clusters.

Studies of the magnetic susceptibility of Fe has produced interesting results concerning clustering [33]. The behaviour of Fe in lead borate glasses was explained by assuming that even at low concentrations, Fe ions are not dispersed uniformly but also exist in the form of clusters consisting of two or more ions sharing common oxygen ions. Studies of Fe_2O_3 in $2SiO_2$.PbO and $2B_2O_3$.PbO

glasses found that the onset of cluster domination occurred at different Fe contents [33]. At 3.3 molar % Fe_2O_3, a greater fraction of Fe ions were clustered in the borate glass than in the silicate glass. However the size of the clusters was larger in the silicate glass, and average inter-cluster distances were greater.

In aluminosilicate glasses, $I_{p\text{-}p}$ (g = 4.3) increased with increasing cation field strength of either alkali or alkaline earth ions [30]. Alkali ions had a greater effect upon $I_{p\text{-}p}$ (g = 4.3) than alkaline earth ions [30]. This is generally in agreement with work on alkali-alkaline earth silicates discussed above.

Linewidth measurements have been used to calculate the average distance *d* between Fe^{3+} ions in lead borate glass [16]. At less than ~3.2 molar % Fe_2O_3, octahedral best described Fe^{3+} coordination. Above ~3.2 molar % Fe_2O_3, tetrahedral gave the best representation of Fe^{3+} coordination. Calculated *d* was greater than obtained from density measurements. It was argued that this was only possible if a significant fraction of the Fe ions form dimers and trimers so that these "connected" ions do not contribute to the g = 4.3 resonance. Thus, it was stated, at low Fe_2O_3 levels, iron-oxygen coordination polyhedra do not share edges. The linewidth was shown to be the sum of dipolar interactions and of a concentration-independent contribution due to some unresolved fine splitting.

Kordas & Oel [34] asserted, on the basis of optical absorption measurements, that by irradiating iron-containing SiO_2-Na_2O-CaO glasses with x-rays the proportion of tetrahedral Fe^{2+} was increased. The optical spectra shown, however, could not confirm that only the band associated with tetrahedral Fe^{2+} ions had changed characteristics upon irradiation. The authors also asserted that the increase in tetrahedral Fe^{2+} was at the expense of Fe^{3+} ions, with the g = 4.3 resonance decreasing upon irradiation. No structural changes could be caused by the level of irradiation, they claimed, therefore the g = 4.3 resonance was due to Fe^{3+} ions in tetrahedral coordination. This disagrees with the majority of ESR work which has discussed the origins of the g = 4.3 and g = 2 resonances (see chapter 5.2.).

Moon et al [13] showed that ESR linewidths have contributions from spin-lattice and spin-spin relaxation times, but also a structural, concentration-independent component. It was also indicated that the spin-lattice contribution was minimal.

Hence the main contributions to the linewidth arise from spin-spin relaxations and the distribution of Fe^{3+} environments in the glass.

5.2.3. Summary of Main Points from the Literature.

i) Fe^{3+} ions exhibit ESR resonances at room temperature, but Fe^{2+} ions do not.

ii) The characteristic Fe^{3+} resonances occur at $g \sim 6$, $g \sim 4.3$ and $g \sim 2$.

iii) These resonances have been attributed by some to specific coordination polyhedra of Fe^{3+}, the $g = 4.3$ resonance to tetrahedral sites and the $g = 2$ resonance to octahedral sites.

iv) A larger and more recent body of work asserts that the $g = 4.3$ resonance is caused by Fe^{3+} ions in rhombically-distorted tetrahedral and octahedral sites. The $g = 2$ resonance can be caused by exchange interactions between clustered Fe^{3+} ions.

v) Linewidth of the $g = 4.3$ resonance increases with iron content until it reaches saturation. Decreases with further iron additions are due to exchange interactions.

vi) Clustering of Fe ions occurs more readily in borate glasses than in comparable silicate glasses.

vii) Major clustering is evidenced by deviation from proportionality between $\Delta H_{p\text{-}p}$ ($g = 4.3$) and Fe_2O_3 content.

viii) Dipolar interactions predominate in silicate glasses at low (~ 0.2 molar % Fe_2O_3) iron contents but there is some exchange interactions due to clusters.

ix) Exchange interactions increase with increasing iron content such that Fe^{3+} ions are mostly clustered at high (~ 5 molar % Fe_2O_3) iron contents in silicate glasses.

x) $I_{p\text{-}p}$ ($g = 2$) / $I_{p\text{-}p}$ ($g = 4.3$) is a function of the type of alkali ion present in a glass.

xi) $I_{p\text{-}p}$ ($g = 2$) / $I_{p\text{-}p}$ ($g = 4.3$) $\propto$ $(Fe_2O_3\ \%)^2$.

xii) ln A ∝ 1 / ionic radius of alkali cation, where A = slope of I_{p-p} (g = 2) / I_{p-p} (g = 4.3).

xiii) Alkaline earth ions contribute to stabilisation of Fe^{3+} ions, but less so than alkali ions.

5.3. Results

The intensity of an ESR resonance is approximated by equation 5.2.1.a. Calculations of intensity of the individual resonances were not carried out in this study owing to difficulties with accurately measuring the linewidth of the g = 2 resonance. It has been shown [20, 21] that ΔH_{p-p} (g = 4.3) ∝ ΔH_{p-p} (g = 2). Comparison of the ratio I_{p-p} (g = 2) / I_{p-p} (g = 4.3), shortened to I_{p-p} (g = 2 / g = 4.3), can therefore give useful information since any changes in the ratio can only be brought about by changes in the I_{p-p} components and not ΔH_{p-p}. This technique has been used previously [20, 21, 27].

The results were evaluated in terms of the ratio of peak-to-peak intensities of the resonance peaks at g = 2 and g = 4.3, I_{p-p} (g = 2 / g = 4.3), and in terms of the peak-to-peak linewidth of the g = 4.3 resonance, ΔH_{p-p} (g = 4.3).

5.3.1. Varying Glass Composition

Both ΔH_{p-p} (g = 4.3) and I_{p-p} (g = 2) / I_{p-p} (g = 4.3) change dramatically with base glass composition at constant molar Fe_2O_3 content, as shown in figure 5.3.1.a.

Figure 5.3.1.a. EPR Spectra of SiO_2-Na_2O-BaO-0.2% Fe_2O_3 and SiO_2-K_2O-MgO-0.2% Fe_2O_3 Glasses (Samples 34 and 40)

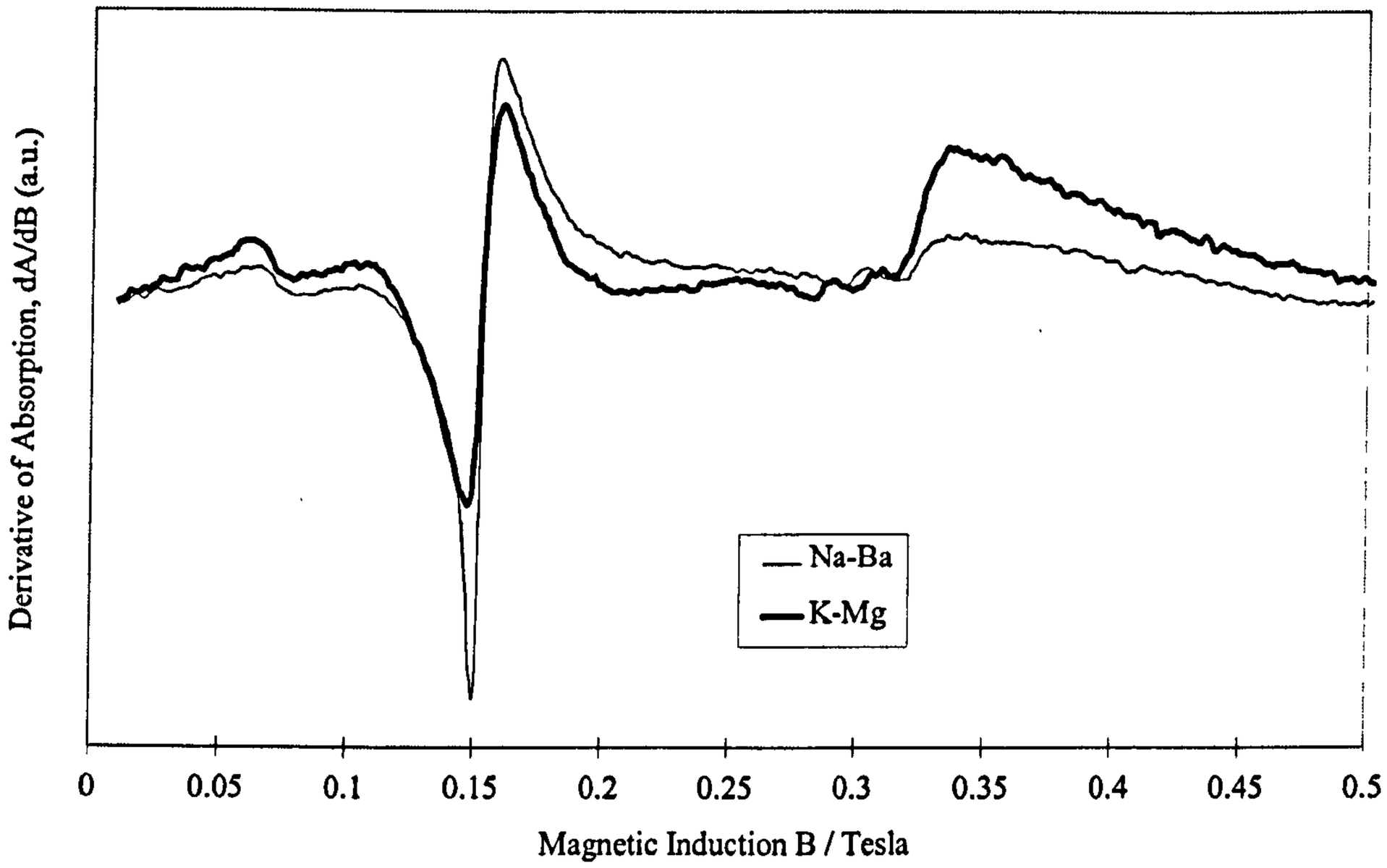

Generally, $\Delta H_{p\text{-}p}$ (g = 4.3) increases with increasing ionic radius of the alkali ion, and decreases with increasing ionic radius of the alkaline earth ion; there are clear trends in the results (see figures 5.3.1.b. and c). Optical observation and x-ray diffraction (see chapter 4.3.2.1.) have shown that some glasses containing Li_2O as the sole alkali oxide were phase-separated. ESR data from the samples containing MgO, CaO and SrO as the alkaline earth oxides was therefore unreliable. Phase separation may affect the distribution of Fe ions in the glass and thus ESR spectra. The BaO glass in this series was not phase separated, and so the ESR spectrum was acceptable. Measurement of $\Delta H_{p\text{-}p}$ (g = 4.3) was straightforward, and errors were estimated at ± 0.3 mT.

Figures 5.3.1.d. and e show relationships in which $I_{p\text{-}p}$ (g = 2) / $I_{p\text{-}p}$ (g = 4.3) increases with increasing alkali / alkaline earth ionic radius ratio. Errors associated with measurement of peak heights were quite large since the data was plotted as a ratio. A small error in the measured intensity of the g = 2 resonance resulted in a larger error in the ratio. The combined errors of technique and ratio measurement have been estimated at ± 10 %.

Figure 5.3.1.b. Linewidth $\Delta H_{p\text{-}p}$ (g = 4.3) with changing Alkali / Alkaline Earth Ionic Radius Ratio showing the effects of Alkaline Earth Type

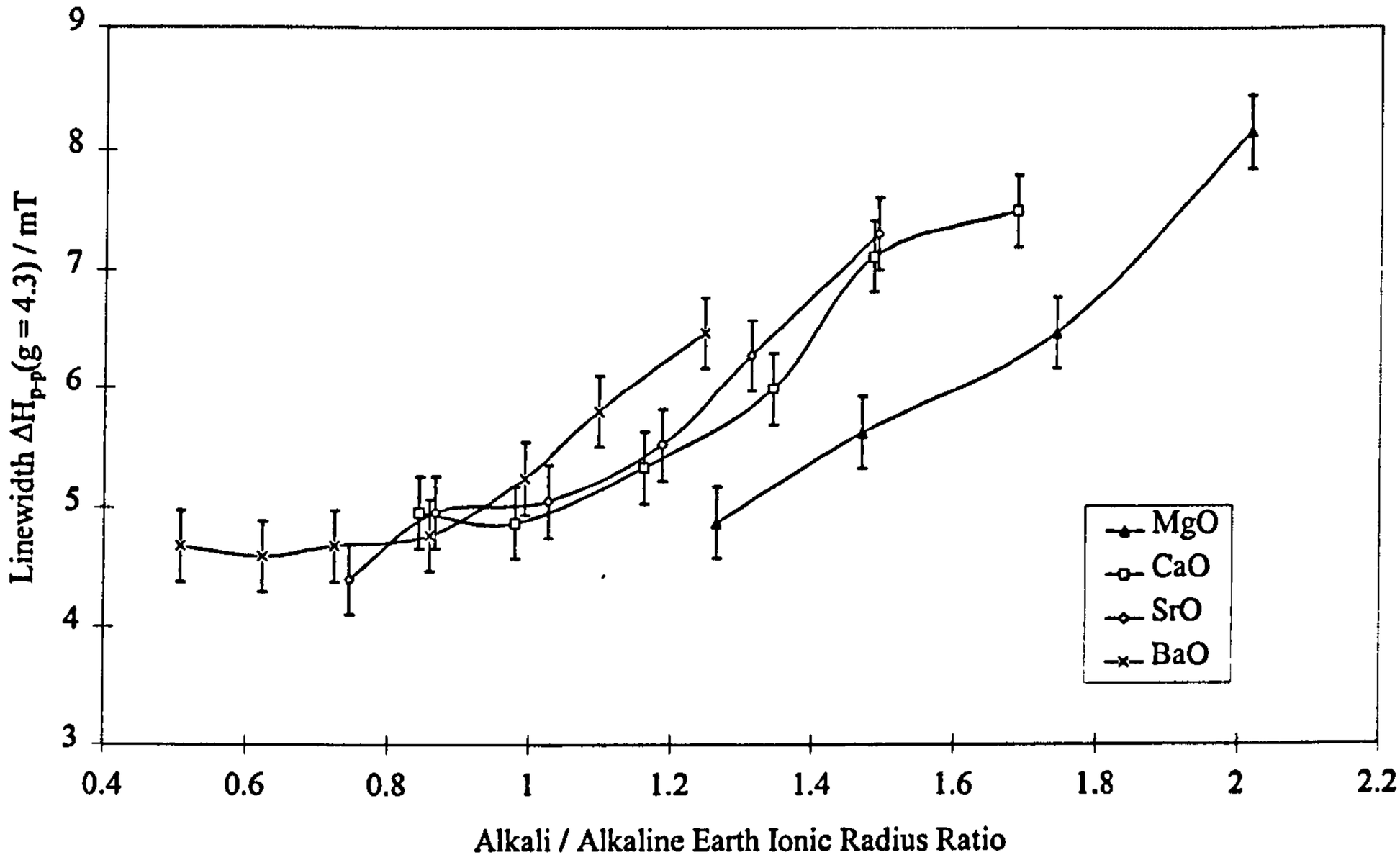

Figure 5.3.1.c. Linewidth $\Delta H_{p\text{-}p}$ (g = 4.3) with changing Alkali / Alkaline Earth Ionic Radius Ratio, showing the effects of Alkali Type

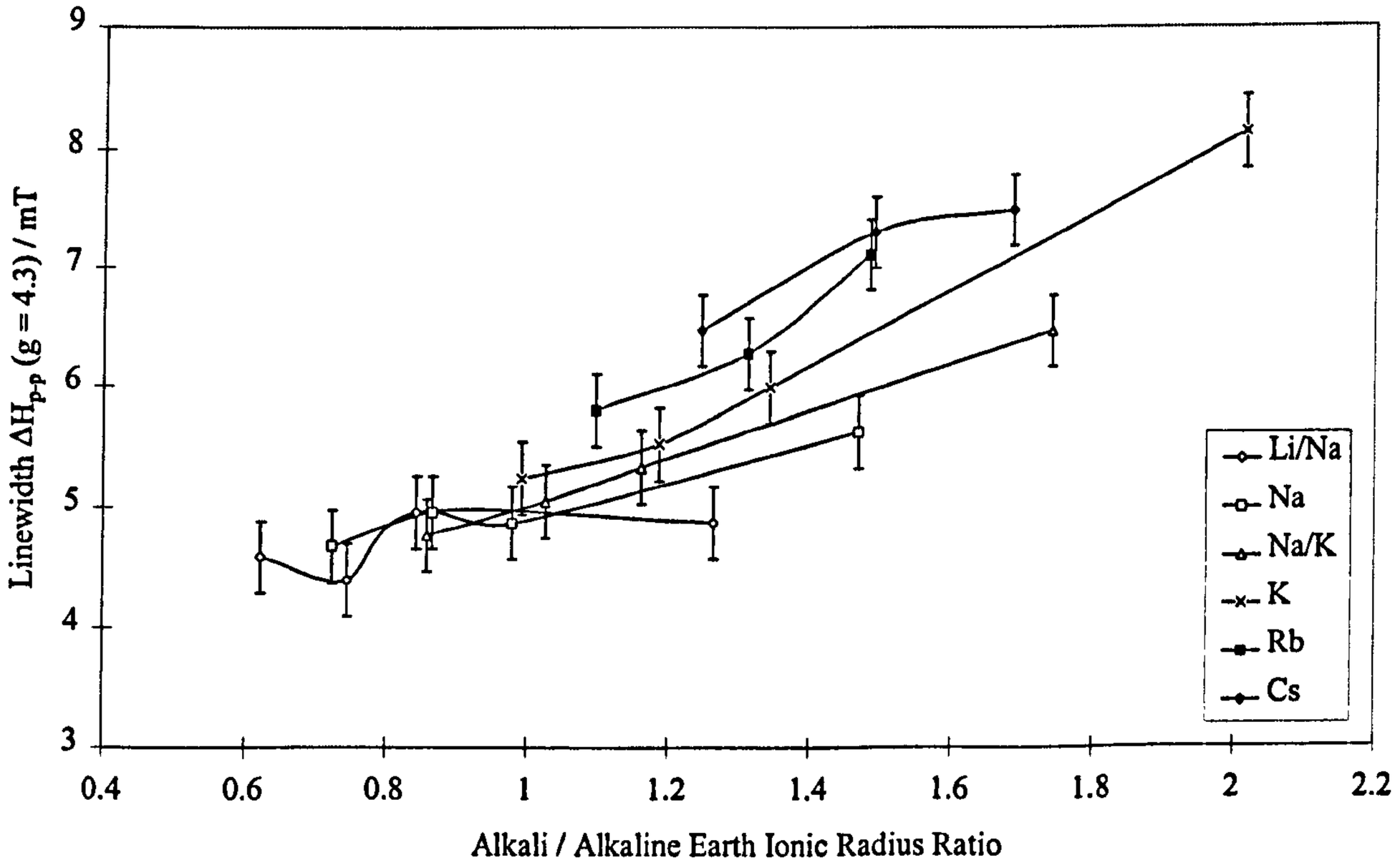

Figure 5.3.1.d. $I_{p\text{-}p}$ (g = 2 / g = 4.3) with changing Alkali / Alkaline Earth Ionic Radius Ratio, showing the effects of Alkaline Earth Type

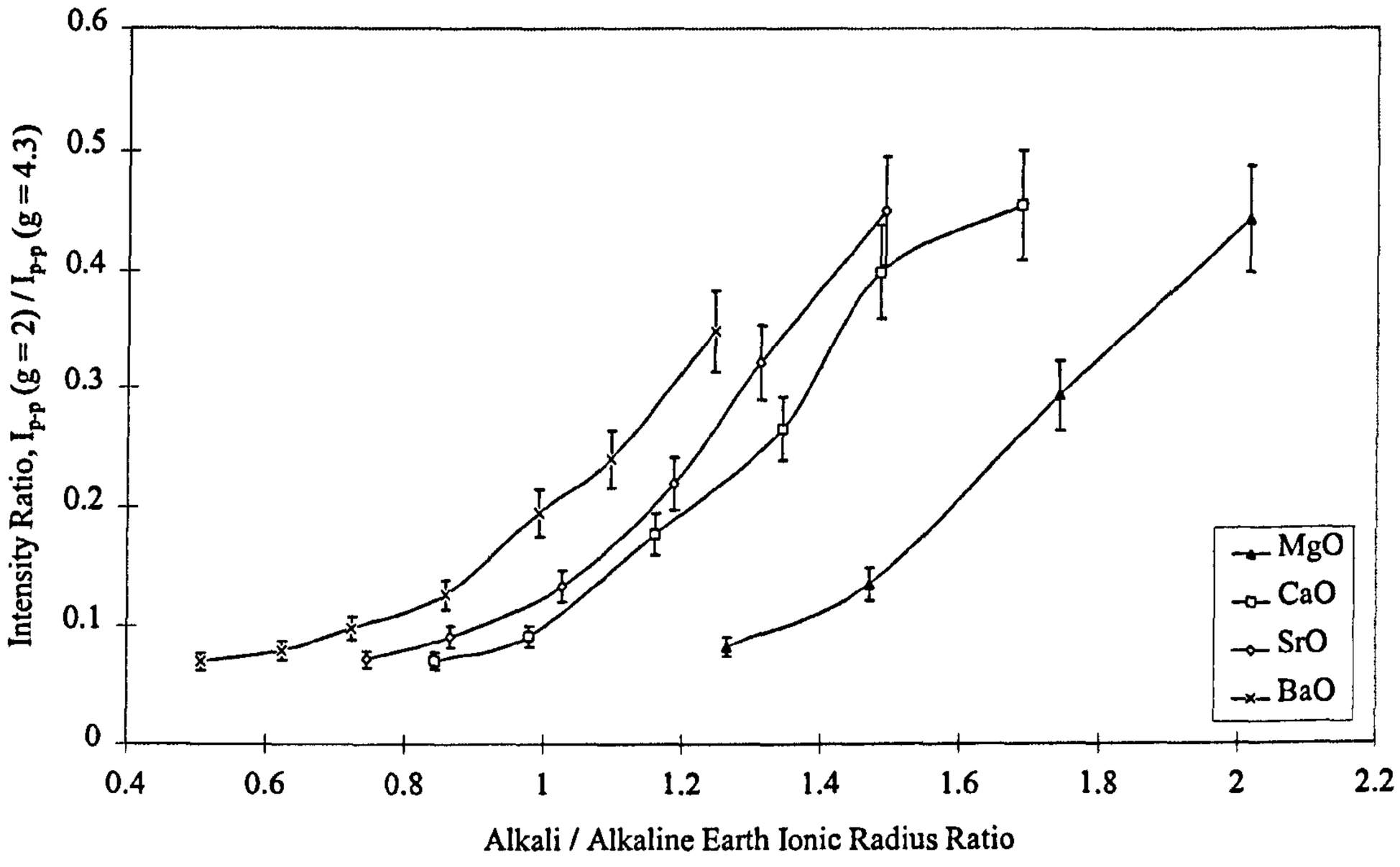

Figure 5.3.1.e. $I_{p\text{-}p}$ (g = 2 / g = 4.3) with changing Alkali / Alkaline Earth Ionic Radius Ratio, showing the effects of Alkali Type

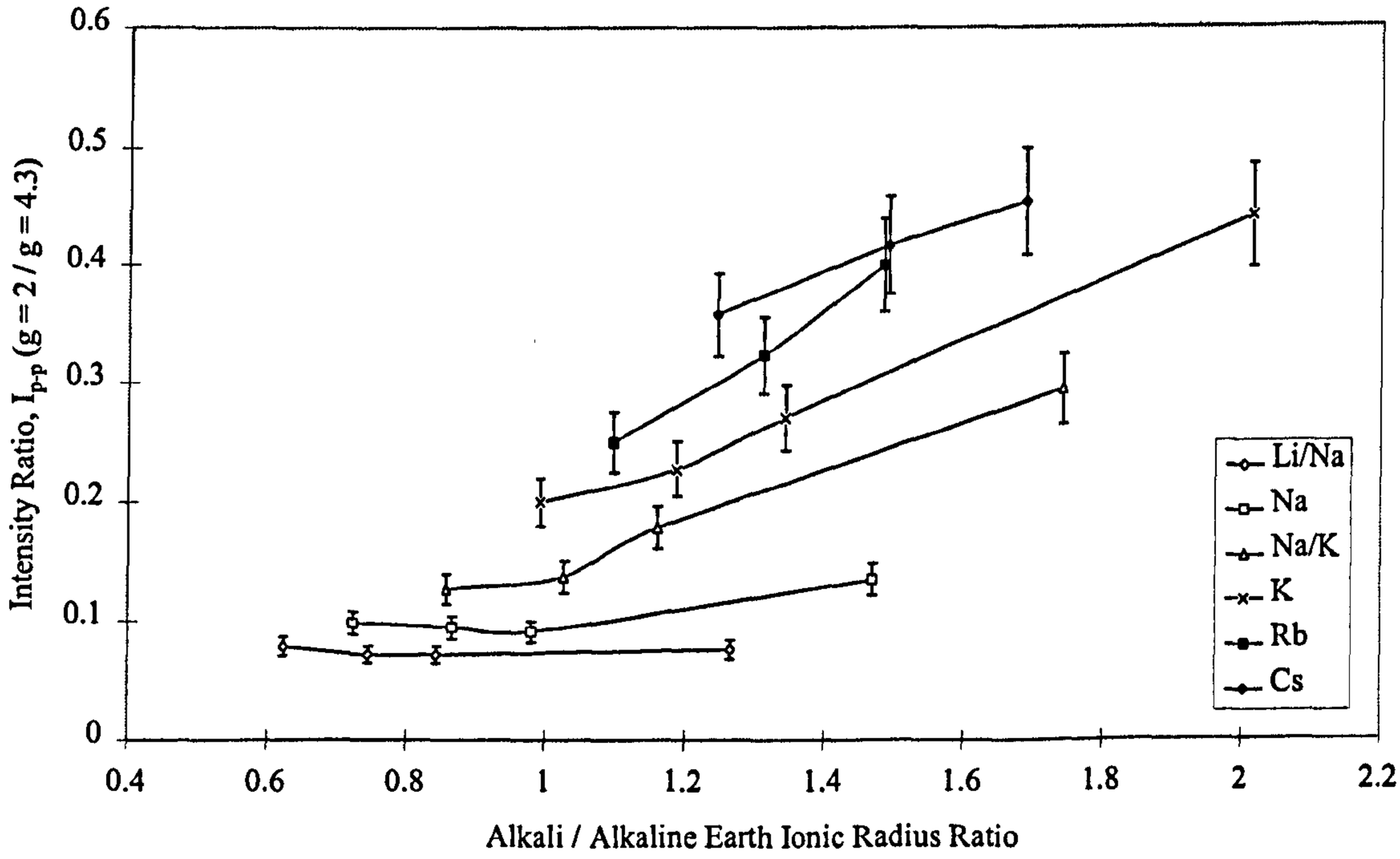

5.3.2. Changing Fe_2O_3 Content

The ESR spectrum of Fe^{3+} in glasses is strongly affected by the concentration of Fe^{3+} ions within the matrix. Figure 5.2.1.a. shows ESR spectra for glasses containing 0.1 %, 1 % and 5 % Fe_2O_3. With increasing Fe_2O_3 content, the g = 2 resonance gains intensity and the g = 4.3 and g = 6 resonances lose intensity such that with 5 % Fe_2O_3 these resonances approach zero intensity. Linewidth $\Delta H_{p\text{-}p}$ of both the g = 2 and g = 4.3 resonances increases with increasing Fe_2O_3 content.

An approximately linear relationship exists between the intensity ratio $I_{p\text{-}p}$ (g = 2 / g = 4.3) and the square of the molar Fe_2O_3 content, highlighted in figure 5.3.2.a. The average slope of the relationship is also affected by base glass composition, shown in the figure as Na_2O is replaced by K_2O. It has been shown in chapter 4.3.2.2. that sodium glasses have greater concentration per unit volume of Fe ions than potassium glasses when molar Fe_2O_3 contents are equal. This therefore cannot be a concentration-based phenomenon. The effects of composition are discussed in chapter 5.4.2.

Figure 5.3.2.b. shows that $\Delta H_{p\text{-}p}$ (g = 4.3) $\propto$ (Fe_2O_3 %) for both SiO_2-Na_2O-CaO and SiO_2-K_2O-CaO base glasses below ~ 1 molar % Fe_2O_3. Above this level $\Delta H_{p\text{-}p}$(g = 4.3) begins to saturate and reaches a maximum at 2-3 % Fe_2O_3. At >3 % Fe_2O_3, $\Delta H_{p\text{-}p}$(g = 4.3) decreases with increasing Fe_2O_3 content. As with the intensity ratio, there is a dependence on base glass composition: the linewidth reaches a maximum at lower Fe_2O_3 contents in glasses containing K_2O than with Na_2O.

Figure 5.3.2.a. Intensity Ratio, I_{p-p} (g = 2) / I_{p-p} (g = 4.3) with Varying $(Fe_2O_3\ \%)^2$ in SiO_2-R_2O-CaO Base Glasses (R = Na, K)

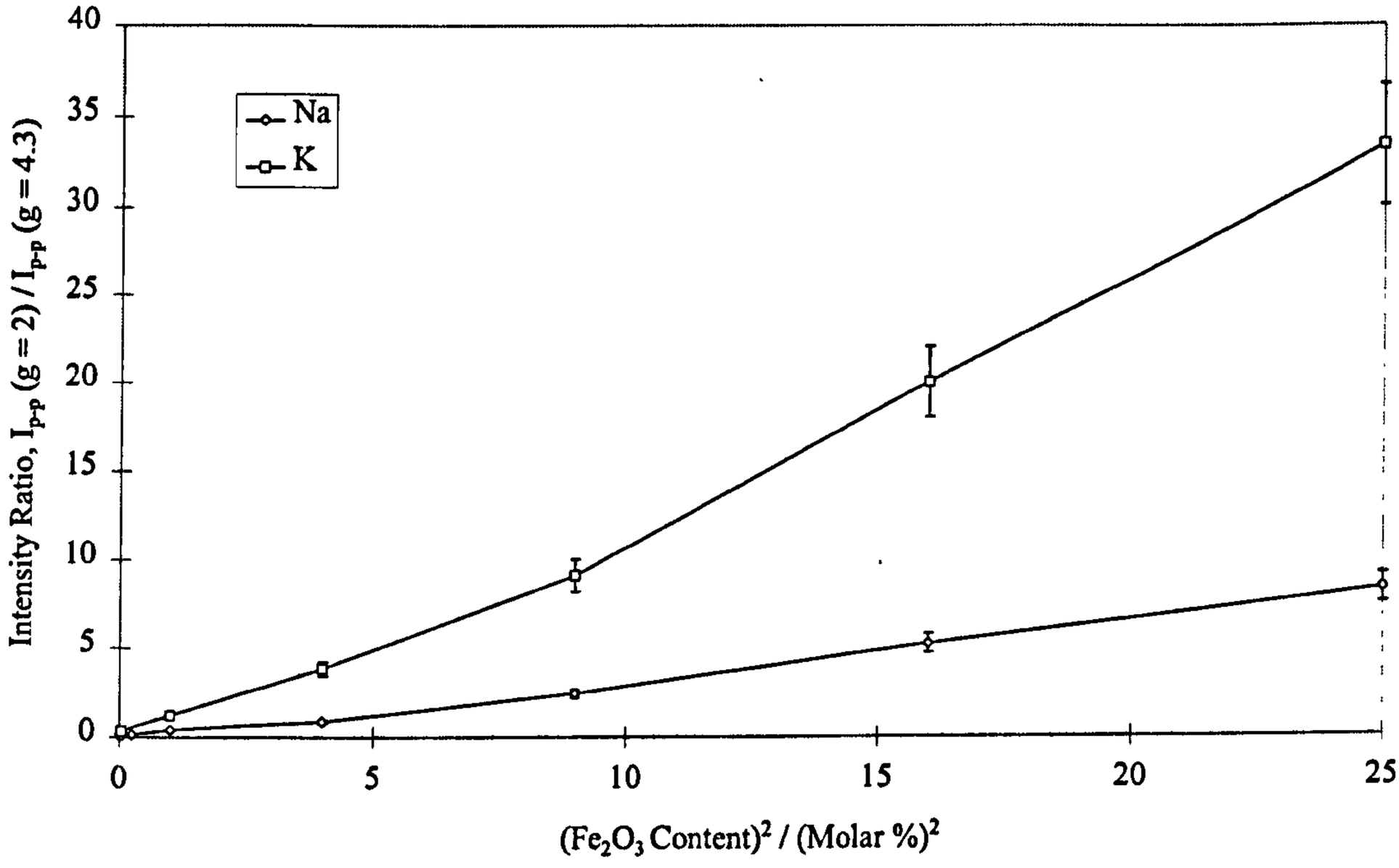

Figure 5.3.2.b. Linewidth ΔH_{p-p} of g = 4.3 Resonance with Fe_2O_3 Content in SiO_2-R_2O-CaO Base Glasses (R = Na, K)

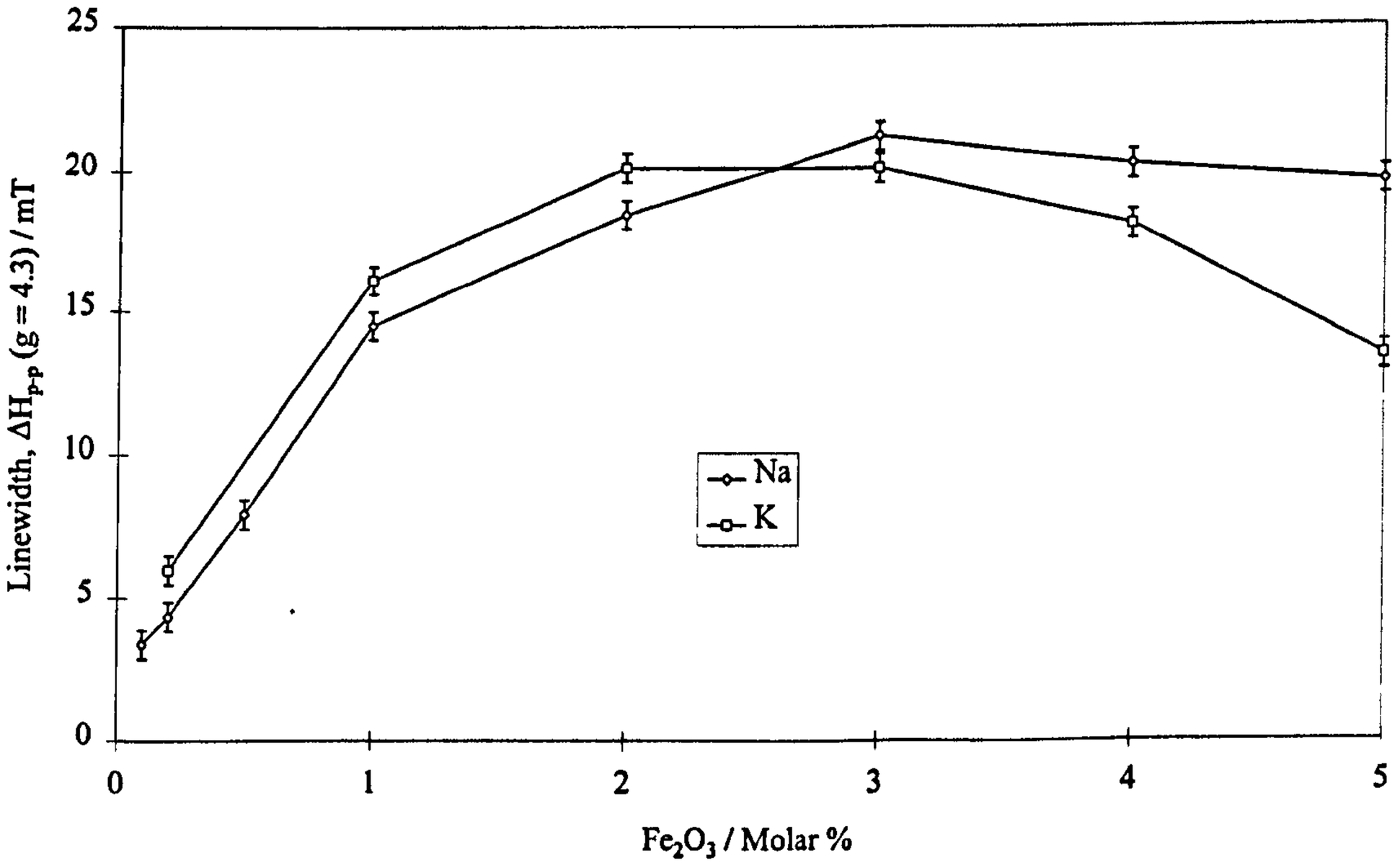

5.3.3. Borate Glass

A borate glass (sample 62) containing 0.2 molar % Fe_2O_3 gave a value of I_{p-p} (g = 2) / I_{p-p} (g = 4.3) of ~0.66, much greater than in comparable silicate glasses. This was due to a much stronger resonance at g = 2.

5.4. Discussion

5.4.1. Distribution of Fe Ions

Interpretation of the ESR results depends greatly upon the origin of the g = 2 resonance. As discussed in chapter 5.2., the majority of the literature surveyed agrees that at medium and high iron concentrations (≥ 1 molar % Fe_2O_3) the g = 2 resonance is caused by clusters of Fe^{3+} ions and not by octahedral Fe^{3+} ions. Interpretation of the g = 2 resonance at low Fe_2O_3 contents, for example 0.2 molar percent, was less straightforward. None of the works which have discussed the clustering of iron in glass and ESR measurements have done so in detail at such low concentrations, although many workers [11 - 13, 17, 22, 26, 34] have indicated that in these situations most Fe^{3+} ions occupy isolated sites. The relative amounts of isolated and clustered Fe^{3+} ions in glasses have only occasionally been measured by ESR [22]. Assuming a random distribution, some iron ions should be members of clusters even at very low concentrations. Additional evidence on the g = 2 resonance was provided by the results for the borate glass, sample 62. This glass contained 0.2 molar % Fe_2O_3, yet gave a spectrum reminiscent of a soda-lime-silica glass containing 1 - 2 molar % Fe_2O_3; the resonance at g = 2 had a greater intensity so the ratio I_{p-p} (g = 2 / g = 4.3) was larger. Considering that Fe ions have been shown to cluster less readily in silicate glasses than in borate glasses (see chapter 5.2.2.), it follows that the g = 2 resonance should be weaker in silicate glasses. This is indeed what occurred, and is yet more evidence that in these ternary silicate glasses, even at low Fe concentrations, the g = 2 resonance is

caused by clustered Fe^{3+} ions.

It was found by Mössbauer studies on float glass compositions that approximately one quarter of the Fe^{3+} ions were exchange-coupled, i.e. in close proximity and therefore clustered, at 0.199 molar % (see chapter 6.2.3.). At these low iron contents in silicate glasses, there is probably not enough clustering to cause measurable exchange narrowing of the g = 4.3 resonance, a fact known because ΔH_{p-p} (g = 4.3) increased linearly up to approximately 1 molar % Fe_2O_3 (see figure 5.3.2.b.) indicating the predominance of dipolar interactions between isolated Fe^{3+} ions at these low iron contents. The exact Fe_2O_3 content at which deviation from linearity occurs was probably slightly lower for the K glass than the Na glass, but there were too few data points to illustrate this. We know this because the linewidth saturates at lower Fe_2O_3 contents in the K glass, indicating the predominance of exchange interactions (i.e. clustering) at lower Fe_2O_3 contents (see chapter 5.2.1.). This is discussed further in chapter 5.4.2.

5.4.2. The Effects of Glass Composition

Figures 5.3.1.b. to e. show that both ΔH_{p-p} (g = 4.3) and I_{p-p} (g = 2 / g = 4.3) are strongly affected by the alkali / alkaline earth ionic radius ratio, such that increases in ΔH_{p-p} (g = 4.3) and I_{p-p} (g = 2 / g = 4.3) occurred with increasing alkali / alkaline earth ionic radius ratio brought about by larger alkali ions or smaller alkaline earth ions.

Some characteristic changes occurred in ΔH_{p-p} (g = 4.3) and the I_{p-p}(g = 2 / g = 4.3) ratio with different alkali and alkaline earth ions. For example, figures 5.3.1.c. and 5.3.1.e. show that when the alkali ion was small, such as in the Li/Na or Na glasses, the type of alkaline earth ion had little effect on either linewidth or intensity ratio. However with increasing alkali ionic size, alkaline earth ions began to have a stronger effect, such that for the larger alkalis, they did affect linewidth and intensity ratio to some degree.

The opposite effects of alkali and alkaline earth ions which were identified in the

literature survey (see chapter 5.2.2.) are evidenced by this work. Unfortunately the dependence of the strength of alkaline earth effect upon the size of the alkali ion makes the relationship a complex one.

How do we know it is alkali ions which primarily determine Fe^{3+} distribution and not alkaline earths? Figures 5.3.1.b. to 5.3.1.e. show that when considering different alkaline earth ions (figures 5.3.1.b and 5.3.1.d.), it is possible to achieve most of the values of linewidth or intensity ratio evidenced by these glasses, using any of the four alkaline earth ions. Conversely, figures 5.3.1.c. and 5.3.1.e. show that when considering different alkali ions, it is *not* possible to achieve most of the values of linewidth or intensity ratio evidenced by these glasses without changing to a different alkali ion.

Interpretation of the effects of compositional change on the intensity ratio, not only at 0.2 molar % Fe_2O_3 (see figures 5.3.1.b. to 5.3.1.e.), but at all the studied Fe_2O_3 contents, indicates that clustering of Fe^{3+} ions increases at the expense of isolated Fe^{3+} ions with increasing alkali ionic size

Structural interpretation of all these findings indicates the following:

i) Larger alkali ions promote the formation of Fe^{3+} clusters.

ii) Smaller alkaline earth ions promote the formation of Fe^{3+} clusters.

iii) The effectiveness of (ii) grows with increasing size of the alkali ion.

These findings are good evidence for *competition* between different ion types for stabilisation of Fe^{3+} ions. For all the glasses studied, there are in theory an abundance of singly-charged alkali ions present to provide sufficient charge balance for all the Fe^{3+} ions present. It has been suggested that alkali – Fe^{3+} complexes are more tightly-bound than alkaline earth – Fe^{3+} complexes and therefore are more stable [31]. The fact that the Fe^{3+} clustered / isolated distribution is primarily determined by alkali ions confirms this statement.

With increasing alkali / alkaline earth ionic radius ratio, the general increase in $I_{p\text{-}p}$ ($g = 2$ / $g = 4.3$) which indicates the presence of increasing numbers of clustered Fe^{3+} ions must be reconciled with the trend in $\Delta H_{p\text{-}p}$ ($g = 4.3$), which appears to indicate stronger dipolar interactions between isolated ions, based on the literature

survey (see figures 5.3.1.b. - c. and chapter 5.2.1.). Figure 4.3.2.2.c. shows that Fe ionic concentration in moles per unit volume *decreases* with increasing alkali / alkaline earth ionic radius ratio, yet we know from figures 5.3.1.b. and 5.3.1.c. that linewidth increases. Dipolar mechanisms are unlikely to cause this broadening because decreasing iron concentration should mean less dipolar interaction. In agreement with Moon et al [13] (see chapter 5.2.2.), the characteristics of the linear relationship between $I_{p\text{-}p}$ (g = 2) / $I_{p\text{-}p}$(g = 4.3) and $(Fe_2O_3\ \%)^2$ indicate the presence of two components. The first is the "Fe^{3+} component", which describes Fe^{3+} distribution in terms of clustered / isolated, and is based on volume concentration. The second is the "structural component", which determines the slope of the linear relationship, i.e. the rate at which the isolated / clustered transition is made with increasing iron content, and this is based on the glass composition. The rate increases with increasing size of the alkali ion, as shown in figure 5.3.2.a. As discussed above, the effects of changes in Fe volume concentration brought about by compositional change on ESR parameters are small compared with the structural component which determines Fe distribution. This effect applies for all Fe_2O_3 contents investigated, i.e. up to 5 molar %. Figure 5.3.2.b. shows that as the Fe_2O_3 content increases above 1 molar % Fe_2O_3 the linewidth tends toward saturation, and then decreases as exchange interactions between nearby Fe^{3+} ions become increasingly strong. This is in agreement with similar studies [13, 15, 16, 22, 25]. The exact Fe_2O_3 content at which saturation occurs is greater for the SiO_2-Na_2O-CaO system than the SiO_2-K_2O-CaO system, ~3 % as opposed to ~2.5 %. This indicates that clustering occurs more readily in the K_2O system, in agreement with the above discussion.

It is probably differences in the second, structural component which also give rise to the differences in $\Delta H_{p\text{-}p}$ (g = 4.3) found with changing composition. These differences are indicative of different distributions of Fe^{3+} ion environments. This disagrees with the results of Russel [20, 21], who found no significant dependence of linewidth on composition for almost identical glasses to those studied here.

The spread of results suggest that ionic radius ratio, i.e. electrostatic space/charge effects, may not be the only factor influencing the $I_{p\text{-}p}$ ratio. Covalency involved

in the bonding is not taken into account by electrostatic or space / charge scales.

The results for glasses containing MgO suggest that Mg interacts slightly differently with Fe^{3+} ions compared with the other alkaline earth ions. If some or all of the Mg^{2+} ions have 4-coordination (see chapter 2.1.) they enter the structure as glass formers rather than glass modifiers. This will produce different interactions with Fe^{3+} ions than for the other alkaline earths, which occupy sites with coordination numbers ≥ 6. It appears from the available ESR data that Mg^{2+} ions are poorer at promoting clustering of Fe^{3+} ions than suggested by alkali / alkaline earth ionic radius ratios. This may be influenced by coordination of Mg^{2+} ions and/or covalency of their bonding.

The onset of major clustering has been shown to be affected by base glass composition. Agreement was found with other work [13, 16] in that clustering predominates above approximately 3 % Fe_2O_3, although the exact Fe_2O_3 content is dictated somewhat by glass composition. Combining results for glasses containing 0.2 molar % Fe_2O_3 (see chapter 5.3.1.) and for glasses having varying iron contents with Na and K as alkalis (see chapter 5.3.2.) show that the percentage of Fe_2O_3 at which clustering predominates decreases with increasing alkali / alkaline earth ionic radius ratio, although as before, the effects of alkali ion type are stronger than the effects of alkaline earth ion type.

5.5. Chapter Summary

The g = 4.3 resonance was attributed to isolated Fe^{3+} ions in rhombically-distorted tetrahedral and octahedral sites. The g = 2 resonance was attributed to clusters of more than one exchange-interacting Fe^{3+} ion.

Study of the linewidth of the g = 4.3 resonance and the ratio of intensities of the g = 2 / g = 4.3 resonances provided information on distribution and environment of the Fe^{3+} ions.

The ratio of clustered / isolated Fe^{3+} ions was approximately proportional to the square of the molar Fe_2O_3 content. The gradient was dependent upon glass

composition. Two components were in effect, one based on Fe^{3+} volume concentration, and the other based on glass composition. Clustering of Fe^{3+} ions predominated above approximately 3 molar % Fe_2O_3 in these glasses, although the exact percentage was affected somewhat by composition, and generally could be expected to decrease with increasing alkali / alkaline earth ionic radius ratio.

Iron content and type of alkali ion primarily determined the Fe^{3+} distribution. Alkaline earth ions generally had a lesser effect. Clustering of Fe^{3+} ions occurred to some degree at all iron contents, and was measurable at 0.2 molar % Fe_2O_3.

The clustered / isolated Fe^{3+} ratio changed with glass composition because larger alkali ions promote clustering. Smaller alkaline earth ions may also promote clustering when present in combination with large alkali ions. These effects were illustrated by a general proportionality with the alkali / alkaline earth ionic radius ratio. This was interpreted as evidence for competition between ion types for stabilisation of Fe^{3+} ions, with alkali complexes being the more stable.

5.6. References

[1] Griscom, D.L., J. Non-Cryst. Solids, 1980, vol. 40, p. 211.

[2] Castner, T., Newell, G.S., Holton, W.C., Slichter, C.P., J. Chem. Phys., 1960, vol. 32, p. 668.

[3] Wong, J., Angell, C.A., Glass Structure by Spectroscopy, Marcel Dekker, New York, 1976, p. 589.

[4] Tucker, R.F., in Advances in Glass Technology, Plenum, New York, 1962, p. 103.

[5] Sands, R.H., Phys. Rev., 1955, vol. 99, p. 1222.

[6] Hirayama, C., Castle, J.G., Kuriyama, M., Phys. Chem. Glasses, 1968, vol. 9, p. 109.

[7] Bishay, A.M., Makar, L., J. Amer. Ceram. Soc., 1969, vol. 52, p. 605.

[8] Camara, B., Glastech. Ber., 1978, vol. 51, p. 87.

[9] Camara, B., J. de Phys., 1982, vol. 43, p. 165.

[10] Schels, T., Camara, B., Dannheim, H., Glastech. Ber., 1992, vol. 65, p. 162.

[11] Kurkjian, C.R., Sigety, E.A., Phys. Chem. Glasses, 1968, vol. 9, p. 73.

[12] Loveridge, D., Parke, S., Phys. Chem. Glasses, 1971, vol. 12, p. 19.

[13] Moon, D.W., Aitken, J.M., MacCrone, R.K., Cieloszyk, G.S., Phys. Chem. Glasses, 1975, vol. 16, p. 91.

[14] Montenero, A., Friggeri, M., Giori, D.C., Belkhiria, N., Pye, L.D., J. Non-Cryst. Solids, 1986, vol. 84, p. 45.

[15] Berger, R., Kliava, J., Yahaioui, E.M., Bissey, J.C., Beziade, P., Verre, 1995, vol. 1, p. 17.

[16] Mendiratta, S.K., De Sousa, E.G., J. Mat. Sci. Lett., 1988, vol. 7, p. 733.

[17] Kishore, N., Bansal, T.K., Kamal, R., Mendiratta, R.G., Phys. Chem. Glasses, 1984, vol. 25, p. 52.

[18] Tanaka, K., Kamiya, K., Yoko, T., Tanabe, S., Hirao, K., Soga, N., Phys. Chem. Glasses, 1991, vol. 32, p. 16.

[19] Chakradhar, R.P.S., Murali, A., Rao, J.L., Opt. Mat., 1998, vol. 10, p. 109.

[20] Rüssel, C., Glastech. Ber., 1993, vol. 66, p. 68.

[21] Rüssel, C., Glastech. Ber., 1997, vol. 70, p. 17.

[22] Sunandana, C.S., Jagannathan, R., Solid State Comm., 1985, vol. 53, p. 985.

[23] Bogomolova, L.D., Henner, E.K., J. Magn. Reson., 1980, vol. 41, p. 422.

[24] Harris, E.A., Phys. Chem. Glasses, 1987, vol. 28, p. 196.

[25] Eissa, N.A., El-Meleigy, W.M., El-Minyawi, S.M., Sheta, N.H., Sallam, H.A., Phys. Chem. Glasses, 1993, vol. 34, p. 31.

[26] Rao, J.L., Murali, A., Rao, E.D., Phys. Chem. Glasses, 1996, vol. 202, p. 215.

[27] Camara, B., Oel, H.J., J. Non-Cryst. Solids, 1984, vol. 65, p. 161.

[28] Vaivada, M.A., Kliava, G.G., Konstants, Z.A., Purans, J.J., Troksh, J.S., Soviet J. Glass Phys. Chem., 1984, vol. 10, p. 44.

[29] Nofz, M., Stösser, R., Wihsmann, F.G., Phys. Chem. Glasses, 1990, vol. 31, p. 57.

[30] Nofz, M., Stösser, R., Wihsmann, F.G., J. Non-Cryst. Solids, 1991, vol. 129, p. 249.

[31] Waff, H.S., Can. Mineral., 1977, vol. 15, p. 198.

[32] Gerlach, S., Clausen, O., Rüssel, C., J. Non-Cryst. Solids, 1998, vol. 238, p. 75.

[33] Valente, M.A., Mendiratta, S.K., De Sousa, E.G., Proc. 16th ICG, madrid, 1992, vol. 4, p. 391.

[34] Kordas, G., Oel, H.J., Phys. Chem. Glasses, 1984, vol. 25, p. 76.

Chapter 6.

Mössbauer Spectroscopy

6.1. Principles of Operation

Mössbauer spectroscopy utilises the recoil-free emission and resonant absorption of γ-radiation by ^{57}Fe nuclei. The effect of recoil energy, which can be neglected for sound and light, becomes dominant in the γ-ray region. For a free ^{57}Fe nucleus, recoil energy is several orders of magnitude greater than the linewidth of the resonance absorption, so the resonance will not be defined. Mössbauer discovered however that in solids, under certain conditions, recoil energy is essentially nil and thus resonance can be observed. By comparing the observed spectrum with that of a reference, for example α-Fe, it is possible to obtain information on co-ordination, bonding and valence. Effects external to the ^{57}Fe nucleus, while very small, can be distinguished due to the very high resolution of this technique. Once the spectra have been measured, they are fitted with Lorentzian lineshapes representing Fe^{2+} and Fe^{3+} components.

6.2. Background and Literature Survey

Mossbauer spectroscopy using the isotope ^{57}Fe has been extensively studied in glasses over the past few decades, and there exist a number of excellent articles

and reviews on this subject [1 – 8].

Metallic Fe gives a distinctive 6-line Mössbauer spectrum, which can easily be fitted using Lorentzian line shapes. Mössbauer spectra of Fe in glasses are more complicated. Linewidths are indicative of the range of site occupancies, and glasses give wider site distributions than crystals due to their disordered nature.

6.2.1. Mössbauer Spectra of Iron in Glasses

Figure 6.2.1.a. shows a typical Mössbauer spectrum of a glass containing iron. There are two distinctive overlapping doublets and computer fitting was required to properly resolve them.

Figure 6.2.1.a. Typical Mössbauer Spectrum of Iron in Glass at Ambient Temperatures

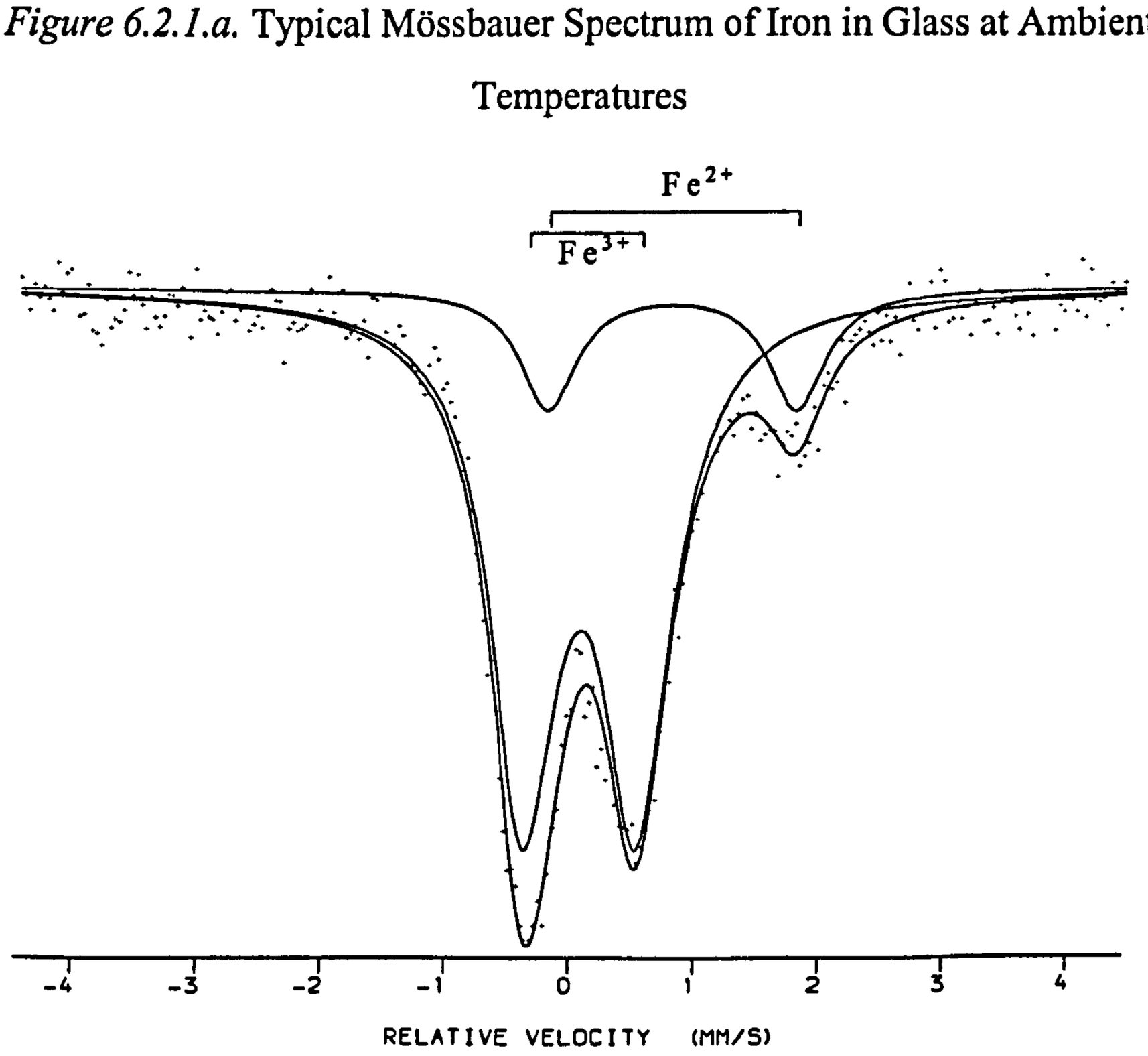

Mössbauer spectra of iron in glasses can give the following parameters: isomer shift or centre shift (δ), quadrupole splitting (Δ), linewidth (Γ) and paramagnetic hyperfine splitting (hfs). These parameters indicate the environment and coordination of the Fe ions present. Changes in the values of these parameters therefore indicate changes in the environment and coordination of Fe ions. By comparing the absorption area ratios of the Fe^{2+} and Fe^{3+} components, it is possible to measure the redox ratio.

A typical Mössbauer spectrum of a silicate glass at low temperature (see figure 6.3.1.a.) with an intermediate iron content of 1 molar % Fe_2O_3, contains two doublets and hfs. One of the doublets is caused by exchange-interacting Fe^{3+} ions with faster spin-spin relaxation times, and the other by Fe^{2+} ions. The hfs is caused by isolated Fe^{3+} ions with slow spin-relaxation times.

The relative areas enclosed by the doublets represent the redox ratio of Fe^{2+}/Fe^{3+} in the glass. In this glass about 15 % of the total Fe is Fe^{2+}. This means 85 % is Fe^{3+}, which is highlighted by the relative areas of the two doublets. It can also be seen that the isomer shift (δ) and quadrupole splitting (Δ) is different for Fe^{2+} and Fe^{3+} ions. The isomer shift (δ) is measured at the midpoint of each doublet and is the distance from zero velocity. The quadrupole splitting (Δ) is the separation between the maxima of the two peaks comprising a doublet.

6.2.2. Centre Shift (δ) and Quadrupole Splitting (Δ)

The centre shift, δ, arises because of small energy differences between source and absorber (sample) matrices. These energy differences are termed centre shifts and are caused by alteration in the energy difference between ground and excited states because of coulombic interactions between electrons and nucleus. Shifts therefore arise if the s-electron density is different for source and absorber nuclei. Since only the difference is measured, values are quoted relative to a "standard". Centre shift δ is a monotonic function of the s-electron density at the ^{57}Fe nucleus.

Decreases in 3s-electron densities amongst the 3*d* transition metal ions are the result of increasing amounts of screening by the 3*d* electrons. Increased covalency in $3d^5$ (Fe^{3+}) and $3d^6$ (Fe^{2+}) compounds is generally the result of increases in the 4s electron contribution [3]. Alpha-iron, α-Fe, has usually been used as a standard.

Quadrupole splitting (Δ) corresponds to the peak separation and is equivalent to the gap of two energy levels in the excited state. It occurs as a result of the interaction of the nuclear electric quadrupole moment with the electric field gradient at the nucleus. Such gradients can be caused by electrons in the chemical bonds of the ^{57}Fe atom, from charges on surrounding ions or from electrons in unfilled shells and /or charges on the ligands. In the case of high-spin Fe^{3+} the electron distribution is spherically symmetrical; therefore they do not give rise to an electric field gradient at the nucleus. Quadrupole splitting is only observed for Fe^{3+} due to deviations from perfect tetrahedral or octahedral symmetry. Thus $\Delta(Fe^{3+})$ is a measure of the distortion from cubic symmetry of Fe^{3+}. Both the electrons and the ligands contribute towards $\Delta(Fe^{2+})$, and large values are observed due to further removal of degeneracy by rhombic or axial distortions of the site. Therefore $\Delta(Fe^{2+}) > \Delta(Fe^{3+})$.

6.2.3. Paramagnetic Hyperfine Splitting (hfs)

Paramagnetic hyperfine splitting (hfs) of Mössbauer spectra can occur in glasses containing small amounts of iron, generally below approximately 3 or 4 molar % in silicate glasses [1 - 3, 9 - 12]. Hfs manifests in Mössbauer spectra as overlapping sextets which occur over a wide velocity range. Figure 6.4.1.a. gives an example of a spectrum containing hfs. Hfs cannot be resolved at ambient temperatures, where it appears as only a broad, smeared signal [1, 3, 9 - 13]. The sample must be cooled to liquid He temperatures in order to resolve the hfs. The reasons for this were discussed in some depth by Kurkjian & Buchanan [1] and by Williams et al [12]. Doublet and sextet components arise when the atomic

relaxation time is respectively shorter and longer than the Mössbauer sensing time τ_m. Atomic relaxation is caused by a combination of spin-lattice (temperature-dependent) and spin-spin (concentration-dependent) mechanisms. The resulting relaxation time τ_R is expressed as follows:

$$\frac{1}{\tau_R} = \frac{1}{\tau_1} + \frac{1}{\tau_2} \qquad \text{(Equation 6.2.3.a.)}$$

where τ_1 = spin-lattice relaxation time and τ_2 = spin-spin relaxation time.

The only requirement to measure the paramagnetic hfs is that the spin relaxation time τ_R be sufficiently long to present a stationary hyperfine field to the nucleus for a sufficiently long time (τ_m).

When the concentration of Fe ions is low, average inter-Fe distances are large and the spin-lattice mechanism predominates. Spin-spin relaxation times are large therefore τ_R is large, and so $\tau_R > \tau_m$. This produces sextets which are only fully resolved at very low temperatures. This is because spin-lattice is by far the quicker of the two mechanisms at ambient temperatures and only by removing all of the thermal energy can this mechanism be slowed enough so as to allow full and accurate resolution of the spectrum. With increasing concentrations of Fe ions, spin-spin relaxation times decrease due to lower average inter-ionic distances, thereby reducing τ_R such that $\tau_R < \tau_m$. This produces only doublet components. The sextet therefore gradually disappears as the iron concentration increases, leaving only the doublet components. The actual iron content at which the sextet disappears is affected by glass composition, but generally appears to be between 3 and 5 molar % Fe_2O_3 [1, 3, 9 - 12].

The spin-lattice relaxation time is short for Fe^{2+} ions, and thus the spin-lattice mechanism ensures that $\tau_R << \tau_m$ at all temperatures for Fe^{2+} ions. This means that Fe^{2+} ions only produce a quadrupole doublet. The sextet is caused by isolated Fe^{3+} ions, which have slow spin-spin relaxation times. Fe^{3+} ions in glass exhibit paramagnetic behaviour whereas Fe^{2+} ions do not, thus paramagnetic hfs for Fe^{3+} ions is observed without applying an external magnetic field.

Mössbauer spectroscopy of very low levels (0.08 atomic %) of Fe^{3+} in corundum [14] resolved three overlapping hyperfine sextets associated with the crystal field sub-levels $S_z = \pm 5/2$, $S_z = \pm 3/2$ and $S_z = \pm 1/2$. Williams et al [12] discussed the implications of this work and concluded that although higher iron levels ($\geq$ 0.2 molar % Fe_2O_3) should give rise to doublet components due to decreased average spin-spin relaxation times, the glassy environment causes Fe^{3+} ions to exist with a range of values of crystal field splittings of the sub-levels S_z. This reduces the frequency with which the spin-spin mechanism occurs. Thus "the glassy nature of the samples lengthens the low temperature atomic relaxation time to yield sextet Mössbauer components in samples with iron concentrations up to 4 molar % Fe_2O_3" [12].

In float glasses containing 0.199 - 4.0 molar % Fe_2O_3 the sextets from the highest two sub-levels, $S_z = \pm 5/2$, $S_z = \pm 3/2$, were resolved at sufficiently low temperatures [12]. The sextet for the $S_z = \pm 5/2$ sub-level gave by far the stronger signal, contributing 40 % of the area of the spectrum as opposed to 16 % from $S_z = \pm 3/2$. The Fe^{3+} components were explained by the following criteria:

$\tau_R < \tau_m$ Fast relaxation between ligand field sub-levels $S_z = \pm 1/2$

$\tau_R \approx \tau_m$ Intermediate rate relaxation between ligand field sub-levels $S_z = \pm 3/2$

$\tau_R > \tau_m$ Slow relaxation between ligand field sub-levels $S_z = \pm 5/2$

Even at the relatively low Fe_2O_3 content of 0.199 molar %, the doublet component associated with exchange-interacting (clustered) Fe^{3+} ions accounted for 17 % of the total area, i.e. the total Fe content [12].

6.2.4. Debye Temperature

Both isomer shift and absorption area are affected by temperature [15 - 17]. The former can be used as a method of measuring the Debye temperatures or lattice specific heats of Fe^{2+} and Fe^{3+} in glass. The energy corresponding to the highest

vibrational frequency of the nucleus is usually expressed in terms of the corresponding temperature, called the Debye temperature, θ_D.

The variations in centre shift with temperature can be explained as second-order Doppler shifts. The measured shift, or centre shift, is a sum of the isomer shift plus this temperature dependence. A simplification of the Debye formula gives equation 6.2.4.a.

$$\theta_D = \sqrt{\frac{6E_R}{k * slope}} \qquad \text{(Equation 6.2.4.a.)}$$

where θ_D = Debye temperature, recoil energy $E_R = 1.9 * 10^{-3}$ eV for ^{57}Fe, k = Boltzmann's constant, and slope = slope of graph of Ln A vs. T, where A = absorption areas of Fe^{2+} and Fe^{3+} components. Thus it is possible to calculate θ_D from fitting parameters. It is also possible to find θ_D from the temperature dependence of the centre shift. Both techniques require measurements at several different temperatures.

As may be expected, θ_D is strongly affected by glass composition. Values of $\theta_D(Fe^{3+})$ in silver vanadate glasses were 344 K and 279 K depending upon network structure [18]. In sodium aluminophosphate glasses, $\theta_D(Fe^{2+}) = 230K$ and $\theta_D(Fe^{3+}) = 385$ K [16]. In borate glasses, $\theta_D(Fe^{3+}) = 296$ K was found [19]. In a series of sodium silicate glasses, Johnson et al [20] found $\theta_D(Fe^{2+}) = 258$ K and $\theta_D(Fe^{3+}) = 312$ K. They found this to be a consequence of different metal-oxygen bond strengths of the two redox states. The higher the value of θ_D, the more tightly-bound the Fe-ion in the network. Indeed, Nishida [8] noted that $\theta_D(Fe^{3+}_{octahedral}) < 280\ K < \theta_D(Fe^{3+}_{tetrahedral})$

The literature indicates that $\theta_D(Fe^{3+}) > \theta_D(Fe^{2+})$, with glass composition having a strong effect on exact values. An approximate "cutoff" appears to occur in the more common glass systems, such that:

$$\theta_D(Fe^{2+}) < 300\ K < \theta_D(Fe^{3+})$$

6.2.5. Recoil-Free Fraction, *f*

Calculation of the recoil-free fraction is possible using equation 6.2.5.a., which applies to Debye solids.

$$f = \exp\left\{-\frac{6E_R}{k\theta_D}\left[\frac{1}{4}+\left(\frac{T}{\theta_D}\right)^2\int_0^{\theta_D/T}\frac{x\,dx}{e^x-1}\right]\right\} \qquad \text{(Equation 6.2.5.a.)}$$

f is the recoil-free fraction, E_R is the recoil energy of the nucleus, k is Boltzmann's constant, θ_D is the Debye temperature, and T is temperature. At low temperatures $T \ll \theta_D$ and the last term in the exponent is negligible.

The recoil-free fraction *f* is a function of glass composition, iron valence and iron coordination [3]. This means that to assume $f^{3+}/f^{2+} = 1.0$ for all redox states and coordinations in a glassy matrix may not be correct. This may in turn lead to inaccurate measurement of Fe^{2+}/Fe^{3+} ratios. In many minerals, $f^{3+}/f^{2+} < 1$. Values of 0.91, 0.87 and 0.91 were found at 300 K for hornblende, crocidolite and cesium trioxalate ferrate [21]. This indicates that Fe^{2+} concentrations would be overestimated by about 10 % with respect to Fe^{3+}.

Coordination also affects *f*, for example $f^{3+}_{octa}/f^{3+}_{tetra}$ values of 0.94, 0.85 and 0.96 are given for yttrium iron garnet, $BaFe_{12}O_{19}$, and $Ca_2Fe_2O_5$ respectively [21]. In chromite, a member of the spinel family, $f^{2+}_{octa}/f^{3+}_{tetra} = 0.94$ [21].

No specific studies could be found on f^{3+}/f^{2+} of iron species in glasses, and most workers have adopted $f^{3+}/f^{2+} = 1.0$ for their calculations. This assumption gives good agreement between redox ratios measured by Mössbauer and wet chemical methods [12, 22]. It was noted by Dyar [6], however, that it is well-known that $f^{2+} < f^{3+}$ in many minerals. Thus it was possible that the same phenomenon could occur in glasses, causing underestimation of $Fe^{2+}/\Sigma Fe$. This statement was not backed up with any quantitative results.

6.2.6. Coordination of Fe^{2+} and Fe^{3+}

Early work by Kurkjian & Buchanan [1] was conducted on $3SiO_2.Na_2O$ glasses containing 0.1 - 5 molar % Fe_2O_3. They observed a hyperfine sextet, or 6-line hyperfine spectrum at very low temperatures. This hyperfine component decreased in intensity as the iron content of the glass increased, and at 5 % Fe_2O_3 it had disappeared and only the quadrupole doublets remained. By comparing values of δ for a number of iron compounds, it was shown that Fe^{2+} exists in octahedral coordination.

Coordinations of iron ions in glasses have often been inferred from Mössbauer data, usually from centre shifts and quadrupole splittings [1 - 4, 6 - 8, 13, 16, 20, 22 - 40]. Dyar [6] proposed a set of general rules after consulting over 150 works up to 1985:

$$\delta\ (Fe^{3+}_{tetrahedral}) = 0.20 - 0.32\ mm\ s^{-1}$$

$$\delta\ (Fe^{3+}_{octahedral}) = 0.35 - 0.55\ mm\ s^{-1}$$

$$\delta\ (Fe^{2+}_{tetrahedral}) < 1.0\ mm\ s^{-1}$$

$$\delta\ (Fe^{2+}_{octahedral}) > 1.0\ mm\ s^{-1}$$

Tomandl [41] proposed the following general rules which are similar to those of Dyar:

$$\delta\ (Fe^{3+}_{tetrahedral}) = 0.2 - 0.4\ mm\ s^{-1}$$

$$\delta\ (Fe^{3+}_{octahedral}) = 0.4 - 0.6\ mm\ s^{-1}$$

$$\Delta\ (Fe^{3+}_{tetrahedral}) = 0.7 - 1.0\ mm\ s^{-1}$$

$$\Delta\ (Fe^{3+}_{octahedral}) = 0.3 - 0.9\ mm\ s^{-1}$$

Values of δ for both Fe^{2+} and Fe^{3+} in glass are a little larger than in crystalline materials because of the decreased 4s-electron density and covalency [41].

Quadrupole splitting, Δ, gives information on coordination since distorted $Fe^{3+}_{tetrahedral}$ generally has a lower symmetry than distorted $Fe^{3+}_{octahedral}$.

It occurs that regardless of matrix composition or valence,

$$\delta \text{ (tetrahedral)} < \delta \text{ (octahedral)}$$

The actual effects of glass composition on δ and Δ are often difficult to measure, since factors such as iron content and redox also play a role.

Between two and four doublets have usually been fitted to measured spectra. Simplest and most popular has been the two-doublet approach, one each for Fe^{2+} and Fe^{3+}. This was done by early workers such as Gosselin et al [15] Belyustin et al [42], and is still used to this day. One doublet each for tetrahedral and octahedral Fe^{3+} ions, plus one for Fe^{2+} has also been used [26, 29, 36, 43, 44]. There has been some reluctance to fit four doublets. This may be due to the general consensus that fitting of a fourth doublet is statistically unjustified. Zhou et al [39] fitted four doublets to spectra of SiO_2-Na_2O-Al_2O_3-ZnO-Fe_3O_4 glasses. The dilemma here is whether fitting more than two doublets, one for Fe^{2+} and one for Fe^{3+}, actually mirrors the site occupancies or whether it simply gives better statistical fitting. This is highlighted by Joseph & Pye [5], who say "Though the assumption that the Mössbauer spectrum is composed of a large number of peaks may lead to a better fit, the results may not represent the actual distribution of iron in the glass. In those cases where the Mössbauer isotope is suspected to exist in all possible configurations, it is necessary to confirm the results.....using other techniques".

Temperature has been shown to affect δ, Γ and Δ [15 - 17]. The variation of Γ with temperature can be explained by the resolution of the hyperfine sextet caused by isolated Fe^{3+} ions at low temperatures. At higher temperatures, the sextet "smears" to become a broad signal which introduces inaccuracies in linewidths of any doublets fitted.

Both δ and Δ decrease with increasing temperature [10, 15 - 17, 45]. The same trends were found in many different systems, hence the effect is not composition-dependent. Approximately linear relationships exists between δ and T and

between Δ and T [15, 16]. The slopes of these relationships differ greatly. Gosselin et al [15] found strong temperature dependence of both $\Delta(Fe^{2+})$ and $\Delta(Fe^{3+})$, but Taragin et al [16] later found $\Delta(Fe^{3+})$ was independent of temperature. Both $\delta\ (Fe^{3+})$ and $\delta\ (Fe^{2+})$ increase with increasing temperature [10, 15 - 17].

Temperature should not affect high-spin $\Delta(Fe^{3+})$, since the only contribution is from the ligand field [16]. Deviations from perfect tetrahedral or octahedral symmetry may introduce a weak temperature effect, so $\Delta(Fe^{3+})$ should be little affected by changes in temperature. Decreasing Δ with increasing temperature indicates increasing lattice symmetry [15].

6.2.7. Linewidth, Γ

Linewidths for ^{57}Fe in glassy materials are greater than in comparable crystalline materials. This is attributed to greater variation in site parameters due to the nature of a distorted glassy matrix [3]. Many workers have discussed the phenomenon of decreasing linewidths with increasing Fe concentration [15, 24, 29, 42, 44]. For some [15, 24] it is explained by the fact that the spectra were not measured at low temperature so the Fe^{3+} hfs was not resolved. Instead it was a broad smear, causing broadening of the observed Fe^{3+} doublet whilst leaving the Fe^{2+} doublet unaffected. Increasing iron content up to about 3 % Fe_2O_3 therefore caused a decrease in the apparent Fe^{3+} linewidth. This effect would decrease with increasing iron content as the hfs disappeared. Detailed work by Williams et al [12] showed that even when measured at 4 K, doublet $\Gamma(Fe^{3+})$ still decreased with increasing Fe_2O_3 content up to 4 molar %. Linewidth indicates the range of site parameters. Results which cannot be explained by wrong measurement temperature thus suggest a wider range of site occupancies at low Fe concentrations. The range of site occupancies is wider for Fe^{3+} than Fe^{2+}. This agrees well with the general view that in silicate glasses, Fe^{3+} ions are present in appreciable numbers in both tetrahedral and octahedral sites and Fe^{2+} ions are

predominantly situated in distorted octahedral sites [1 - 3, 9, 15, 16, 25, 26, 30, 37, 39, 46 - 54]. An increase in Γ indicates a wider range of site occupancies, probably involving a change in average coordination number.

Linewidth is influenced by glass composition. Silicate glasses exhibit a larger range of site occupancies than borate and phosphate glasses, according to the detailed review of Dyar [6]:

$$\text{Phosphate Glasses } \Gamma \approx 0.4 - 0.6 \text{ mm s}^{-1}$$

$$\text{Borate Glasses } \Gamma \approx 0.6 - 0.9 \text{ mm s}^{-1}$$

$$\text{Silicate Glasses } \Gamma \approx 0.4 - 1.2 \text{ mm s}^{-1}$$

Linewidths of Fe^{2+} and Fe^{3+} doublets have been found to change with composition in binary alkali silicate glasses containing Fe_2O_3 [40]. Increasing the size of the alkali ion from Li to Na to K showed a progressive decrease in $\Gamma(Fe^{3+})$. This indicates that the range of site occupancies and distortions decreased with increasing size of alkali ion, probably because as they become larger they are less polarising and exert weaker influences on Fe-O polyhedra. There was some variation in $\Gamma(Fe^{2+})$, but no obvious trend.

6.2.8. Effects of Iron Concentration

Conflicting evidence exists concerning other Mössbauer parameters of glasses with varying iron content. Several workers found that $\Delta(Fe^{3+})$ increased with increasing iron content in a number of glass systems including silicates [29, 30, 32, 39, 44] and borosilicates [34]. The size of these increases was affected by composition and possibly by fitting methods. Other work on silicate glasses showed no change in $\Delta(Fe^{3+})$ with increasing iron content [15, 24]. The reasons for this disagreement are not clear. One notable difference is that all the papers showing increasing $\Delta(Fe^{3+})$ with iron content used two doublets to fit the Fe^{3+} component, one each for tetrahedral and octahedral sites. The papers showing

little or no change in $\Delta(Fe^{3+})$ used only one doublet to fit the Fe^{3+} component.

Early work [15, 23, 24, 42] highlighted differences when comparing redox ratios measured by Mössbauer spectroscopy with those measured by wet chemical analysis. Results indicated that the two techniques essentially agreed at iron contents above about 3 molar % Fe_2O_3. Below this level, Mössbauer measurements indicated large changes in the redox which increasingly favoured Fe^{2+} with decreasing iron content. The possibility that *f* - values were not equal to 1.0 was considered, but if this was the case there would be disagreement between the techniques at *all* Fe_2O_3 concentrations and not just low levels.

Williams et al [12] have shown how by measuring spectra at liquid He temperatures and wide velocity ranges where the absorption due to hfs relaxation is included, there are good correlations between wet chemical and Mössbauer measurements of $Fe^{2+}/\Sigma Fe$ at all Fe_2O_3 contents in silicate glasses. Other workers [11, 22] have found good agreement between the techniques for iron contents where no hfs was expected.

6.2.9. Composition - Redox - Coordination Interactions

In a series of papers, Mysen & co-workers [13, 31, 33, 36, 37] investigated and discussed the interaction between redox and changes in Mössbauer parameters of alkaline earth silicate and alkaline earth aluminosilicate glasses containing iron. Changes in δ and Δ of the Fe^{2+} and Fe^{3+} components with changing redox were interpreted as being due to coordination changes. Isomer shift of Fe^{3+}, $\delta(Fe^{3+})$, was found to be sensitive to redox regardless of the bulk composition, temperature and oxygen fugacity of the melt. When $Fe^{3+}/\Sigma Fe > 0.6$, $\delta(Fe^{3+})$ was approximately constant at 0.3 mm s^{-1} and Fe^{3+} ions were in tetrahedral sites. When $Fe^{3+}/\Sigma Fe < 0.3$, $\delta(Fe^{3+})$ was approximately constant at 0.5 mm s^{-1} and Fe^{3+} ions were in octahedral sites. Between these two levels a rapid transition took place such that an increase in oxidation led to a drop in $\delta(Fe^{3+})$ and Fe^{3+} ions occupied a

combination of tetrahedral and octahedral. Quadrupole splitting of Fe^{3+}, $\Delta(Fe^{3+})$, decreased approximately linearly with increasing values of $Fe^{2+}/\Sigma Fe$, but was approximately constant when $Fe^{2+}/\Sigma Fe < 0.2$. Both the changes in $\delta(Fe^{3+})$ and $\Delta(Fe^{3+})$ indicated that the average Fe^{3+} coordination became more tetrahedral with increasing $Fe^{3+}/\Sigma Fe$.

Isomer shift and quadrupole splitting values have indicated that in lithium, sodium and potassium silicate glasses containing Fe_2O_3, the Fe^{3+} ions occur mostly in tetrahedral coordination [2, 3, 33], even more so in the K_2O glass than the Na_2O glass [3]. In phosphate glasses, $\delta(Fe^{3+})$ indicated that Fe^{3+} ions were mostly in octahedral coordination [2, 3].

In soda-lime-silica glasses containing 20-35 % Fe_2O_3, the Fe^{2+}/Fe^{3+} ratio increased with decreasing glass basicity and the replacement of Na_2O by CaO [26]. The $Fe^{3+}_{octahedral} / Fe^{3+}_{tetrahedral}$ ratio appeared to be unaffected by the replacement of Na_2O by CaO, however both δ and Δ increased almost linearly with the replacement, which could be interpreted as indicating a change in average coordination.

In alkali silicate glasses containing iron, it was found that valence and coordination of iron were functions of, amongst other parameters, iron content and amount and type of alkali ion [2, 40]. Measurements showed decreases in $\delta(Fe^{3+})$ and $\Delta(Fe^{3+})$ with increasing alkali ionic size or decreasing cation field strength because of an increasing s-electron density at the Fe nucleus. These decreases were almost linear when plotted against increasing optical basicity of the glass [40]. Hence the observed dependence of δ with alkali ionic size or cation field strength or optical basicity means that the electron density at the Fe nucleus is determined by second nearest neighbour cations [40].

Slight differences can be found when comparing the results of Kurkjian & Sigety [2] and Burkhard [40]. Both papers concerned alkali silicate glasses although with slight compositional differences. Increasing alkali ionic radius from Li to Na to K resulted in a small decrease in $\delta(Fe^{3+})$ and no change in $\Gamma(Fe^{3+})$ in the work of Kurkjian & Sigety [2], however Burkhard [40] showed a more pronounced decrease in $\delta(Fe^{3+})$, accompanied by a substantial decrease in $\Gamma(Fe^{3+})$, with

increasing alkali ionic radius. Both sets of results showed a substantial decrease in $\Delta(Fe^{3+})$ with increasing ionic radius. In the earlier paper [2], the lithium silicate glass crystallised and had to be re-melted under different conditions from the sodium and potassium silicates. The crystallisation problem was avoided in the later paper [40] by quenching the glass upon pouring. These differences in preparation probably contributed to the differences in measured Mössbauer parameters.

In lead borate glasses containing 5-50 % iron, $\delta(Fe^{3+})$ decreased with increasing Fe_2O_3 content and $\Delta(Fe^{2+})$ increased with increasing Fe_2O_3 content [30]. The $Fe^{3+}_{octahedral}$ / $Fe^{3+}_{tetrahedral}$ ratio was unaffected by Fe_2O_3 content in the range studied. Redox was strongly affected by Fe_2O_3 content, decreasing from $Fe^{2+}/Fe^{3+} = 0.8$ to 0.4 as Fe_2O_3 % increased from 10 – 50 %. It is possible, however, that insufficient equilibration time was allowed during melting and this would have seriously affected the results.

In CaO-MgO-SiO_2 glasses, both Fe^{3+} and Fe^{2+} occupy octahedral sites [13]. It was thought that this is because $CaFe_2O_4$ and $MgFe_2O_4$ complexes are not stable in molten silicates. It was therefore concluded that only alkali ions such as Na^+ and K^+ etc. stabilise Fe^{3+} in tetrahedral coordination, and providing sufficient alkali metal ions are present in a melt then Fe^{3+} ions occur in tetrahedral coordination. Waff [55] found that (Na, K) $Fe^{3+}O_2$ complexes are more tightly-bound and therefore, more stable than (Mg, Ca) $Fe^{3+}O_2$ complexes. This work agreed with Mysen et al [13], who found that a progressive decrease of M^+ / M^{2+} of a magma resulted in Fe^{3+} ions shifting from tetrahedral to octahedral coordination.. These results disagreed with those of Levy et al [26], who found no effect in silicate glasses with the progressive replacement of Na_2O by CaO, although perhaps within the range studied there was sufficient Na^+ present to stabilise Fe^{3+} in tetrahedral sites regardless of the number of Ca^{2+} ions added. Gerlach et al [56] found that alkaline earth ions can stabilise Fe^{3+} in tetrahedral sites. Mössbauer parameters of Mysen et al [33] indicated increasing distortion of the Fe^{3+} tetrahedra as the cation field strength of the charge-balancing cation increased.

The value of $\Delta(Fe^{3+})$ increased with increasing cation field strength of the alkali ion [33]. This was suggested to be the result of increasing distortion of the Fe^{3+} tetrahedra as the cation field strength of the charge-balancing cation increases. Quadrupole splitting of Fe^{2+} components was generally found to increase with decreasing $Fe^{2+}/\Sigma Fe$, which again may be indicative of the coordination changes discussed previously.

Linear increases in δ and Δ for Fe^{2+} and Fe^{3+} were found in lithium vanadium borosilicate glasses containing up to 12.5 % Fe_2O_3 [34]. At low iron contents, results indicated that iron was a network modifier, whilst at higher iron contents it was a network former. Slight increases in isomer shifts with increasing iron content indicated a decrease in the degree of covalency of both Fe^{2+} and Fe^{3+}.

6.3. Results

Mössbauer spectra were analysed in terms of the $Fe^{2+}/\Sigma Fe$ ratio, centre shift (δ), quadrupole splitting (Δ), and linewidth (Γ). Most spectra were fitted with two Lorentzian doublets, one each for Fe^{2+} and Fe^{3+} ions. Two samples were measured with wide velocity ranges at 7 K and the resulting spectra were fitted with two doublets and two sextets.

Results from wet chemical redox analysis and optical spectroscopy indicated that there was little change in $Fe^{2+}/\Sigma Fe$ ratio throughout the series of SiO_2-Na_2O-CaO glasses containing 1 – 5 % Fe_2O_3. This prompted the questioning of the accuracy of the 293 K Mössbauer results for the glasses containing 1 and 2 molar % Fe_2O_3.

When the concentration of Fe_2O_3 in glasses is very low, overestimation of the $Fe^{2+}/\Sigma Fe$ ratio from Mössbauer measurements can occur (see chapter 6.2.8.). In order to measure these samples accurately, they must be cooled to near liquid He temperatures (~ 7 K), and measured with a wider velocity range of ± 12 mm s^{-1} (see chapter 6.2.3.).

Subsequent measurement of spectra under these conditions showed hyperfine

splitting in the 1 % and 2 % Fe_2O_3 samples. Fitting the spectra gave $Fe^{2+}/\Sigma Fe$ ratios closer to those for the 3 – 5 % Fe_2O_3 samples, and there was much better agreement with wet chemical and optical results.

6.3.1. Varying Fe_2O_3 Content

SiO_2-Na_2O-CaO glasses containing 1, 2, 3, 4, 5 molar % Fe_2O_3 were analysed by Mössbauer spectroscopy. The samples containing 1 % and 2 % Fe_2O_3 were measured at 7 K and in the velocity range of ± 12 mm s^{-1} in order to resolve the hyperfine splitting components. The samples containing 3 %, 4 % and 5 % Fe_2O_3 were measured at 293 K and in the velocity range ± 5 mm s^{-1}. It was expected that there would be little or no hfs present in these samples, on the basis of results from previous studies [1 - 3, 9, 10, 12, 54]. Figures 6.3.1.a., 6.3.1.b., and 6.3.1.c. show the fitted spectra for the 1 %, 2 % and 5 % Fe_2O_3 samples, respectively. All measured parameters are given in table 6.3.1.a.

Figure 6.3.1.a. Mössbauer Spectrum of SiO_2-Na_2O-CaO-1 % Fe_2O_3 Glass at 7 K

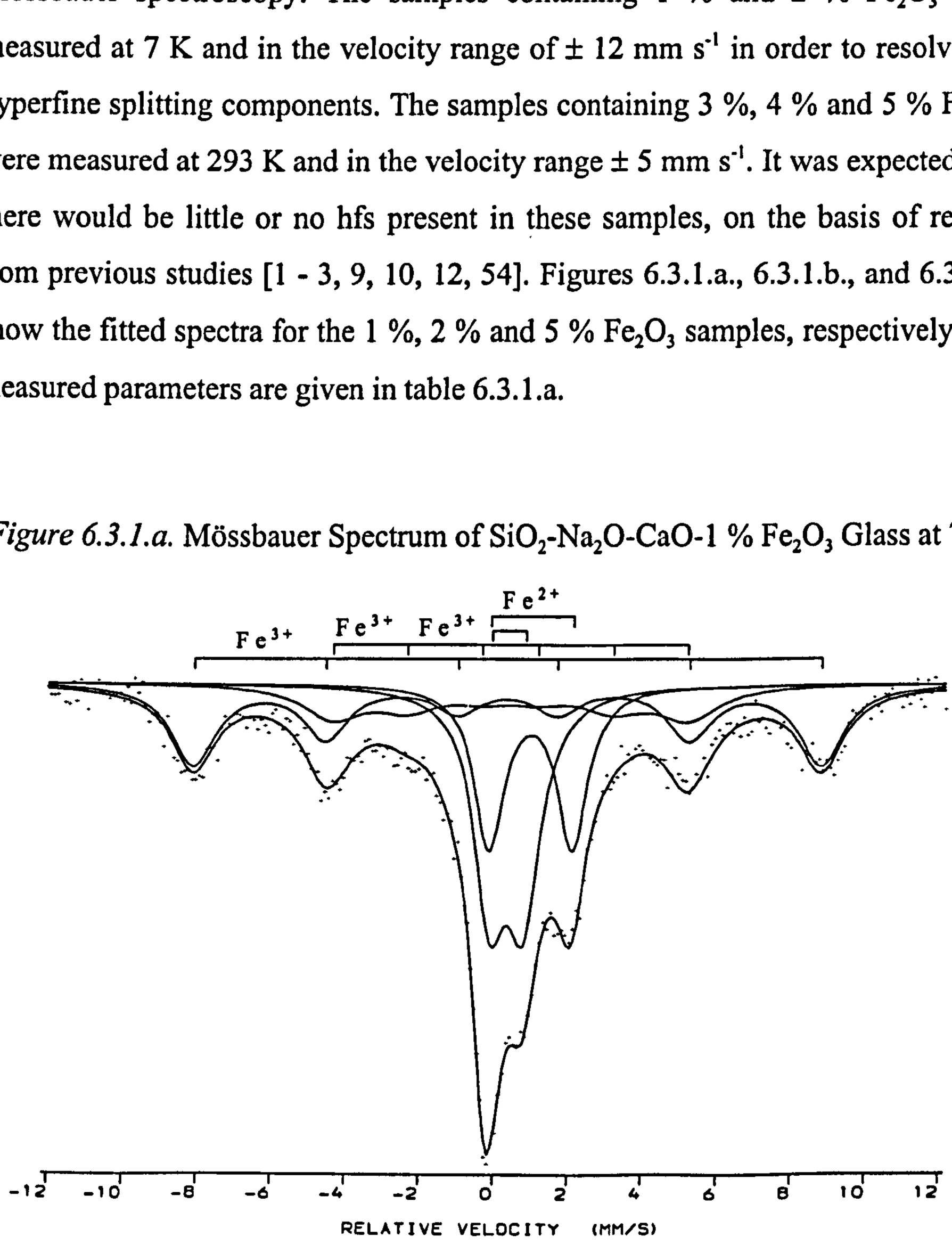

Figure 6.3.1.b. Mössbauer Spectrum of SiO_2-Na_2O-CaO-2 % Fe_2O_3 Glass at 7 K

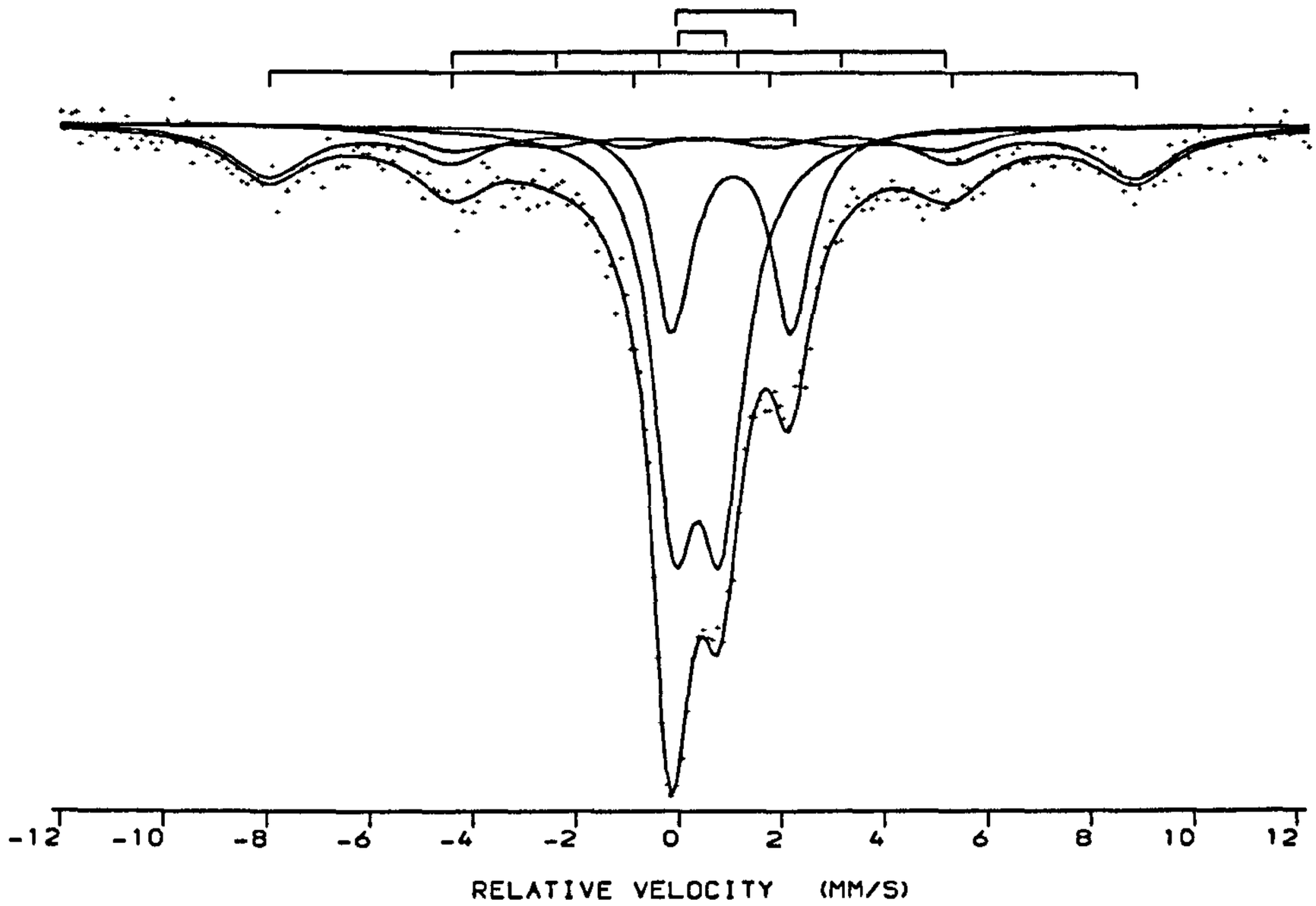

Figure 6.3.1.c. Mössbauer Spectrum of SiO_2-Na_2O-CaO-5% Fe_2O_3 Glass at 293 K

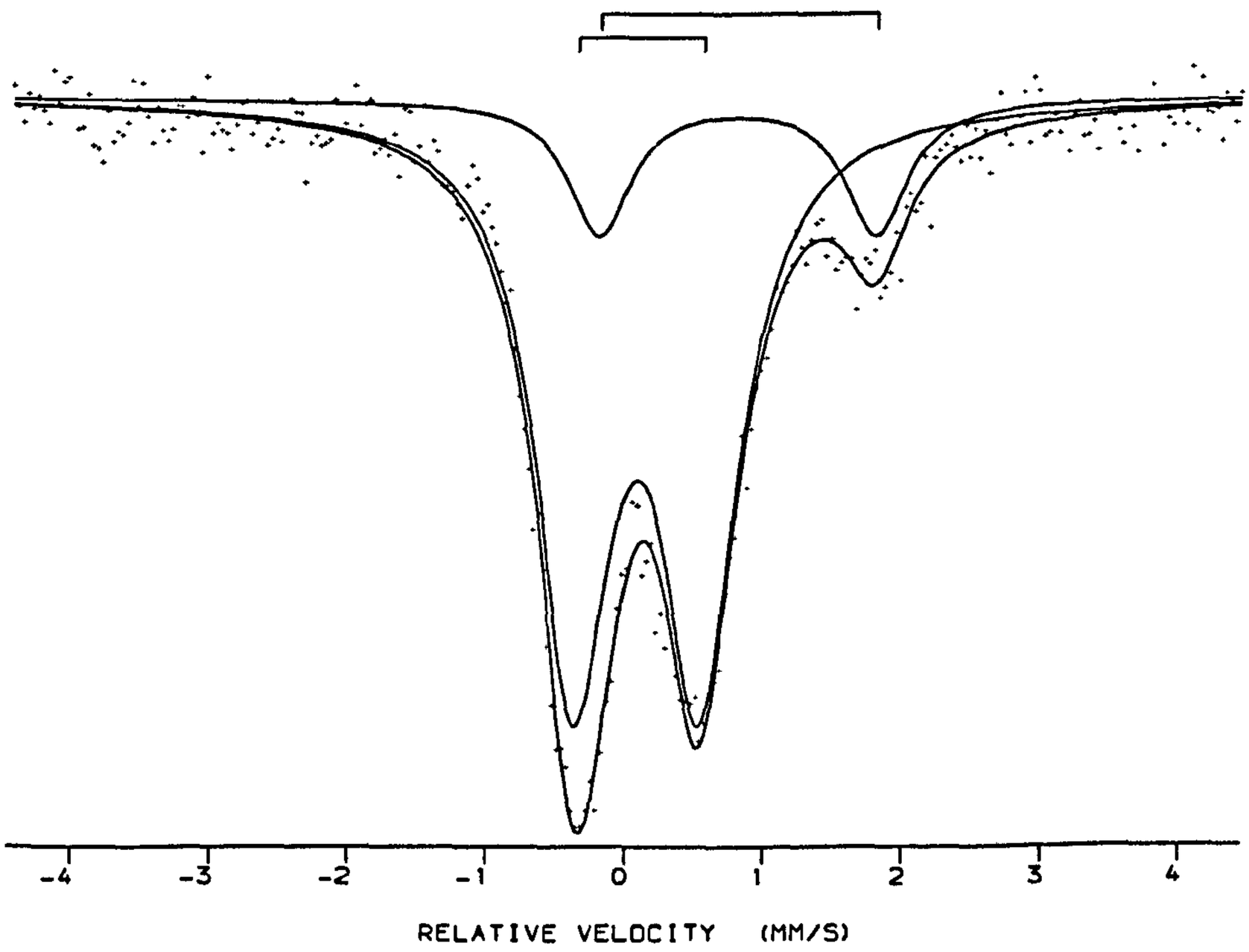

Table 6.3.1.a. Mössbauer Parameters of SiO_2-Na_2O-CaO Glasses containing 1 – 5 % Fe_2O_3

Fe_2O_3 Molar %	1	2	3	4	5
$Fe^{2+}/\Sigma Fe$ * 100 %, ± 2	21.16	21.99	19.38	13.28	16.33
CS (Fe^{2+}) / mm s^{-1}, ± 0.02	1.06	1.07	1.02	1.00	0.98
QS (Fe^{2+}) / mm s^{-1}, ± 0.03	2.24	2.31	2.07	2.03	1.99
LW (Fe^{2+}) / mm s^{-1}, ± 0.03	0.99	0.89	0.67	0.56	0.55
Area (Fe^{2+}) %	21.16	21.99	19.38	13.28	16.33
CS (Fe^{3+} doublet) / mm s^{-1}, ± 0.02	0.44	0.44	0.29	0.28	0.27
QS (Fe^{3+} doublet) / mm s^{-1}, ± 0.03	0.91	0.91	0.91	0.92	0.91
LW (Fe^{3+} doublet) / mm s^{-1}, ± 0.03	1.08	1.02	0.72	0.64	0.66
Area (Fe^{3+} doublet) %	29.54	44.93	80.62	86.72	83.67
CS (Fe^{3+} sextet A) / mm s^{-1}, ± 0.02	0.40	0.44	-	-	-
LW (Fe^{3+} sextet A) / mm s^{-1}, ± 0.03	1.46	1.81	-	-	-
Area (Fe^{3+} sextet A) / %	31.75	22.35	-	-	-
CS (Fe^{3+} sextet B) / mm s^{-1}, ± 0.02	0.47	0.38	-	-	-
LW (Fe^{3+} sextet B) / mm s^{-1}, ± 0.03	2.000	2.000	-	-	-
Area (Fe^{3+} sextet B) / mm s^{-1}	17.55	10.74	-	-	-

The areas contained by the doublets and sextets indicate the relative abundances of Fe^{2+} and Fe^{3+} ions, hence the $Fe^{2+}/\Sigma Fe$ ratio. This assumes that the recoil-free fraction, *f*, of Fe^{2+} and Fe^{3+} ions is equal, which has not been proven in silicate glasses (see chapter 6.2.5.). The Mössbauer results suggest a change in redox with Fe_2O_3 content (see table 6.3.1.a.), but these results should not be used without corroborating evidence, as the 1 % and 2 % samples were measured under

different conditions to the 3 – 5 % samples. The $Fe^{2+}/\Sigma Fe$ ratios measured were generally 15 - 20 %, showing differences of only a few percent with changing Fe_2O_3 content.

A linear regression was used to predict the amounts of Fe^{3+} ions giving rise to doublet and sextet components at all the studied iron contents (see table 6.3.1.b). This regression followed the relationship $C \propto (Fe_2O_3)^2$, established from ESR measurements in both this study and other work (see chapter 5). Values of redox were from Mössbauer measurements where possible, and wet chemistry for < 1 % Fe_2O_3.

Table 6.3.1.b. Predicted Distribution of Sites Based on $C \propto (Fe_2O_3)^2$

Fe_2O_3 %	$(Fe_2O_3\ \%)^2$	Fe^{2+} / ΣFe %	$Fe^{3+}_{isolated}$ / ΣFe %	$Fe^{3+}_{clustered}$ / ΣFe %
0.1	0.01	15	63.0	22.0
0.2	0.04	16	61.9	22.1
0.5	0.25	16	59.6	24.4
1	1	21.16	49.3	29.6
2	4	21.99	33.1	44.9
3	9	19.38	22.2	58.4
4	16	13.28	16.1	70.6
5	25	16.33	10.9	72.8

Centre shifts of Fe^{2+} and Fe^{3+} doublets show a general decrease with increasing Fe_2O_3 content, highlighted in table 6.3.1.a. and figure 6.3.1.d. The apparent "jump" in δ between 2 % and 3 % Fe_2O_3 is caused by the difference in measurement temperature for the 1 % and 2 % samples.

Values of $\Delta(Fe^{2+})$ show that despite the difference in measurement temperature for

the 1 % and 2 % samples, a general decrease in $\Delta(Fe^{2+})$ occurs with increasing Fe_2O_3 content. The value of $\Delta(Fe^{3+})$ is unaffected by Fe_2O_3 content.

Linewidth may be affected by the difference in measurement conditions between the 1 – 2 % and 3 – 5 % Fe_2O_3 samples, however table 6.3.1.a. and figure 6.3.1.e. show that there is a general decrease in Γ with increasing Fe_2O_3 content. The rate of change in $\Gamma(Fe^{2+})$ and $\Gamma(Fe^{3+})$ is greatest at low Fe_2O_3 contents.

Figure 6.3.1.d. Centre Shift (Relative to α-Fe) of Doublets Fitted to SiO_2-Na_2O-CaO Glasses Containing 1-5 Molar % Fe_2O_3

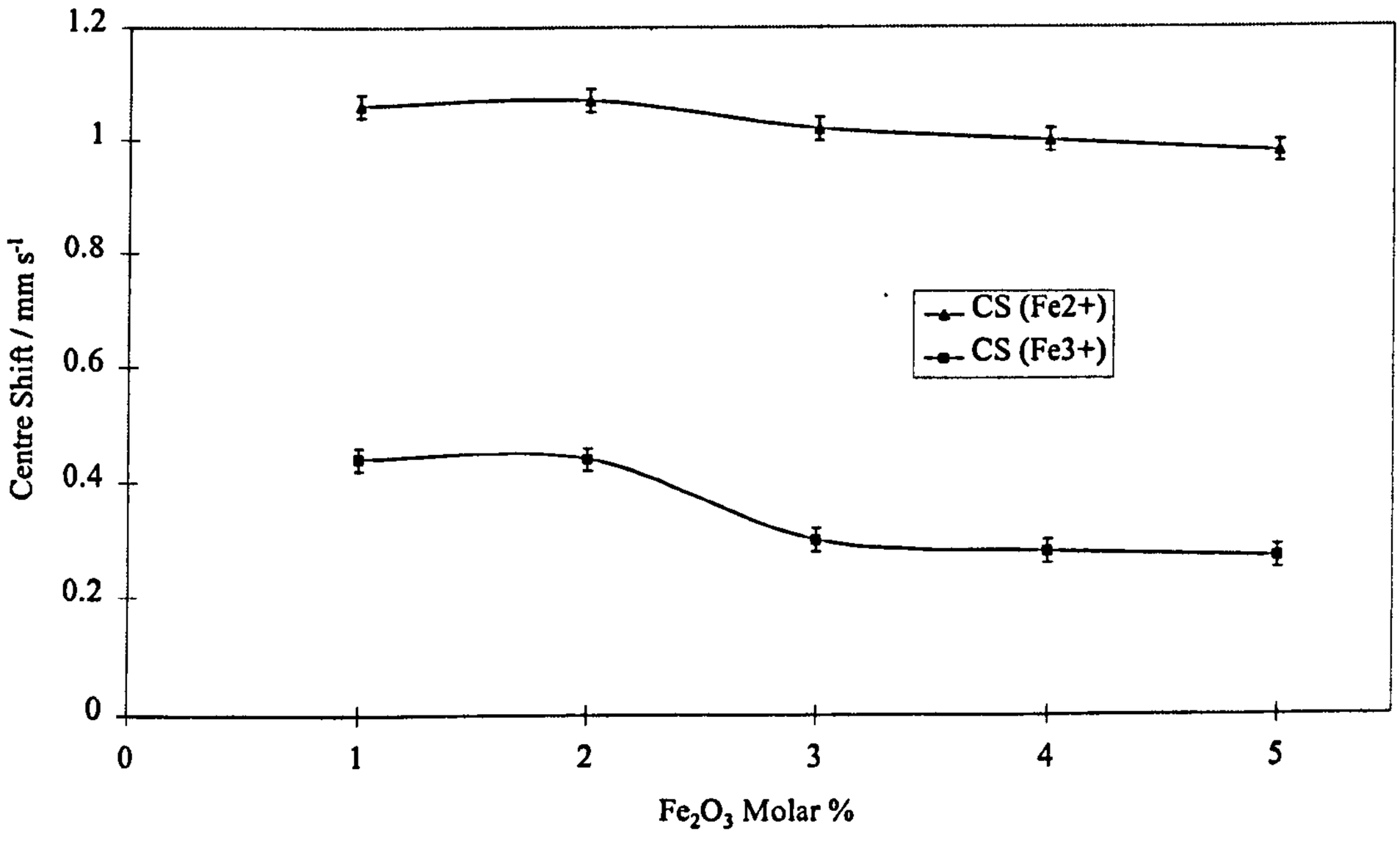

Figure 6.3.1.e. Linewidths of Doublets Fitted to SiO_2-Na_2O-CaO Glasses Containing 1-5 Molar % Fe_2O_3

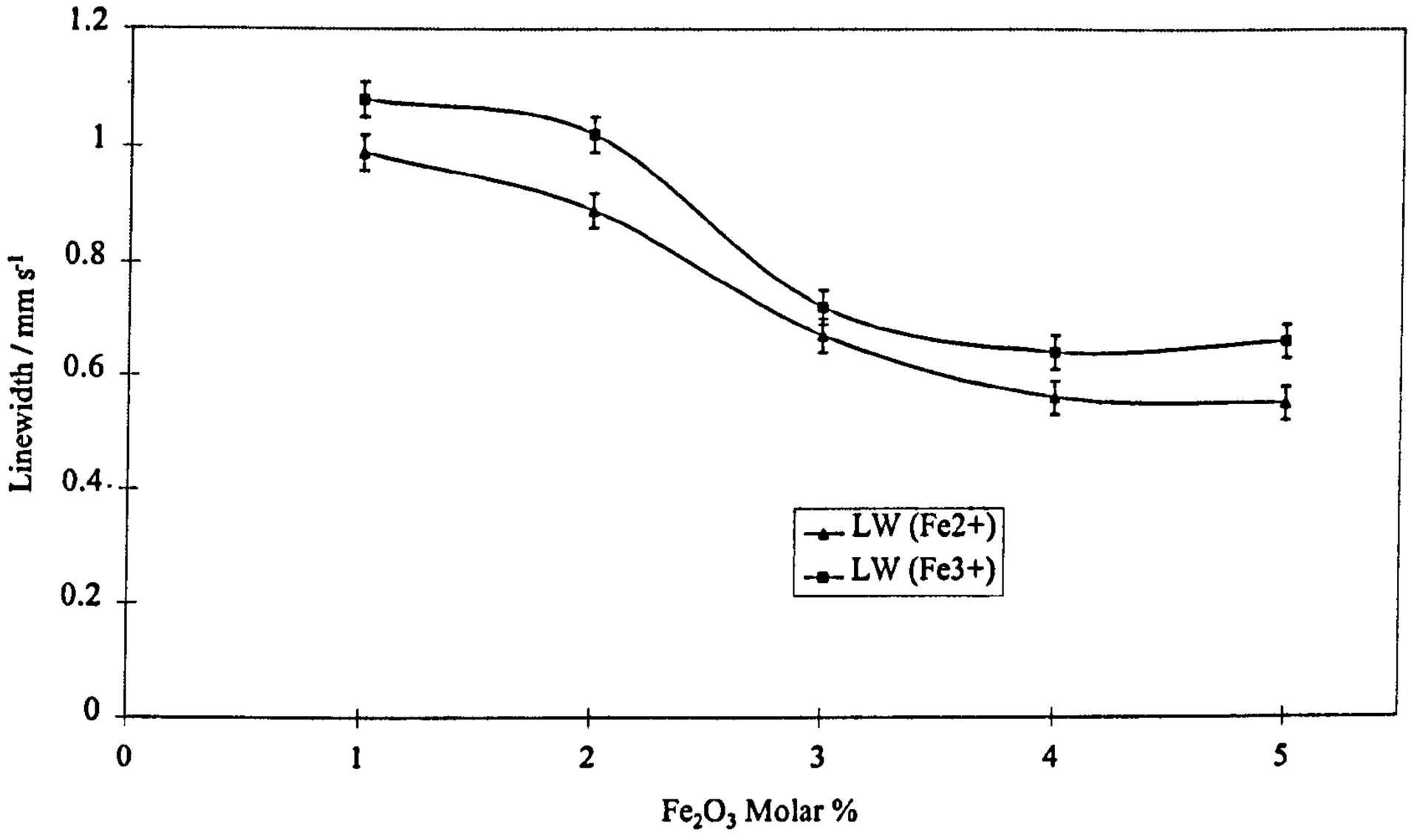

6.3.2. Varying Glass Composition

Glasses of the general compositions SiO_2-R_2O-BaO and SiO_2-Na_2O-RO, each containing 5 molar % Fe_2O_3 were analysed at 293 K and in the velocity range ± 5 mm s^{-1}. Fitted parameters for each sample are shown in tables 6.3.2.a. and 6.3.2.b. The effects of composition on centre shift, quadrupole splitting, and linewidth are shown in figures 6.3.2.a., b and c, respectively. Trends are as follows:

i) The $Fe^{2+}/\Sigma Fe$ ratio decreased strongly with increasing ionic radius of the alkali ion, but was largely unaffected by alkaline earth ion type. The behaviour of the MgO glass was anomalous.

ii) $\delta(Fe^{2+})$ and $\delta(Fe^{3+})$ decreased with increasing alkali ionic radius and decreasing alkaline earth ionic radius and were inversely proportional to ionic radius ratio.

iii) With increasing optical basicity, $\Delta(Fe^{2+})$ increased proportionately and $\Delta(Fe^{3+})$ decreased proportionately.

iv) $\Gamma(Fe^{2+})$ and $\Gamma(Fe^{3+})$ have similar values and decrease approximately linearly with increasing optical basicity.

Table 6.3.2.a. Mössbauer Parameters for SiO_2-R_2O-BaO-5 Molar % Fe_2O_3 Glasses

Alkali Oxide	Li_2O + Na_2O	Na_2O	K_2O	Rb_2O	Cs_2O
$Fe^{2+}/\Sigma Fe$ * 100 %, ± 2	14.55	16.84	9.52	11.33	9.35
CS (Fe^{2+}) / mm s^{-1}, ± 0.02	1.09	1.07	0.96	0.99	0.91
QS (Fe^{2+}) / mm s^{-1}, ± 0.03	1.96	1.95	2.18	2.08	2.04
LW (Fe^{2+}) / mm s^{-1}, ± 0.03	0.59	0.53	0.57	0.52	0.46
CS (Fe^{3+}) / mm s^{-1}, ± 0.02	0.31	0.30	0.27	0.26	0.26
QS (Fe^{3+}) / mm s^{-1}, ± 0.03	0.90	0.89	0.80	0.78	0.75
LW (Fe^{3+}) / mm s^{-1}, ± 0.03	0.59	0.59	0.57	0.52	0.53

Table 6.3.2.b. Mössbauer Parameters for SiO_2-Na_2O-RO-5 Molar % Fe_2O_3 Glasses

Alkaline Earth Oxide	MgO	CaO	SrO	BaO
$Fe^{2+}/\Sigma Fe$ * 100 %, ± 2	16.67	16.33	18.30	16.84
CS (Fe^{2+}) / mm s^{-1}, ± 0.02	0.98	0.98	1.05	1.07
QS (Fe^{2+}) / mm s^{-1}, ± 0.03	1.95	2.00	1.94	1.95
LW (Fe^{2+}) / mm s^{-1}, ± 0.03	0.69	0.55	0.60	0.53
CS (Fe^{3+}) / mm s^{-1}, ± 0.02	0.24	0.27	0.30	0.30
QS (Fe^{3+}) / mm s^{-1}, ± 0.03	0.92	0.91	0.91	0.89
LW (Fe^{3+}) / mm s^{-1}, ± 0.03	0.65	0.66	0.60	0.59

Figure 6.3.2.a. Centre Shifts for 5 Molar % Fe_2O_3 Glasses

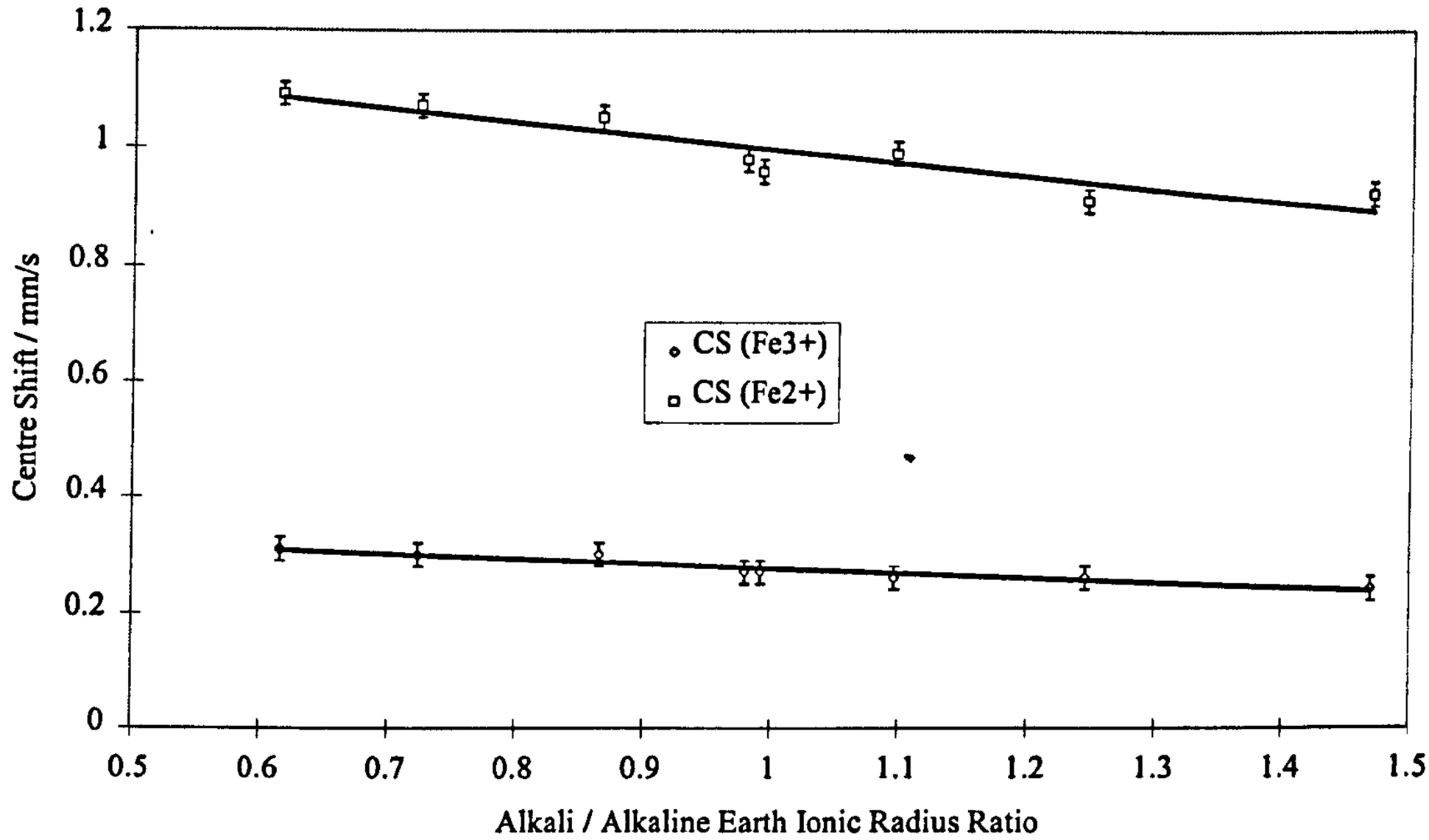

Figure 6.3.2.b. Quadrupole Splittings for 5 Molar % Fe_2O_3 Glasses

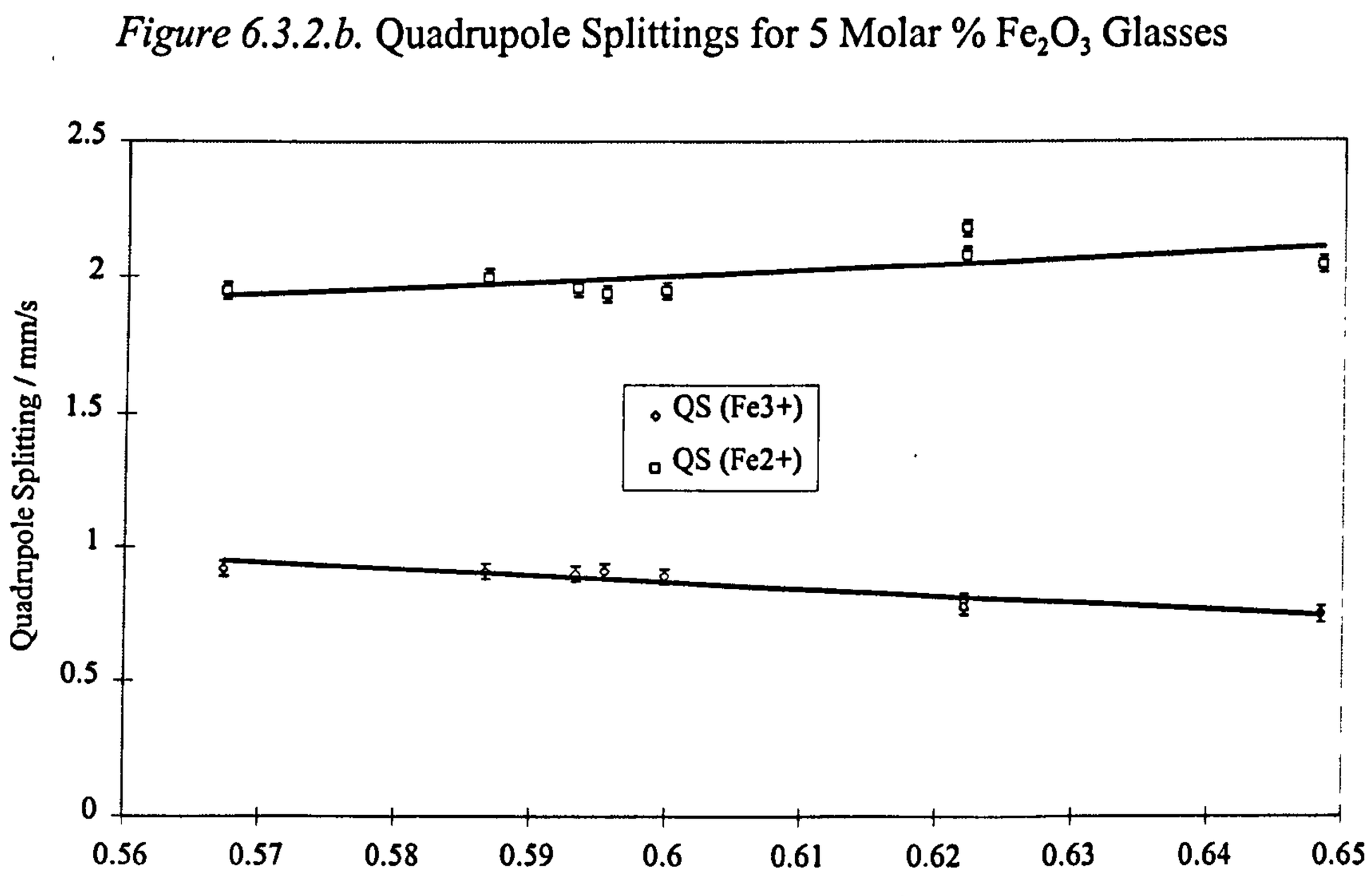

Figure 6.3.2.c. Linewidths for 5 Molar % Fe_2O_3 Glasses

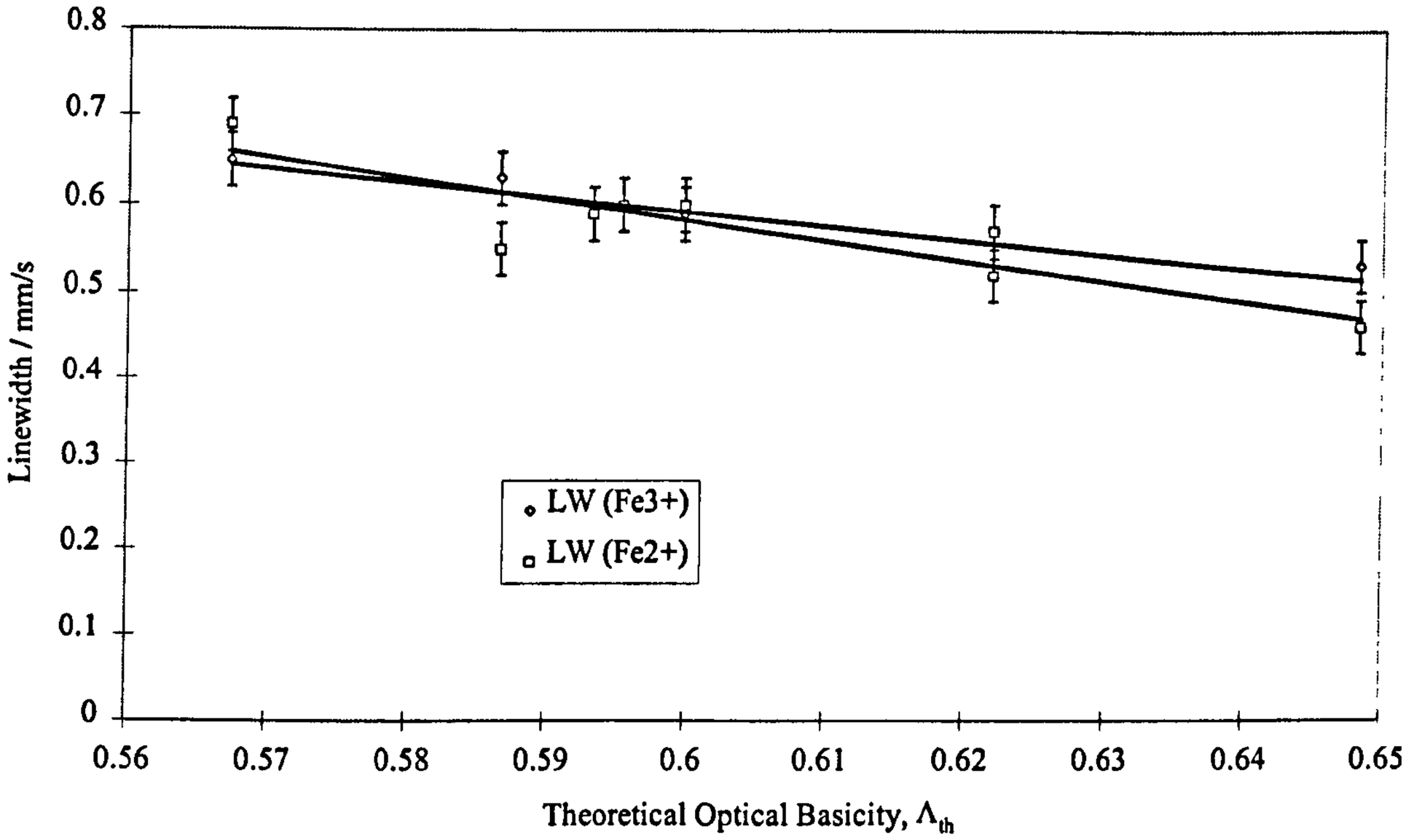

Redox ratios measured by Mössbauer spectroscopy for these glasses were strongly affected by alkali type, but remained largely unaffected by alkaline earth type. These trends can be plotted against either alkali / alkaline earth ionic radius ratio or optical basicity, and yield rough relationships showing that the $Fe^{2+}/\Sigma Fe$ ratio decreases with increases in either scale.

6.4. Discussion

6.4.1. The Effects of Fe_2O_3 Content

Caveat: Ideally, centre shift values should be corrected for both temperature and volume effects in order to look specifically at the contribution from local chemistry. Unfortunately this requires a large number of samples and was not possible in this work. Therefore caution must be taken when using some centre shifts in this study. For example the direct comparison of Mössbauer parameters gained from spectra measured at different temperatures, such as comparing those for the 1 % and 2 % Fe_2O_3 glasses (7 K) with those for the 3 – 5 % Fe_2O_3 glasses

(293 K) can be problematic.

As discussed in chapters 6.2.4. and 6.2.6., temperature has been shown to affect δ, Δ and Γ. Table 6.3.1.a. shows that a "jump" occurs in parameters between those measured at 7 K and at 293 K. Despite the expected differences due to temperature effects, it can be seen that generally, trends in results continue through 1-2 % (7 K) and 3-5 % (293 K). This indicates that although they may be exaggerated by the temperature effects, nonetheless they are real.

Two hyperfine sextets were fitted to the 1 % and 2 % Fe_2O_3 spectra, in accordance with similar work by Williams et al [12]. These represent slow and intermediate rate relaxations between ligand field sub-levels $S_z = \pm 5/2$ and $S_z = \pm 3/2$, respectively. The sextet due to fast relaxations between the $S_z = \pm 1/2$ sub-levels was not fitted for two reasons:

i) This sextet appears in the velocity range normally associated with quadrupole doublets and would be masked by these stronger signals.

ii) The area contained by this sextet is the smallest of the three sextets, and hence is unlikely to have much effect on the fitted spectrum.

Values of $\delta(Fe^{2+})$ and $\delta(Fe^{3+})$ doublets are in agreement with a large body of work on similar glasses discussed in chapter 6.2.6. for all iron concentrations studied. The values of $\delta(Fe^{2+})$ occur near the "borderline" between values associated with octahedral and tetrahedral coordinations, according to Dyar [6]. Other workers gave values of $\delta(Fe^{2+})$ which are in close agreement with those found in this study [2, 9, 17, 23, 40]. The general consensus is that Fe^{2+} is mainly octahedrally-coordinated in soda-lime-silica and similar glasses, and the values of $\delta(Fe^{2+})$ obtained in this study are in agreement. There is a suggestion that a small amount of Fe^{2+} ions may be tetrahedral in coordination.

The decrease in $\delta(Fe^{2+})$ with increasing Fe_2O_3 content indicates a slight move towards more tetrahedral character of Fe^{2+}. The size of this change is small, and thus the change in the ratio of octahedral / tetrahedral sites must also be small. Centre shift is strongly affected by temperature, and so the results for the 1 % and 2 % samples could be expected to be higher, however the decrease continues

through 3 – 5 % Fe_2O_3, which were measured at the same temperature, so is real.

Hyperfine sextets notwithstanding, only one doublet was fitted for Fe^{3+} ions, whereas some workers [9, 41] fitted 2 doublets for Fe^{3+}, one each for tetrahedral and octahedral sites. It is agreed that $\delta(Fe^{3+}_{octahedral}) > \delta(Fe^{3+}_{tetrahedral})$. The single doublet fitted in this study gives a centre shift that indicates increasingly tetrahedral coordination of Fe^{3+} ions with increasing Fe_2O_3 content. The 1 % and 2 % Fe_2O_3 samples gave $\delta(Fe^{3+})$ values within the range associated with octahedral sites, however it is likely that this is caused by the effects of low temperature which increase the centre shift and should thus be disregarded. Centre shifts indicate increasingly tetrahedral coordination of both Fe^{2+} and Fe^{3+} ions with increasing Fe_2O_3 content. It is not possible to quantify the extent of this change in terms of site occupancies.

Quadrupole splitting for the Fe^{2+} and Fe^{3+} doublets agree with values quoted for similar glasses in the literature. They are consistent with octahedral Fe^{2+} and tetrahedral Fe^{3+}, although some octahedral Fe^{3+} may also be present. Values of $\Delta(Fe^{2+})$ fell slightly with increasing Fe_2O_3 content, indicating the move towards more tetrahedral coordination deduced from centre shifts. The $\Delta(Fe^{3+})$ remains constant at all measured Fe_2O_3 contents. Possible reasons for this were discussed by Taragin et al [16]; the charge distribution in Fe^{3+} is spherically symmetric when the electrons are in high-spin configuration, hence the only contribution to the quadrupole splitting comes from the crystal field and the splitting should be independent of temperature. The quadrupole splitting in Fe^{3+} compounds is a result of the distortion of the site from cubic symmetry. The lack of change in $\Delta(Fe^{3+})$ with iron content was slightly surprising, since a large body of literature suggested it would change (see chapter 6.2.8.). The literature which does agree with these findings generally fitted one doublet, and not two, to the Fe^{3+} component (see also chapter 6.2.8.). Interpretation of the data becomes somewhat difficult, because it was concluded from centre shift data that Fe^{3+} ions become more tetrahedral in their coordination with increasing iron content. This may accompany clustering. One may expect this to be accompanied by a change in symmetry, hence a change in $\Delta(Fe^{3+})$, but this does not occur. A possible

explanation is that the Fe^{3+} quadrupole doublet is attributable to exchange-interacting Fe^{3+} ions, often referred to as "clustered". Within these clusters, which are present at all iron contents, the symmetry surrounding Fe^{3+} ions may be well-defined relative to the symmetry around isolated Fe^{3+} ions. If with increasing iron content, the "extra" Fe^{3+} ions either form new clusters or add to existing ones, they would take up symmetries similar to those already in existence, hence very little change in average symmetry. Some of the "extra" Fe^{3+} ions would be isolated and therefore not contribute to the quadrupole doublet so are of no concern when discussing $\Delta(Fe^{3+})$. This does not, however, explain the discrepancies in the literature and with these results. Fitting methods probably play a role, yet it seems likely that if $\Delta(Fe^{3+})$ increases, it would do so no matter which fitting procedure was used.

Linewidths for the quadrupole doublets show large decreases with increasing Fe_2O_3 content. Gosselin et al [15] showed that Γ remained approximately constant for both Fe^{2+} and Fe^{3+} below ~500 K, so the measurements should be unaffected by temperature and are easier to interpret. The behaviour of each linewidth closely mirrors that of the other; although $\Gamma(Fe^{3+}) > \Gamma(Fe^{2+})$ for all Fe_2O_3 concentrations measured. These data indicate a much wider range of site occupancies by both Fe^{2+} and Fe^{3+} at low (< 2 %) Fe_2O_3 contents. If the move towards tetrahedral coordination with increasing Fe_2O_3 content indicated by δ and Δ is taken into account, some octahedral sites with varying degrees of distortion must become tetrahedral sites. This may accompany a narrower range of sites and distortions, which would cause line narrowing in Mössbauer spectra, i.e. smaller linewidths. The greater values of $\Gamma(Fe^{3+})$ indicate a wider range of site occupancies for Fe^{3+} than for Fe^{2+}. This agrees with the evidence that Fe^{2+} is predominantly octahedral but Fe^{3+} occurs in a mixture of tetrahedral and octahedral sites.

Perhaps equally importantly, increasing iron content leads to increased exchange interactions, i.e. clustering of Fe ions, which is manifested in the gradual disappearance of the hfs caused by isolated Fe^{3+} ions. As the relative fraction of clustered Fe ions increases, values of Γ suggest a narrower range of site occupancies. Hence the sites occupied by Fe ions within a "cluster" may be more

constrained than those of isolated ions. This is reasonable if the next-nearest-neighbour ions are less random for a member of a cluster than in an isolated site.

Additional evidence for the influence of clustering on linewidth is the fact that linewidth is the same, within error limits, between 4 % and 5 % Fe_2O_3. It is evident from chapters 5.2. and 6.2., considering mainly ESR and Mössbauer measurements respectively, that Fe ions are predominantly clustered in many glasses at Fe_2O_3 contents > 3 molar %. Increasing from 4 % to 5 % Fe_2O_3 will thus affect the relative numbers of isolated and clustered Fe ions far less than the change from 1 % to 2 % Fe_2O_3.

The amounts of isolated and clustered Fe^{3+} ions were estimated (see chapter 6.3.1.). This was made possible by the proof that the amount of isolated and clustered Fe ions is proportional to the square of the Fe_2O_3 content. Additional corroboration is provided in the work of Williams et al [12], who used Mössbauer spectroscopy to study similar glasses between 0.2 and 4.0 molar % Fe_2O_3. Estimated percentages of clustered and isolated Fe^{3+} ions agree well with their work. Perhaps interestingly, it highlights the fact that even at iron contents as low as 0.2 molar % Fe_2O_3 approximately 20 % of all Fe ions occur as clustered Fe^{3+} ions.

Mössbauer measurements of the iron redox ratio, $Fe^{2+}/\Sigma Fe$, have been carried out. Disagreement has sometimes been shown with other techniques at low iron contents. The reasons for this have been discussed in chapters 6.2.3. and 6.2.8. Comparisons with results from other techniques such as wet chemical analysis or optical spectroscopy are required to test the Mössbauer results properly.

Results for the 1 % - 5 % Fe_2O_3 series of glasses indicate a slight decrease in $Fe^{2+}/\Sigma Fe$ with increasing iron content up to 3 %, above which it remains approximately constant. Generally, $Fe^{2+}/\Sigma Fe$ = 15 – 20 %. This is typical of iron in soda-lime-silica glasses fully equilibrated in air at approximately 1450°C [54, 57, 58].

It is expected that a small amount of hfs should be present in even the 3 – 5 % Fe_2O_3 samples, but which was not detected due to the measurements being made

at 293 K. From comparison with the work of Williams et al [12], which was conducted on glasses of very similar composition to the glasses studied here, it can be inferred that the amount of hfs in these samples would be small. Even at 3 % Fe_2O_3 it should be weak enough to have little effect on the measured parameters, and this effect decreases further with increasing Fe_2O_3 content. It would certainly be interesting further work to compare and contrast measurements made for all samples at 7 K and at 293 K in the velocity range ± 12 mm s^{-1}. There probably exists a "cut-off", below which ambient temperature spectra contain too much unresolved hfs to give accurate measurements. It is predicted that this cut-off exists in these glasses between 2 % and 3 % Fe_2O_3.

Mössbauer studies of 0.2 - 4 molar % Fe_2O_3 in float glass compositions by Williams et al [12] produced results which suggested that $Fe^{2+}/\Sigma Fe$ decreased with increasing Fe_2O_3 contents, from $Fe^{2+}/\Sigma Fe$ = 29 % at 0.32 molar % Fe_2O_3 to $Fe^{2+}/\Sigma Fe$ = 15 % at 4 molar % Fe_2O_3. These results were in agreement with wet chemical analysis of the redox.

Mössbauer results do show a slight decrease in $Fe^{2+}/\Sigma Fe$ with increasing Fe_2O_3 content, from perhaps 21 % at 1 molar % Fe_2O_3, to 16 % at 5 molar % Fe_2O_3. This change is small but disagrees with wet chemical and optical redox measurements for the same glasses (see chapters 4.3.7. and 4.3.8.). One possible source of disagreement with the work of Williams et al [12] may lie in differences in the melting schedule of the glasses.

6.4.2. The Effects of Glass Composition

The redox ratio $Fe^{2+}/\Sigma Fe$ decreased approximately linearly within error limits with increasing ionic radius of the alkali ion. Similar relationships exist if the data are plotted against the cation field strength (z/a^2) of the alkali ion. Despite some differences between values of $Fe^{2+}/\Sigma Fe$ obtained with Ba as the alkaline earth (comparison of table 6.3.2.a. with table 4.3.7.3.a.) using Mössbauer and wet

chemical techniques, both sets of results do agree that increasing ionic radius of the alkali ion leads to a decrease in $Fe^{2+}/\Sigma Fe$. This is in agreement with a large body of literature (see chapter 2.2.5.), which indicates that increasing glass basicity leads to an increasingly oxidised melt.

The type of alkaline earth ion, however, did not affect the redox in these glasses beyond the limits of error. This was unexpected, since it is known that alkaline earth ions do affect iron redox (see chapter 2.2.5.). Indeed, wet chemical and optical results for 0.2 molar % Fe_2O_3 glasses in this study show that alkaline earth ions affect redox at low iron contents (see chapter 4.3.7.1.).

It is known that $\delta(Fe^{3+})$ and $\Delta(Fe^{3+})$ are affected by the redox ratio of iron, or vice-versa (see chapter 6.2.9.). Large changes in redox in the glass affect $\delta(Fe^{3+})$ and $\Delta(Fe^{3+})$ in opposite manners. The redox changes in the glasses studied here were relatively small with changing composition, and no opposite changes in $\delta(Fe^{3+})$ and $\Delta(Fe^{3+})$ were observed with changing alkali ion. Therefore the differences in redox brought about by using different alkali ions are not responsible for the changes in $\delta(Fe^{3+})$ and $\Delta(Fe^{3+})$. The coordination changes are unlikely to be influenced by the small changes in redox, rather it is structural changes brought about by the presence of different cations which is the cause.

All the Mössbauer parameters show distinct changes with changing glass composition. Centre shifts, $\delta(Fe^{2+})$ and $\delta(Fe^{3+})$, are inversely proportional to the alkali / alkaline earth ionic radius ratio, exhibiting relatively large changes, ~15 % and ~25 % respectively, throughout the series of glasses studied. These decreases with increasing alkali / alkaline earth ionic radius ratio signal increases in the covalency of bonding.

From comparison with information in chapters 6.2.6. - 6.2.9., the following conclusions can be drawn;

i) $\delta(Fe^{2+})$ and $\Delta(Fe^{2+})$ indicate that the majority of Fe^{2+} ions are octahedrally coordinated, but increasing alkali / alkaline earth ionic radius ratio leads to an increase in the number of Fe^{2+} ions in tetrahedral coordination. A greater dependency is shown on type of alkali ion than alkaline earth ion.

ii) $\delta(Fe^{3+})$ and $\Delta(Fe^{3+})$ show that the majority of Fe^{3+} ions occur in tetrahedral coordination regardless of composition. Increasing alkali / alkaline earth ionic radius ratio leads to greater predominance of tetrahedral sites. Again, greater dependency is shown on type of alkali ion than alkaline earth ion.

Clearly the s-electron density at the nucleus does not remain constant with changing alkali ionic radius, indeed it appears to follow approximately linear changes for both Fe^{2+} and Fe^{3+}. Increasingly tetrahedral coordination would cause this phenomenon. Thus within the "range" of centre shifts associated with a given coordination, a change towards or away from the "crossover point" between the different coordination states signifies greater population of the dominant coordination state. It is also possible that mixtures of 4, 5 and 6-coordinated sites are populated [40], and the value of δ represents that distribution. For a given valence state the centre shift decreases with increasing electronegativity (or decreasing cation field strength) of the ligand ion, due to increasing s-electron density at the Fe nucleus. This is shown by the centre shifts for this series of glasses.

According to Burkhard [40], for a given glass system, $\Delta(Fe^{3+})$ decreases with increasing optical basicity meaning that the polyhedral geometry becomes more cubic. This change was certainly exhibited by the behaviour of $\Delta(Fe^{3+})$, which decreased from 0.92 mm s^{-1} to 0.75 mm s^{-1} over the range of glasses studied here. These values indicate the predominance of tetrahedral sites, but further interpretation is difficult. The value of $\Delta(Fe^{3+})$ is a measure of distortion from cubic of the Fe^{3+} coordination polyhedron. The differences in distortion may be due largely to changes in Fe-O bond lengths caused by the different cations. These bond lengths are affected most by small, highly polarising ions such as Li^{+}, hence there is decreasing distortion of the polyhedron with increasing size of alkali ion. Moreover, introducing different alkaline earth ions affects $\Delta(Fe^{3+})$ far less than different alkali ions. Alkaline earth ions therefore appear to have far less influence on polyhedral distortion. Values of $\Delta(Fe^{2+})$ cannot be interpreted in this way (see chapter 6.2.2.).

Linewidths of Fe^{2+} and Fe^{3+} doublets were inversely proportional to optical basicity. They indicate a wider range of site parameters for Fe^{2+} and Fe^{3+} ions with smaller, more acidic modifier ions present. On average, $\Gamma(Fe^{3+})$ is slightly greater than $\Gamma(Fe^{2+})$, supporting the conclusion that Fe^{3+} ions occupy a combination of tetrahedral and octahedral sites and Fe^{2+} ions are predominantly octahedral.

6.5. Chapter Summary

Mössbauer spectra consisted of a doublet attributed to Fe^{2+} ions, a doublet attributed to exchange-interacting Fe^{3+} ions, and hyperfine splitting sextets attributed to isolated Fe^{3+} ions.

Parameters generally showed that the majority of Fe^{2+} ions occupy octahedral sites, and the majority of Fe^{3+} ions occupy tetrahedral sites. Increasing Fe_2O_3 content gave rise to increases in the tetrahedral / octahedral ratio for both Fe^{2+} and Fe^{3+} ions, particularly for Fe^{3+} ions. Mössbauer parameters also indicated that within clusters, the symmetry surrounding Fe^{3+} ions is more constrained and well-defined than for isolated Fe^{3+} ions.

The relative numbers of isolated and clustered Fe^{3+} ions were estimated for Fe_2O_3 contents between 0 and 5 molar %. At Fe_2O_3 contents as low as 0.2 molar %, it was estimated that approximately 20 % of all Fe ions occur as clustered Fe^{3+} ions.

Mössbauer redox measurements suggested slightly higher Fe^{2+} contents at 1 and 2 molar % Fe_2O_3 than at 3-5 molar % Fe_2O_3. This difference was considered small, but comparisons with results from wet chemical and optical techniques indicated the Mössbauer results for 1 and 2 molar % Fe_2O_3 overestimated the Fe^{2+} content slightly.

The $Fe^{2+}/\Sigma Fe$ redox ratio measured by Mössbauer spectroscopy for glasses containing 5 molar % Fe_2O_3 had an approximate negative linear relationship with the alkali ionic radius. This was in agreement with wet chemical analysis and a large body of literature. Alkaline earth ions appeared to have little effect on redox

at these Fe_2O_3 contents.

Parameters show that increasing alkali / alkaline earth ionic radius ratio leads to an increase in the number of Fe^{2+} and Fe^{3+} ions occupying tetrahedral sites. Greater dependency was shown on alkali type than on alkaline earth type A wider range of site parameters occur for both Fe^{2+} and Fe^{3+} ions with smaller, more acidic alkali *or* alkaline earth ions such as Li^+ or Mg^{2+} present.

6.6. References

[1] Kurkjian, C.R., Buchanan, D.N.E., Phys. Chem. Glasses, 1964, vol. 5, p. 63.

[2] Kurkjian, C.R., Sigety, E.A., Proc. 7th ICG, Brussels, 1965, ch. 39.

[3] Kurkjian, C.R., J. Non-Cryst. Solids, 1970, vol. 3, p. 157.

[4] Wong, J., Angell, C.A., Glass Structure by Spectroscopy, Marcel Dekker, New York, 1976, ch. 3.

[5] Joseph, I., Pye, L.D., in Experimental Techniques of Glass Science, Ed. Simmons, C.J., El-Bayoumi, O.H., Amer. Ceram. Soc., ch. 4, p. 101.

[6] Dyar, M.D., Amer. Mineral., 1985, vol. 70, p. 304.

[7] Sekhon, S.S., Kamal, R., Phys. Chem. Glasses, 1988, vol. 29, p. 157.

[8] Nishida, T., J. Non-Cryst. Solids, 1994, vol. 177, p. 257.

[9] Bizi, M., Hannoyer, B., Lenglet, M., Riv. Staz. Sper. Vetro, 1989, vol. 1, p. 75.

[10] Chavez-Rivas, F., Regnard, J.R., Chappert, J., J. de Phys., 1980, vol. 41, p. C1-275

[11] Hannoyer, B., Lenglet, M., Dürr, J., Cortes, R., J. Non-Cryst. Solids, 1992, vol. 151, p. 209.

[12] Williams, K.F.E., Johnson, C.E., Thomas, M.F., J. Non-Cryst. Solids, 1998, vol. 226, p. 19.

[13] Mysen, B.O., Seifert, F., Virgo, D., Amer. Mineral., 1980, vol. 65, p. 867.

[14] Wertheim, G.K., Remeika, J.P., Phys. Lett., 1964, vol. 10, p. 14.

[15] Gosselin, J.P., Shimony, U., Grodzins, L., Cooper, A.R., Phys. Chem. Glasses, 1967, vol. 8, p. 56.

[16] Taragin, M.F., Eisenstein, J.C., Haller, W., Phys. Chem. Glasses, 1972, vol. 13, p. 149.

[17] Varret, F., Naudin, F., Rev. de Phys. Appl., 1979, vol. 14, p. 613.

[18] Nishida, T., Ide, H., Takashima, Y., J. Ceram. Soc. Jpn., 1989, vol. 97, p. 284.

[19] Bahgat, A.A., Shaisha, E.E., Fayek, M.K., Phys. Chem. Glasses, 1983, vol. 24, p. 5.

[20] Johnson, J.A., Johnson, C.E., Holland, D., Mekki, A., Appleyard, P., Thomas, M.F., J. Non-Cryst. Solids, 1999, vol. 246, p. 104.

[21] Pollak, H., Karfunkel, U., Hyperfine Interactions, 1993, vol. 77, p. 235.

[22] Mysen, B.O., Carmichael, I.S.E., Virgo, D., Contrib. Min. Petrol., 1985, vol. 90, p. 101.

[23] Taragin, M.F., Eisenstein, J.C., J. Non-Cryst. Solids, 1970, vol. 3, p. 311.

[24] Labar, C., Gielen, P., J. Non-Cryst. Solids, 1973/74, vol. 13, p. 107.

[25] Boon, J.A., Fyfe, W.S., Chem. Geol., 1972, vol. 10, p. 287.

[26] Levy, R.A., Lupis, C.H.P., Flinn, P.A., Phys. Chem. Glasses, 1976, vol. 17, p. 94.

[27] Nolet, D.A., Burns, G., Flamm, S.L., Besancon, J.R., Proc. 10th Lunar Planet. Sci. Conf., 1979, p. 1775.

[28] Nolet, D.A., J. Non-Cryst. Solids, 1980, vol. 37, p. 99.

[29] De Grave, E., Van Iseghem, P., Batist, R., Chambaere, D., J. de Phys., 1980, vol. 41, p. C1-269.

[30] Burzo, E., Ardelean, I., Phys. Chem. Glasses, 1979, vol. 20, p. 15.

[31] Mysen, B.O., Virgo, D., Seifert, F.A., Amer. Mineral., 1985, vol. 70, p. 88.

[32] Eissa, N.A., Sanad, M., El-Saghier, A.A., Sallam, H.A., Mostafa, A.G., Acta Phys. Hungar., 1986, vol. 59, p. 297.

[33] Mysen, B.O., Virgo, D., Amer. Mineral., 1989, vol. 74, p. 58

[34] Kashif, I., Gomaa, S.S., Mostafa, A.G., Hamad, S.M., Sanad, A.M., Phys. Chem. Glasses, 1988, vol. 29, p. 72.

[35] Lipinska-Kalita, K.E., Görlich, E., J. Non-Cryst. Solids, 1988, vol. 107, p. 73.

[36] Mysen, B.O., Virgo, D., Neumann, E.R., Seifert, F.A., Amer. Mineral., 1985, vol. 70, p. 317.

[37] Mysen, B.O., Virgo, D., Seifert, F.A., Amer. Mineral., 1984, vol. 69, p. 834.

[38] Wang, C.M., Chen, H., Phys. Chem. Glasses, 1987, vol. 28, p. 39.

[39] Zhou, Z., Yuan, Y., Hu, Z., Liu, R., Xia, Y., Wang, S., J. Non-Cryst. Solids, 1986, vol. 84, p. 34.

[40] Burkhard, D.J.M., Phys. Chem. Glasses, 1997, vol. 38, p. 317.

[41] Tomandl, G., in Glass: Science and Technology, vol. 4B, Ed. Uhlmann, D.R., and Kriedl, N.J., Academic Press, New York, 1990, ch. 5.

[42] Belyustin, A.A., Ostanevich, Y.M., Pisarevskii, A.M., Tomilov, S.B., Baishi, U., Cher, L., Soviet Phys. Solids State, 1965, vol. 7, p. 1163.

[43] Goldman, D.S., Bewley, D.E., J. Amer. Ceram. Soc., 1985, vol. 68, p. 691.

[44] Pagnier, T., Souquet, J.L., Ribes, M., Mats. Res. Bull., 1985, vol. 20, p. 225.

[45] Friedt, J.M., Bonnenfant, A., Laville, H., Bernier, J.C., J. de Phys., 198, vol. 41, p. C1-273.

[46] Fenstermacher, J.E., J. Non-Cryst. Solids, 1980, vol. 38 & 39, p. 239.

[47] Calas, G., Petiau, J., in The Structure of Non-Crystalline Materials, Ed., Gaskell, P.H., parker, J.M., Davis, E.A., Taylor-Francis, 1983, p.18.

[48] Calas, G., Petiau, J., Solid State Comms.,1983, vol. 48, p. 625.

[49] Ades, C., Toganidis, T., Traverse, J.P., J. Non-Cryst. Solids, 1990, vol. 125, p. 272.

[50] Baiocchi, E., Bettinelli, M., Montenero, A., J. Amer. Ceram. Soc., 1982, vol. 65, p. C-39.

[51] Wang, C.M., Chen, H., Phys. Chem. Glasses, 1987, vol. 28, p. 39.

[52] Edwards, R.J., Paul, A., Douglas, R.W., Phys. Chem. Glasses, 1972, vol. 13, p. 131.

[53] Creux, S., Proc. Fundamentals of Glass Sci Tech., 1997, p. 41.

[54] Hannoyer, B., Lenglet, M., Durr, J., Cortes, R., J. Non-Cryst. Solids, 1992, vol. 151, p. 209.

[55] Waff, H.S., Can. Mineral., 1977, vol. 15, p. 198.

[56] Gerlach, S., Clausen, O., Rüssel, C., J. Non-Cryst. Solids, 1998, vol. 238, p. 75.

[57] Hahn, B., Buhler, P., Weissmann, R., Fundamentals Glass Sci. Tech., Venice, 1993, p. 205.

[58] Schreiber, H.D., Kochanowski, B.K., Schreiber, C.W., Glastech. Ber., 1995, vol. 68(C2), p. 233.

Chapter 7.

Discussion

This chapter is intended to bring all the evidence from previous chapters together. Properties of the glasses studied are discussed in terms of redox, coordination, and distribution of iron species, and the effects on each of Fe_2O_3 content and glass composition. The interrelationships between these properties are then discussed. Finally the structural implications, both for local structure of Fe species and longer-range order, are covered.

Most of the results of this study concerning the effects of glass composition have followed one of two behavioural patterns. These have been classed as "collective" and "selective" behaviour.

Collective behaviour occurred when both alkali and alkaline earth ions affected properties in a similar manner, having a cumulative effect. An example of this would be the effects of glass composition as quantified by optical basicity, on $Dq(Fe^{2+})$.

Selective behaviour occurred when alkali and alkaline earth ions had opposing effects on properties. An example of this type of behaviour is the effect of glass composition, quantified by the alkali / alkaline earth ionic radius ratio, on the Fe^{3+} extinction coefficient, $\varepsilon(Fe^{3+})$.

7.1. Iron Redox

As discussed in chapter 2.2., the redox of iron in glass is governed by several variables. The effects of Fe_2O_3 content and glass composition were investigated in detail by this study. The effects of melting time were also studied briefly.

The Mössbauer studies by Mysen and co-workers [1 - 5], which were reviewed in chapter 6.2.9., suggested that no appreciable change in coordination would accompany the redox changes which occurred in this study, where $Fe^{2+}/\Sigma Fe < 20$ % in almost every case. Much higher $Fe^{2+}/\Sigma Fe$ ratios would probably be required to induce appreciable coordination changes.

Comparison of redox ratios measured by Mössbauer spectroscopy (see tables 6.3.2.a. and 6.3.2.b.) with wet chemical measurements of the same samples (see table 4.3.7.3.a.) indicates some disagreement between the different sets of results. Both sets do agree, however, that Fe^{2+} content decreased with increasing alkali ion size (hence with both increasing alkali / alkaline earth ionic radius ratio and optical basicity). Certainly a wider range of measurements would need to be taken at 5 molar % Fe_2O_3 before it could be said with any confidence that the behaviour was different from that at 0.2 molar % Fe_2O_3.

7.1.1. The Effects of Fe_2O_3 Content and Melting Conditions on Redox

The results presented in chapters 4 and 6 showed that Fe_2O_3 content does not appreciably affect redox in the glasses studied. This was demonstrated not only in the SiO_2-Na_2O-CaO system, but also in SiO_2-R_2O-BaO glasses where R = Li/Na, Rb and Cs (see chapter 4.3.7.3.). Hence we can infer that for all the silicate systems investigated, redox was unaffected by Fe_2O_3 content.

The redox ratio $Fe^{2+}/\Sigma Fe$ was at or very close to equilibrium for a SiO_2-Na_2O-CaO glass melted by the standard regime (see chapter 4.3.4.1.). It is reasonable to assume that this applied to all glasses melted in this study under the same regime.

These results disagree with the findings of a sizeable proportion of the literature on the subject of iron redox in glass which was reviewed in chapter 2.2. Many workers found that the $Fe^{2+}/\Sigma Fe$ ratio was affected by iron content: it increased quite sharply below a certain iron content. Some workers who carefully equilibrated their melts before measurement [6 - 8] found results which agree with those presented here. It has been suggested that the oxidising action of Fe_2O_3 on the unequilibrated melt causes the discrepancy [6]. The results of this study

therefore show that in properly equilibrated glassmelts, Fe_2O_3 content does not affect redox within the range studied. This conclusion was reached by combining wet chemical and optical spectroscopy (see chapters 4.3.7. and 4.3.8.) measurements, as well as Mössbauer results (see chapters 6.3. and 6.4.). Some discrepancies were found at lower iron contents between Mössbauer spectroscopy and the other two techniques, but generally they were in complete agreement.

It was shown in chapter 4.3.2.2. that the actual concentration per unit volume of Fe ions was strongly affected by glass composition, such that small alkali and alkaline earth ions, except in the particular case of Mg^{2+}, maximised the Fe ion concentration, and large ions minimised it. The Fe_2O_3 content did not affect redox, regardless of composition. This means that for the 0.2 molar % Fe_2O_3 series of glasses, any variations in redox with different compositions were not influenced by differences in Fe concentration.

7.1.2. The Effects of Glass Composition on Redox

The results of this study show that alkali and alkaline earth ions exert different influences upon many properties, including redox and extinction coefficients. It was found that $Fe^{2+}/\Sigma Fe$, $\varepsilon(Fe^{2+})$ and $\varepsilon(Fe^{3+})$ had linear relationships with the alkali / alkaline earth ionic radius ratio. Glasses with MgO as the alkaline earth oxide exhibited slightly different behaviour from the other glasses.

It has generally been found that redox equilibria in glass melts shift toward the oxidised state as the glass basicity increases (see chapter 2.2.5.). This phenomenon has been demonstrated in binary alkali silicate glasses.

Results of this study agree with the trend if considering different alkali ions alone, e.g. SiO_2-CaO-R_2O (R = Li → Cs). This also includes mixed-alkali glasses (e.g. Li-Na series). Where the optical basicity model failed to predict the redox ratio was when considering the effects of different alkaline earth ions. The opposite trend occurred to that predicted by optical basicity: increasing Λ_{th} (i.e. MgO → CaO → SrO → BaO) increased the $Fe^{2+}/\Sigma Fe$ ratio (see chapter 2.2.5.)

It has been noted that in many cases, redox equilibria do not correlate very well with the optical basicity, indicating the existence of additional mechanisms [9].

Gerlach et al [10], using square-wave voltammetry, found similar results for ternary alkali magnesium silicate and alkali calcium silicate glasses containing iron. The standard potential (Fe^{3+}/Fe^{2+}) increased with increasing size of alkali ion, but decreased with changing from MgO to CaO. Hence the effects of alkali and alkaline earth ions were in opposition to one another. In another voltammetric study of a soda-lime-silica glass, replacement of some Na_2O by CaO kept the optical basicity approximately constant, yet standard potentials were found to change [11]. The findings of this study regarding the effects of glass composition on iron redox are in agreement with these voltammetric studies [10, 11], in that the effects of composition on redox cannot be fully explained by the concept of optical basicity.

The optical basicity is an average basicity for the whole glass, hence the local optical basicity of an Fe-ion may be different from the average glass optical basicity. It is known that the distributions of alkali and alkaline earth ions in silicate glasses are not completely random (see chapter 2.1.), and results from this study also show that clustering of Fe ions can occur at low iron contents such that nearby Fe ions may also exert an influence.

Taking the very simple method of directly comparing the alkali / alkaline earth ionic radii by plotting them as a ratio against $Fe^{2+}/\Sigma Fe$ showed they were proportional. This occurred for all compositions, although $Fe^{2+}/\Sigma Fe$ ratios for glasses with MgO as the alkaline earth oxide were slightly higher than for the other alkaline earths. This may have been caused by the difference in coordination of Mg^{2+} ions, as discussed earlier in this chapter and in chapter 2.1.

Wet chemical and Mössbauer results were generally in agreement regarding redox at 5 % Fe_2O_3 in terms of alkali ions; both techniques showed that an increase in the size of the alkali ion decreased $Fe^{2+}/\Sigma Fe$. Only Mössbauer redox results were available for changing alkaline earth ions at 5 % Fe_2O_3. They appeared to indicate that alkaline earth ions had little effect on redox in these particular glasses. The errors associated with the wet chemical technique were larger at 5 % Fe_2O_3 than at 0.2 % Fe_2O_3 (± 2 % compared with ± 1 %). Optical spectra showed some corroboration: the Fe^{2+} absorption peak near 10,000 cm^{-1} was stronger in Li/Na

and Na glasses than the others (see figure 4.3.3.1.b.), i.e. the Fe^{2+} content was higher.

It has been widely agreed that for binary alkali silicate glasses and binary alkaline earth silicate glasses, the ratio of Fe [oxidised/reduced] increases with increasing glass basicity or cation field strength, e.g. as the modifier ions increase in size (see chapter 2.2.5.).

When we move to the ternary systems covered by this study there is a change in behaviour. The effects of alkali are still the same as in the binary systems, but now with changing alkaline earth ion the ratio [oxidised/reduced] decreases with increasing glass basicity, i.e. Λ. These effects are highlighted in figures 4.3.7.1.a. and 4.3.7.1.b. Hence the linear relationship with the alkali / alkaline earth ionic radius ratio. Plotting cation field strength ratio or oxide basicity ratio yields similar trends.

Waff [12] noted that Na^+ and K^+ ions form more stable complexes with Fe^{3+} ions than do Mg^{2+} or Ca^{2+} ions. This may be one reason why the behaviour remains the same for alkali ions. Discussion of ESR results in chapter 5.4.2. identified alkali ions as being primarily responsible for determining Fe^{3+} ion distribution. It is possible that this dominance of alkali ions extends to redox as well.

It is interesting to note that the trend in redox with composition tallies with observed glass viscosities when molten at 1450°C and when being poured: the more viscous the glass, the lower the $Fe^{2+}/\Sigma Fe$ ratio.

7.2. Coordination of Iron Species

Results from optical absorption, luminescence, ESR and Mössbauer spectroscopy have shown that the coordination and environment of Fe species can be strongly affected by both iron content and glass composition.

7.2.1. The Effects of Fe_2O_3 Content on Coordination

Optical, ESR and Mössbauer techniques have shown that the distribution of Fe ions changes with Fe_2O_3 content. Thus any changes in coordination and environment are probably linked with changing interactions between Fe ions, since other parameters such as composition and redox remained approximately constant with changing iron content. The following results were found:

a) The number of Fe ions occupying tetrahedral sites increases with Fe_2O_3 content. This effect is greater for Fe^{3+} ions than for Fe^{2+} ions.
b) The amount of distortion of sites occupied by both Fe^{2+} and Fe^{3+} ions decreases with increasing Fe_2O_3 content.

Little evidence was found from optical spectroscopy of changes in the average coordination of Fe^{2+} ions with increasing iron content (see chapter 4.4.3.1.). This is slightly at odds with evidence from Mössbauer spectroscopy, which indicated a small increase in the tetrahedral / octahedral ratio of Fe^{2+} ions. Due to the large differences in optical extinction coefficients of tetrahedral and octahedral Fe^{2+} ions, one may have expected optical spectroscopy to have shown this change.
The Fe_2O_3 content had a stronger effect on Fe^{3+} coordination than on Fe^{2+}. This may in part be simply because the majority of Fe ions occurred as Fe^{3+} in these glasses. It proved difficult to extract information on the effects of Fe_2O_3 content on Fe^{3+} coordination due to the fact that many characteristic absorption bands occurred in the same parts of the spectrum regardless of coordination. Luminescence spectroscopy was only useful up to 1 molar % Fe_2O_3 due to concentration quenching, and showed no obvious effects of iron concentration on measured spectra below this level (see chapter 4.3.9.1.).
ESR was very useful for studying Fe^{3+} ion distribution, but gave little information on coordination. As discussed in chapter 5.2., interpretation of ESR spectra cannot be done in terms of tetrahedral and octahedral sites. It is clear that the distribution of Fe^{3+} ions is strongly affected by Fe_2O_3 content, and this is likely to

also affect coordination. Distribution and its relationship with coordination is discussed in chapters 7.3. and 7.5.

Mössbauer spectroscopy showed that the character of both Fe^{2+} and Fe^{3+} ions becomes more tetrahedral with increasing Fe_2O_3 content (see chapter 6.4.1.). This effect was greater for Fe^{3+} ions than for Fe^{2+} ions. In addition, the range of site distortions, evidenced by linewidth, decreased sharply with increasing Fe_2O_3 content up to about 3 molar %. These changes in both coordination and site distortion may be linked with ion distribution, as discussed in chapters 7.3. and 7.5.

7.2.2. The Effects of Glass Composition on Coordination

Whilst it was shown in chapters 5 and 6 that Fe ions can occur in clusters at low iron concentrations, the majority occurred as isolated ions at 0.2 molar % Fe_2O_3 (see table 6.3.1.b.). For this reason one can surmise that whilst distribution may influence coordination and environment of Fe ions at these low concentrations, it is not the determining factor. Systematic changes in coordination are brought about by the introduction of different alkali and alkaline earth cations.

The results of this study have shown that:

a) Fe^{2+} ions mainly occupy distorted octahedral sites with some distortion splitting, attributable to the dynamic Jahn-Teller effect. A small number of Fe^{2+} ions may occupy tetrahedral sites, though the ratio of $Fe^{2+}_{octahedral}$ / $Fe^{2+}_{tetrahedral}$ was largely unaffected by changes in glass composition.

b) The parameter $Dq(Fe^{2+})$ is proportional to optical basicity of the glass for both octahedral and tetrahedral sites.

c) Fe^{3+} ions occupied both tetrahedral and octahedral sites. The ratio of $Fe^{3+}_{tetrahedral}$ / $Fe^{3+}_{octahedral}$ is strongly affected by glass composition, and increases proportionately with the alkali / alkaline earth ionic radius ratio.

d) $Dq(Fe^{3+})$ is affected by composition, and Racah B and C parameters show proportionality with the alkali / alkaline earth ionic radius ratio.

No obvious trends occurred in optical absorption spectra to suggest that the $Fe^{2+}_{tetrahedral}$ / $Fe^{2+}_{octahedral}$ ratio was affected by glass composition. Despite this, Mössbauer parameters showed systematic changes with composition. Covalency of Fe-O bonding increased with increasing alkali / alkaline earth ionic radius ratio for both redox states, and in particular for Fe^{3+} ions. Changes in Fe^{3+}-O bond covalency were also indicated by proportionality between the Fe^{3+} Racah B and C parameters and the alkali / alkaline earth ionic radius ratio. In addition, polyhedral distortion and the range of site distortions decreased with increasing optical basicity, for both redox states.

There was agreement between information from Mössbauer parameters and the optical extinction coefficient $\varepsilon(Fe^{3+})$ that the $Fe^{3+}_{tetrahedral}$ / $Fe^{3+}_{octahedral}$ ratio was proportional to the alkali / alkaline earth ionic radius ratio. Stabilisation of Fe^{3+} ions in tetrahedral sites is best achieved by a combination of large alkali cations and small alkaline earth cations. Such combinations also served to increase Fe-O bond covalency.

7.3. Distribution of Iron Species

Ionic distribution of Fe was strongly affected by both glass composition and Fe_2O_3 content. This was indicated by optical, ESR and Mössbauer results. The effects of clustering have been shown in chapters 4, 5 and 6 to manifest as the inter-valence charge transfer (IVCT) band near 16,000 cm^{-1} in optical absorption; the $g = 2$ resonance and saturation of $\Delta H_{p\text{-}p}$ ($g = 4.3$) in ESR spectra; and the relative areas of Fe^{3+} doublet and sextets in Mössbauer spectra. Iron distribution has also been linked with changes in coordination and site parameters.

7.3.1. The Effects of Fe_2O_3 Content on Fe Ion Distribution

The following points have been confirmed by this work:

a) Amount of clustering of the type (Fe^{3+}-O-Fe^{3+}) $\propto$ (Fe_2O_3 %)^2.

b) Amount of clustering of the type (Fe^{2+}-O-Fe^{3+}) $\propto$ (Fe_2O_3 %)^2.

c) Percentages of isolated and clustered Fe^{3+} ions have been estimated for all Fe_2O_3 contents studied.

d) The crossover from predominance of isolated to clustered Fe ions occurs at ~3 molar % Fe_2O_3; glass composition affects the exact value somewhat.

Iron ion distribution at low concentrations (<1 molar % Fe_2O_3) has not been widely investigated. Some literature indicated that measurable clustering of Fe ions only occurs at higher Fe_2O_3 contents (see chapter 5.2.). A combination of ESR (see chapter 5) and Mössbauer (see chapters 6.3.1. and 6.4.1.) work in this study illustrated that at 0.2 molar % Fe_2O_3, some Fe^{3+}-O-Fe^{3+} exchange interactions do occur, i.e. some clustered Fe^{3+} ions are present. This work has indicated that measurable clustering occurs at all iron contents. It is estimated that at 0.2 molar % Fe_2O_3, approximately 20 % of all Fe ions occur as clustered Fe^{3+} ions (see chapters 6.3.1. and 6.4.1.). The actual percentage is affected by glass composition, and particularly by alkali ions.

Hence clustering of both types Fe^{3+}-O-Fe^{3+} and Fe^{3+}-O-Fe^{2+} obey the same relationship with Fe_2O_3 content, indicating no obvious preference for like-like clustering.

7.3.2. The Effects of Glass Composition on Fe Ion Distribution

Glass composition strongly affects the distribution of Fe ions:

a) Clustered / Isolated Ratio C = b * (Fe_2O_3 %)^2 where b is a constant determined by glass composition.

b) b $\propto$ (alkali / alkaline earth ionic radius ratio) for the glasses studied

c) Hence for glasses of equimolar Fe_2O_3 contents, C $\propto$ (alkali / alkaline earth ionic radius ratio).

d) Inconsistencies exist concerning MgO-containing glasses

As discussed in chapter 5.4.2., ESR results from both this work and others have shown that larger alkali ions and smaller alkaline earth ions promote Fe^{3+} cluster formation. An approximately linear relationship exists between the ratio of the two main ESR resonances (figure 6.4.1.c.), hence between isolated and clustered ions, and the alkali / alkaline earth ionic radius ratio. This is perhaps a simplification: it was noted in chapter 5.4.2. that alkali ions have a stronger influence on Fe^{3+} distribution, although alkaline earth ions have a greater influence when present in conjunction with large alkali ions such as K^+, Rb^+ or Cs^+.

The extinction coefficient of the main Fe^{3+} *d-d* absorption band is also proportional to the alkali / alkaline earth ionic radius ratio (see chapter 4.3.6.2.). It is possible that the Fe^{3+} extinction coefficient is affected by the relative proportions of isolated and clustered Fe^{3+} ions. In addition, MgO-containing glasses behaved in relative fashions, i.e. both the amount of clustering and $\varepsilon(Fe^{3+})$ were lower than predicted on the basis of results for the other cations. The anomalous results for MgO glasses were probably due to different bonding requirements of the Mg^{2+} ion, shown in chapter 2 to occupy tetrahedral network-forming sites. Bonding is partially covalent in glasses, and may be instrumental in this discrepancy.

7.4. The Effects of Other Compositional Changes

The effects of changing the base glass from silicate to borate, as well as minor substitutions of other ions for Si^{4+} will be covered by this chapter.

Optical absorption and ESR spectra showed important differences between borate and silicate glasses containing equimolar amounts of Fe_2O_3 (see chapters 4.3.2.5. and 5.3.3.). The UV edge in the borate glass was so strong that it obscured most of the absorptions normally attributed to Fe^{3+} *d-d* transitions in the range 20,000 – 30,000 cm^{-1}. The absorption at ~10,000 cm^{-1} associated with the $^5T_{2g} \rightarrow {}^5E_g$ transition of Fe^{2+} ions in octahedral coordination (see chapter 4.1.4.1.) is so weak that it indicates almost all iron is in the 3+ state in this glass.

In the borate glass, an absorption near 15,000 cm^{-1} can be distinguished. Its relative broadness and weakness are consistent with the $^6A_1 \rightarrow {}^4T_1$ transition of Fe^{3+} ions in tetrahedral sites, as predicted form Tanabe-Sugano diagrams [13 – 20]. The main effect of adding small amounts of B_2O_3 in silicate glasses containing iron is to shift the UV edge to lower wavenumbers (see chapter 4.3.2.4.). The addition of B_2O_3 to silicate glasses containing nominally zero Fe actually increases the UV transmission [21]. It is possible therefore that the addition of B_2O_3 to silicate glasses modifies the behaviour of the oxygen-metal charge transfer (OMCT) bands in the UV. It affects the strength and / or position of these bands such that the UV edge is stronger. The strength of the Fe^{2+} absorption ~10,000 cm^{-1} decreases, indicating that the addition of boron either reduces $\varepsilon(Fe^{2+})$ or the $Fe^{2+}/\Sigma Fe$ ratio. Further replacement of SiO_2 by B_2O_3 gives a glass similar in composition to sample 62. The UV edge has moved to much lower wavenumbers and the Fe^{2+} absorption is all but gone. This therefore indicates that it is the redox which has changed in the 5 % B_2O_3 glass. The shift in redox may partially contribute to the change in UV edge position, but it was concluded earlier that composition has a far greater influence than redox. The differences are therefore mainly caused by structural and environmental effects. The suggestion that Fe^{3+} ions in borate glasses exist in part in colloidal form [22] may be an explanation for this phenomenon. Such colloidal dispersions could affect the values of extinction coefficients in the UV. Indeed, ESR measurements discussed in chapter 5.3.3. suggest much greater clustering of Fe^{3+} ions in the borate glass compared with the silicate glass.

The addition of Al_2O_3 and GeO_2 to silicate base glasses had lesser effects on UV edges than the addition of B_2O_3. Changes occurred in optical spectra with all these additions, suggesting changes in redox or extinction coefficients.

7.5. Connections between Redox, Coordination and Distribution

Does distribution affect the redox, coordination and environment of Fe ions, and vice-versa? At low Fe_2O_3 contents such as 0.2 molar %, it would be useful to

know more about the relationships between composition, redox, coordination and distribution.

Many of the properties associated with Fe^{3+} ions are governed by selective behaviour. Larger alkali cations and smaller alkaline earth cations give rise to decreases in the $Fe^{2+}/\Sigma Fe$ redox ratio and increases in the amount of clustering and the tetrahedral / octahedral site ratio.

This study has shown that an increase in the Fe^{3+} tetrahedral / octahedral ratio is accompanied by an increase in the Fe^{3+} clustered / isolated ratio. Both of these changes are large compared with any changes in redox which may also occur, meaning that the relationship between coordination and distribution is probably little affected by these changes in redox. Hence we can consider coordination and distribution alone. This means that isolated Fe^{3+} ions are more likely to occupy octahedral sites, and clustered Fe^{3+} ions are more likely to occupy tetrahedral sites.

The following parameters have been identified as behaving selectively, i.e. they exhibit proportionality to some ratio of alkali / alkaline earth ions:

a) $Fe^{2+}/\Sigma Fe$ redox ratio.

b) Stabilisation of Fe^{3+} ions in tetrahedral sites.

c) Distribution of Fe^{3+} ions between clustered and isolated sites.

So why should selective behaviour occur for redox and also for many properties associated with Fe^{3+} ions, but collective behaviour apply more to Fe^{2+} ions?

One reason may be coordination: for the glasses studied there was a major difference in coordination of the different redox states: Fe^{2+} ions mostly occupied octahedral sites, and Fe^{3+} ions occupied a mixture of tetrahedral and octahedral sites. Tetrahedral Fe^{3+} ions require charge balance of +1 from one alkali or half an alkaline earth ion [12]. As discussed in chapter 5.4.2., Waff [12] found that alkali complexes are more tightly bound and therefore more stable than alkaline earth-iron complexes. This explains selective behaviour wherein tetrahedral Fe^{3+} ions preferentially use alkali ions for charge balance. A combination of larger alkali and smaller alkaline earth ions give the best stabilisation of $Fe^{3+}_{tetrahedral}$ ions.

There may be two different structural possibilities governing these selective properties; redox, coordination of Fe^{3+} ions, and distribution of Fe^{3+} ions:

a) Only alkali cations perform the necessary stabilisations of Fe^{3+} ions, and alkaline earth ions merely hinder their effectiveness by varying degrees based upon space / charge effects. The ability of the alkali ions to perform these various stabilisations is proportional to their size, and the ability of alkaline earth ions to hinder the stabilisation is proportional to their size.

b) Both alkali and alkaline earth cations perform the necessary stabilisations of Fe^{3+} ions. A combination of large alkali ions and small alkaline earth ions best achieves this. The ability of the alkali ions to perform these stabilisations is proportional to their size, and the ability of alkaline earth ions to perform the stabilisation is inversely proportional to their size.

This is one of the main questions posed by these results: we know that tetrahedral, clustered Fe^{3+} ions are best stabilised by alkali ions, especially by larger alkali ions, but do alkaline earth ions participate? If so, how? If not, do they hinder alkali ions from performing the stabilisations, and how? These questions require further work to be fully answered.

7.6. Local Structure Surrounding Fe Species

Optical basicity represents the *average* electron donor capability of oxygen ions in a glass. A linear relationship between a property and optical basicity with changing composition therefore indicates that both types of modifier cation, alkali and alkaline earth, affect the behaviour of Fe ions in similar ways but to varying degrees, and the overall effect is additive. For example, $Dq(Fe^{2+})$ was proportional to the optical basicity of the glass for octahedral and tetrahedral ions. The alkali / alkaline earth ionic radius ratio is a scale which represents *selective* rather than *collective* behaviour. Many properties of Fe have been found in this work to be quantified by these scales, for example various optical parameters, the

relative amounts of isolated and clustered Fe^{3+} ions and of tetrahedral and octahedral Fe^{3+} ions, and the $Fe^{2+}/\Sigma Fe$ redox ratio. Selective structural behaviour affects Fe^{3+} ions more strongly and with respect to more of their properties than Fe^{2+} ions. It is possible that this may be related to differences in coordination; the majority of Fe^{3+} ions occupy tetrahedral sites, whereas the majority of Fe^{2+} ions occupy octahedral sites.

As discussed in chapter 2.1., work on glass structure has revealed that cation distributions are not random as proposed by the original random network theory. Channels or regions of high alkali content percolate alkali silicate glasses [23]. In addition, regions of high barium content were found in SiO_2-Na_2O-BaO glasses [24].

Application of these more recent findings to the question of Fe coordination and environment presents certain difficulties; Fe^{2+} ions occur predominantly in octahedral sites in the glasses studied. They display collective behaviour in terms of *Dq*, so their next-nearest-neighbour cation coordination spheres must contain alkali and alkaline earth cations, though not necessarily both types in any one coordination sphere. It is therefore possible that Fe^{2+} ions occupy regions in the glass which are rich with modifier ions. On the other hand there is no evidence that the Fe^{2+} ions do not define their own environment and use appropriate cations from their surroundings to satisfy bonding requirements and maintain charge neutrality.

Fe^{3+} ions occupy both tetrahedral and octahedral sites, and exhibit selective behaviour with respect to modifier cations. Tetrahedral sites in particular show this selectivity, as demonstrated by luminescence spectroscopy. Mössbauer spectroscopy could not distinguish individual behaviours of Fe^{3+} ions in tetrahedral and octahedral sites. Selectivity indicates that Fe^{3+} ions largely define their own immediate environments in terms of their coordination spheres, although the distribution of Fe^{3+} ions between isolated and clustered sites must also be considered: tetrahedral Fe^{3+} ions are associated with clustering. This distribution is governed by similar selectivity to that which governs coordination and redox, albeit with slight differences which were discussed in chapter 5.4.2.

Clearly the medium-range order surrounding Fe ions in the glasses studied here is relatively well-defined and not random. This applies to Fe ions in both possible

redox states and both possible coordinations. It also means that the environments surrounding these ions are not average representations of environments within the bulk glass. Caution should therefore be taken when using Fe as a probe ion for examining the structure of glass.

Medium-range order surrounding Fe ions may also include other Fe ions, even at low iron concentrations such as 0.2 molar % Fe_2O_3. Whilst not having a great affect on existing optical parameters, it does introduce a new absorption band near 16,000 cm^{-1}. In addition it may be one reason for decreases in site distortion with increasing clustering.

7.7. Other Structural Implications

Density measurements and other data have given useful information on the structure of these glasses. In particular the behaviour of MgO – containing glasses was unlike the other alkaline earth oxides. This has been attributed to a fraction of the Mg^{2+} ions occupying tetrahedral sites, resulting in a voluminous structure (see chapter 2.1.). This affected the behaviour of Fe ions, and particularly Fe^{3+} ions, in terms of redox, coordination, distribution and environment. The $Fe^{2+}/\Sigma Fe$ ratio was higher than expected and the proportions of tetrahedral and of clustered Fe^{3+} ions were lower than expected. This is yet further evidence for the inter-dependence of tetrahedral and clustered Fe^{3+} ions.

7.8. Suggestions for Future Work

During the course of this study, this author became aware of how few detailed structural studies have been made on alkali-alkaline earth silicate systems. Generally such work has tended to cover alkali silicate or aluminosilicate systems. Considering that alkali – alkaline earth silicates present a much closer approximation to container glass and float glass, more work should be conducted to give a better structural understanding of these common glasses. With this in mind, techniques such as x-ray absorption and neutron diffraction can provide information on bulk properties such as were shown by Brosset [24]. Detailed

environmental information on Fe ions, for example Fe-O bond lengths, can be obtained from techniques such as neutron diffraction or EXAFS. A combination of detailed studies of Fe local environments and bulk glass structure using such techniques would provide yet further insight into the behaviour of the glasses covered by this study.

An expansion of the luminescence work discussed in this study should include an investigation of the effects of glass composition on the luminescence band near 11,000 cm^{-1}, established as being due to Fe^{3+} ions in octahedral sites. This would offer further evidence on the connections between coordination and distribution of Fe^{3+} ions.

Transmission electron microscopy and EDS analysis may give information on phase separation phenomena and the makeup of different phases, if any. The distribution of both modifier ions and Fe ions between such phases (if they exist) would allow a better understanding of the behaviour of Fe ions in these glasses. Imaging of iron clusters may be possible using electron microscopy. Calculation of the statistics involved with iron clusters would allow better insight into the behaviour of Fe ions and their tendency to cluster.

The addition of other ions to the compositions already studied could be made; a few percent Al_2O_3; more mixed-alkali glasses; these would bring the composition even closer to those of container and float glass, and hence studies of such glasses would be directly useful to manufacturers and developers of such glasses.

7.9. References

[1] Mysen, B.O., Seifert, F., Virgo, D., Amer. Mineral., 1980, vol. 65, p. 867.

[2] Mysen, B.O., Virgo, D., Seifert, F.A., Amer. Mineral., 1985, vol. 70, p. 88.

[3] Mysen, B.O., Virgo, D., Amer. Mineral., 1989, vol. 74, p. 58.

[4] Mysen, B.O., Virgo, D., Neumann, E.R., Seifert, F.A., Amer. Mineral., 1985, vol. 70, p. 317.

[5] Mysen, B.O., Virgo, D., Seifert, F.A., Amer. Mineral., 1984, vol. 69, p. 834.

[6] Goldman, D.S., J. Amer. Ceram. Soc., 1983, vol. 66, p. 205.

[7] Cable, M., Xiang, Z., Glastech. Ber., 1989, vol. 62, p. 382.

[8] Schreiber, H.D., Kozak, S.J., Merkel, R.C., Balazs, G.B., Jones, P.W., J. Non-Cryst. Solids, 1986, vol. 84, p. 186.

[9] Jeddeloh, G., Phys. Chem. Glasses, 1984, vol. 25, p. 163.

[10] Gerlach, S., Clausen, O., Rüssel, C., J. Non-Cryst. Solids, 1998, vol. 238, p. 75.

[11] Claussen, O., Rüssel, C., Phys. Chem. Glasses, 1998, vol. 39, p. 200.

[12] Waff, H.S., Can. Mineral., 1977, vol. 15, p. 198.

[13] Tanabe, Y., Sugano, S., J. Phys. Soc. Japan, 1954, vol. 9, p. 753.

[14] Tanabe, Y., Sugano, S., J. Phys. Soc. Japan, 1954, vol. 9, p. 766.

[15] Ades, C., Toganidis, T., Traverse, J.P., J. Non-Cryst. Solids, 1990, vol. 125, p. 272.

[16] Fox, K.E., Furukawa, T., White, W.B., Phys. Chem. Glasses, 1982, vol. 23, p. 169.

[17] Knight, D.S., White, W.B., J. Amer. Ceram. Soc., 1988, vol. 71, p. C-342.

[18] Fox, K.E., Furukawa, T., White, W.B., J. Amer. Ceram. Soc., 1981, vol. 64, p. C-42.

[19] Kinawi, A.A., Transition Met. Chem., 1982, vol. 7, p. 335.

[20] Kinawi, A.A., J. Inorg. Nucl. Chem., 1981, vol. 43, p. 1989.

[21] Sigel, G.H., Optical Absorption of Glass, in Treatise on Materials Science and Technology, vol. 12, Ed., Tomozawa, M., Doremus, R.H., Academic Press, 1977.

[22] Steele, F.N., Douglas, R.W., Phys. Chem. Glasses, 1965, vol. 6, p. 246.

[23] Greaves, G.N., J. Non-Cryst. Solids, 1985, vol. 71, p. 203.

[24] Brosset, C., J. Soc. Glass Tech., 1958, vol. 42, p. 125.

Chapter 8.

Summary and Conclusions

In this thesis a multi-technique approach has been used to study iron in ternary silicate glasses. A wide range of glass compositions and iron concentrations have been thoroughly investigated and characterised.

It has been established that coordination, redox, ion distribution, ligand field and bonding parameters associated with Fe^{2+} and Fe^{3+} ions are strongly affected by either or both of iron content and glass composition.

Conclusions apply only to the glass systems studied, and whilst they indicate possible behaviour in other systems, identical behaviour should not be assumed.

8.1. The Effects of Fe_2O_3 Content

A combination of techniques has shown that redox is not affected by Fe_2O_3 content *provided that the glass melt is sufficiently close to equilibrium with the surrounding atmosphere.* Mössbauer, wet chemical and optical methods gave $Fe^{2+}/\Sigma Fe$ ratios which were generally the same.

Coordinations of Fe^{2+} and Fe^{3+} ions were affected by Fe_2O_3 content, and this accompanied clustering. Increasing Fe_2O_3 content gave rise to increases in the tetrahedral / octahedral ratio, more so for Fe^{3+} ions than for Fe^{2+} ions. This was accompanied by a narrowing of site parameters and increasing site symmetry, which may be linked with clustering.

The Fe_2O_3 content strongly affected all measured spectra. Some spectral changes were the results of the effects of Fe_2O_3 content on the distribution of Fe^{2+} and Fe^{3+} ions between isolated and clustered sites. The amounts of clustering of the types

Fe^{3+}-O-Fe^{3+} and Fe^{2+}-O-Fe^{3+} were both approximately proportional to the square of the Fe_2O_3 content in molar percent. Clustering was found to manifest in optical spectra as an absorption band attributable to inter-valence charge transfer at approximately 16,000 cm^{-1}. The disappearance of hyperfine sextets in Mössbauer spectra and the increasing intensity of the g = 2 resonance in ESR spectra were indicative of Fe^{3+} clustering. The crossover in predominance between isolated and clustered Fe^{3+} ions was affected by glass composition, but generally occurred at ~3 molar percent Fe_2O_3. Estimates of the relative numbers of clustered and isolated Fe^{3+} ions were made for different Fe_2O_3 contents, and indicated that even at low iron contents of 0.2 molar % Fe_2O_3, considerable numbers of Fe ions were clustered.

Optical absorption spectra were greatly affected by changes in Fe_2O_3 content, however the ligand field and Racah parameters were not. The changes in optical spectra manifested as increasing strength of all *d-d* transitions, but also the movement of the UV edge to lower wavenumbers and the increasing strength of an inter-valence charge transfer absorption.

8.2. The Effects of Glass Composition

The effects of glass composition on the properties investigated by this study could be separated into two general categories: *collective* and *selective*.

Collective relationships took the form of proportionality between a property and the theoretical optical basicity Λ_{th} of a glass, which is a measure of the *average* electron donor power of constituent oxides. The ligand field parameter $Dq(Fe^{2+}_{oct})$ fell into this category, indicating that the next-nearest neighbour coordination shells of octahedral Fe^{2+} ions include both alkali and alkaline earth cations.

Selective relationships took the form of proportionality between a property and the ratio of alkali / alkaline earth ions, as expressed in this case by ionic radii. Many parameters describing redox, coordination, environment and ion distribution fell into this category, especially those pertaining to Fe^{3+} ions.

A combination of wet chemical and optical techniques showed that regardless of the Fe_2O_3 content, the redox ratio $Fe^{2+}/\Sigma Fe$ was inversely proportional to the ratio

of alkali / alkaline earth ions in terms of their ionic radii. This was typical of selective behaviour.

Optical spectra exhibited changes with composition which could be attributed to redox, coordination and ion distribution.

Coordination and environment of Fe^{2+} and Fe^{3+} ions were strongly affected by composition, and generally tended to be governed by selective behaviour. A shift in coordination of Fe^{3+} ions from octahedral towards tetrahedral was caused by increasing the alkali / alkaline earth ionic radius ratio.

Two possibilities were put forward to explain selective behaviour: either alkali and alkaline earth ions act in opposition to one another with regards to Fe (particularly Fe^{3+}) ions to which they are coordinated, or it is mostly alkali ions which coordinate and charge-balance Fe^{3+} ions and alkaline earth ions hinder their ability to do so by varying degrees.

Fitting of optical spectra confirmed the existence of absorptions which were attributed to the dynamic Jahn-Teller effect and to inter valence charge transfer caused by clustering, in addition to d-d transitions and the UV edge.

8.3. The Unique Case of MgO

Glasses containing MgO exhibited behaviour dissimilar to the other alkaline earths. These differences manifested as unexpectedly high molar volumes, indicating a voluminous structure. These had a diluting effect upon Fe dopants, so that glasses with CaO as the alkaline earth oxide contained a higher volume concentration of Fe ions than equivalent MgO glasses. It was also found that Mg^{2+} ions give rise to greater amounts of clustering of Fe^{3+} ions than the other alkaline earth ions.

These differences also affected many other properties: the redox ratio $Fe^{2+}/\Sigma Fe$, was higher than expected, so Fe^{3+} ions were less stable than suggested by ionic radii predictions. Extinction coefficients were lower than expected for both valencies, hence for Fe^{3+} ions the tetrahedral / octahedral ratio was lower than expected.

These phenomena may be due to some fraction of Mg^{2+} ions occupying tetrahedral network-forming sites.

Appendix A

Table A1. Compositions

Sample Code	SiO_2 molar %	Alkali Oxide and molar %	Alkaline Earth Oxide and molar %	Fe_2O_3 molar %	Other Component and molar %	Melting Conditions	Crucible Type	Comments
1	70	Na_2O 15	MgO 15	0		Standard	Pt-2 % Rh	
2	70	Na_2O 15	CaO 15	0		Standard	Pt-2 % Rh	
3	70	Na_2O 15	SrO 15	0		Standard	Pt-2 % Rh	
4	70	Na_2O 15	BaO 15	0		Standard	Pt-2 % Rh	
5	70	Na_2O 15	BaO 15	0		Gas 1	Mullite	
6	70	K_2O 15	BaO 15	0		Gas 1	Mullite	
7	70	Rb_2O 15	BaO 15	0		Gas 1	Mullite	
8	69.9	Na_2O 15	MgO 15	0.1		Standard	Pt-2 % Rh	
9	69.9	Na_2O 15	CaO 15	0.1		Standard	Pt-2 % Rh	
10	69.8	Li_2O 15	MgO 15	0.2		Standard	Pt-2 % Rh	
11	69.8	Li_2O 15	MgO 15	0.2		Gas 1	Mullite	
12	69.8	Li_2O 15	CaO 15	0.2		Standard	Pt-2 % Rh	
13	69.8	Li_2O 15	CaO 15	0.2		Gas 1	Mullite	
14	69.8	Li_2O 15	SrO 15	0.2		Standard	Pt-2 % Rh	

Sample Code	SiO_2 %	Alkali Oxide and %	Alkaline Earth Oxide and %	Fe_2O_3 %	Other Components and %	Melting Conditions	Crucible	Comments
15	69.8	Li_2O 15	BaO 15	0.2		Standard	Pt-2 % Rh	
16	69.8	Li_2O 15	BaO 15	0.2		Gas 1	Mullite	
17	69.8	Li_2O 7.5 Na_2O 7.5	MgO 15	0.2		Standard	Pt-2 % Rh	
18	69.8	Li_2O 7.5 Na_2O 7.5	CaO 15	0.2		Standard	Pt-2 % Rh	
19	69.8	Li_2O 7.5 Na_2O 7.5	SrO 15	0.2		Standard	Pt-2 % Rh	
20	69.8	Li_2O 7.5 Na_2O 7.5	BaO 15	0.2		Standard	Pt-2 % Rh	
21	69.8	Na_2O 15	MgO 15	0.2		Standard	Pt-2 % Rh	
22	69.8	Na_2O 15	MgO 15	0.2		Gas 2	Pt-2 % Rh	
23	69.8	Na_2O 15	MgO 15	0.2	Carbon	Gas 2	Pt-2 % Rh	Reduced
24	69.8	Na_2O 15	CaO 15	0.2		Standard	Pt-2 % Rh	
25	69.8	Na_2O 15	CaO 15	0.2		Standard	Pt-2 % Rh	3-Hour Melt
26	69.8	Na_2O 15	CaO 15	0.2		Standard	Pt-2 % Rh	22-Hour Melt

Sample Code	SiO_2 %	Alkali Oxide and %	Alkaline Earth Oxide and %	Fe_2O_3 %	Other Components and %	Melting Conditions	Crucible	Comments
27	69.8	Na_2O 15	CaO 15	0.2		Gas 2	Pt-2 % Rh	
28	69.8	Na_2O 15	CaO 15	0.2	Carbon	Gas 2	Pt-2 % Rh	Reduced
29	69.8	Na_2O 15	SrO 15	0.2		Standard	Pt-2 % Rh	
30	69.8	Na_2O 15	SrO 15	0.2		Gas 2	Pt-2 % Rh	
31	69.8	Na_2O 15	SrO 15	0.2	Carbon	Gas 2	Pt-2 % Rh	Reduced
32	69.8	Na_2O 15	BaO 15	0.2		Standard	Pt-2 % Rh	
33	69.8	Na_2O 15	BaO 15	0.2		Gas 1	Mullite	
34	69.8	Na_2O 15	BaO 15	0.2		Gas 2	Pt-2 % Rh	
35	69.8	Na_2O 15	BaO 15	0.2	Carbon	Gas 2	Pt-2 % Rh	Reduced
36	69.8	Na_2O 7.5 K_2O 7.5	MgO 15	0.2		Gas 1	Mullite	
37	69.8	Na_2O 7.5 K_2O 7.5	CaO 15	0.2		Gas 1	Mullite	
38	69.8	Na_2O 7.5 K_2O 7.5	SrO 15	0.2		Gas 1	Mullite	
39	69.8	Na_2O 7.5	BaO 15	0.2		Gas 1	Mullite	

		K_2O 7.5						
Sample Code	**SiO_2 %**	**Alkali Oxide and %**	**Alkaline Earth Oxide and %**	**Fe_2O_3 %**	**Other Components and %**	**Melting Conditions**	**Crucible**	**Comments**
40	69.8	K_2O 15	MgO 15	0.2		Standard	Pt-2 % Rh	
41	69.8	K_2O 15	MgO 15	0.2	Carbon	Gas 1	Pt-2 % Rh	Reduced
42	69.8	K_2O 15	CaO 15	0.2		Standard	Pt-2 % Rh	
43	69.8	K_2O 15	CaO 15	0.2		Gas 1	Pt-2 % Rh	
44	69.8	K_2O 15	CaO 15	0.2	Carbon	Gas 1	Pt-2 % Rh	Reduced
45	69.8	K_2O 15	SrO 15	0.2		Standard	Pt-2 % Rh	
46	69.8	K_2O 15	SrO 15	0.2		Gas 1	Pt-2 % Rh	
47	69.8	K_2O 15	SrO 15	0.2	Carbon	Gas 1	Pt-2 % Rh	Reduced
48	69.8	K_2O 15	BaO 15	0.2		Standard	Pt-2 % Rh	
49	69.8	K_2O 15	BaO 15	0.2		Gas 1	Pt-2 % Rh	
50	69.8	K_2O 15	BaO 15	0.2	Carbon	Gas 1	Pt-2 % Rh	Reduced
51	69.8	Rb_2O 15	CaO 15	0.2		Standard	Pt-2 % Rh	
52	69.8	Rb_2O 15	SrO 15	0.2		Standard	Pt-2 % Rh	
53	69.8	Rb_2O 15	BaO 15	0.2		Standard	Pt-2 % Rh	
54	69.8	Cs_2O 15	CaO 15	0.2		Standard	Pt-2 % Rh	

Sample Code	SiO_2 %	Alkali Oxide and %	Alkaline Earth Oxide and %	Fe_2O_3 %	Other Components and %	Melting Conditions	Crucible	Comments
55	69.8	Cs_2O 15	SrO 15	0.2		Standard	Pt-2 % Rh	
56	69.8	Cs_2O 15	BaO 15	0.2		Standard	Pt-2 % Rh	
57	64.8	Na_2O 15	CaO 15	0.2	Al_2O_3 5	Standard	Pt-2 % Rh	
58	64.8	Na_2O 15	CaO 15	0.2	B_2O_3 5	Standard	Pt-2 % Rh	
59	64.8	Na_2O 15	CaO 15	0.2	PbO 5	Standard	Pt-2 % Rh	
60	64.8	Na_2O 15	CaO 15	0.2	GeO_2 5	Standard	Pt-2 % Rh	
61	64.8	Na_2O 15	CaO 15	0.2	ZnO 5	Standard	Pt-2 % Rh	
62	20	Na_2O 5	-	0.2	B_2O_3 74.8	Standard	Pt-2 % Rh	Borate Glass
63	69.5	Na_2O 15	CaO 15	0.5		Standard	Pt-2 % Rh	
64	69.34	Na_2O 15	CaO 15	0.66		Standard	Pt-2 % Rh	
65	69.3	Na_2O 14.85	MgO 14.85	1		Standard	Pt-2 % Rh	
66	69.3	Na_2O 14.85	CaO 14.85	1		Standard	Pt-2 % Rh	
67	69.3	Na_2O 14.85	SrO 14.85	1		Standard	Pt-2 % Rh	
68	69.3	Na_2O 14.85	BaO 14.85	1		Standard	Pt-2 % Rh	
69	68.6	Na_2O 14.70	CaO 14.70	2		Standard	Pt-2 % Rh	
70	67.9	Na_2O 14.55	CaO 14.55	3		Standard	Pt-2 % Rh	

Sample Code	SiO_2 %	Alkali Oxide and %	Alkaline Earth Oxide and %	Fe_2O_3 %	Other Components and %	Melting Conditions	Crucible	Comments
71	67.2	Na_2O 14.40	CaO 14.40	4		Standard	Pt-2 % Rh	
72	66.5	Na_2O 14.25	CaO 14.25	5		Standard	Pt-2 % Rh	
73	69.3	K_2O 14.85	CaO 14.85	1		Standard	Pt-2 % Rh	
74	68.6	K_2O 14.70	CaO 14.70	2		Standard	Pt-2 % Rh	
75	67.9	K_2O 14.55	CaO 14.55	3		Standard	Pt-2 % Rh	
76	67.2	K_2O 14.40	CaO 14.40	4		Standard	Pt-2 % Rh	
77	66.5	K_2O 14.25	CaO 14.25	5		Standard	Pt-2 % Rh	
78	66.5	Na_2O 14.25	MgO 14.25	5		Standard	Pt-2 % Rh	
79	66.5	Na_2O 14.25	SrO 14.25	5		Standard	Pt-2 % Rh	
80	66.5	Na_2O 14.25	BaO 14.25	5		Standard	Pt-2 % Rh	
81	66.5	Li_2O 7.125 Na_2O 7.125	BaO 14.25	5		Standard	Pt-2 % Rh	
82	66.5	K_2O 14.25	BaO 14.25	5		Standard	Pt-2 % Rh	
83	66.5	Rb_2O 14.25	BaO 14.25	5		Standard	Pt-2 % Rh	
84	66.5	Cs_2O 14.25	BaO 14.25	5		Standard	Pt-2 % Rh	

Table A2. Raw Material Analyses

Raw Material	Oxide Supplied	Manufacturer	Assay	Impurities
Japanese Quartz	SiO_2	Unknown	99.9 %	$Na_2O < 0.05$ %, $Fe_2O_3 < 3$ ppm
Fe_2O_3	Fe_2O_3	Aldrich	> 99 %	-
Li_2CO_3	Li_2O	BDH	99%	Cl < 0.005 %, SO_4 < 0.01 %, Pb < 0.001 %, Fe < 0.001 %, Mg < 0.005 %, Na < 0.005 %
Na_2CO_3	Na_2O	Fisher	> 99.5 %	Ca < 0.05 %, Cu < 0.002 %, Fe < 0.002 %, Pb < 0.002 %, Mg < 0.01 %, K < 0.02 %, S < 0.02%, Cl < 0.02 %, Zn < 0.01 %, P < 0.005 %, Si < 0.02 %
K_2CO_3	K_2O	BDH	> 99 %	Cl < 0.001 %, N < 0.001 %, PO_4 < 0.0005 %, SiO_2 < 0.0025 %, Al < 0.001 %, Ca < 0.002 %, Cu < 0.0005 %, Fe < 0.0005 %, Pb < 0.001 %, Na < 0.08 %
Rb_2CO_3	Rb_2O	Penn	99.8%	-
Cs_2CO_3	Cs_2O	Avocado	97%	-
$MgCO_3$	MgO	Fisons	99%	Ca < 1 %, Cu < 0.001 %, Fe < 0.05 %, Pb < 0.001 %, K < 0.02 %, Na < 0.5 %, Zn < 0.01 %, S < 0.5 %, P < 0.01 %, Cl < 0.05 %, Si < 0.05 %
$CaCO_3$	CaO	BDH	> 99%	Cl < 0.005 %, N < 0.001 %, SO_4 < 0.01 %, Al < 0.005 %, Ba < 0.005 %, Cu < 0.0005 %, Fe < 0.001 %, Pb < 0.0005 %, Mg < 0.05 %, K < 0.01 %, Na < 0.2 %, Sr < 0.1 %
$SrCO_3$	SrO	BDH	> 99%	Ba < 0.05 %, Ca < 0.07 %, Pb < 0.005 %, Fe < 0.003 %, Mg < 0.002 %

Raw Material	Oxide Supplied	Manufacturer	Assay	Impurities
$BaCO_3$	BaO	BDH	> 99%	Cl < 0.005 %, S < 0.01 %, Pb < 0.002 %, Fe < 0.005 %, K < 0.01 %, Na < 0.05 %
GeO_2	GeO_2	Koch-Light	> 99.999%	-
B_2O_3	B_2O_3	Fisher	> 98%	-
Al_2O_3	Al_2O_3	Fisher	> 99.5%	Cl < 0.005 %, Fe < 0.005 %, SO_4 < 0.005 %
ZnO	ZnO	Fisher	99.5%	-
Pb_3O_4	PbO	BDH	> 99%	-

Appendix B

Table B1. Density, Luminescence and Absorption Data

Sample	Composition In Brief	Density / gcm^{-3}	Fe^{3+} PL Peak Max. / cm^{-1} ± 200	Fe^{2+} Peak Max. / cm^{-1} ± 100
10	Si-Li-Mg-0.2Fe	2.2954	-	-
12	Si-Li-Ca-0.2Fe	2.4841	-	-
14	Si-Li-Sr-0.2Fe	2.7051	-	-
15	Si-Li-Ba-0.2Fe	3.0044	13,160	9,900
17	Si-Li/Na-Mg-0.2Fe	2.4367	14,285	10,750
18	Si-Li/Na-Ca-0.2Fe	2.5560	13,890	10,100
19	Si-Li/Na-Sr-0.2Fe	2.7856	13,795	9,800
20	Si-Li/Na-Ba-0.2Fe	3.0027	13,425	9,600
21	Si-Na-Mg-0.2Fe	2.4444	14,390	9,900
24	Si-Na-Ca-0.2Fe	2.5554	14,085	9,200
29	Si-Na-Sr-0.2Fe	2.8011	13,605	9,300
32	Si-Na-Ba-0.2Fe	3.0297	13,160	9,000
36	Si-Na/K-Mg-0.2Fe	2.4399	14,815	-
37	Si-Na/K-Ca-0.2Fe	2.5042	14,705	-
38	Si-Na/K-Sr-0.2Fe	2.7705	14,085	-
39	Si-Na/K-Ba-0.2Fe	2.9902	13,335	-
40	Si-K-Mg-0.2Fe	2.4007	14,925	9,000

Sample	Composition In Brief	Density / gcm^{-3}	Fe^{3+} PL Peak Max. / cm^{-1} ± 200	Fe^{2+} Peak Max. / cm^{-1} ± 100
42	Si-K-Ca-0.2Fe	2.5184	14,495	8,600
45	Si-K-Sr-0.2Fe	2.7434	14,390	8,500
48	Si-K-Ba-0.2Fe	2.9709	13,890	8,400
51	Si-Rb-Ca-0.2Fe	2.9088	14,705	8,550
52	Si-Rb-Sr-0.2Fe	3.1156	14,600	8,400
53	Si-Rb-Ba-0.2Fe	3.3207	14,285	8,300
54	Si-Cs-Ca-0.2Fe	3.2205	14,705	8,500
55	Si-Cs-Sr-0.2Fe	3.4923	14,390	8,500
56	Si-Cs-Ba-0.2Fe	3.6136	14,390	8,200
9	Si-Na-Ca-0.1Fe	2.5546	14,185	9,300
63	Si-Na-Ca-0.5Fe	2.5662	14,185	9,300
66	Si-Na-Ca-1Fe	2.5825	14,285	9,300
69	Si-Na-Ca-2Fe	2.6106	-	9,400
70	Si-Na-Ca-3Fe	2.6474	-	9,600
71	Si-Na-Ca-4Fe	2.6787	-	10,000
72	Si-Na-Ca-5Fe	2.7067	-	10,200
60	Si-Ge-Na-Ca-0.2 Fe	-	-	9,200
58	Si-B-Na-Ca-0.2 Fe	-	-	9,250
57	Si-Al-Na-Ca-0.2 Fe	-	-	9,400
81	Si-Li-Na-Ba-5 Fe	-	-	10,300
80	Si-Na-Ba-5 Fe	-	-	9,500
82	Si-K-Ba-5 Fe	-	-	8,800
83	Si-Rb-Ba-5 Fe	-	-	8,700
84	Si-Cs-Ba-5 Fe	-	-	8,700
78	Si-Na-Mg-5 Fe	-	-	11,200
79	Si-Na-Sr-5 Fe	-	-	9,900

Table B2. Electron Spin Resonance (ESR) Data

Sample	Composition	Fe_2O_3 / molar %	ΔH_{p-p} (g = 4.3) / mT ± 0.3	I_{p-p} (g = 2 / g = 4.3) ± 10 %
15	Si-Li-Ba	0.2	4.68	0.0654
17	Si-Li-Na-Mg	0.2	4.87	0.0763
18	Si-Li-Na-Ca	0.2	4.96	0.0719
19	Si-Li-Na-Sr	0.2	4.4	0.0719
20	Si-Li-Na-Ba	0.2	4.59	0.0787
21	Si-Na-Mg	0.2	5.62	0.135
24	Si-Na-Ca	0.2	4.87	0.0909
29	Si-Na-Sr	0.2	4.96	0.0943
32	Si-Na-Ba	0.2	4.68	0.0980
36	Si-Na-K-Mg	0.2	6.46	0.294
37	Si-Na-K-Ca	0.2	5.33	0.179
38	Si-Na-K-Sr	0.2	5.05	0.137
39	Si-Na-K-Ba	0.2	4.77	0.127
40	Si-K-Mg	0.2	8.14	0.442
42	Si-K-Ca	0.2	5.99	0.270
45	Si-K-Sr	0.2	5.52	0.227
48	Si-K-Ba	0.2	5.24	0.2
51	Si-Rb-Ca	0.2	7.11	0.4
52	Si-Rb-Sr	0.2	6.27	0.323
53	Si-Rb-Ba	0.2	5.8	0.25
54	Si-Cs-Ca	0.2	7.49	0.455
55	Si-Cs-Sr	0.2	7.3	0.417
56	Si-Cs-Ba	0.2	6.46	0.357
62	Borate	0.2	6.98	0.659
9	Si-Na-Ca	0.1	3.38	0.080
63	Si-Na-Ca	0.5	7.94	0.145
66	Si-Na-Ca	1	14.49	0.377

Sample	Composition	Fe_2O_3 / molar %	ΔH_{p-p} (g = 4.3) / mT ± 0.3	I_{p-p} (g = 2 / g = 4.3) ± 10 %
69	Si-Na-Ca	2	18.46	0.862
70	Si-Na-Ca	3	21.24	2.439
71	Si-Na-Ca	4	20.25	5.263
72	Si-Na-Ca	5	19.65	8.333
73	Si-K-Ca	1	16.1	1.176
74	Si-K-Ca	2	20.13	3.846
75	Si-K-Ca	3	20.13	9.091
76	Si-K-Ca	4	18.12	20.00
77	Si-K-Ca	5	13.42	33.33

Table B3. Wet Chemical and Optical Redox Measurements

Sample	Composition	Fe_2O_3 / molar %	Wet Chemical $(Fe^{2+}/\Sigma Fe)$ * 100%	Optical $(Fe^{2+}/\Sigma Fe)$ * 100%
15	Si-Li-Ba	0.2	-	20.6
17	Si-Li-Na-Mg	0.2	17 ± 1	17.0
18	Si-Li-Na-Ca	0.2	-	17.5
19	Si-Li-Na-Sr	0.2	-	18.5
20	Si-Li-Na-Ba	0.2	20 ± 1	20.0
21	Si-Na-Mg	0.2	15 ± 1	15.0
24	Si-Na-Ca	0.2	16 ± 1	16.0
29	Si-Na-Sr	0.2	17 ± 1	17.0
32	Si-Na-Ba	0.2	18 ± 1	18.1
40	Si-K-Mg	0.2	-	9.7
42	Si-K-Ca	0.2	12 ± 1	12.2
45	Si-K-Sr	0.2	15 ± 1	15.1
48	Si-K-Ba	0.2	16 ± 1	16.1
51	Si-Rb-Ca	0.2	-	11.4
52	Si-Rb-Sr	0.2	-	13.1
53	Si-Rb-Ba	0.2	15 ± 1	14.9
54	Si-Cs-Ca	0.2	-	9.5
55	Si-Cs-Sr	0.2	-	11.5
56	Si-Cs-Ba	0.2	14 ± 1	14.1
9	Si-Na-Ca	0.1	15 ± 1	15.1
63	Si-Na-Ca	0.5	16 ± 1	16.8
66	Si-Na-Ca	1	16 ± 1	16
69	Si-Na-Ca	2	21 ± 2	19.3
70	Si-Na-Ca	3	17 ± 2	17
71	Si-Na-Ca	4	16 ± 2	14.5
72	Si-Na-Ca	5	15 ± 2	21.2
88	Si-Li-Na-Ba	5	18 ± 2	-

90	Si-Rb-Ba	5	14 ± 2	-
91	Si-Cs-Ba	5	15 ± 2	-

Table B4. Mathematical Fitting Parameters for Optical Absorption Spectra

Peak	Parameter	Sample 15	Sample 17	Sample 18	Sample 19	Sample 20
A	Position	4830	4901	4864	4774	4750
	Intensity	0.2141	0.1545	0.1803	0.2093	0.1970
	Width	957	1308	1066	1035	977
B	Position	7706	8143	7732	7665	7624
	Intensity	0.0615	0.0989	0.0941	0.0972	0.1076
	Width	1345	1473	1341	1433	1520
C	Position	10069	10881	10288	10113	9985
	Intensity	0.7972	0.7439	0.7384	0.7465	0.7432
	Width	4101	3892	3972	4080	4054
D	Position	16282	16625	16226	15906	15912
	Intensity	0.0891	0.0678	0.0602	0.0565	0.0689
	Width	2551	2456	2576	2461	2283
E	Position	20522	20053	19805	20044	20256
	Intensity	0.0970	0.0615	0.0493	0.0584	0.0829
	Width	2450	1534	1802	2718	2702
F	Position	23288	22954	23135	23321	23271
	Intensity	0.1364	0.1698	0.1488	0.1041	0.1205
	Width	1586	1582	1727	1578	1455
G	Position	25016	24727	25167	25116	24811
	Intensity	0.0930	0.0889	0.0772	0.0581	0.0638
	Width	694	880	664	638	754
H	Position	26149	26274	26225	26196	26150
	Intensity	0.2305	0.3537	0.3281	0.2113	0.2291
	Width	642	729	654	642	812
	Exponent B_0	2.47 E -14	5.90 E -13	8.36 E -14	5.82 E -14	3.95 E -14
	Exponent B_1	0.001045	0.000909	0.001004	0.001001	0.001015

Peak	Parameter	Sample 21	Sample 24	Sample 29	Sample 32	Sample 40
A	Position	4654	4788	4748	4693	4547
	Intensity	0.1712	0.203	0.1990	0.2257	0.1667
	Width	1100	1011	956	922	983
B	Position	7798	7653	7608	7647	7641
	Intensity	0.0956	0.1737	0.1571	0.1622	0.1901
	Width	1953	1653	1670	1688	2128
C	Position	10608	10012	10001	9797	10467
	Intensity	0.6294	0.7250	0.6895	0.7292	0.5291
	Width	4039	4062	3985	4015	4364
D	Position	16246	16954	16657	16689	17173
	Intensity	0.0477	0.0611	0.0561	0.0541	0.0367
	Width	2158	2559	3219	3005	1474
E	Position	20152	20008	20194	20254	20371
	Intensity	0.0611	0.0501	0.0367	0.0245	0.0691
	Width	2541	1467	1447	984	1933
F	Position	22574	23026	23111	23024	22380
	Intensity	0.0240	0.159	0.1390	0.0965	0.0332
	Width	615	1902	1833	1972	544
G	Position	23765	25307	25422	25590	23668
	Intensity	0.1345	0.0683	0.0735	0.0625	0.0154
	Width	2084	1072	937	731	1728
H	Position	26289	26253	26236	26161	26289
	Intensity	0.3093	0.2585	0.2078	0.1536	0.4134
	Width	688	680	647	533	659
	Exponent B_0	2.70 E -13	7.97 E -13	1.58 E -13	1.51 E -14	2.19 E -12
	Exponent B_1	0.000931	0.000912	0.000971	0.001049	0.000854

Peak	Parameter	Sample 42	Sample 45	Sample 48	Sample 51	Sample 52
A	Position	4490	4595	4564	4489	4518
	Intensity	0.1982	0.1787	0.1839	0.1885	0.1977
	Width	1041	860	827	1024	933
B	Position	7292	7293	7221	7136	7033
	Intensity	0.212	0.1974	0.2109	0.2235	0.2220
	Width	2085	1941	2077	1920	1952
C	Position	9940	9722	9693	9859	9672
	Intensity	0.5155	0.5692	0.5239	0.5457	0.5580
	Width	4007	4070	4047	3710	3677
D	Position	16014	15658	15795	13945	14843
	Intensity	0.0399	0.0568	0.0513	0.0711	0.1047
	Width	2299	2327	2202	1974	2567
E	Position	20861	20218	20113	17284	19538
	Intensity	0.0822	0.0609	0.0586	0.0624	0.0730
	Width	3982	2779	2527	3228	2990
F	Position	22780	23291	23100	23032	23167
	Intensity	0.169	0.134	0.131	0.1208	0.1388
	Width	1478	1672	1604	1879	1763
G	Position	24446	25089	24847	25253	25232
	Intensity	0.0904	0.0466	0.0514	0.0314	0.0481
	Width	962	531	736	356	409
H	Position	26103	26084	26037	26081	26047
	Intensity	0.3755	0.3215	0.2907	0.3262	0.3339
	Width	699	618	651	593	575
	Exponent B_0	5.34 E -12	7.99 E -13	4.68 E -14	7.87 E -13	4.15 E -12
	Exponent B_1	0.000851	0.000920	0.001017	0.000841	0.000869

Peak	Parameter	Sample 53	Sample 54	Sample 55	Sample 56	Sample 25
A	Position	4492	4448	4337	4529	4787
	Intensity	0.1711	0.1308	0.2093	0.1546	0.1765
	Width	858	1017	1191	877	1003
B	Position	7124	7133	6982	6864	7653
	Intensity	0.1819	0.1099	0.0700	0.1221	0.1591
	Width	2057	1882	1190	1530	1672
C	Position	9582	9543	9068	9089	10076
	Intensity	0.4994	0.4434	0.5887	0.5316	0.6331
	Width	4217	4148	4032	3677	3998
D	Position	16161	14113	15022	14079	15894
	Intensity	0.0662	0.0713	0.1917	0.1599	0.0547
	Width	2799	2349	3552	2858	2414
E	Position	19757	18507	20017	19872	20267
	Intensity	0.0507	0.0421	0.0925	0.0621	0.0636
	Width	1556	4143	934	2644	2532
F	Position	22562	22219	22314	23110	23262
	Intensity	0.1278	0.03134	0.1873	0.1210	0.1445
	Width	1555	605	1620	1729	1638
G	Position	24545	23532	24279	24956	25084
	Intensity	0.0741	0.0766	0.1041	0.0424	0.0644
	Width	1325	1400	1278	510	668
H	Position	26011	25985	25851	25907	26203
	Intensity	0.2673	0.2941	0.3692	0.3026	0.3219
	Width	668	665	655	593	649
	Exponent B_0	2.29 E -13	6.69 E -11	1.58 E -11	1.92 E -13	1.46 E -12
	Exponent B_1	0.000964	0.000850	0.000836	0.000978	0.000896

Peak	Parameter	Sample 26	Sample 9	Sample 63	Sample 66	Sample 69
A	Position	4811	4764	4829	4843	4872
	Intensity	0.1819	0.0839	0.4526	0.8597	2.248
	Width	964	984	982	977	1035
B	Position	7626	7585	7686	7692	7644
	Intensity	0.1641	0.0642	0.4231	0.7967	2.257
	Width	1575	1617	1633	1665	1717
C	Position	10041	10041	10113	10108	10249
	Intensity	0.7307	0.2849	0.2849	1.7322	3.3957
	Width	4014	3982	3982	3995	4024
D	Position	15245	15795	15795	15986	15965
	Intensity	0.0473	0.0205	0.0205	0.1869	0.4939
	Width	2062	2379	2379	2368	2394
E	Position	18646	19333	19963	20064	19510
	Intensity	0.0382	0.01331	0.225	0.7286	2.697
	Width	2420	1810	2358	2652	2833
F	Position	23106	23019	23197	23153	22990
	Intensity	0.0997	0.0480	0.450	1.073	3.267
	Width	1794	1901	1793	1757	1994
G	Position	25206	25711	25428	25333	25388
	Intensity	0.0472	0.0374	0.232	0.524	1.124
	Width	554	639	915	929	952
H	Position	26193	26303	26253	26201	26214
	Intensity	0.2549	0.0846	0.597	1.132	2.001
	Width	612	513	590	561	576
	Exponent B_0	8.56 E -14	4.93 E -13	1.72 E -10	1.42 E -8	1.44 E -6
	Exponent B_1	0.000991	0.000977	0.000764	0.000644	0.000052

Peak	Parameter	Sample 70	Sample 71	Sample 72		
A	Position	4867	4885	4906		
	Intensity	2.393	2.948	5.602		
	Width	1005	1065	1075		
B	Position	7766	7653	7705		
	Intensity	2.306	1.940	4.24		
	Width	1771	1438	1638		
C	Position	10419	.9892	10094		
	Intensity	9.509	11.736	21.100		
	Width	4152	3773	3806		
D	Position	17027	16501	16314		
	Intensity	4.276	6.932	14.923		
	Width	2798	4420	3984		
E	Position	19909	20483	20241		
	Intensity	2.127	3.830	9.312		
	Width	934	2141	2458		
F	Position	22219	22452	22453		
	Intensity	6.303	5.206	9.351		
	Width	2323	1228	1433		
G	Position	-	-	-		
	Intensity	-	-	-		
	Width	-	-	-		
H	Position	25952	-	-		
	Intensity	2.077	-	-		
	Width	602	-	-		
	Exponent B_0	1.98 E -5	0.000273	9.79 E -4		
	Exponent B_1	0.000453	0.000038	0.000351		